Biomarker qualification for drug-induced liver injury across species using immunoaffinity mass spectrometry

Dissertation
der Mathematisch-Naturwissenschaftlichen Fakultät
der Eberhard Karls Universität Tübingen
zur Erlangung des Grades eines
Doktors der Naturwissenschaften
(Dr. rer. nat.)

vorgelegt von
Viktoria Anselm
aus Ishmorski/Russland

Tübingen
2021

Gedruckt mit Genehmigung der Mathematisch-Naturwissenschaftlichen Fakultät
der Eberhard Karls Universität Tübingen

Tag der mündlichen Qualifikation:	28.03.2022
Dekan:	Prof. Dr. Thilo Stehle
1. Berichterstatter:	Prof. Dr. Thilo Stehle
2. Berichterstatter:	Prof. Dr. Boris Maček

Declaration

The experimental work presented in this thesis was performed at the Natural and Medical Sciences Institute at University of Tübingen (NMI) between October 2017 and January 2019 and continued at SIGNATOPE GmbH between February 2019 and October 2021. This thesis was supervised by Prof. Dr. Thilo Stehle (Eberhard Karls Universität Tübingen), Prof. Dr. Boris Maček (Eberhard Karls Universität Tübingen), and Dr. Oliver Pötz (SIGNATOPE GmbH, Reutlingen).

Experiments related to trypsin and chymotrypsin activity assays were performed in conjunction with Jasmin Knoll, a master student who worked on this project with me. She presented data from preliminary experiments of this research area in her master thesis.

Cornelia Sommersdorf supported this project to a great extent by preparing peptide-specific antibodies and by performing all K18, ccK18, HMGB1, and OPN sandwich immunoassays (bead-based and ELISA). Tissue and cell lysis was performed by me in conjunction with Cornelia Sommersdorf (liver), by Katharina Bendel (other tissue), or by Dr. Helen Hammer (primary human hepatocytes), all working at SIGNATOPE GmbH.

Samples for matrix and sampling comparison (human EDTA plasma & serum) were kindly provided by Genentech (Montserrat Carrasco-Triguero and Paula Katavolos) through the Genentech employee sample donation program. Project-relevant preclinical EDTA plasma and tissue samples were kindly provided by Sanofi (Sébastien Laurent) and by Merck Sherp & Dohme (Katerina Vlasakova). Furthermore, data of ALT enzyme tests were kindly provided by the respective companies and I analyzed and presented the data in this work. GLDH activity results were kindly provided by Sanofi.

List of publications related to this work

Parts of the data presented in this work were already published or are in preparation.

Anselm, V., Meisinger, T., Laurent, S., Sautier, L., Poetz, O., Elevated GLDH and OPN levels in plasma of rats treated with APAP or DAPM.
In preparation.

Anselm, V., Sommersdorf, C., Carrasco-Triguero, M., Katavolos, P., Planatscher, H., Steinhilber, A., Joos, T., Poetz, O., Matrix and Sampling Effects on Quantification of Protein Biomarkers of Drug-Induced Liver Injury. *Journal of Proteome Research.* 20(11):4985-4994. doi:10.1021/acs.jproteome.1c00478 (Nov 2021).

Anselm V., Steinhilber, A., Sommersdorf, C., Poetz, O. Immunoaffinity-Based Liquid Chromatography Mass Spectrometric Assay to Accurately Quantify the Protein Concentration of HMGB1 in EDTA Plasma. *Methods in Molecular Biology (Clifton, N.J.)* 2261,277–289. doi:10.1007/978-1-0716-1186-9_17 (2021).

List of poster presentations related to this work

Anselm, V, Sommersdorf, C., Merz, M., Knoll, J., Steinhilber, A., Schmidt, F., Naboulsi, W., Hammer, H. S., Tausch, A., Planatscher, H., Joos, T., Pötz, O.
Development of MS-based immunoassays for quantification of drug-induced liver injury candidate biomarkers across species, Eurotox 2019, Helsinki, Finland, 2019

Anselm, V., Naboulsi, W., Joos, T., Pötz, O.
Development of mass spectrometry-based immunoassays for quantification of drug-induced liver injury biomarkers across species, 12th European Summer School Advanced Proteomics, Brixen, Italy, 2018

Danksagung

Zunächst möchte ich Dr. Oliver Pötz für die Möglichkeit danken, meine Arbeit bei SIGNATOPE GmbH und am NMI ermöglicht zu haben. Die engagierte Betreuung, das stets offene Ohr und die vielen zielführenden Diskussionen haben die Ergebnisse dieser Arbeit maßgeblich ermöglicht.

Zudem möchte ich mich bei Prof. Dr. Thilo Stehle and Prof. Dr. Boris Maček für die Betreuung meiner Arbeit als Gutachter durch die Mathematisch-Naturwissenschaftliche Fakultät der Eberhard Karls Universität Tübingen sehr bedanken. Die vorhergehenden Arbeiten in Betreuung durch Prof. Dr. Thilo Stehle and Prof. Dr. Boris Maček (Bachelor- und Masterarbeit) haben das wissenschaftliche Fundament für diese Arbeit gelegt.

Großer Dank gilt Dr. Montserrat Carrasco-Triguero, Dr. Paula Katavolos, Dr. Katerina Vlasakova, Dr. Sébastien Laurent, und Dr. Björn Tränkle für die Bereitstellung der Proben für diese Arbeit.

Meinen Kollegen danke ich sehr für ihre Unterstützung, die wissenschaftlichen Diskussionen und die schöne gemeinsame Zeit. Dabei möchte ich mich vor allem bei Dr. Hannes Planatscher und Cornelia Sommersdorf für ihre große Hilfsbereitschaft und die Zusammenarbeit im Zuge dieser Arbeit bedanken.

Meinen Freunden und meiner Familie danke ich für die außerordentliche Unterstützung in jeglicher Hinsicht während dieser Zeit. Meinem Mann, David, danke ich aus tiefstem Herzen ihn an meiner Seite zu haben und von seiner guten Laune angesteckt zu werden. Meinen Eltern, Olga und Alexander, und meiner Schwester, Evelyn, danke ich vor allem, mich auf diesen Weg gebracht zu haben und mir über die vielen Jahre hinweg einen starken Rückhalt gegeben zu haben. Heike danke ich überaus für ihr Anfeuern zu allen möglichen Zeiten. Saskia bin ich für ihre tatkräftige Unterstützung während der Entstehung dieser Arbeit sehr dankbar.

Contents

List of Figures VIII

List of Tables X

Abbreviations XI

Summary 1

Zusammenfassung 3

1 Introduction 5
1.1 Liver - organ of detoxification and toxification . . . 5
1.2 Drug-induced liver injury - DILI . . . 7
1.2.1 Effects of DILI-related drugs or compounds on the liver . . . 9
1.2.2 Current and potential DILI biomarkers . . . 10
1.3 Mass spectrometry for protein analysis . . . 14
1.3.1 Targeted and non-targeted proteomics . . . 14
1.3.2 Instrumentation . . . 16
1.3.3 Plasma proteomics . . . 17
1.4 Accurate quantification & validation . . . 19
1.4.1 Quantification strategies . . . 19
1.4.2 Validation strategies . . . 20

2 Aims of the thesis 21

3 Material and Methods 23
3.1 Material . . . 23
3.1.1 Consumables . . . 23
3.1.2 Chemicals and reagents . . . 24
3.1.3 Solutions and buffers . . . 25
3.1.4 Enzymes, proteins, and kits . . . 26
3.1.5 Samples . . . 27
3.1.6 Laboratory equipment . . . 27
3.1.7 Databases and software . . . 28
3.2 IA-LC-MS/MS assays for DILI biomarker quantification . . . 29
3.2.1 Surrogate matrix . . . 29
3.2.2 Samples for method development and method validation . . . 30
3.2.3 Samples for matrix and sampling comparison . . . 31
3.2.4 Samples for translational DILI biomarker investigation in preclinical studies . . . 32
3.2.5 Proteotypic peptides of DILI biomarkers . . . 33

3.2.6 Capture antibodies for peptide enrichment . . . 34
3.2.7 Tissue and cell lysis . . . 34
3.2.8 Total protein determination . . . 34
3.2.9 Proteolysis of tissue, cells, plasma, and serum . . . 35
3.2.10 Peptide immunoaffinity enrichment (immunoprecipitation) . . . 36
3.2.11 LC-MS/MS and MS data public access . . . 37
3.2.12 General MS data analysis and quantification . . . 38
3.2.13 Data analysis for validation experiments . . . 38
3.2.14 Replicates and statistical analysis . . . 40
3.3 Sandwich immunoassays for DILI biomarker quantification . . . 40
3.3.1 ELISAs for quantification of HMGB1, K18, and ccK18 . . . 41
3.3.2 Bead-based sandwich immunoassays for quantification of OPN and MCSF1R . . . 41
3.4 Enzyme activity-based assays . . . 42
3.4.1 Enzyme activity assay for GLDH . . . 42
3.4.2 Enzyme activity assay for ALT . . . 43
3.4.3 Tryptic and chymotryptic activity assays . . . 43

4 Results 47
4.1 General factors influencing IA-LC-MS/MS assays applied to plasma analyses . . . 47
4.1.1 Optimization of peptide measurement by parallel reaction monitoring . . . 47
4.1.2 K18 and ccK18 peptide stability and chromatographic performance 51
4.1.3 Effect of antibody and spiked internal standard amount on peptide recovery . . . 52
4.1.4 Impact of trypsin on peptide release and recovery . . . 54
4.1.5 New insights into the rat MCSF1R protein sequence . . . 64
4.1.6 DILI biomarker quantification in human and rat specimen . . . 68
4.2 Method validation of IA-LC-MS/MS assay for protein quantification in rat specimen . . . 71
4.2.1 Accuracy & precision . . . 71
4.2.2 Parallelism of endogenous analyte diluted in surrogate matrix . . 75
4.2.3 Reproducibility of quantification of endogenous analyte . . . 76
4.3 Matrix and sampling effects on quantification of potential human protein biomarkers of DILI . . . 78
4.3.1 Effects of sample matrix on DILI biomarkers . . . 78
4.3.2 Effects of sample benchtop time on DILI biomarkers . . . 84
4.3.3 Correlation between standard methods and IA-LC-MS/MS . . . 86

4.4 Translational protein biomarkers for DILI investigation in preclinical studies with APAP, DAPM, thioacetamide, bromobenzene, and CCl_4 . 87
4.4.1 ALT . . . 88
4.4.2 OPN . . . 90
4.4.3 GLDH . . . 92
4.4.4 HMGB1 . . . 96
4.4.5 MCSF1R . . . 98
4.4.6 ccK18 . . . 100
4.5 Specificity of DILI protein biomarkers in rat tissue . . . 102

5 Discussion 105
5.1 IA-LC-MS/MS assays applied to analyses in plasma . . . 105
5.1.1 Combining sensitivity and selectivity in IA-LC-MS/MS assays . 105
5.1.2 Peptide rescue by inhibition of trypsin side reactivity . . . 109
5.2 Matrix, sampling, and methodological effects on quantification of human protein biomarkers of DILI . . . 111
5.3 Translational protein biomarkers as potential DILI markers in preclinical studies . . . 116
5.3.1 ALT . . . 116
5.3.2 OPN . . . 118
5.3.3 GLDH . . . 120
5.3.4 HMGB1 . . . 121
5.3.5 MCSF1R . . . 122
5.3.6 ccK18 . . . 123
5.3.7 Relationship between potential biomarkers and their preclinical value for DILI . . . 123

6 Conclusions 125

References 128

Appendices 147

Curriculum Vitae 162

List of Figures

1 Structural organization of liver lobules. 5
2 Biotransformation in the liver. 7
3 Mechanistic 3-step model for drug-induced liver injury. 8
4 Current and potential biomarkers of DILI. 13
5 Peptide identification via full-scan MS and parallel reaction monitoring (PRM). 15
6 Overview of mass spectrometer instrumentation and peptide fragmentation. 17
7 Dynamic range of the plasma proteome. 18
8 General IA-LC-MS/MS workflow. 29
9 Sample preparation for matrix and sampling comparison. 31
10 General sandwich immunoassay workflow 41
11 General enzyme activity assay workflow for GLDH 43
12 General IA-LC-MS/MS workflow for serum or plasma specimen. 47
13 Impact of normalized collision energy (NCE) on peptide detection and quantification. 49
14 Carryover or intensity loss of ccK18 or K18 peptide. 51
15 Impact of antibody (AB) and internal standard amount on HMGB1 peptide quantification in human plasma. 53
16 Endogenous DILI-related proteins measured by IA-LC-MS/MS in human plasma. 54
17 Loss of endogenous K18 peptide in plasma. 55
18 Impact of sample matrix on K18 and HMGB1 peptide recovery. 55
19 Different effect of trypsin to protein ratio on K18 and HMGB1 recovery. 57
20 Digest kinetics for the K18 and HMGB1 peptides. 57
21 Full-length and chymotryptic fragments of the K18 and HMGB1 peptides on MS/MS level. 58
22 Conversion of trypsin and chymotrypsin substrate and its inhibitiony. . 60
23 Effect of PMSF addition before proteolysis on K18 and HMGB1 peptide recovery. 61
24 K18 peptide rescue in rat plasma and rat liver tissue. 62
25 Improvement of HMGB1 peptide measurement in rat plasma and rat liver tissue. 63
26 MCSF1R analyses in human, mouse, and rat plasma. 64
27 MCSF1R rat sequence comparison. 65
28 MS and MS/MS measurement of recombinant MCSF1R rat with the protein sequence according to Uniprot ID D4ACA7 66
29 Immunoaffinity enrichment of peptides from recombinant MCSF1R rat (Uniprot ID D4ACA7). 67

30 Exemplary calibration curves and QC samples for the GLDH and MCSF1R rat peptides. 69
31 DILI biomarker concentrations in serum gel, serum, and EDTA plasma. 79
32 Correlation of DILI biomarker concentrations in serum gel, serum, and EDTA plasma of matched samples by IA-LC-MS/MS (MPh-dev) and ELISA (ccK18). 82
33 Correlation of DILI biomarker concentrations in serum gel, serum, and EDTA plasma by immunoassays and enzyme activity. 83
34 Change in analyte concentrations during benchtop stability between 15 min and 60 min benchtop time. 85
35 IA-LC-MS/MS and immunoassay or enzyme assay method comparison. 86
36 Enzymatic ALT activity in serum of preclinical DILI studies with rats. 89
37 OPN concentration in EDTA plasma of preclinical DILI studies with rats. 91
38 OPN concentration in liver tissue of preclinical DILI studies with rats. . 92
39 GLDH concentration in EDTA plasma of preclinical DILI studies with rats. 93
40 GLDH activity results in studies with APAP (1,500 mg/kg) and DAPM and correlation with protein concentration data. 95
41 GLDH concentration in liver tissue of preclinical DILI studies with rats. 96
42 HMGB1 concentration in EDTA plasma of preclinical DILI studies with rats. 97
43 HMGB1 concentration in liver tissue of preclinical DILI studies with rats. 98
44 MCSF1R peptide ratio in EDTA plasma of preclinical DILI studies with rats. 99
45 MCSF1R peptide ratio in liver tissue of preclinical DILI studies with rats. 100
46 ccK18 peptide ratio in EDTA plasma of preclinical DILI studies with rats. 101
47 ccK18 peptide ratio in liver tissue of preclinical DILI studies with rats. 101
48 Specificity of DILI biomarkers in rat tissue 103
49 Tryptic and chymotryptic activity in plasma 147
50 Enriched endogenous human ccK18 from cell lysate of taxol-treated HepG2 cells. 147

List of Tables

1 Classification for drug-induced liver injury . . . 11
2 Consumables . . . 23
3 Chemicals and reagents . . . 24
4 Solutions and buffers . . . 25
5 Enzymes, proteins, and kits . . . 26
6 Samples . . . 27
7 Laboratory equipment . . . 27
8 Databases, software and version . . . 28
9 Composition of quality control (QC) samples . . . 30
10 Study set-up DILI rat, MSD . . . 32
11 Semi-automated procedure for immunoprecipitation in amagnetic bead processor . . . 37
12 General parameters of proteins related to DILI and relevant peptides . . 48
13 Precursor ions and fragments selected for peptide quantification . . . 50
14 Assay-related specifications for IA-LC-MS/MS assays . . . 70
15 Peak area ratio data of calibrators S1-S8 and blank B for GLDH (MPr) 72
16 Peak area ratio data of calibrators S1-S8 and blank B for MCSF1R (MPr) 72
17 Calibrator validation results for GLDH (MPr) . . . 73
18 Calibrator validation results for MCSF1R (MPr) . . . 73
19 QC inter assay validation results for GLDH and MCSF1R (MPr) . . . 74
20 QC intra assay validation results for GLDH and MCSF1R (MPr) . . . 74
21 Parallelism of endogenous GLDH in plasma samples diluted in surrogate matrix (MPr) . . . 75
22 Reproducibility of endogenous GLDH levels in rat plasma (MPr) . . . 76
23 Validation results for the assay MPr . . . 77
24 Statistical comparison between DILI biomarker concentration in matched serum gel, serum, and EDTA plasma samples. . . . 79
25 Mean difference between DILI biomarker concentration in matched serum gel, serum, and EDTA plasma samples measured by IA-LC-MS/MS. . . 80
26 Peak area ratio data of calibrators S1-S8 and blank B for OPN (MPr) . 148
27 Peak area ratio data of calibrators S1-S8 and blank B for HMGB1 (MPr) 148
28 Peak area ratio data of calibrators S1-S8 and blank B for ccK18 (MPr) 149
29 Calibrator validation results for OPN (MPr) . . . 149
30 Calibrator validation results for HMGB1 (MPr) . . . 150
31 Calibrator validation results for ccK18 (MPr) . . . 150
32 QC inter assay validation results for OPN and HMGB1 (MPr) . . . 151
33 QC inter assay validation results for ccK18 (MPr) . . . 151
34 QC intra assay validation results for OPN and HMGB1 (MPr) . . . 152
35 QC intra assay validation results for ccK18 (MPr) . . . 152

36 Parallelism of endogenous OPN in plasma samples diluted in surrogate matrix (MPr) . . . 153
37 Parallelism of endogenous HMGB1 in plasma samples diluted in surrogate matrix (MPr) . . . 154
38 Parallelism of endogenous GLDH in liver tissue samples diluted in surrogate matrix (MPr) . . . 155
39 Parallelism of endogenous HMGB1 in liver tissue samples diluted in surrogate matrix (MPr) . . . 156
40 Reproducibility of endogenous OPN levels in rat plasma (MPr) . . . 157
41 Reproducibility of endogenous HMGB1 levels in rat plasma (MPr) . . . 157
42 Reproducibility of endogenous GLDH levels in liver tissue (MPr) . . . 157
43 Reproducibility of endogenous HMGB1 levels in rat liver tissue (MPr) . 157
44 DILI biomarker concentration in matched serum gel, serum, and EDTA plasma samples. . . . 158
45 Calibration curves for matrix and sampling comparison (MPh-dev assay, MCSF1R, OPN, HMGB1) . . . 159
46 Calibration curves for matrix and sampling comparison (MPh-dev assay, GLDH). . . . 160
47 Quality control samples for matrix and sampling (MPh-dev assay, GLDH).160
48 Quality control samples for matrix and sampling (MPh-dev assay, MCSF1R, OPN, HMGB1). . . . 161

Abbreviations

Abbreviation	Description
aa	Amino acid
ABC	Ammonium hydrogen bicarbonate
ABCC	Ammonium hydrogen bicarbonate with 0.03% CHAPS
Acc.	Accuracy
ACN	Acetonitrile
AGC	Automatic gain control
ALF	Acute liver failure
ALP	Alkaline phosphatase
AST	Apartate aminotransferase
APAP	Acetaminophen
approx.	Approximately
AQUA	Absolute quantification
AUC	(Peak) area under the curve
B	Blank sample
BCA	Bicinchoninic acid
Bcl-2	B-cell lymphoma 2
BSA	Bovine serum albumin
ccK18	Caspase-cleaved keratin 18
CCl_4	Carbon tetrachloride
CV	Coefficient of variation
CYP	Members of the cytochrome P450 superfamiliy
DAPM	4,4'-methylene dianiline
DDA	Data-dependet acquisition
DF	Dilution factor
DIA	Data-independet acquisition
DILI	Drug-induced liver injury
ECM	Extracellular matrix
EDTA	Ethylenediaminetetraacetic acid
ELISA	Enzyme-linked immunosorbent assay
EMA	European Medicines Agency
e.g.	Exempli gratia (for example)
EPA	U.S. Environmental Protection Agency
ESI	Electrospray ionization
EtOH	Ethanol
FA	Formic acid
FDA	United States Food and Drug Administration

Abbreviation	Description
GLDH	Glutamate Dehydrogenase 1
GSH	Glutathione
HAc	Acetic acid
HCD	Higher-energy collisional dissociation
HLA	human leukocyte antigen
HMGB1	High mobility group protein B1
HSC	Hepatic stellate cell
i.e.	Id est (that is to say)
IA-MS	Immunoaffinity mass spectrometry
IA-LC-MS/MS	Immunoaffinity liquid chromatography tandem mass spectrometry
IAA	Iodoacetamide
IgG	Immunglobulin
IP	Immunoprecipitation
iTRAQ	Isobaric tags for relative and absolute quantification
K	Lysine
K18	Keratin 18
kDa	Kilo dalton
L	Leucine
LC-MS	Liquid chromatography coupled to mass spectrometry
LC-MS/MS	Liquid chromatography tandem mass spectrometry
LFQ	Label-free quantification
LLOQ	Lower limit of quantification
m/z	mass-to-charge
MCSF1R	Macrophage colony stimulating factor 1 receptor
MPT	Mitochondrial permeability transition
MPh-dev	Multiplex human
MPr	Multiplex rat
MRP	Multidrug resistance protein
MS	Mass spectrometry
MSD	Merck Sherp & Dohme
min	Minute
ms	Millisecond
n/a	Not applicable
NAPQI	N-acetyl-p-benzoquinone imine
NCE	Normalized collision energy
OPN	Osteopontin
o\n	Overnight
PBS	Phosphate-buffered saline
PBSC	Phosphate-buffered saline with 0.03% CHAPS
PE	Phycoerythrin

Abbreviation	Description
PMSF	Phenylmethylsulfonyl fluoride
PRM	Parallel reaction monitoring
PTM	Post-translational modification
QC	Quality control
R	Arginine
rec.	Recombinant
rep	Replicate
RT	Room temperature
ROS	Reactive oxygen species
S1-S8	Calibration samples S1 to S8
SD	Standard deviation
SIS	Stable isotope-labeled standard
SISCAPA	Stable isotope standards and capture by anti-peptide antibodies
SLC	Solute carrier
SNP	Single nucleotide polymorphism
SRM	Selected reaction monitoring
TBIL	Total bilirubin
TCEP	Tris(2-carboxyethyl)phosphine
TEA	Triethanolamine
TEA-NOG	N-Octyl glycoside in triethanolamine
TE	Total error
TLCK	Nα-tosyl-L-lysine chloromethyl ketone hydrochloride
TMT	Tandem mass tags
TNFα	Tumor necrosis factor alpha
TPCK	N-p-tosyl-L-phenylalanine chloromethyl ketone
TXP	Triple X proteomics
(U)HPLC	(Ultra) high-performance liquid chromatography
ULN	Upper limit of normal
ULOQ	Upper limit of quantification
vs	Versus

Summary

Drug-induced liver injury remains one of the major complications during patient treatment and accounts for more than 10% of all cases of acute liver failure. Accordingly, drug withdrawals from the global market still occur frequently. Standard diagnosis and prediction of DILI involves assessment of alanine aminotransferase (ALT) combined with careful evaluation and exclusion of other underlying liver impairments as current gold standard. However, the predictive value of this assessment method is rarely DILI-specific. Current efforts in investigating clinical DILI studies revealed potential new DILI protein biomarkers including glutamate dehydrogenase (GLDH), high-mobility group protein B1 (HMGB1), full-length and caspase-cleaved keratin 18 (K18, ccK18), macrophage colony stimulating factor 1 receptor (MCSF1R), and osteopontin (OPN). As potential mechanistic markers for immune response and hepatocyte apoptotis and necrosis upon drug treatment, these proteins may increase the specificity of DILI diagnosis and potentially have higher predictive value for DILI diagnosis. The use of these proteins as potential DILI biomarkers in animal studies, thus, their translatability from human to animal for preclinical studies, is of particular interest to intervene earlier in drug development with improved DILI diagnosis. Furthermore, serum and plasma are both used as clinically relevant samples but their comparability regarding preanalytical matrix and sampling effects is not completely examined for the proteins under investigation.

Immunoaffinity liquid chromatography tandem mass spectrometry (IA-LC-MS/MS) was used to develop multiplexed assays for quantification of the potential DILI biomarkers. The multiplexed assays were used to elucidate matrix and sampling effects in human plasma and serum samples. Sandwich immunoassays were compared with IA-LC-MS/MS read-out. Furthermore, the effect of drugs and compounds, which are known to induce hepatic injury, was examined in preclinical studies in rat models to test for biomarker translatability. Acetaminophen (APAP), 4,4'-methylene dianiline (DAPM), thioacetamide, bromobenzene, and carbon tetrachloride (CCl_4) were used for this purpose. APAP, thioacetamide, and bromobenzene were tested for dose effects, while time-dependent effects were monitored for DAPM and CCl_4 and daily drug treatment was tested for CCl_4.

HMGB1 and MCSF1R were affected the most by matrix effects in serum and plasma. Serum HMGB1 levels were significantly higher than plasma levels by up to 12-fold, whereas MCSF1R content was higher in plasma than in serum by about 20%. Analyte release within the first 60 min between sample collection and centrifugation was observed for HMGB1 in serum with up to 200% increase during the sampling procedure. Other analytes showed either no significant change over time or remained within 10% of the base level. IA-LC-MS/MS provided a powerful tool to investigate the protein sequence of MCSF1R in rat plasma revealing more experimental evidence for the unre-

viewed protein sequence with Uniprot ID D4ACA7 compared to the reviewed protein sequence with Uniprot ID Q00495. However, chromatographic and stability-related challenges were observed with the initially targeted K18 and ccK18 peptides for measurement. Therefore, ELISA kits were used for read out of matrix and sampling effects for K18 and ccK18. The IA-LC-MS/MS approach was better applicable to quantify OPN in serum and plasma due to better correlation compared to the sandwich immunoassay approach. K18 and one of the investigated HMGB1 peptides were found to be susceptible to tryptic side-reactivity, likely produced by autolytic production of pseudotrypsin with chymotryptic-like activity. Addition of PMSF before proteolysis was found to rescue the according K18 and HMGB1 peptides. Analysis of preclinical studies with the presented drugs and compounds confirmed GLDH as potential marker for acute hepatic cell death. Furthermore, OPN levels were shown in concordance with GLDH levels except for CCl_4 treatment, where GLDH levels further increased with longer treatment time, while OPN remained at the same level. Since elevated OPN concentration upon drug treatment was observed in this animal model, OPN may serve as translational immune response marker for DILI. HMGB1 might be rather a biomarker for liver fibrosis than for acute liver failure since APAP and DAPM treatment showed steady HMGB1 levels, whereas thioacetamide and CCl_4 as known fibrosis-inducing agents resulted in elevated HMGB1 levels. Corresponding to previous RNA expression results, GLDH was observed predominantly in liver followed by kidney and brain tissue.

In summary, this work contributes to better understanding for the use of trypsin in IA-LC-MS/MS assays and for matrix and sampling effects on the potential DILI biomarkers. Most importantly, translational value of GLDH and OPN as potential DILI biomarker in rats as animal model is supported by the observed results, while HMGB1 as marker for acute liver injury is further under question.

Zusammenfassung

Medikamenteninduzierte Leberschädigung (*drug-induced liver injury*, DILI) ist nach wie vor eine der größten Nebenwirkungen bei der Behandlung von Patienten und macht mehr als 10% aller Fälle von akutem Leberversagen aus. Dementsprechend kommt es immer noch häufig zu Rücknahmen von Arzneimitteln vom Weltmarkt. Der Goldstandard zur Diagnose und Vorhersage von DILI umfasst insbesondere die Bestimmung der Alaninaminotransferase (ALT) in Verbindung mit einer sorgfältigen Bewertung und dem Ausschluss anderer zugrundeliegender Leberschäden. Die Vorhersage für DILI nach dieser Mess- und Bewertungsmethode ist jedoch selten spezifisch. Aktuelle Untersuchungen klinischer DILI-Studien ergaben potenzielle neue Proteinbiomarker für DILI, darunter *glutamate dehydrogenase* (GLDH), *high-mobility group protein B1* (HMGB1), *keratin 18* (K18 in voller Länge und ccK18 als durch Kaspase gespaltenes Produkt), *macrophage colony stimulating factor 1 receptor* (MCSF1R), and *osteopontin* (OPN). Diese Proteine könnten möglicherweise durch ihre Funktion als potenzielle mechanistische Marker sowohl für die Immunreaktion, als auch für Apoptose und Nekrose von Hepatozyten bei medikamentöser Behandlung eine bessere Diagnose und Vorhersage spezifisch für DILI liefern. Die Verwendung dieser Proteine als potenzielle Biomarker für DILI in Tierversuchen und damit ihre Übertragbarkeit vom Menschen auf das Tier für präklinische Studien ist von besonderem Interesse, um mit einer verbesserten Diagnose von DILI in Fällen von Leberschädigung früher in der Arzneimittelentwicklung einzugreifen. Sowohl Serum als auch Plasma werden als klinische Probenmatrix verwendet, aber ihre Vergleichbarkeit hinsichtlich präanalytischer Matrix- und Probenbearbeitungseffekten ist nicht vollständig untersucht.

Basierend auf der Methode *immunoaffinity liquid chromatography tandem mass spectrometry* (IA-LC-MS/MS) wurden Assays zur multiplexen Quantifizierung der potenziellen Biomarker für DILI entwickelt. Diese Assays wurden zur Aufklärung von Matrix- und Probenbearbeitungseffekten in humanen Plasma- und Serumproben verwendet. Herkömmliche Sandwich-Immunassays wurden mit den Ergebnissen der IA-LC-MS/MS-Methode verglichen. Um die Übertragbarkeit von Biomarkern zu testen, wurde die Wirkung von Arzneimitteln und Reagenzien, von denen bekannt ist, dass sie Leberschäden hervorrufen, in präklinischen Studien mit Ratten als Tiermodell untersucht. Acetaminophen (APAP), 4,4'-Methylendianilin (DAPM), Thioacetamid, Brom-benzol und Tetrachlorkohlenstoff (CCl_4) wurden hierfür verwendet. APAP, Thioacetamid und Brombenzol wurden auf Dosiseffekte hin getestet, während für DAPM und CCl_4 zeitabhängige Effekte und für CCl_4 eine tägliche Medikamentenbehandlung untersucht wurden.

HMGB1 und MCSF1R waren am stärksten von Matrixeffekten in Serum und Plasma betroffen. Die Konzentrationen von HMGB1 im Serum waren signifikant höher als in Plasma, und zwar um das bis zu 12-fache, während die Konzentration von MCSF1R in

Plasma um etwa 20% höher war als in Serum. Ein Anstieg von bis zu 200% wurde für HMGB1 in Serum innerhalb der ersten 60 min zwischen Probenentnahme und Zentrifugation beobachtet, während andere Biomarkerkonzentrationen entweder keine signifikante Veränderung über diese Zeitspanne hinweg zeigten oder innerhalb von 10% Varianz blieben. IA-LC-MS/MS stellt eine leistungsfähige Methode zur Untersuchung der Proteinsequenz von MCSF1R in Rattenplasma dar, mithilfe derer experimentelle Beweise für die Proteinsequenz mit der Uniprot-ID D4ACA7 gesammelt wurden, die als nicht geprüft gilt, als im Vergleich zur Proteinsequenz mit der Uniprot-ID Q00495. Bei den ursprünglich zur Untersuchung herangezogenen Peptiden K18 und ccK18 gab es allerdings chromatografische und stabilitätsbedingte Herausforderungen zur Messung, weshalb ELISA-Kits zum Auslesen von Matrix- und Probenbearbeitungseffekten für K18 und ccK18 verwendet wurden. Der IA-LC-MS/MS-Ansatz war für die Quantifizierung von OPN aufgrund der Serum- /Plasmakorrelation der Ergebnisse besser geeignet als der Sandwich-Immunassay-Ansatz. K18 und eines der untersuchten HMGB1-Peptide erwiesen sich als anfällig für eine tryptische Nebenreaktion, die wahrscheinlich durch die autolytische Produktion von Pseudotrypsin, welches eine chymotryptischer Aktivität aufweist, hervorgerufen wird. Die Zugabe von PMSF vor der Proteolyse konnte die entsprechenden Peptide für K18 und HMGB1 wiederherstellen und im Falle von K18 sogar messbar machen. Die Analyse der präklinischen Studien mit den untersuchten Arzneimitteln und Reagenzien bestätigte GLDH als potenziellen Marker für den akuten Leberzelltod. Außerdem zeigte sich, dass die Konzentration von OPN sich analog zur Konzentration von GLDH verhält, mit Ausnahme während der Behandlung mit CCl_4. Hierbei erhöhte sich die Konzentration von GLDH mit verlängerter Behandlungszeit immer weiter, während der OPN-Gehalt gleich hoch blieb. Da in diesem Tiermodell eine erhöhte Konzentration von OPN bei medikamentöser Behandlung beobachtet wurde, könnte OPN als translationaler Immunreaktionsmarker für DILI dienen. HMGB1 stellt eher einen Biomarker für Leberfibrose als für akutes Leberversagen dar, da die Behandlung mit APAP und DAPM einen gleichbleibenden HMGB1-Gehalt ergab, während Thioacetamid und CCl_4 als bekannte Fibrose-induzierende Mittel zu erhöhter HMGB1-Konzentration in Plasma behandelter Ratten führten. In Übereinstimmung mit früheren RNA-Expressionsergebnissen wurde GLDH vorwiegend in der Leber, gefolgt von Nieren- und Hirngewebe, nachgewiesen.
Zusammenfassend lässt sich sagen, dass diese Arbeit zu einem besseren Verständnis der Verwendung von Trypsin in der IA-LC-MS/MS-Methodik und der Auswirkungen von Matrix und Probebearbeitung auf die potenziellen Biomarker für DILI beiträgt. Vor allem aber wird der Wert von GLDH und OPN als potenzielle Biomarker für DILI in Ratten als Tiermodell durch die hier erzielten Ergebnisse unterstützt, während HMGB1 als Marker für akute Leberschäden in Frage gestellt wird.

1 Introduction

1.1 Liver - organ of detoxification and toxification

The liver combines vital metabolic functions within its organ structure ranging from carbohydrate and fatty acid metabolism to ureagenesis[1]. Hepatocytes take over these functions building up to 90% of the liver mass. This cell type clusters in chords forming hexagonal structures around the central veins of the liver, termed liver lobules[2] (**Figure 1**). Each lobule comprises three zones with a gradient in oxygen and nutrients going from saturated at the portal vessel (zone 1) to low saturation at the central vein (zone 3) and shows a differential gene expression in hepatocytes within these zones. Genes for gluconeogenesis or β-oxidation for fatty acid break-down are primarily expressed in the periportal region, whereas genes for glycolysis and fatty acid synthesis are expressed in the pericentral region[2,3].

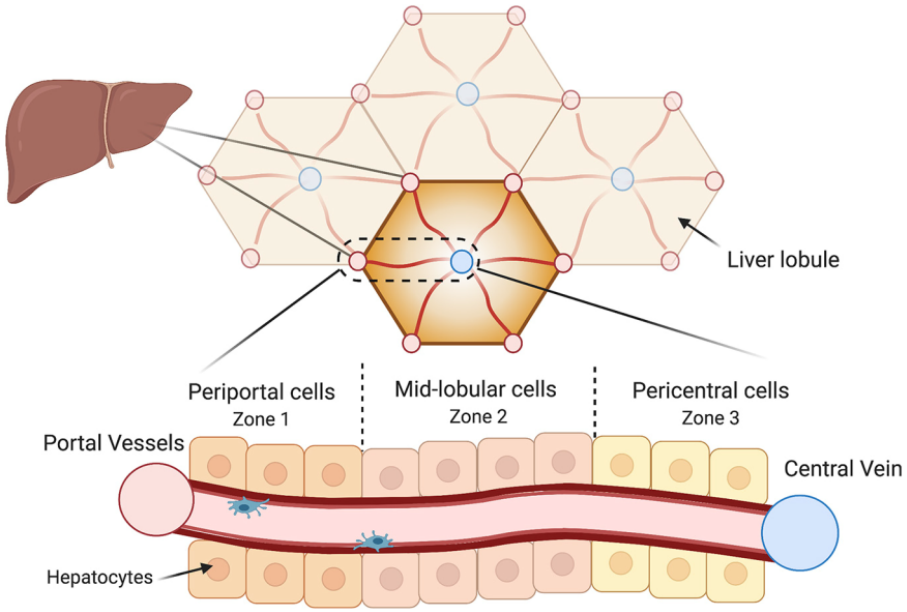

Figure 1: Structural organization of liver lobules. The liver is structurally formed in clusters of liver lobules. Hexagonal liver lobules consist of hepatic cords with blood flow from portal vessels (red) to the central vein (blue). Three zones of hepatic cells form the liver lobule ranging from the periportal, oxygen- and nutrient-rich site (zone 1) to the pericentral site, which is low in oxygen and nutrients (zone 3). Hepatocytes cluster along the portal circulation, while immune cells (Stellate and Kupfer cells) circulate within the blood flow. Adapted from Cunningham & Porat-Shliom[2].

Oxygen and nutrient-rich blood flows from the portal vein at the corners of the lobules towards the central vein. These corners comprise the portal triad consisting of the portal vein, the hepatic artery and the bile duct[1]. Within the portal circulation, immune cells such as Stellate and Kupffer cells are present, which are involved in promoting collagen organization in the liver (Stellate cells) or in promoting the inflammatory response as macrophages of the liver (Kupffer cells)[4,5]. Cholangiocytes are responsible for forming a barrier of epithelial cells between hepatocytes and the bile duct[6]. Bile is primarily produced in hepatocytes as a product of fatty acid and carbohydrate metabolism and consists of water, lipids, bile acids, and bilirubin[7]. Cholesterol is converted in hepatocytes to bile acids to facilitate lipid adsorption during digestion[8]. After bile secretion from hepatocytes via the bile canaliculus into the bile duct, cholangiocytes modify the bile composition mainly by increasing the bicarbonate concentration in bile. Bile is further delivered to the gallbladder or duodenum by the biliary system[9]. Bile acid can also be transported from hepatocytes back to plasma and is further eliminated in the kidney by renal elimination via urine excretion. Under normal conditions, biliary excretion is the major pathway for bile acids. As end product of heme catabolism, bilirubin is conjugated in hepatocytes with glucuronic acid and subsequently excreted into plasma or bile[10]. In plasma, bilirubin is taken up again by hepatocytes. In bile, conjugated bilirubin hydrolyzes again into unconjugated bilirubin and is further processed by gut microbiota in the intestine resulting finally in excretion via the intestine. About one fifth of the unconjugated bilirubin from intestine reenters the enterohepatic circulation to be processed again by hepatocytes.

Along with its function to maintain metabolic processes related to homeostasis, the liver plays the body's key role in xenobiotic biotransformation of chemical compounds or drugs. After the initiating step of xenobiotic uptake, its biotransformation can be divided into three phases I, II, and III[2,11] (**Figure 2**). During phase I, functional groups are introduced to the molecule by oxidation, reduction, or hydrolytic processes[11]. This step is mediated by members of the cytochrome P450 superfamiliy (CYPs), other monooxigenases, oxidoreductases, or peroxidases resulting in production of more polar and reactive metabolites. Further solubilization and detoxification is achieved by conjugation of, for instance, glutathione (GSH), glucuronic acid, or acetyl groups to the reactive metabolite. Enzymes such as glutathione S-transferases, N-acetyl transferases, or UDP-glucurono-syltransferases mediate these processes termed phase II of xenobiotic metabolism[12]. Urinary or biliary excretion of metabolites during phase III is mediated by transporters such as ATP binding cassette or solute carrier (SLC) transporters[13]. Drug turn-over according to the biotransformation processes mainly takes place in pericentral hepatocytes but can be dynamically modulated by induction of the corresponding genes[2,14]. When the elimination of reactive metabolites is disturbed or drug excess leads to accumulation of reactive metabolites, toxification and resulting liver injury occurs.

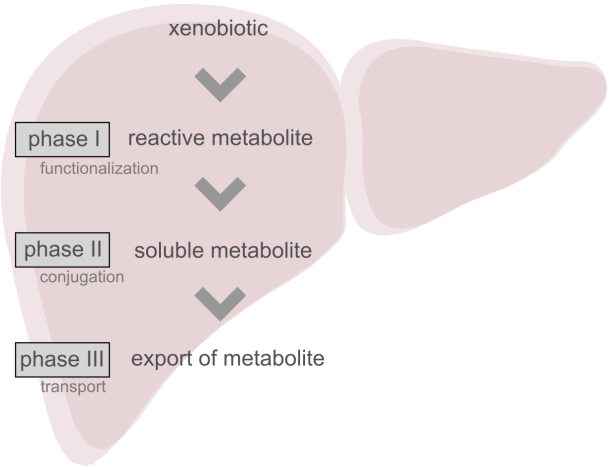

Figure 2: Biotransformation in the liver. During phase I, xenobiotics are chemically modified via various functionalization routes by hydrolysis, oxidation, or reduction mediated mainly by members of the cytochrome P450 superfamily. The resulting reactive metabolites are then conjugated in phase II with glutathione, glucuronic acid, or acetyl groups by transferases, whereby the metabolites are detoxified and their solubility is increased. Conjugated metabolites are eliminated by urinary or biliary excretion during the phase III reaction, which is enabled by transporters. Adapted and modified from Esteves *et al.*[11].

1.2 Drug-induced liver injury - DILI

Drug-induced liver injury (DILI) can be categorized in three types comprising intrinsic, idiosyncratic, and indirect DILI[15,16]. While intrinsic DILI is predictable and dose-dependent, idiosyncratic DILI occurs rarely and dose-independent. Indirect DILI was recently proposed as unintended liver injury upon drug administration, which might be a synergetic effect of underlying chronic liver or inflammatory disease[16]. Mechanistic classification of DILI is rather challenging since multiple mechanism are involved in liver injury induced by drugs. Russmann *et al.*[17] summarized the series of mechanism during liver toxification in a 3-step model (**Figure 3**). Reactive metabolites can cause direct cell stress during biotransformation in hepatocytes by binding to all forms of macromolecules including lipids, enzymes or nucleic acid or by depletion of substrates required for conjugation, e.g., glutathione. When reactive metabolites bind to enzymes of the respiratory chain of mitochondria, they can directly inhibit mitochondria leading to lack in ATP and accumulation of reactive oxygen species (ROS). Furthermore, specific immuno response can be triggered within the first step of this model by activation of cytotoxic T-cells. Reactive metabolites forming protein adducts can be presented by major histocompatibility complexes (MHC) resulting in neoantigen presentation and subsequent T-cell activation[18].
The proposed liver-injury initiating pathways lead to mitochondrial permeability transition (MPT), thus, permeability of the outer mitochondrial membrane, either by direct mitochondrial inhibition or indirectly by intrinsic or extrinsic pathways defining

the second step of DILI. Severe intracellular stress triggers activation of pro-apoptotic members of the B-cell lymphoma 2 (Bcl-2) protein family resulting in MPT[19]. Once activated, the extrinsic pathway via immune response leads to death receptor-mediated activation of MPT[20]. The immune response can be enhanced when hepatic cytokines are out of balance making hepatocytes more affected by cell death promoted by tumor necrosis factor alpha (TNFα) during immune response. When MPT is triggered, apoptosis or necrosis form the third step of this model. Depending on how fast mitotoxicity is triggered, ATP might still be available in the injured hepatocyte leading to apoptosis. If no ATP is available, hepatocytes will undergo necrosis, leading to further stimulating the immune response by cytokine secretion and neoantigen presentation via Kupffer

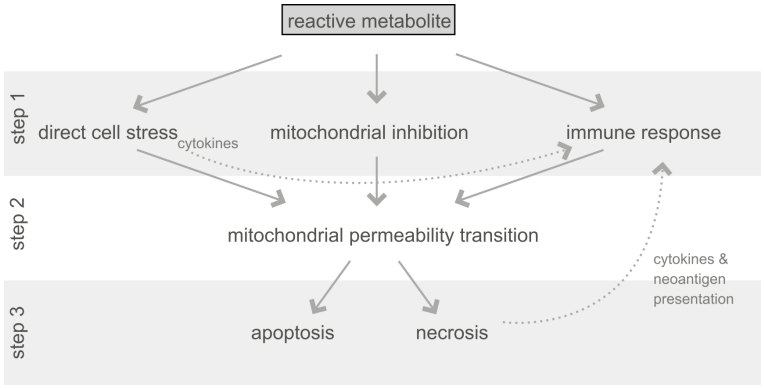

Figure 3: Mechanistic 3-step model for drug-induced liver injury. The first step of this model involves activation of at least one of multiple pathways. Reactive metabolites can induce direct cell stress by binding to macromolecules in hepatocytes, can inhibit the mitochondrial respiratory chain, or trigger specific immune response against hepatocytes. In all cases, permeability of the the outer mitochondrial membrane is induced in a second step termed mitochondrial permeability transition (MPT). Initiation of MPT leads to apoptosis or necrosis, depending on if enough ATP is prevalent to move towards apoptosis. Hepatocytes with cytokine production out of balance may enhance the reaction during immune response. Necrotic cells lead to further activation of the immuno response by release of pro-inflammatory cytokine or neoantigen presentation after their uptake by Kupffer cells. Adapted and modified from Russmann *et al.*[17].

cells, which are involved in clearance of necrotic hepatocytes. Idiosyncratic DILI is considered to be more represented by the immune response pathway[21] since genetic variability in human leukocyte antigen (HLA) was linked to adverse reactions during hepatotoxicity[22,23]. However, their use for DILI prediction remains under question since HLA gene sequencing is not applied before general drug administration in clinics. Prediction of DILI is still challenging since the mechanisms for DILI are versatile and may mimic acute or chronic liver disease. Over the past years, DILI was recognized as the major cause for acute liver failure (ALF) at least in western countries[24,25]. About 11% of ALF cases were determined as idiosyncratic DILI cases in the USA within the year 2013[24]. Furthermore, more than 30% of the drug withdrawals between 1975 and 2007 accounted for DILI making it one of the major reasons for failure in drug

development[26]. Diverse animal models are used for preclinial investigation of DILI including rat, mouse, cat, and dog animal models[27]. However, translational value between human patients and animal models remains challenging due to differences in proteins across species causing, e.g., altered drug turn-over rates, changed protein binding capability during xenobiotic biotransformation, or differential CYP expression due to carnivore or herbivore diet[27,28].

1.2.1 Effects of DILI-related drugs or compounds on the liver

The high percentage in DILI cases for ALF cannot only be caused by idiosyncratic DILI, therefore translatability of intrinsic DILI from clinic to preclinial animal models and *vice versa* is still valuable to improve drug development. Several compounds and drugs are known to cause DILI of which the mechanism is by far best understood for acetaminophen (APAP), commonly known as paracetamol. APAP or paracetamol can be freely purchased on the market and is used as analgesic with a maximum dosage of 4 g per day for adults[29]. Due its dose-dependent hepatotoxic effect, APAP is in particular useful to investigate intrinsic DILI. The conversion of APAP to the reactive metabolite N-acetyl-p-benzoquinone imine (NAPQI) is catalyzed by P450 cytochrome enzymes and conjugated with GSH[30]. In excessive doses of APAP, GSH is depleted and reactive NAPQI is not metabolized rapidly enough. NAPQI then binds especially mitochondrial proteins[31], e.g., by binding to complex I/II of mitochondrial electron transport chain, ultimately producing more oxidative stress by H_2O_2 production, which promotes further GSH depletion[32]. As a result, mitochondrial membrane potential is lost and hepatocytes undergo necrosis as mode in cell death[33]. This manifests as hepatitis with impaired liver functionality due to damaged hepatocytes. Rapidly dying hepatocytes can then result in total liver failure.
Carbon tetrachloride (CCl_4) is another cell stress-inducing compound with a reactive metabolite produced during biotransformation causing hepatocellular damage. CYPs convert CCl_4 to the trichloromethyl radical $CCl_3^{\bullet}$, which can bind to proteins, lipids, or nucleic acid producing oxidative stress in hepatocytes followed by cell death and subsequent inflammation[34]. Furthermore, CCl_4 mediates liver fibrosis by activation of hepatic stellate cells (HSCs) via released cytokines as key players during hepatic cell death, which is induced by $CCl_3^{\bullet}$[35,36]. Activated HSCs transdifferentiate to myofibroblasts which are responsible for production of extracellular matrix (ECM) proteins such as type-I collagen[37]. Excessive HSC activation leads to excessive ECM production resulting in impaired liver function, which is termed liver fibrosis[38]. Chronic liver fibrosis can turn into irreversible scarring of the liver structure by impaired blood flow, which is then termed cirrhosis. Overexposure to $CCl_3^{\bullet}$ can lead to hepatocellular carcinoma because of its binding to nucleic acid thereby inducing mutagenesis. Based on this carcinogen feature and its role in ozone depletion, its former use as organic solvent or precursors for refrigerants is not pursued anymore[39].

Acute toxicity can be investigated by the organic compound 4,4'-methylene dianiline (DAPM), which is used in polymer chemistry for industrial production of polyurethan foams[40]. It was found to induce biliary injury by damaging epithelial cells of the bile duct[41]. Hereby, the bile flow is impaired and bile acids accumulate in hepatocytes and systemic circulation by increased levels in enterohepatic circulation instead of biliary excretion manifesting as cholestatic liver disease (cholestasis)[9]. Chronic cholestasis can lead to fibrosis followed by cirrhosis and ultimately leading to liver failure. Under non-chronic conditions, hepatocytes undergo transdifferentiation into biliary epithelial cells for recovery from DAPM-induced damage[42].
Initially used as fruit preservative and fungicide, thioacetamide was early recognized as hepatotoxicant[43]. Thioacetamide is metabolized by CYPs by a 2-step mechanism to thioacetamide sulfoxide followed by production of the reactive metabolite thioacetamide sulfdioxide. Subsequently to binding hepatocellular macromolecules, the liver cells undergo hepatic apoptosis and necrosis and thioacetamide was shown to induce liver fibrosis[44,45]. Bromobenzene is used as additive to motor oils and industrial solvent and is known for hepatotoxic effects due to formation of bromobenzene 3,4-epoxide as reactive metabolite during biotransformation[46,47]. Hepatocellular damage is induced by GSH depletion, followed by increased oxidative stress resulting in hepatocyte necrosis[48].
In general, antibiotics and anti-inflammatory analgesic drugs are highly associated with DILI with amoxicillin-clavulanate and ximelagatran as prominent examples with known DILI cases[15,49]. DILI remains one of the main reasons for drug withdrawals from the market. Since DILI phenotypes can cover cell death of hepatocytes, inflammation, fibrosis, or cholestasis and histopathologic evaluation is not sufficient for specific DILI indication[50], biomarkers improving DILI diagnosis are required.

1.2.2 Current and potential DILI biomarkers

The current gold standard for DILI assessment is provided by measurement of alanine amino transferase (ALT), aspartate aminotransferase (AST), alkaline phosphatase (ALP), total bilirubin (TBIL) and application of Hy's law[21]. ALT is responsible for L-alanine conversion to α-ketoglutarate conversion during gluconeogenesis in hepatic mitochondria and its *vice versa* reaction during glycolysis in muscle tissue[51]. Its prevalence in liver is highest followed by kidney or other tissue such as muscle or heart in humans. Accordingly, AST catalyzes the transamination between L-aspartate to α-ketoglutarate. However, AST is more widely expressed than ALT in other tissues such as kidney, muscle, or heart. ALP includes enzymes, which hydrolyze phosphate esthers at alkaline pH in a variety of metabolic functions such as bone mineralization or bile modification, as such expressed predominantly in bone marrow and in epithelial cells of the bile duct[52,53]. Hence, elevated ALP represents a marker for cholestasis, when the bile duct flow is impaired. However, elevated ALP levels were associated with pregnancy or metastatic cancer and were demonstrated to be age-dependent[53,54]. The sum

of conjugated and unconjugated bilirubin, which is represented by TBIL, can serve as marker for impaired liver function since bilirubin uptake in hepatocytes and bilirubin elimination via biliary excretion are impaired, thus, serum levels of total bilirubin are increased[10].
All of the presented markers can be elevated in hepatic damage events other than DILI such as muscle impairement, metastatic cancer, alcoholic liver disease, or bone disease. Furthermore, ALT levels may reflect hepatocellular injury well, but they are also increased after treatment with heparins or statins[55,56]. Taken together, these markers are not specific for DILI. Dr. Hyman Zimmerman found that between 10% and 50% of patients were affected with liver transplant or death during DILI, when the following criteria where met, summarized as "Hy's law" for DILI prognosis[57]. When ALT or AST levels are higher then 3-fold of the upper limit of normal (ALT or AST $>$ 3 x ULN) and jaundice and / or elevated levels of serum TBIL (TBIL $>$ 2 x ULN) are diagnosed, then the drug under investigation induces hepatocelluar injury. This applies when cholestatic injury can be excluded by ALP measurement with ALP $<$ 2 x ULN and when other interfering diseases such as viral hepatitis, alcoholic liver disease, or bone disease can be excluded for the investigated subject. Hy's law currently serves as the best clinical model to predict severe DILI although specificity is low. Hy's law is generally accepted as basic rule to classify DILI and was extended resulting in the following classification criteria[21,58] (**Table 1**). The R factor was introduced by Aithal *et al.*[58] to differentiate drug-induced hepatocellular, cholestatic, and mixed liver injury by dividing the measured ALT value with the measured ALP value. Hepatocellular liver injury is met when Hy's law regarding ALT, AST and TBIL is fulfilled or when R is ≥ 5. Cholestatic liver injury can be expected when ALP values are $>$ 2 x ULN or R $\leq$ 2. Hepatocellular injury mixed with cholestatic injury can be expected when R is between 2 and 5. However, determination of ULN remains challenging for global clinical DILI studies since reference values were determined country-wise[59]. Clinical studies rely on ALT, AST, ALP, and TBIL measurement before start of the study to account for the right ULN values. Still, the lack in specificity and prediction value for adverse DILI remains low.

Table 1: Classification for drug-induced liver injury (DILI). R = ALT / ALP

Hepatocellular DILI	**Cholestatic DILI**	**Mixed DILI**
ALT or AST $>$ 3 x ULN and TBIL $>$ 2 x ULN or R $\geq$ 5	ALP $>$ 2 x ULN or R $\leq$ 2	2 $<$ R $<$ 5

Emerging potential DILI biomarkers with higher specificity and predictive value have been proposed from investigations of human DILI studies[21,60]. These potential biomarkers include proteins from apoptotic and necrotic processes as well as from immune re-

sponse. The proteins glutamate dehydrogenase (GLDH), high-mobility group protein B1 (HMGB1), and keratin 18 (K18) are considered to be released in circulation during hepatocellular necrosis, while caspase-cleaved keratin 18 (ccK18) is released during apoptosis[21] (**Figure 4**). Together, their assessment may serve for early damage detection induced by DILI. Macrophage colony stimulating factor 1 receptor (MCSF1R) and osteopontin (OPN) are involved in activation of innate immune cells triggered by necrosis.

GLDH is especially expressed in mitochondria of pericentral-located hepatocytes due to its function in amino acid oxidation und the urea cycle by catalyzing the reaction between L-glutamate and α-ketoglutarate[61]. Similarly to ALT, lower levels of GLDH can be found in other tissue such as brain and kidney[62]. Clinical studies with patients exhibiting APAP-induced liver injury showed, that GLDH and ALT levels in serum at least showed comparable DILI diagnosis value or that GLDH even outperforms ALT[60,63]. Patients with underlying muscle damage showed elevated ALT levels in otherwise healthy subjects and in subjects with liver injury, whereas GLDH was only elevated in serum of patients with liver injury[63,64]. GLDH levels were not affected by the underlying muscle injury in subjects without liver injury.

Intracellular HMGB1 acts as nuclear DNA-binding factor and regulates transcription by structural bending of DNA. HMGB1 comprises two nuclear localization sequences, which are masked when acetylated, in turn, leading to secretion of HMGB1 into extracellular matrix[65,66]. Secreted HMGB1 acts as cytokine promoting macrophage activation including HSCs and Kupffer cells[67]. When released from necrotic cells, HMGB1 promotes innate immune response by acting as damage-associated molecular pattern (DAPM). HMGB1 was associated with acute liver disease and fibrosis in human studies and animal model[67].

Clusters of the protein K18 form the intermediate filament in single-layered epithelial cells and is predominantly expressed in inner organs[68]. Despite its prevalence in other organs such as kidney, K18 was demonstrated as predictive marker for adverse DILI outcome including death or liver transplant[69]. MicroRNA-122 (miR-122), a small, non-coding RNA expressed specifically in hepatocytes, was also found with predictive value in the same study. However, large inter- and intra-individual variability of miR-122 levels was demonstrated among serum samples of healthy volunteers[60]. Release of the fragment ccK18 is a result of intermediate filament fragmentation mediated by caspase-3 during apoptosis. Together with K18, ccK18 forms the "apoptotic index" where levels of ccK18 and K18 are divided to account for keratin released rather by apoptosis than by necrosis. The apoptotic index might be used to diagnose more severe injury, which is reflected by apoptosis[70]. However, background differences across various kits for K18 and ccK18 measurement impair its predictive value[60].

OPN is a multifunctional protein involved in bone remodeling by serving as structural protein[71] and is involved in processes of the immune system. OPN promotes immune cell infiltration in the liver by acting as cytokine[72]. It is expressed and secreted from

macrophages and T-cell and further activates macrophages by binding to integrins and the CD44 hyaluronic acid receptor[73]. The predictive value of OPN measurement for potential adverse DILI outcome was demonstrated in a clinical study with DILI patients[60].
MCSF1R is a tyrosine kinase receptor specific to macrophages and was observed in plasma samples of patients treated with ximelagatran[74]. Thereby, receptor shedding after macrophage activation was hypothesized as reason for finding MCSF1R in this body fluid. A predictive value for DILI with fatal outcome was attributed to elevated MCSF1R levels in patients of clinical studies[60]. Interestingly, MCSF1R was shown elevated in flupirtine treated patients compared to MCSF1R levels in plasma of patients with APAP-induced hepatotoxicity presenting MCSF1R as potential marker for idiosyncratic DILI. K18, HMGB1, OPN, and MCSF1R are supported by the United States Food and Drug Administration (FDA) for further investigation and exploratory use of these proteins as DILI biomarkers[75]. GLDH entered recently the biomarker qualification program for DILI due to its superiority in specific DILI diagnosis for patients with underlying muscle impairment compared to ALT as biomarker[64,76].

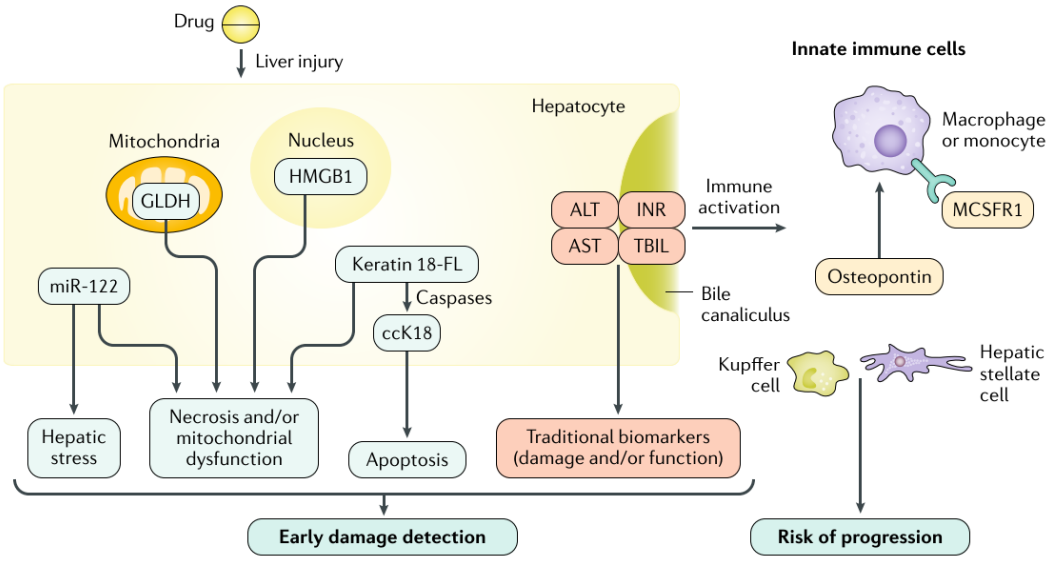

Figure 4: Current and potential biomarkers of DILI. Current DILI diagnosis is performed by the combined analysis of alanine aminotransferase (ALT), aspartate aminotransferase (AST), and total bilirubin levels (TBIL) as international normalized ratio (INR) to classify and predict DILI. MicroRNA (miR-122), a hepatocyte-specific non-coding RNA, was shown to specificly indicate hepatic stress, but was later abandoned as supported biomarker due to high inter-variability between healthy volunteers. Glutamate dehydrogenase (GLDH), high-mobility group protein B1 (HMGB1), and keratin 18 (K18) are released during necrosis, while caspase-cleaved keratin 18 shows apoptotic hepatocyte death, together considered as early damage detection for DILI. Immune activation mediated by activated macrophages via osteopontin (OPN) and macrophage colony stimulating factor 1 receptor (MCSF1R) might be assessed for prediction of adverse DILI outcome, ultimately serving as factors to determine the risk in DILI progression. Taken from Andrade *et al.*[21].

1.3 Mass spectrometry for protein analysis

Proteins serve multiple functions ranging from structure formation and enzymatic conversion of substrate to signal transfer as cytokines within cells, tissue or body fluids. The entity of all proteins within the subject of investigation was termed proteome[77] and its analysis is part of the research field of proteomics. Over the past two decades, mass spectrometry (MS) emerged as tool for protein analysis with regard to complex protein profiling[78], post-translational modifications (PTMs)[79], and protein interaction studies[80,81]. One strategy in form of top-down proteomics is to analyze intact proteins by direct injection into mass spectrometers and investigating the entire protein's mass and its fragments[82]. While this approach enables the investigation of proteins of even more than 100 kDa and especially facilitates analysis of the entire protein sequence and PTMs, top-down proteomics is mainly limited to purified proteins or low complex protein mixtures. In contrast, bottom-up proteomics provides the advantage to analyze highly complexe mixtures by identification of numerous proteins on the basis of their unique peptides[83]. Within this commonly used protein profiling technique, proteins are fragmented into peptides by proteolysis. The most commonly used protease is trypsin, which cleaves proteins usually after lysine or arginine generating 10 to 20 amino acid long peptide fragments[84]. The peptide mixture is analyzed using liquid chromatography coupled to mass spectrometry (LC-MS). Peptides are subjected to tandem MS and the resulting fragment spectra are matched to theoretical spectra for identification. By read-out of the mass-to-charge ratio (m/z) of proteotypic peptides, which are unique in their composition of amino acids, proteins can be identified by their corresponding unique peptide[85]. Thereby, the proteome can be studied in non-targeted approach to study complex interaction networks or in targeted approach by focusing on a subset of proteins to elucidate their function or to quantify them in a highly sensitive and selective manner.

1.3.1 Targeted and non-targeted proteomics

Both targeted and non-targeted proteomics have their value in studying the proteome of organisms. Non-targeted proteomics is in particular useful to build knowledge on whole metabolic or signaling pathways and functions of proteins within these pathways. Shotgun proteomics can be used hereby to monitor as many as possible peptides from a proteolyzed sample mixture. The peptides are monitored in form of precursor ions (MS1) with the mass analyzer of a high performance mass spectrometer und subsequent fragmentation of these precursors into ion fragments, which are termed transitions (MS2 or MS/MS)[83] (**Figure 5A**). The acquired fragment spectra with the respective transition intensities are then matched against spectra from corresponding *in silico* databases to identify unique peptides representing the identified proteins. Over the recent years, advances in prefractionation of peptides by liquid chromatography coupled to a mass spectrometer enabled identification of over 16,000 proteins in mammalian

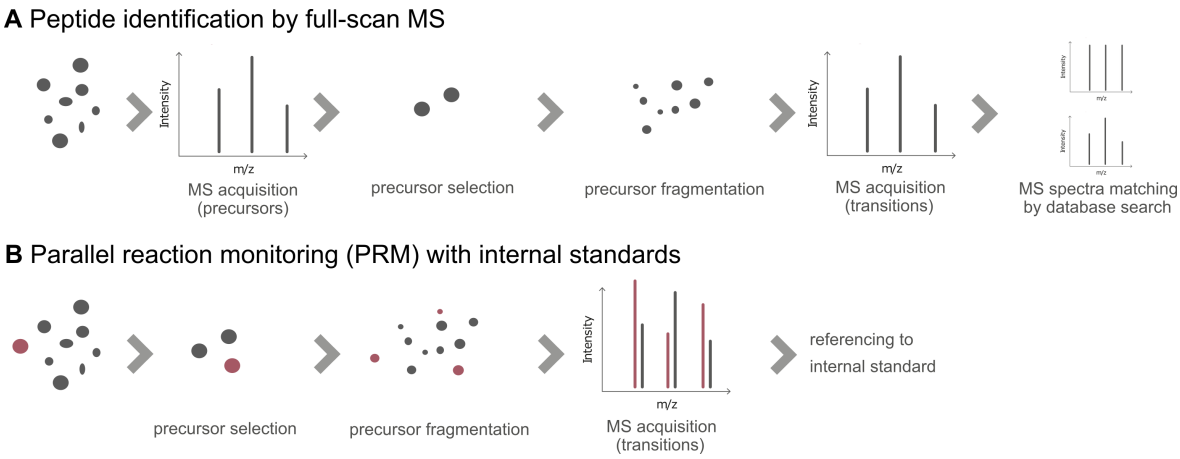

Figure 5: Peptide identification via full-scan MS and parallel reaction monitoring (PRM). **(A)** MS spectra of precursor ions are monitored and precursors are selected for fragmentation. MS spectra of the resulting transitions are recorded and identified during database search by matching to *in silico* MS spectra. **(B)** Precursors of target peptides and their corresponding internal stable isotope-labeled standard peptide (red) are selected for fragmentation during parallel reaction monitoring (PRM). MS spectra of the resulting transitions are recorded and compared between target and reference peptide for identification and quantification.

tissue by this approach[86]. This technique is summarized as liquid chromatography tandem mass spectrometry (LC-MS/MS) including precursor and transition monitoring with several coupled mass analyzers in a mass spectrometer. Reproducible peptide measurement with this method based on data-dependent acquisition (DDA) is rather limited since it is driven by stochastic prevalence of peptides due to the selection of precursor ions starting with the most intense ions in a sample. In contrast, all precursors within a defined m/z range can be selected for simultaneous fragmentation with the more recently introduced MS technique termed data-independet acquisition (DIA)[87]. Since all precursors are fragmented within this method, the resulting MS2 spectra are highly complex and require complex data processing including matching against spectral libraries acquired in preceeding DDA measurements. This method is termed SWATH MS when synthetic peptides are used to build a spectral library in preceeding targeted LC-MS/MS measurements[88]. More reproducible protein identification within each measurement run is better provided by targeted proteomics. In contrast to monitoring as much peptides as possible as in shotgun proteomics, targeted proteomics involves selection of a subset of peptides for MS read-out. This has the advantage of measuring the peptides of interest within each run regardless of the prevalence of other peptides. One prominent method for targeting peptides is parallel reaction monitoring (PRM). A pre-specified set of precursor ions is determined with an inclusion list to direct the mass spectrometer towards selection of these precursors (**Figure 5B**). Once the precursor with the correct m/z is selected, this precursor is fragmented in the mass spectrometer and all available transitions (MS/MS) are monitored[89]. By addition of

stable isotope-labeled reference peptides as internal standards, identification of unique peptides is provided with high confidence. Compared to other targeted methods in proteomics such as selected reaction monitoring (SRM), where transitions are determined *a priori* and measured one by one, PRM enables simultaneous monitoring of all possible transitions[89,90]. Changes in transitions across matrices, thus, their influence on peptide quantification, can be monitored easier by PRM with less method development[89,91].

1.3.2 Instrumentation

In targeted as well as in non-targeted proteomics, peptide mixtures of proteolyzed samples are separated by liquid chromatography based on their hydrophobicity using reversed-phase chromatography by ultra-high performance liquid chromatography (UHPLC) instruments in nanoflow mode[92,93]. Online coupling of LC systems to their respective mass spectrometers is commonly enabled by electrospray ionization (ESI)[94]. Hereby, charged peptides are ionized under high voltage and their transfer from liquid to gas phase is induced. After entering the mass spectrometer, these precursor ions are focused by electronic lenses and prefiltered through an inject flatapole and an active beam guide into a quadrupole as presented by Scheltema *et al.*[95] (**Figure 6A**).
Within the quadrupole, precursor ions can be filtered by their m/z ratio and sent to the HCD cell, where the ions are fragmented, for instance by higher-energy collisional dissociation[96] (HCD). Peptides are fragmented via HCD by mainly breaking the amide bonds between amino acids resulting in C-terminal y-ions and N-terminal b-ions[97] (**Figure 6B**). When fragments are monitored which overlap in their amino acid sequence, the exact amino acid sequence can be deduced from the corresponding mass difference. Peptide fragments are bundled in the C-trap and further injected in the orbitrap mass analyzer and mass spectra are recorded (**Figure 6A**). The monitored intensity of the transitions can be used for quantification via PRM, while either transitions or precursor ions can be used for quantification via full-scan MS.

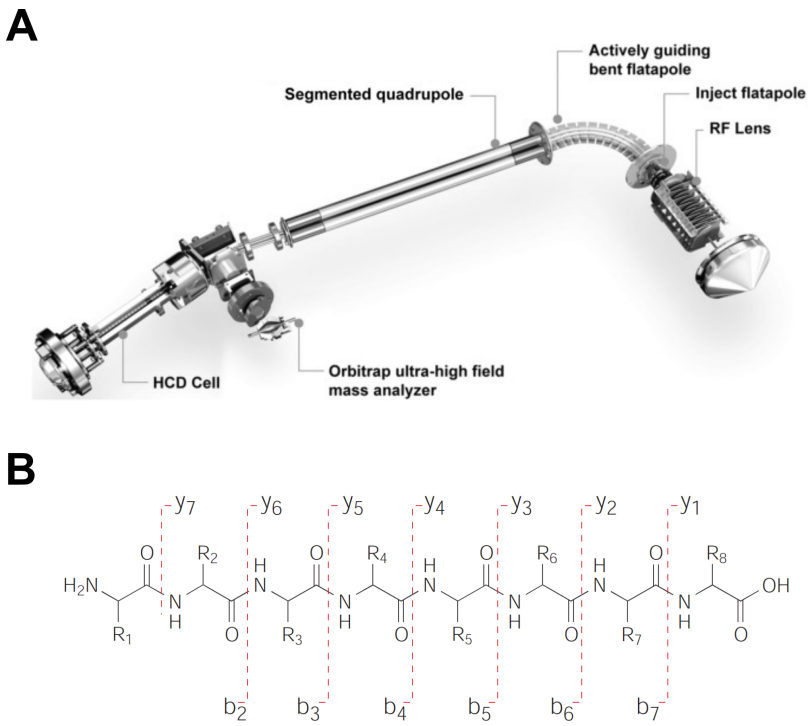

Figure 6: Overview of mass spectrometer instrumentation and peptide fragmentation. **(A)** After entering the mass spectrometer, precursor ions are focused by electronic lenses and pre-filtered by an inject flatapole and a guiding bent flatapole. Precursor filtering is performed in the quadrupole and fragmentation is induced in the HCD cell by higher-energy collisional dissociation (HCD) when a MS/MS event is triggered. Mass spectra of precursors (MS1) and transitions (MS/MS or MS2) are recorded in the orbitrap mass analyzer. **(B)** Peptides are commonly fragmented by breaking the amide bond between adjacent amino acids during the HCD process. Adapted from Scheltema *et al.*[95] and Steen & Mann[97]

1.3.3 Plasma proteomics

One major obstacle of non-targeted bottom-up proteomics is the limited sensitivity either when mixtures are highly complex, thus, comprising numerous peptides that require fast and precise data acquisition via MS, or when samples have an enormous dynamic range of up to 10^{11} in protein concentration as it is for plasma or serum specimen[98](**Figure 7**). Functional proteins such as albumin, which is responsible for maintaining homeostasis in blood, or immunglobulins (IgGs) are highly abundant making it more complicated to assess tissue leakage or signaling proteins within the lower ng/mL or pg/mL range of blood specimen. Peptides of such high abundant proteins may mask low abundant peptides since common orbitrap mass analyzers reach only a dynamic range of about 5,000 due to limitations in number of analyzed ions per run[99]. Depletion techniques utilizing immunoprecipitation with antibodies against abundant proteins[100] are quantitatively not reliable for low abundant proteins[101] and plasma fractionation for deep plasma proteomics[102] is work-intensive making it less accessible

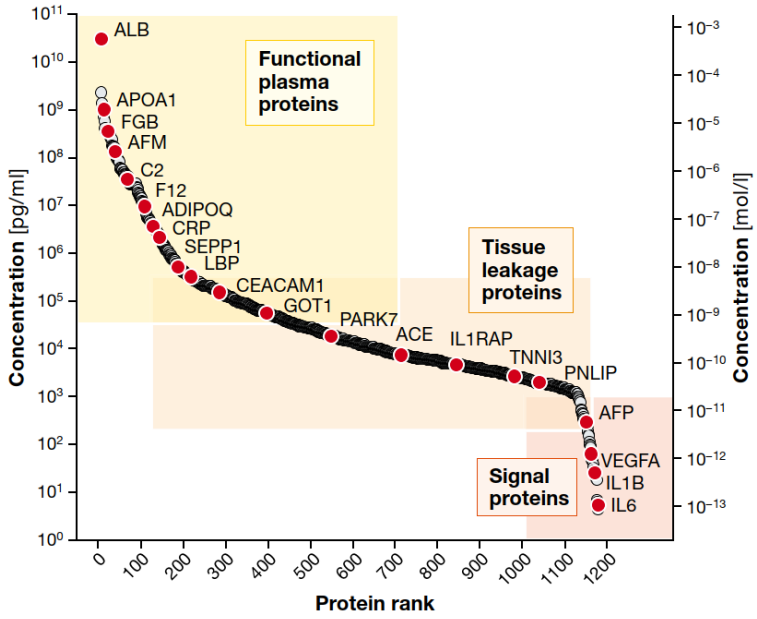

Figure 7: Dynamic range of the plasma proteome. Protein concentration ranges over several orders of magnitude (10^{11}) in plasma with high abundant functional proteins, tissue leakage proteins in the lower ng/mL range and signal proteins in the lower pg/mL range. Taken from Geyer *et al.*[98]

for high-throughput plasma proteome profiling. Apart from LC-MS-based read-out, plasma is commonly investigated using sandwich immunoassays by capturing plasma proteins with two antibodies and colorimetric analysis summarized as enzyme-linked immunosorbent assays (ELISAs)[103–105]. The target protein is bound at two sites by a solid-phase coupled capture antibody and a detection antibody. Commonly, horseradish peroxidase is coupled to the detection antibody, which converts its chromogenic substrate, if the target protein is present in the sample of interest and is bound between both antibodies. The converted substrate is then measured colorimetrically, e.g., using a photometer. This method is easily accessible but struggles for example with lack of concordance across different kits, physiologically present autoantibodies, and with cross reactivity to other proteins[106,107]. Combining peptide-tageted antibody enrichment with LC-MS/MS measurement enables highly selective and sensitive identification of proteins of interest based on their unique peptides. This peptide-targeted approach is termed stable isotope standards and capture by anti-peptide antibodies (SISCAPA)[108]. As part of the field of immunoaffinity liquid chromatography tandem mass spectrometry (IA-LC-MS/MS)[109], this method combines the sensitivity of immunoassays with highly selective read-out by mass spectrometry. Thyroglobulin, a tumor marker for thyroid carcinoma which is known for difficult quantification due to the presence of autoantibodies in serum, could be detected with this approach with a detection limit of 2.6 ng/mL[110]. Group-specific antibodies can be used to maximize the number of peptides enriched per antibody known as concept of triple X proteomics (TXP)[111–113]. Hereby, peptides with the same short C-terminal peptide sequence are enriched with

one antibody and the peptides of interest are monitored by mass spectrometry. However, the high protein content and potential non-specific antibody binding still make plasma and serum difficult body fluids to study.

1.4 Accurate quantification & validation

1.4.1 Quantification strategies

Robust plasma protein quantification remains challenging and accurate protein quantification strategies are required. LC-MS provides several approaches for quantitative protein analysis including label-free methods and methods relying on sample labeling or addition of stable isotope-labeled standards. Label-free protein quantification can be used for relative quantification of peptides on the precursor level[114] or by counting fragment spectra[115]. Quantification on the precursor level involves normalization of the measured precursor intensity to the total measured peptide intensity in a MS run, thereby generating normalized label-free quantification (LFQ) intensities. The LFQ intensities of peptides eluting at the same time between different runs can then be compared. However, label-free quantification does not account for variability in sample preparation, differences in total peptide intensity introduced by sample fractionation, or use of different software[116]. Therefore, the use of stable-isotope labels is preferred for accurate peptide quantification. When comparing different sample conditions in cell culture, stable isotope-labeling with amino acids in cell culture (SILAC) is the method of choice by introducing isotopically labeled amino acids via the cell growth medium in the conditions to be compared[117,118]. By use of either isotope-labeled lysine or arginine, three conditions can be compared in total[119]. Samples can be mixed after harvesting, processed and peptide intensities obtained from the LC-MS/MS measurements are then compared, thus, studying the relative abundance of proteins. Similarly, proteins can be chemically labeled by dimethyl labeling[120], samples can be mixed and set in relation by comparing precursor intensities of non-labeled and labeled peptides.
Up to 10 conditions or samples can be multiplexed in one MS run by isobaric labeling of peptides after proteolysis using isobaric tags for relative and absolute quantification (iTRAQ) or tandem mass tags (TMT)[121,122]. Thereby, peptides can be distinguished on their MS2 level by different reporter ions released during fragmentation, hence, resulting in fragments with different m/z ratios. Isobaric labeling is a widely used method to quantify peptides on their MS2 level in deep proteome profiling[86,123]. In summary, the presented methods enable quantification of proteins in proteome-wide investigations using LC-MS, while confident analyte identification and quantification in targeted proteomics is provided by addition of stable isotope-labeled standards (SIS) as strategy for absolute quantification (AQUA) presented by Gerber *et al.*[124]. Known amounts of synthetic isotope-labeled peptides are thereby added as internal standards to the samples of interest. Endogenous peptides and their corresponding peptide ana-

log elute at the same time within the LC system and the peptide intensity ratios are formed to normalize against the intensity of the internal standard. When antibodies are used for enrichment of endogenous and synthetic peptides, this approach resembles common protein quantification methods such as sandwich immunoassays in form of ELISAs best. In both approaches, analytes in unknown samples are enriched by antibodies and quantified based on calibration curves of known analyte material either in form of proteins (ELISA) or peptides (SISCAPA as part of IA-LC-MS/MS).

1.4.2 Validation strategies

Moving from biomarker identification towards biomarker validation for confident and reliable protein quantification for clinically relevant proteins as biomarkers is considered as the next step in clinical proteomics[125]. Analytical method validation is generally recommended by institutions represented by the FDA and the European Medicines Agency (EMA)[126,127]. Parameters for analytical method validation comprise and are not limited to the assessment of accuracy and precision of calibration curves and quality control samples, effect of sample dilution in substitute matrix (parallelism), and reproducibility of sample measurement[126–128]. Accuracy is determined by how close the measured value represents the theoretically aimed value, whereas precision describes the agreement between several independent measurements represented by the coefficient of variation (CV) in percent. Furthermore, analytical methods should be tested for their upper and lower limits of calibration (ULOQ, LLOQ), matrix effects and sample and reagent stability should be investigated. Ideally, analytes in unknown samples should be measured within the calibration range combined with evaluation of quality control samples within each run to increase the confidence of protein quantification for the corresponding assay.

2 Aims of the thesis

The main aim of this thesis was to further elucidate the potential of emerging new protein biomarkers to evaluate drug-induced liver injury (DILI). Candidate biomarkers were found to exceed the potential of the current DILI marker alanine aminotransferase (ALT) for diagnosis or even prediction of DILI in human DILI studies[60]. Hereby, the performance of these candidate biomarkers in combination is fairly little examined in preclinical studies with animals such as rats. Hence, the impact of known liver injury inducing agents on a subset of these biomarkers was aimed to investigate in preclinical studies with rats including acetaminophen (APAP), 4,4'-methylene dianiline (DAPM), thioacetamide, bromobenzene, and carbon tetrachloride (CCl_4). To enable accurate quantification of these biomarkers, method development was required to determine OPN, MCSF1R, GLDH, HMGB1, K18, and ccK18 protein concentration in serum or plasma. Biofluids such as serum or plasma are widely used to investigate the stated biomarkers but there is growing concern whether some of them can be compared across studies based on different sample matrices[129–131]. Thus, preanalytical effects such as matrix or sampling effects during serum and plasma production were of interest within this thesis. Immunoaffinity liquid chromatography tandem mass spectrometry (IA-LC-MS/MS) was employed to enrich unique peptides of the proteins of interest with antibodies and to measure these proteins highly specific by mass spectrometry in peptide-targeted mode. The following objectives were established on the basis of the stated aims:

1. Method development for DILI-related protein quantification using IA-LC-MS/MS
   - 1.1. Optimization of the IA-LC-MS/MS method for quantification of potential DILI biomarkers in human and rat specimen regarding peptide and antibody features.
   - 1.2. Investigation on the impact of trypsin on peptide release and recovery.
   - 1.3. Comparison of MCSF1R rat protein variants based on their amino acid sequence.
   - 1.4. Partial method validation of DILI-related protein quantification in rat plasma and liver tissue.

2. Study of preanalytical matrix and sampling effects in human serum and plasma specimen regarding DILI biomarker quantification
   - 2.1. Examination of differences between matrices such as EDTA plasma and two commonly types of serum collection tubes (with gel and without gel) regarding candidate DILI biomarkers.

2.2. Identification of time-dependent changes in DILI biomarker concentration during benchtop incubation between sample collection and centrifugation.

2.3. Comparison between the IA-LC-MS/MS method and sandwich immunoassays or enzymatic assays for DILI-related protein quantification.

3. Study of translational protein biomarkers for DILI investigation in preclinical studies including rat animal models

3.1. Analysis of candidate DILI protein biomarkers in EDTA plasma of rats treated with APAP, DAPM, thioacetamide, bromobenzene, and CCl_4.

3.2. Analysis of candidate DILI protein biomarkers in liver tissue of rats treated with APAP and DAPM.

3.3. Comparison of DILI protein biomarker content in various rat tissues to evaluate their tissue specificity.

3 Material and Methods

3.1 Material

All reagents were prepared in demineralized water if not specified otherwise. Components for UHPLC buffers were purchased in LC-MS grade quality.

3.1.1 Consumables

Table 2: Consumables

Consumable	**Manufacturer**
0.2 mL PCR reaction vessels 8-tube strips	Eppendorf, Hamburg, Germany
0.2 mL Skirted 96-well robotic PCR plate	Thermo Fisher Scientific, Waltham, USA
1.5 mL reaction vessel	Eppendorf, Hamburg, Germany
15 mL PP reaction vessel	Greiner Bio-One, Frickenhausen, Germany
50 mL PP reaction vessel	Greiner Bio-One, Frickenhausen, Germany
96 PLATE+ GL 7MM RD V 220UL PP, glass-coated plates	Thermo Fisher Scientific, Waltham, USA
Acclaim PepMap100 C18 µ-precolumn, 0.3 mm, I.D. x 5 mm, 5 µm	Thermo Fisher Scientific, Waltham, USA
Acclaim PepMap RSLC C18, 75 µm I.D. x 150 mm, 2 µm	Thermo Fisher Scientific, Waltham, USA
Axygen AxySeal sealing film	Corning, New York, USA
BD Vacutainer® serum and plasma tubes	BD, Franklin Lakes, USA
DURAN Laboratory bottle with DIN thread, GL 45, 250 mL; 500 mL, 1000 mL	Duran Group GmbH, Wertheim/Mainz, Germany
epT.I.P.S. Standard 0.5 - 20 µL	Eppendorf, Hamburg, Germany
epT.I.P.S. Standard 100 - 5000	Eppendorf, Hamburg, Germany
epT.I.P.S. Standard 2 - 200 µL	Eppendorf, Hamburg, Germany
epT.I.P.S. Standard 50 - 1000 µL	Eppendorf, Hamburg, Germany
Micro Amp 8-CAP Strip	Thermo Fisher Scientific, Waltham, USA
KingFisher™ 96 tip comb	Thermo Fisher Scientific, Waltham, USA
Micro insert, clear glass, 15 mm opening	VWR, Radnor, USA
Micromat CLR, 96 RD flat, clear silicone	Thermo Fisher Scientific, Waltham, USA
Microtiter plate, 96 well, PS, F-Bottom, clear	Greiner Bio-One, Frickenhausen, Germany
Nitrile gloves	VWR, Radnor, USA
pH indicator paper range 1-14	Carl Roth, Karlsruhe, Germany
Pierce™ Protein G Magnetic Beads	Thermo Fisher Scientific, Waltham, USA
Pipette tips GPS LTS 20 µL	Mettler Toledo, Columbus, USA

Consumable	Manufacturer
Pipette tips GPS LTS 250 µL	Mettler Toledo, Columbus, USA
Pipette tips GPS LTS 300 µL	Mettler Toledo, Columbus, USA
Pipette tips GPS LTS 300 µL	Mettler Toledo, Columbus, USA
Steel balls	Qiagen, Düsseldorf, Germany
Sterile filter, 0.2 µm	Sarstedt, Nümbrecht, Germany
Syringe, 30 mL	B. Braun, Melsungen, Germany
Screw caps, 9 mm, natural rubber red-orange	VWR, Radnor, USA
Vial short thread, 1.5 mL, amber glass with label	VWR, Radnor, USA
Viper Inline Filter	Thermo Fisher Scientific, Waltham, USA

3.1.2 Chemicals and reagents

Table 3: Chemicals and reagents

Substance	Manufacturer
3-[(3-Cholamidopropyl) dimethylammonio]-1-propanesulfonate (CHAPS)	Carl Roth, Karlsruhe, Germany
Acetic acid (HAc)	Carl Roth, Karlsruhe, Germany
Acetonitrile (ACN), ultrapure LC-MS grade	WICOM
Ammonia solution 25%, Rotipuran	Carl Roth, Karlsruhe, Germany
Ammonium bicarbonate (ABC) Sigma-Aldrich, St. Louis, USA Albumin fraction V, protease-free, for matrix preparation (BSA)	Carl Roth, Karlsruhe, Germany
Calcium chloride dihydrate	Carl Roth, Karlsruhe, Germany
Custom-made polyclonal antibody sera	Pineda GmbH, Berlin, Germany
Custom-made monoclonal antibodies	ASKA Biotech GmbH, Berlin, Germany
Custom-made synthetic isotope-labeled and non-labeled peptides	INTAVIS AG, Tübingen, Germany
Dimethyl sulfoxide (DMSO)	Thermo Fisher Scientific, Waltham, USA
Disodium phosphate (Na_2HPO_4 x 2 H_2O)	Carl Roth, Karlsruhe, Germany
Ethanol, >99.8%, p.a.	Carl Roth, Karlsruhe, Germany
Ethylenediaminetetraacetic acid (EDTA)	Carl Roth, Karlsruhe, Germany
Ethanol (EtOH) >99.8%, p.a.	Carl Roth, Karlsruhe, Germany
Formic acid 99.0%, Optima™ (FA), LC-MS grade	Fisher Scientific
Hydrochloric acid 37% fuming (HCl)	Carl Roth, Karlsruhe, Germany

Substance	Manufacturer
Iodoacetamide (IAA)	SigmaAldrich, St. Louis, USA
Methanol, ROTISOLV ≥99.98%, LC-MS grade	Carl Roth, Karlsruhe, Germany
Nα-benzoyl-L-arginine-4-nitroanilide hydrochloride	SigmaAldrich, St. Louis, USA
Nα-tosyl-L-lysine chloromethyl ketone hydrochloride (TLCK)	SigmaAldrich, St. Louis, USA
N-Octyl β-D- glucopyranoside (NOG)	Carl Roth, Karlsruhe, Germany
NP40 Surfact Amps Detergent Solution	Thermo Fisher Scientific, Waltham, USA
N-p-tosyl-L-phenylalanine chloromethyl ketone (TPCK)	SigmaAldrich, St. Louis, USA
N-Succinyl-Ala-Ala-Pro-Phe-p-nitroanilide	SigmaAldrich, St. Louis, USA
Phenylmethanesulfonyl fluoride (PMSF)	Thermo Fisher Scientific, Waltham, USA
Phosphate-buffered saline (PBS)	Thermo Fisher Scientific, Waltham, USA
Sodium chloride (NaCl)	Carl Roth, Karlsruhe, Germany
Sodium dodecyl sulfate (SDS)	SigmaAldrich, St. Louis, USA
Sodium hydroxide ≥99% (NaOH)	Carl Roth, Karlsruhe, Germany
Technical buffer solutions pH 4.01, pH 7.00, pH 9.21	Mettler Toledo, Columbus, USA
Triethanolamine hydrochloride (TEA/TEA-HCl)	Carl Roth, Karlsruhe, Germany
Trifluoroacetic acid (TFA), HPLC-MS Optigrade	VWR, Radnor, USA
Tris-(2-carboxyethyl)-phosphin (TCEP)	Carl Roth, Karlsruhe, Germany
Tris-(hydroxymethyl)-aminomethane hydrochloride (Tris-HCl)	Carl Roth, Karlsruhe, Germany
Water, ultrapure LC-MS grade	Honeywell, Charlotte, USA

3.1.3 Solutions and buffers

Table 4: Solutions and buffers

Solution or buffer	Components	Use
ABC buffer	50 mM ABC buffer	Immunoprecipitation
ABCC	0.03% CHAPS in ABC buffer	Immunoprecipitation
HAc	50 mM HAc in H_2O	Proteolysis
Digestion buffer (TEA-NOG)	0.5% NOG in 100 mM TEA	Proteolysis
Eluent A	0.1% FA in H_2O	LC elution solvent
Eluent B	0.1% FA + 80% ACN in H_2O	LC elution solvent
Eluent C	10% 2-propanol in H_2O	LC needle wash solvent
FA solution	1% FA in H_2O	Immunoprecipitation

Solution or buffer	Components	Use
IAA stock	1 M IAA in H_2O	Proteolysis
Loading buffer	0.05% TFA + 2% ACN in H_2O	LC loading solvent
Lysis buffer	1% NP40, 0.01% SDS, 0.15 M NaCl, 0.01 M Na_2HPO_4 x 2 H_2O, 2 mM EDTA, 2.5 Units/mL Benzonase in H_2O, pH 7.2	Lysis & total protein determination
PBSC	0.03% CHAPS in PBS	Immunoprecipitation
PMSF stock	0.2 mM PMSF in EtOH	Proteolysis
Rear seal wash buffer	10% methanol in H_2O	LC rear seal wash solvent
TCEP stock	1 M TCEP in H_2O	Proteolysis
Tris-HCl working buffer	100 mM Tris-HCl, pH 8.0	Enzyme activity assay
Tris-HCl working buffer with $CaCl_2$	100 mM Tris-HCl, 10 mM $CaCl_2$, pH 7.8	Enzyme activity assay

3.1.4 Enzymes, proteins, and kits

Table 5: Enzymes, proteins, and kits

Enzymes, proteins, and kits	Provider
Antibody and protein kits for OPN & MCSF1R	R&D, Minneapolis, USA
ccK18 ELISA, Apoptosense®	Peviva (VLVbio), Nacka, Schweden
Chymotrypsin, sequencing-grade	Promega, Walldorf, Germany
GLDH, recombinant protein (human)	ProSpec-Tany TechnoGene Ltd., Ness-Ziona, Israel
GLDH activity assay kit	SigmaAldrich, Munich, Germany
HMGB1 ELISA	IBL, Hamburg, Germany
HMGB1, recombinant protein (rat, used for human & rat)	HMGBiotech, Milano, Italy
K18, recombinant protein (human)	OriGene Technologies, Inc., Rockville, USA
K18 ELISA, EpiDeath®	Peviva (VLVbio), Nacka, Schweden
MCSF1R, recombinant protein (human)	R&D, Minneapolis, Canada
MCSF1R, recombinant protein (rat)	Sino Biological Inc., Beijing, China
OPN, recombinant protein (human)	SigmaAldrich, Munich, Germany
OPN, recombinant protein (rat)	SigmaAldrich, Munich, Germany
Pierce™ Bicinchoninic acid protein assay (BCA) kit	Thermo Fisher Scientific, Waltham, USA
Pierce™ Bovine Serum Albumin Standard (BSA) for total protein determination	Thermo Fisher Scientific, Waltham, USA
Pierce™ Protein G magnetic beads	Thermo Fisher Scientific, Waltham, USA
Trypsin, modified, TPCK treated	Worthington Biochemical Corporation, Lakewood, USA
Trypsin Gold, mass spectrometry-grade	Promega, Madison, USA

3.1.5 Samples

Table 6: Samples

Sample	Provider	Use
Hepatoma G2 cell pellets	Workgroup Rothbauer, University of Tuebingen, Germany	Method development
Human EDTA plasma	Biotrend, Köln, Germany	Method development
Human serum and EDTA plasma	Genentech, San Francisco, USA	Matrix and sampling comparison
Primary human hepatocytes	hepacult GmbH, Martinsried, Germany	Method development
Rat EDTA plasma	Biotrend, Köln, Germany	Method development
Rat EDTA plasma	MSD, Landsdale, USA	DILI investigation (1,000 mg/kg APAP, thioacetamide, bromobenzene, CCl_4)
Rat EDTA plasma and liver tissue	Sanofi, Montpellier, France	DILI investigation (1,500 mg/kg APAP, DAPM)

3.1.6 Laboratory equipment

Table 7: Laboratory equipment

Apparatus and type	Manufacturer
Analytical balance CPA225D-0CE	Sartorius Stedim Biotech, Göttingen, Germany
Analytical balance, Explorer scale	OHAUS Waagen, Bad Hersfeld, Germany
AU analyzer	Beckman Coulter, Brea, USA
Ball mill, Micro-Dismembrator U	Sartorius Stedim Biotech, Göttingen, Germany
Centrifuge, Mini Star	VWR, Radnor, USA
Chromatography system, UltiMate 3000 RSLCnano	Thermo Fisher Scientific, Waltham, USA
FlexMap3D instrument	Luminex xMAP, Luminex Corp., Austin, USA
DynaMag- 15 Magnet	Thermo Fisher Scientific, Waltham, USA
Magnet KingFisher™ 96 PCR head	Thermo Fisher Scientific, Waltham, USA
Magnetic particle processor, KingFisher™96-purification system	Thermo Fisher Scientific, Waltham, USA
Mass spectrometer, Q Exactive Plus™	Thermo Fisher Scientific, Waltham, USA
Microplate reader, BioTek ELx808	BioTek, Bad Friedrichshall, Germany
Microplate reader, FLUOstar Optima	BMG Labtech, Ortenberg, Germany
Mixer, Vortex-Genie 2	Scientific Industries, Bohemia, USA
Multichannel Electronic Pipette, E4 XLS, 100 - 1200 µL	Mettler Toledo, Columbus, USA
Multichannel pipette, Pipet-Lite XLS, 2 - 20 µL	Mettler Toledo, Columbus, USA

Apparatus and type	Manufacturer
Multichannel pipette, Pipet-Lite XLS, 20 - 300 µL	Mettler Toledo, Columbus, USA
Multichannel pipette, Pipet-Lite XLS, 5 - 50 µL	Mettler Toledo, Columbus, USA
pH-meter, 766 Calimatic	Knick, Berlin, Germany
Pipette 2 - 20 µL, Eppendorf Research plus	Eppendorf, Hamburg, Germany
Pipette 10 - 100 µL, Eppendorf Research plus	Eppendorf, Hamburg, Germany
Pipette 100 - 1,000 µL, Eppendorf Research plus	Eppendorf, Hamburg, Germany
Pipette 20 - 200 µL, Eppendorf Research plus	Eppendorf, Hamburg, Germany
Pipette 50 - 5,000 µL, Eppendorf Research plus	Eppendorf, Hamburg, Germany
Refrigerated microcentrifuge 5417R	Eppendorf, Hamburg, Germany
Sample mixer, HulaMixer	Thermo Fisher Scientific, Waltham, USA
Single Channel Electronic Pipette, E4 XLS, 20 - 300 µL	Mettler Toledo, Columbus, USA
SWC Safety Weighing Cabinet	Sartorius Stedim, Biotech, Göttingen, Germany
Thermo Mixer Comfort	Eppendorf
Universal 320/320R centrifuge with plate rotor	Hettich
Water purification system, Milli Q Plus	Sartorius Stedim, Biotech, Göttingen, Germany

3.1.7 Databases and software

Table 8: Databases and software

Databases and software	Distributor
Chromeleon version 6.8 or later	Thermo Fisher Scientific, Waltham, USA
Gen version 5.1.10.8	BioTek, Winooski, USA
Inkscape version 0.92	GNU GEeneral Public License
Microsoft Office Home and Business 2016	Microsoft, Redmond, USA
Origin version 2017	OriginLab, Northampton, USA
PeptideCutter	SIB Swiss Institute of Bioinformatics, Lausanne, Switzerland
ProtParam	SIB Swiss Institute of Bioinformatics, Lausanne, Switzerland
Skyline version 19.1 or later	MACOSS Lab, Department of genome sciences, University of Washington, Seattle, USA
Tune 2.8	Thermo Fisher Scientific, Waltham, USA
UniProtKB Protein knowledgebase	UniProt Consortium
Xcalibur 4.0	Thermo Fisher Scientific, Waltham, USA

3.2 IA-LC-MS/MS assays for DILI biomarker quantification

Assays for protein biomarker quantification in human or rat samples were established using the IA-LC-MS/MS method **(Figure 8**). Depending on the specimen, this method included sample lysis and total protein determination (tissue and cell pellets) and proteolysis followed by peptide-targeted immunoprecipitation using antibodies (tissue and cell pellets, serum and plasma). For all types of specimen, read-out by LC-MS/MS was performed. The following assays were qualified or partially validated: multiplex human (MPh-dev) and multiplex rat (MPr). Depending on the assay, several workflow steps could vary as described in section **3.2.1** to **3.2.12**.

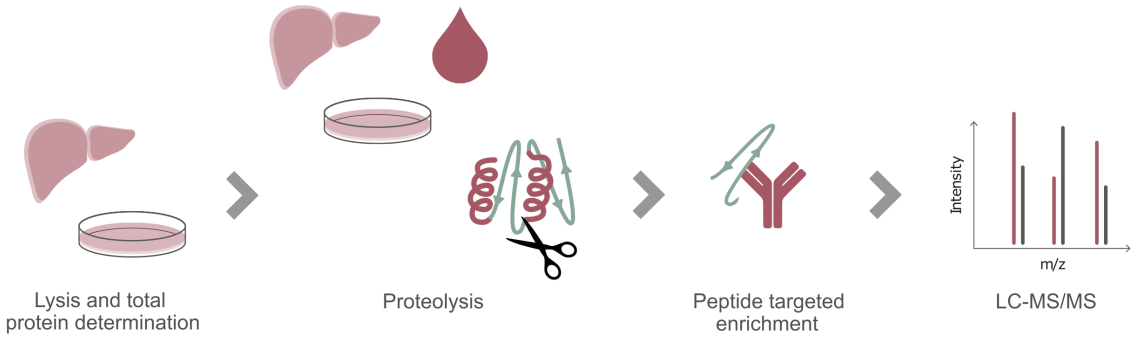

Figure 8: General IA-LC-MS/MS workflow for various specimen. Tissue and cell specimen were lyzed and total protein content was determined. Tissue and cell lysates as well as serum or plasma specimen were proteolyzed, synthetic peptides were added as internal standards, and peptide-targeted immunoaffinity enrichment was performed. Read-out was performed with LC-MS. Adapted from Anselm *et al.* 2021.

3.2.1 Surrogate matrix

A surrogate matrix was used as general calibration curve matrix or for dilution of recombinant proteins to mimic the protein content in serum or plasma samples. The surrogate matrix consisted of bovine serum albumin (BSA) with a concentration of 60 µg/µL in sterile filtered phosphate-buffered saline (PBS). This matrix and protein concentration was chosen, since serum albumin is the highest abundant protein in serum or plasma and the approximate total protein concentration in serum or plasma samples between 60 µg/µL to 80 µg/µL[133]. The surrogate matrix was stored in aliquots at approx. -20 °C up to 6 months. Hereafter, this matrix is termed surrogate matrix or BSA control. Surrogate matrix was processed in the same way as the corresponding volume of unknown test samples and used as matrix for calibration and blank samples for all assays. For validated assays, surrogate matrix was also spiked in tissue or cell lysate samples during processing to provide matrix conditions comparable to serum or

plasma. Unknown serum or plasma samples and quality control samples were prepared without surrogate matrix.

3.2.2 Samples for method development and method validation

Between 1 µL and 15 µL plasma sample was tested for sample processing during method development. Cell pellets from hepatoma G2 (HepG2) non-treated or treated with 100 nM taxol for 18 h were kindly provided by Dr. Björn Tränkle (workgroup of Prof. Dr. Rothbauer, University of Tuebingen) and processed for method development.
Several types of samples were prepared to address different parameters following "Bioanalytical Method Validation Guidance for Industry" published by the United States Food and Drug Administration[126] (FDA).
Quality control (QC) samples were prepared and processed according to unknown plasma samples and were used to assess the general assay performance regarding inter / intra assay accuracy and precision. QC samples were prepared from endogenous plasma samples spiked with recombinant protein or liver tissue lysate depending on protein availability and the assay. Detailed QC sample composition is shown in Table **9**. QC samples presented in Anselm *et al.* 2021 are also listed here and QC samples were termed differently as in the publication (QCL = QC1, QCM = QC2, QCH = QC3). Calibration samples (calibrators S1-S8, blank B) were prepared as described below (see section **3.2.5** and **3.2.10**) for general analyte quantification and for addressing intra / inter accuracy and precision.

Table 9: Composition of quality control (QC) samples

Assay	Sample	Composition
MPh-dev	QC1	- Human EDTA plasma (Biotrend, Köln, Germany)
	QC2	- Human EDTA plasma, 2,160.00 ng/mL rec. MCSF1R, 283.21 ng/mL rec. OPN, 33.17 ng/mL rec. HMGB1, 447.79 ng/mL rec. GLDH
	QC3	- Human EDTA plasma, 6,480.00 ng/mL rec. MCSF1R, 2,832.10 ng/mL rec. OPN, 333.71 ng/mL rec. HMGB1, 4,477.87 ng/mL rec. GLDH
MPr	QC1	- Rat EDTA plasma (MSD, Kenilworth, USA); 18.83 ng/mL rec. rat MCSF1R, 12.44 ng/mL synthetic ccK18 peptide
	QC2	- Rat EDTA plasma, 150.67 ng/mL rec. rat MCSF1R, 454.67 ng/mL rec. rat OPN, 46.64 ng/mL synthetic ccK18 peptide, 0.5 µg rat liver tissue lysate (Sanofi, Montpellier, France)
	QC3	- Rat EDTA plasma, 1,506.67 ng/mL rec. rat MCSF1R, 4546.67 ng/mL rec. rat OPN, 466.38 ng/mL synthetic ccK18 peptide, 8 µg rat liver tissue lysate

Parallelism was tested using at least six samples with high endogenous protein levels. Plasma samples were diluted serially three times 1:2 in surrogate matrix (P1-6_dil1-4) for assay validation. Liver tissue was spiked with up to 8 µg into surrogate matrix and serially diluted three times 1:2 in surrogate matrix (PT1-6_dil1-4) for testing parallelism in case of MPr.

3.2.3 Samples for matrix and sampling comparison

Samples for matrix and sampling comparison were provided by the Genentech (San Francisco, USA) employee sample donation program. Information consent form, sampling procedures, forms, and recruitment material was approved by the Western Institutional Review Board. Samples were kindly prepared by Connie Mahood using the following sample tubes: EDTA plasma: BD Vacutainer® #367844; serum without gel: BD Vacutainer® #366668; serum with gel: BD Vacutainer® #367981. For each time point to be investigated, serum with gel, serum without gel, and EDTA plasma was drawn from each healthy volunteer (HV), in total ten HVs. After collection and gentle inversion (5 - 8 times), the tubes were kept up right at room temperature (RT) for 15 min, 30 min, or 60 min prior to centrifugation at 1,600 rpm for 10 min at RT to test different benchtop intervalls (**Figure 9**).

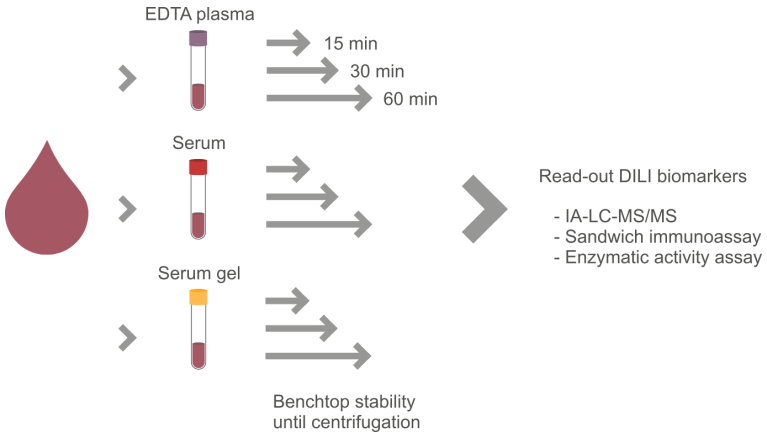

Figure 9: Sample preparation for matrix and sampling comparison. EDTA plasma, serum without gel and serum with gel samples were collected from ten healthy volunteers. Benchtop stability was tested by incubating samples 15 min, 30 min, and 60 min at RT between collection and centrifugation. Read-out was performed with various assay types including IA-LC-MS/MS assays, sandwich immunoassays and enzymatic activity assays. Taken from Anselm *et al.* 2021.

For storage at -80 °C, the plasma or serum supernatants were transferred carefully to cryo tubes. Apart from analysis by the IA-LC-MS/MS method (MCSF1R, OPN, HMGB1, GLDH), these samples were also analyzed using sandwich immunoassays (K18, ccK18, MCSF1R, OPN, HMGB1), and enzyme activity-based assay (GLDH) as described below (see sections **3.3** and **3.4.1**).

3.2.4 Samples for translational DILI biomarker investigation in preclinical studies

EDTA plasma specimen of research animals from carbon tetrachloride (CCl_4), thioacetamide, bromobenzene, and acetaminophen (APAP) studies for DILI investigation were kindly provided by Merck Sherp & Dohme (MSD, Landsdale, USA). The respective vehicle solutions without drug or compound were administered to the rat control groups. Study details are summarized in **Table 10**.

Table 10: Study set-up DILI rat, MSD

Study #	**Compound**	**Rat strain**	**Animal #**	**Dosing**	**Day of sampling**
06-2502	Thioacetamide	Sprague-Dawley	4	Control (water)	2
			5	50 mg/kg	
			5	100 mg/kg	
			3	200 mg/kg	
08-2532	Bromobenzene	Wistar-Han	5	Control (corn oil)	3
			4	300 mg/kg	
			4	750 mg/kg	
13-1140	APAP	Sprague-Dawley	5	Control (0.5% (w/v) methylcellulose)	2
			5	1,000 mg/kg	
08-9942	CCl_4	Sprague-Dawley	3	Control (corn oil)	3
			3		4
			4		8
			4		15
			3	120 mg/kg/day	3
			3		4
			4		8
			6		15

Further EDTA plasma and liver specimen of research animals for DILI investigation were kindly provided by Sanofi (Montpellier, France). The animals were housed in a facility accredited by the Association for Assessment and Accreditation of Laboratory

Animal Care International. The study and all procedures were in accordance with the Directive 2010/63/EU of the European parliament and the related French transposition texts, and were approved by the Sanofi Animal Care and Use Committee. Several groups of male Sprague-Dawley rats (9-10 weeks old) of the study NTD0644 were treated either with APAP or with DAPM according to the following specifications. The corresponding vehicle solutions without drug or compound were administered to the rat control groups. Six animals were dosed once with 1,500 mg/kg APAP and were sacrificed at 24 h post dose together with six control animals without treatment. EDTA plasma and liver specimen were collected. Liver samples were preserved in RNAlater-like buffer for RNA analysis (performed at Sanofi). Furthermore, 18 animals were dosed once with 250 mg/kg DAPM (plus 18 animals as control). Blood sampling and animal sacrificing was performed 3 h, 24 h, and 96 h after dosing for 6 animals of each group. Liver samples were provided from the animal group with 24 h treatment time after dosing.

3.2.5 Proteotypic peptides of DILI biomarkers

In preparation for the IA-LC-MS/MS assay development, proteotypic peptides were selected and purchased. Labeled and non-labeled reference peptides were supplied by INTAVIS AG (Tübingen, Germany) in a purity of at least 95%. Isotope-labeled peptides comprised either arginine ($^{13}C_6$ / $^{15}N_4$) or lysine ($^{13}C_6$ / $^{15}N_2$) at their C-terminus depending on the tryptic cleavage site. When no C-terminal K or R was available, then N-terminal leucine ($^{13}C_6$ / $^{15}N_1$) was used. Peptides were reconstituted in 100% DMSO. The peptide solutions were then diluted in ultrapure LC-MS-grade water to a final DMSO concentration of 20% to a peptide stock concentration of 1 mmol/L and stored at approximately -20 °C. Exact peptide concentrations were determined by amino acid analysis (enantiomer labeling) at C.A.T. GmbH & Co (Tübingen, Germany).
Stable isotope-labeled standard (SIS) peptides were used as internal standards spiked in a constant concentration to all samples prior to the immunoprecipitation (calibrator, QC, and unknown samples). The SIS peptide stock solutions were mixed in PBSC and were further diluted in PBSC to the corresponding SIS working solution. The first dilution of SIS peptide mix was aliquoted and stored at -20 °C for further usage (see **3.2.10**).
Synthetic non-labeled peptides were reconstituted, quantified and stored as described above for SIS peptides. The non-labeled peptides were mixed in PBSC and serially diluted 1:3 in PBSC to establish calibration curves (calibrators S1-S8). The first dilution of non-labeled peptide mix was aliquoted and stored at -20 °C for further usage (see **3.2.10**). Labeled peptides for normalized collision energy (NCE) testing were diluted either in loading buffer or in 1% FA, prepared in glass vials and measured via LC-MS/MS (see **3.2.11**).

3.2.6 Capture antibodies for peptide enrichment

In preparation for the IA-LC-MS/MS assay development, polyclonal antibodies were generated by SIGNATOPE GmbH for peptid-specific enrichment. Monoclonal antibodies were generated and provided by ASKA Biotech GmbH (Berlin, Germany) using monoclonal mouse hybridoma. Polyclonal antibodies were kindly prepared by Cornelia Sommersdorf (SIGNATOPE GmbH, Reutlingen, Germany) according to the antibody generation protocol described elsewhere[111]. Briefly, peptides with a chosen amino acid length (either at least four amino acids from the C-terminus or the full peptide length) and a spacer sequence were conjugated to the protein keyhole limpet hemocyanin. Rabbits were immunized for about 70 days at Pineda GmbH (Berlin, Germany) using this conjugate. Polyclonal antibodies were then purified by affinity chromatography. Sepharose, presenting the peptide antigen via a spacer, linker, and ovalbumin, served as the column material.

3.2.7 Tissue and cell lysis

Sample preparation for tissue or cell pellet samples started with lysis to extract proteins. Liver tissues were homogenized using a ball mill (Sartorius Stedim Biotech, Göttingen, Germany). Briefly, fresh frozen liver samples were added to cryo vials and weighed. Then, 7 mm steel balls (Qiagen, Düsseldorf, Germany) were added and the samples were kept frozen in liquid nitrogen. Homogenization was performed in the ball mill for 2 min at 2,000 rpm.
After homogenization, tissue samples were treated accordingly to the general lysis procedure for cell pellets as follows. A 20-fold weight (volume) of lysis buffer was added compared to the sample weight. For cell pellets, the approximate volume of cell pellet was estimated by eye and the double volume of lysis buffer was added. Samples with lysis buffer were incubated in a sample mixer (HulaMixer, Thermo Fisher Scientific, Waltham, USA) for 1 h at 4 °C. Intensive vortexing was performed every 15 min during this incubation time. Samples were then centrifuged for 10 min at 13,000 rpm at 4 °C. Supernatants were transferred in fresh tubes, aliquoted, and stored at -80 °C until analysis. No lysis was required for serum or plasma samples. Tissue and cell lysis was performed with the support of Cornelia Sommersdorf (HepG2 cells, liver), Katharina Bendel (other tisse), or Helen Hammer (primary human hepatocytes).

3.2.8 Total protein determination

The protein concentration in tissue or cell lysate samples was determined according to the bicinchoninic acid (BCA) method[135] using the Pierce™ Bicinchoninic acid protein assay kit (Thermo Fisher Scientific, Waltham, USA). The assay was performed according to the manufacturer's instructions with the following modifications. The calibrators were prepared by spiking diluted lysis buffer (20% lysis buffer in demineralized water)

with BSA according to the concentration levels proposed by the manual (25 µg/mL to 2,000 µg/mL). No total protein determination was performed for serum or plasma samples since the total protein concentration in these samples is mainly determined high abundant proteins such as serum albumin and globulis (IgG)[133]. Thus, total protein concentration in serum or plasma samples was assumed 60 µg/µL as described in section **3.2.1**.

3.2.9 Proteolysis of tissue, cells, plasma, and serum

For enzymatic fragmentation of intact proteins to peptides (digestion / proteolysis), samples were mixed with digestion reagents and digested by trypsin as follows. All incubation steps were performed at 700 rpm shaking in a Thermo Mixer Comfort. Digestion buffer (0.5% NOG in 100 mM TEA) and plasma samples (1 µL to 15 µL) were mixed to give a final volume of 110 µL per well in a 96-well microtiter plate, closed with microcap strips and proteins were denatured at 99 °C for 5 min. Accordingly, digestion buffer, 15 µL surrogate matrix and liver tissue or lysate (1 µg to 8 µg) were mixed to give a final volume of 110 µL and heated for preparation of lysate samples. After cooling the samples down to room temperature (RT), protein disulfide bonds were reduced by adding 10 µL 60 mM TCEP for a final concentration of 5 mM TCEP and an incubation at RT for 5 min. For alkylation of cysteine residues, the samples were complemented with 10 µL 130 mM IAA for a final concentration of 10 mM IAA and incubated at RT in the dark for 20 min. Trypsin was added for proteolytic protein digestion in a trypsin to protein ratio of 1:20. The pH was confirmed at about pH 8 with pH indicator paper. Proteolysis with trypsin was performed at 37 °C for 16 h. The reaction was stopped by a heating step to 99 °C for 5 min, cool-down to RT, and subsequent addition of PMSF (final 10 mM). Samples were diluted at least 10-fold during the proteolysis step by subsequent addition of proteolysis reagents, i.e., 15 µL sample volume resulted in a final digestion volume of 150 µL. A volume of 15 µL surrogate matrix (60 µg/µL BSA in PBS) was used for proteolysis to prepare calibration samples, which were finalized in the following peptide immunoaffiniy enrichment procedure. The following proteolysis parameters were investigated during method development for the proteins K18 and HMGB1. For testing impact of trypsin concentration, the trypsin to protein ratio was decreased to 1:100. Proteolysis times from 0 h, 2 h, 4 h, 6 h to 16 h were tested for digestion kinetics. PMSF was added directly before trypsin addition in peptide recovery experiments to reduce cleavage within the sequence of the K18 and HMGB1 peptides.

3.2.10 Peptide immunoaffinity enrichment (immunoprecipitation)

Proteolyzed samples were further used for peptide-specific immunoaffinity enrichment as follows. Immunoprecipitation (IP) reagents including peptide solution and antibody solution were added to the digested samples in the 96-well microtiter PCR plate. Peptide solutions were prepared as described in section **3.2.5**. A volume of 10 µL SIS working solution (internal standard) was added to the digested surrogate matrix (for calibrators), QC samples, and unknown samples resulting in definded SIS peptide amounts in fmol per well. A volume of 10 µL calibrator was added to the samples with proteolyzed surrogate matrix to complete calibration samples. A volume of 10 µL PBSC was added to proteolyzed surrogate matrix to generate blank samples (B).
Antibody mixtures were prepared in PBSC and between 10 µL to 25 µL antibody mixture was added depending on the total antibody concentration. Depending on the assay, CHAPS was added to give a final concentration of 0.03% as a detergent to reduce surface tension, since this is a prerequisite for the magnetic bead transfer by the following automatic magnetic bead transfer steps in the magnetic bead processor.
Additionally to the described sample plate, bead (source) plate and wash plates in 96-well format were prepared as follows. Pierce™ Protein G magnetic beads (Thermo Fisher Scientific, Waltham, USA) were washed and prepared in PBSC according to the manufacturer's instructions using a magnet (DynaMag- 15 Magnet, Thermo Fisher Scientific, Waltham). Usually, a volume of 2 µL bead suspension was used per 1 µg antibody. To increase sensitivity, more bead suspension was added depending on the assay. PBSC and bead suspension were added up to 100 µL volume per well in the source plate. The immunoprecipitation procedure with two wash steps in PBSC (0.03% CHAPS in PBS) and three wash steps in ABCC (0.03% CHAPS in 50 mM ABC buffer) were performed in semi-automated format in a magnetic bead processor (KingFisher™, Thermo Fisher Scientific, Waltham, USA). During a total run time of 2 h 45 min, the plates were processed by bead transfer to the corresponding plates and the respective incubation steps (see procedure **Table 11**). Peptide elution from their corresponding antibody was performed in 1% formic acid (FA). The obtained elution was transferred to a new 96-well plate to avoid remnants of beads (transfer plate), subsequently pipetted into a glass-coated 96-well plate, and closed with a silicone mat (for MPr). Alternatively, samples were pipetted from the transfer plate into glass inserts in glass vials (for MPh-dev).

Table 11: Semi-automated procedure for immunoprecipitation in a magnetic bead processor

Step number	Plate description	Solvent / condition	Volume (µL)
1	Sample	Samples, peptides, antibodies	max. 195
2	Source	Bead suspension in PBSC	100
3	Washing	PBSC	100
4	Washing	PBSC	100
5	Washing	ABCC	100
6	Washing	ABCC	100
7	Washing	ABCC	100
8	Elution	1% FA	20

3.2.11 LC-MS/MS and MS data public access

After immunoprecipitation, sample read-out was performed using an liquid chromatorgraphy (LC) system coupled to a mass spectrometer (MS). The peptide eluates were loaded onto a nanoflow UHPLC system (Ultimate 3000 RSLCnano, Thermo Fisher Scientific) with an injection volume of 5 µL per sample. Peptide trapping was performed with loading buffer as mobile phase (2% acetonitrile (ACN) and 0.05% trifluoroacetic acid (TFA)) on a precolumn (Acclaim PepMap100 C18, µ-precolumn, Thermo Fisher Scientific, Waltham, USA). Chromatographic peptide separation was performed on an analytical column (Acclaim PepMaP RSLC C18, Thermo Fisher Scientific Waltham, USA) with a flowrate of 1 µL/min at 55 °C column oven temperature. During a total run time of 10 min, peptides were separated within a 5.75 min gradient from 4% to 40% eluent B (80% ACN), the analytical column was washed with 99% eluent B and equilibrated again to 4% eluent B (96% eluent A: 0.1% FA). LC needle wash was performed with eluent C (10% 2-propanol) and the rear seal wash buffer (10% methanol). Between each run, 2 min equilibration was set resulting in a total run time of 12 min per sample. Final read-out of peak intensities was performed with a mass spectrometer (QExactive Plus™, Thermo Scientific, Waltham, USA). PRM was chosen for targeted MS data acquisition and MS parameters were set as follows: resolution of 35,000, maximum injection time of 60 ms, automatic gain control (AGC) target of $2x10^5$, peptide isolation window of 1.4 m/z, MSX count of 2. For precursor selection, an inclusion list was used with the corresponding mass-to-charge (m/z) values for non-labeled and labeled peptides. Peptide isolation time was scheduled to maximize data points for the chromatographic peaks when more than three peptides were part of the inclusion list (at least ten data points per peak). Charge state and normalized collision energy (NCE) was optimized for all peptides.
Full-scan MS analysis was performed for measurement of the rat MCSF1R peptides during method development. The same LC conditions from above were combined with the following full-scan MS parameters. A resolution of 70,000, a maximum injection

time of 100 ms, an isolation window of 2 m/z and an AGC target of $3x10^6$ were applied to measure the top 10 peptides per MS cycle.
The mass spectrometry data for matrix and sampling comparison of human serum and plasma specimen[134] have been deposited the ProteomeXchangeConsortium (http://proteomecentral.proteomexchange.org) via the PRIDE partner repository[136] with the data set identifier PXD028274.

3.2.12 General MS data analysis and quantification

Chromatograms were recorded using the software XCalibur version 4.0 or later, raw data was imported to the software Skyline[137] version 19.1 or later and peak areas were determined for each analyte and isotope-labeled analog. The summed peak areas of at least four fragment ions were used for calculation. For assays under development, either peak areas under the curve (AUC) (non-labeled peptide) or AUC ratios (endogenous or non-labeled peptide vs. labeled standard peptide) were reported. For MPh-dev and the validated assay MPr, peptide quantification was based on the calibration curve S1-S8 plus blank (B). This calibration curve was obtained by the AUC ratio (synthetic non-labeled vs. labeled analog) using a logistic fit model. Protein concentrations in EDTA plasma were calculated by converting measured absolute peptide amount (fmol) into ng/mL considering the molecular weight of the corresponding protein and the corresponding sample volume (1 µL to 15 µL). Quantification results for liver tissue samples in fmol were calculated in ng and normalized to total protein input for proteolysis (ng analyte / µg total protein). The protein molecular weight values were calculated by the amino acid sequence only because not all relevant protein weights were available at Uniprot (e.g., shedded MSCF1R part or caspase-cleaved K18). The corresponding amino acid sequences were used from UniProt[138] (FASTA sequence) and the theoretical molecular weight was calculated using the corresponding amino acid sequence with the online tool ProtParam[139].

3.2.13 Data analysis for validation experiments

Several analysis parameters were investigated for partial validation experiments for the assay MPr following the recommendations of the FDA guideline[126]. Analytes were quantified according to the general analysis method described above (see section **3.2.12**) and the obtained results were used for the following calculations. In general, three independent runs were applied per validation criterion for partial validation.
QC samples were characterized by repeated multiple measurements (n = 3). The nominal values of the corresponding protein concentrations in each QC sample (QC1, QC2, and QC3) were determined by calculating the mean from three runs with two processings and measurements per QC level and run. Inter assay accuracy and precision over the calibrator concentration range was assessed by the repeated analysis of calibration

samples (S1-S8, B), and QC samples in three independent runs. Accuracy was determined as the relative deviation of the measured concentration from the respective nominal concentration (**Equation 1**). Precision was determined as the standard deviation of the individual measurements at one concentration level relative to the arithmetic mean value (**Equation 2**).

$$accuracy\ (\%)\ =\ \frac{concentration_{measured} - concentration_{nominal}}{concentration_{nominal}}\ *100 \tag{1}$$

$$precision\ (\%\ CV)\ =\ \frac{standard\ deviation_{\ measured}}{arithmetic\ mean_{measured}}\ *100 \tag{2}$$

Intra assay accuracy and precision were calculated from the sixfold measurement of QC samples on one sample plate. The mean accuracy of the measurement should not exceed ±20% CV from the determined nominal value (except at LLOQ & ULOQ, ±25%, see below). Intra assay precision should not exceed 20% (except at LLOQ & ULOQ, 25%). Total error (TE) sets precision and accuracy into relation and was calculated as follows to determine the quantification limits (**Equation 3**).

$$Total\ error\ (\%\ TE)\ =\ \%\ precision\ +\ |\%\ accuracy| \tag{3}$$

The lower limit of quantification (LLOQ) was derived as the lowest concentration level which could be measured with an accuracy of ±25%, a mean precision of better than CV ≤25%, and total error of ≤40%. Furthermore, the LLOQ should be higher than the mean blank signal per batch summed with six times standard deviation of the blank signal. The upper limit of quantification (ULOQ) was defined as the highest concentration level which could be measured with an accuracy of ±25%, a mean precision of better than CV ≤25%, and total error of ≤40%.

For parallelism, the accuracy between back-calculated diluted samples and undiluted sample was determined using **Equation 1** for at least six animal samples.

For reproducibility, the percentage difference of the results of at eight animals from two independent measurement runs was investigated according to the recommendation from the European Medicines Agency[127] (EMA) with the following **Equation 4**.

$$difference\,(\%) = \frac{concentration_{replicate1} - concentration_{replicate2}}{concentration_{mean}}\ *100 \tag{4}$$

3.2.14 Replicates and statistical analysis

All samples were processed (digest & IP) and measured by LC-MS/MS three times during early method development. Samples at a later development stage (MPh-dev) or validated assay (MPr) were processed and measured twice. Only samples with a coefficient of variation (% CV) below 30% were reported in ng/mL and results with a CV below were shown as half the corresponding LLOQ values (LLOQ/2) as proposed by Wakefield & Racine-Poon[140].
All statistical tests were performed using the software OriginPro (version 2017) and figures were edited using the software Inkscape (version 0.92). Regression analyses were performed by assessing the regression coefficient adjusted relative to the number of samples (adjusted R^2). The strength of correlation was assessed during method development for endogenous analyte in 1 µL to 15 µL plasma sample or for correlation of analyte concentrations in matched serum and plasma samples or method comparison (see **3.2.3** and **4.4.3**). The levels in strength of correlation were termed according to the guide proposed by Mukaka in 2012[141].
Significant increase or decrease in analyte levels between sample collection and centrifugation time from matched human serum and plasma specimen (see **3.2.3**) were investigated with a one-way repeated measures analysis of variance (ANOVA) test and Bonferroni correction (significance level: $p < 0.05$). Results from samples with a benchtop time of 15 min were used as reference value (100%). Matching serum and EDTA plasma samples from the same donor were investigated using paired t-tests (significance level: $p < 0.05$).
Since different animals were tested for each condition or investigated time period for drug or compound treatment, the nonparametric Mann-Whitney test was applied to assess statistically significant difference (significance level: $p < 0.05$).

3.3 Sandwich immunoassays for DILI biomarker quantification

Samples for matrix and sampling comparison (see **3.2.3**) were investigated with various sandwich immunoassays including enzyme-linked immunosorbent assay (ELISA) kits and bead-based sandwich immunoassays depending on assay availability. Both assays involved a two-step procedure using two antibodies (capture & detection) and read-out via absorbance or fluorescence measurement (**Figure 10**). All samples were analyzed once due to sample availability and the procedures were kindly performed by Cornelia Sommersdorf (SIGNATOPE GmbH, Reutlingen). Statistical analysis was performed by me.

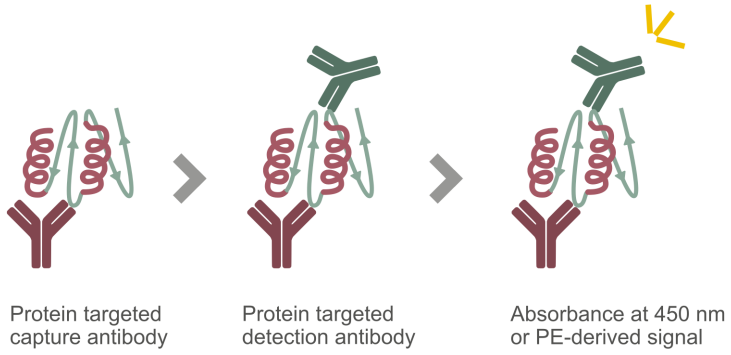

Figure 10: General sandwich immunoassay workflow for protein quantification. ELISAs: absorbance at 450 nm, bead-based sandwich immunoassays: Fluorescence of phycoerythrin (PE). Adapted from Anselm *et al.* 2021.

3.3.1 ELISAs for quantification of HMGB1, K18, and ccK18

ELISA kits were used for quantification of the proteins HMGB1 (IBL, Hamburg, Germany, #ST51011), K18 (Peviva (VLVbio), Nacka, Schweden, EpiDeath® #10020) and ccK18 (Peviva (VLVbio), Nacka, Schweden, Apoptosense® #10011) in samples for matrix and sampling comparison (**3.2.3**) according to their manufacturer's instructions. Briefly, antibody-coated microtiter strips were incubated with 50 µL neat sample for HMGB1 or 25 µL neat sample for K18 or ccK18 for their according assay incubation times. Calibrators and blank samples were generated and added according to the kit protocol. The high sensitivity calibration range was used for the HMGB1 ELISA. Endogenous plasma samples (HMGB1) or samples provided with the kit (K18, ccK18) were used as batch control samples. After antibody and sample incubation, enzyme-conjugated antibodies were added to the microtiter strips followed by addition of color solution. After reaction stop using the stop solution, read-out was performed by measuring the absorbance at 450 nm using a microplate reader (BioTek ELx808, BioTek, Bad Friedrichshall, Germany). Analyte quantification was performed based on the according calibration curves and reported in ng/mL (HMGB1) or picomole per liter (K18, ccK18).

3.3.2 Bead-based sandwich immunoassays for quantification of OPN and MCSF1R

Bead-based sandwich immunoassays were performed for quantification of the proteins OPN and MCSF1R in single analyte format. Antibodies and protein stocks for preparation of the calibration curves were used from the corresponding kits (R&D, Minneapolis, Canada: OPN: DuoSet #DY1433, MCSF1R: DuoSet #DY329) and adapted to the Luminex bead-based assay platform (Luminex xMAP, Luminex Corp., Austin, USA) as described by Poetz *et al.* in 2018. Briefly, capture antibodies were coupled to magnetic

polystyrene beads and detection antibodies were biotinylated. Unknown samples were diluted 1:100 for MCSF1R and 1:10 for OPN. Endogenous human plasma samples were used as batch control samples. Capture antibody beads were incubated with unknown samples, calibrators, blanks and controls for 2 h followed by further incubation with the biotinylated detection antibodies for 2 h. Phycoerythrin (PE)-conjugated streptavidin was added for 45 min and read-out of the fluorescence signal was performed on a FlexMap3D instrument (Luminex xMAP, Luminex Corp., Austin, USA) according to the manufacturer's instructions. Analyte quantification was performed based on the respective calibration curves and reported in pg/mL.

3.4 Enzyme activity-based assays

Since no sandwich immunoassay was available for GLDH quantification in plasma or serum, an enzyme activity-based assay (see below **3.4.1**) was used for GLDH activity measurement in serum samples for matrix and sampling comparison (see **3.2.3**). Activity of alanine amino-transferase (ALT) was measured in serum specimen according to the procedure described below (**3.4.2**). Furthermore, tryptic and chymotryptic activity of trypsin was investigated using the corresponding activity assays (**3.4.3**).

3.4.1 Enzyme activity assay for GLDH

An enzyme activity assay kit (SigmaAldrich, Munich, Germany, #MAK099-1KT) was used to assess GLDH activity in serum samples for matrix and sampling comparison (see **3.2.3**). The procedure was performed according to the manufacturer's instructions with a sample volume of 25 µL serum per sample. Plasma was not measured since the manufacturer established this assay only for serum samples. GLDH activity was assessed by enzymatic conversion of the substrate glutamate to α-ketoglutarate generating NADH from NAD^+ and H^+ (**Figure 11**) by GLDH. A probe reacted then with NADH resulting in a probe product having a maximum absorbance at 450 nm using a microplate reader. Calibration curves were prepared as recommended by the manufacturer using specified concentrations of NADH (provided by the kit) and endogenous plasma was used as batch control samples for both measured batches. Results were reported in enzyme activity per time in U/L. Reaction times were determined for optimal absorbance signal of the unknown samples to be within the assay's working range between 2 and 10 nmole NADH per well. A reaction time of 30 min (batch 1) or 40 min (batch 2) was chosen to determine the GLDH activity per batch, respectively. Serum samples were collected and measured at Sanofi for GLDH activity with the same method using a Roche Cobas 6000 c501 system (Roche Diagnostics, Basel, Switzerland) for read-out and data were kindly provided by Sanofi for further analysis.

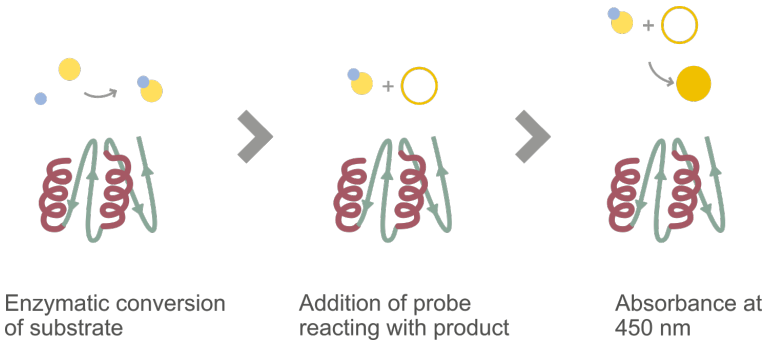

Figure 11: General enzyme activity assay workflow for GLDH. GLDH converts glutamate enzymatically to α-ketoglutarate generating NADH from NAD^+ and H^+. NADH reacts with a probe and the product can be read out with an absorbance at 450 nm. Adapted from Anselm *et al.* 2021.

3.4.2 Enzyme activity assay for ALT

Alanine aminotransferase (ALT) activity was measured in animal serum samples on Beckman Coulter AU analyzers (Brea, USA). The underlying coupled enzyme assay was proposed by Wroblewski & Ladue[143] and modified as recommended by the International Federation of Clinical Chemistry[144]. Briefly, L-alanine and α-oxoglutarate is transformed to pyruvate by ALT under usage of glutamate. NADH and generated pyruvate is then converted by lactate dehydrogenase to NAD^+. The decrease in absorbance at 340 nm (by conversion of NADH to NAD^+) is proportional to ALT activity. The analyses were performed at the sample collection sites of Sanofi and MSD, respectively. ALT data in U/L were kindly provided and statistically analyzed by me.

3.4.3 Tryptic and chymotryptic activity assays

Chymotryptic activity of trypsin was tested by tryptic and chymotryptic activity assays as described by DelMar *et al.* in 1979[145] with the following modifications. For testing tryptic activity of trypsin, microtiter plate wells were prepared with Tris-HCl working buffer (100 mM tris-HCl, pH 8.0) and trypsin substrate (100 nmol per well Nα-Benzoyl-L-arginine-4-nitroanilide hydrochloride, SigmaAldrich, #B3133-100MG). Wells without substrate or without substrate and enzyme served as negative controls. Read-out was performed at 405 nm (absorbance of the product 4-nitroaniline) with a microplate reader (FLUOstar Optima, BMG Labtech, Ortenberg, Germany) before enzyme addition to obtain absorbance of blanks without enzyme. Trypsin of the following manufacturers were added to each well except the corresponding negative control wells: 1 µg trypsin provided by Worthington Biochemical Corporation, #LS003744; 1 µg trypsin (Trypsin Gold, mass spectrometry-grade) provided by Promega,#V5280. Buffer, substrate and enzyme solution was added up to 100 µL. Read-out was performed at the following time points after trypsin addition: 0 min, 5 min, 10 min, 15 min, 20 min, 25 min, 30 min,

60 min, 120 min, 180 min, 240 min, 960 min, 1,020 min, 1,080 min. Inhibitors were prepared freshly before usage in the following solutions or buffers: PMSF in EtOH, N-p-tosyl-L-phenylalanine chloromethyl ketone (TPCK) (SigmaAldrich, #T4376-100MG) in tris-HCl working buffer, Nα-tosyl-L-lysine chloromethyl ketone hydrochloride (TLCK) (SigmaAldrich, #T7254-100MG) in 1 mM HCl (due to instability in working buffer). Inhibitors were added 20 min after trypsin addition (final concentrations per well: 1 mM PMSF, 100 µM TPCK, 100 µM TLCK). Inbetween read-out time points 30 min and 1,080 min, the plate was covered with a sealing film and incubated at 25 °C shaking at 450 rpm in a Thermo mixer comfort. Enzyme substrates were dissolved in 100% DMSO and then further diluted in their corresponding working buffer for usage during the assay. The complete activity test set-up with trypsin was also investigated in presence of 15 µL human plasma per well.
For testing chymotryptic activity of trypsin, several workflow steps were modified as follows. Tris-HCl working buffer with $CaCl_2$ (100 mM tris-HCl, 10 mM $CaCl_2$, pH 7.8) and a substrate specifically cleavable by chymotryptic activity were used (100 nmol per well N-succinyl-Ala-Ala-Pro-Phe-p-nitroanilide, SigmaAldrich, #S7388-100MG). The same inhibitors were added after 180 min instead of 20 min due to lower chymotryptic activity. As described for trypsin, tryptic and chymotryptic activity was tested accordingly using 1 µg chymotrypsin (sequencing-grade, #V1062, Promega) as control.

The obtained absorption results were used for calculating the nmol substrate conversion per time intervall (min) as follows. Absorption values were corrected by their blank value (**Equation 5**). Samples comprising the corresponding buffer and substrate before time point 0 min were considered as blanks. The optical path length (**Equation 6**) was determined by the well dimensions given by the microtiter plate (Greiner Bio-One, Frickenhausen, Germany) and the used reaction volume. Concentrations of converted substrate were then calculated according to the law of Beer-Lambert[146] using the extinction coefficient of 4-nitroaniline (8,800 $M^{-1}cm^{-1}$) and considering the optical path length (**Equation 7**). This extinction coefficient was used for both activity calculations since 4-nitroaniline is the reaction product after cleavage of both types of substrates. Concentration results were multiplied with 100 µL well volume for plotting converted substrate in nmol against time intervall in min.

$$A_{corrected} = A_{measured} - A_{blank} \tag{5}$$

$A_{corrected}$: Blank-corrected absorption

$A_{measured}$: Measured absorption of sample after enzyme addition

A_{blank}: Absorption of blank (working buffer with substrate & without enzyme)

$$l = \frac{V}{\pi * r^2} \tag{6}$$

l: Optical path length (cm)

V: Well volume (cm^3)

r: Well radius (cm)

$$c = \frac{A}{\epsilon * l} * 1000 \tag{7}$$

c: Concentration of measured substance (mM)

A: Blank-corrected absorption

ϵ: Extinction coefficient of measured substance ($M^{-1}cm^{-1}$)

l: Optical path length (cm)

4 Results

4.1 General factors influencing IA-LC-MS/MS assays applied to plasma analyses

4.1.1 Optimization of peptide measurement by parallel reaction monitoring

The general workflow for the IA-LC-MS/MS assay approach mainly used in this work included proteolytic digestion of proteins into peptides, immunoaffinity enrichment using antibodies for capturing peptides of interest and read-out by LC-MS/MS using the targeted acquisition mode parallel reaction monitoring (PRM). Specimen such as serum or plasma were directly proteolyzed (**Figure 12**), whereas tissue or cell pellet samples required lysis and total protein determination extending the processing time from 23 hours by approximately 5 hours to 28 hours until start of LC-MS/MS read-out. This assay approach was developed on the basis of the SISCAPA method[108] and a detailed step-by-step presentation of this peptide-targeting method was published in

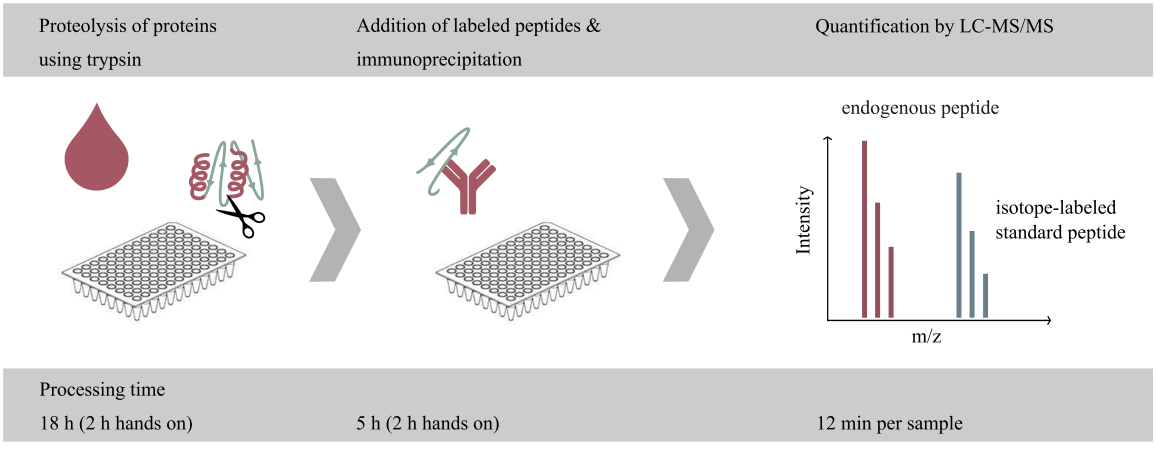

Figure 12: General IA-LC-MS/MS workflow for serum or plasma specimen. This workflow included proteolysis of proteins to peptides, enrichment with peptide-targeted antibodies in 96-well format and read-out by LC-MS/MS. A total processing time of 23 h with approximately 4 h hands on time is required and measurement time per sample is only about 12 min. Processing time is increased by about 5 h when tissue or cells are measured due to sample lysis and total protein determination (not shown here). Taken from Anselm *et al.* 2021[132].

Anselm *et al.* 2021[132]. Measurements during development were analyzed either by peak intensity of the non-labeled peptide or by the peak intensity ratio between non-labeled peptide and labeled peptide standard. Non-labeled peptide was either a product from digested endogenous or recombinant protein or was synthesized for preparation of a calibration curve. The peak intensity is displayed generally as area under the curve (AUC), whereas peak intensity ratio is termed ratio AUC. The following peptides were targeted for measurement of DILI-relevant proteins in biofluids and tissue or cell specimen from human or rat (**Table 12**). Only parts of the full molecular weights of MCSF1R and K18 annotated in Uniprot were used to calculate from peptide to protein since only the shedded receptor part of MCSF1R or the caspase-cleaved part of K18 (for ccK18) were of interest for these particular proteins. Peptides were chosen based on their sequence length and their position within the protein. For instance, the MCSF1R peptides were chosen to be in the extracellular receptor part of the protein for accessibility in serum and plasma specimen. The ccK18 peptide was chosen based on the specific caspase 3 cleavage site[147].

Table 12: General parameters of proteins related to DILI and relevant peptides

Protein name	**Species**	**Uniprot ID[1]**	**MW (Da)**	**Peptide**	**aa position**
OPN	Human	P10451	35,401	YPDAVATWLNPDPSQK	36-51
	Rat	P08721	33,228	HSDAVATWLKPDPSQK	36-51
HMGB1	Human	P09429	24,878	GEHPGLSIGDVAK	115-127
	Rat	P63159	24,747	GEHPGLSIGDVAK	115-127
	Human	P09429	24,878	RPPSAFFLFCSEYRPK	97-112
GLDH	Human	P00367	55,973	HGGTIPIVPTAEFQDR	481-496
	Rat	P10860	61,377	HGGTIPVVPTAEFQDR	481-496
K18	Human	P05783	47,897	AQIFANTVDNAR	138-149
	Rat	Q5BJY9	47,761	AQIFANSVDNAR	131-142
	Human	P05783	47,897	LLEDGEDFNLGDALDSS--NSMQTIQK	383-407
ccK18	Human	P05783	18,118[2]	LLEDGEDFNLGDALD	383-397
	Human	P05783	3,726[3]	SSNSMQTIQK	398-407
	Rat	Q5BJY9	3,729[3]	SSNSMQTVQR	391-400
MCSF1R	Human	P07333	56,982[4]	VIPGPPALTLVPAELVR	198-214
	Rat	Q00495	57,660[4]	ESTSTGIWLK	185-194
	Rat	D4ACA7	60,415[4]	AHNNVGNSSQFFR	529-541
	Rat	D4ACA7	60,415[4]	ESTSIGIR	228-236
	Rat	D4ACA7	60,415[4]	VILQSQLPIGTLK	168-179

[1] Data based on UniProt release 2021_06 (rat) and Uniprot release 2019_04 (human)
[2] Middle part of caspase-cleaved keratin 18
[3] C-terminal part of caspase-cleaved keratin 18
[4] Shedded soluble receptor part of MCSF1R

General factors regarding assay conditions can influence the measurement of each peptide, thus, several optimization steps were required for quantification via IA-LC-MS/MS. First of all, each peptide required optimization of the normalized collision energy (NCE) for optimal peptide fragmentation in the MS instrument. Thus, all peptides were measured with a NCE range between 10 and 35 as shown exemplary for the human MCSF1R peptide in **Figure 13** and optimal NCEs were summarized for each peptide in **Table 13**. Not only fragment intensity was important for peptide quantification, but also the fragment pattern after collision was considered when deciding for an optimal NCE (**Figure 13**). More fragments show a higher intensity with a NCE of 25 compared to 20 in case of the MCSF1R peptide (y6+, y13++, y15++), hence, providing more specificity to measure the peptide of interest.

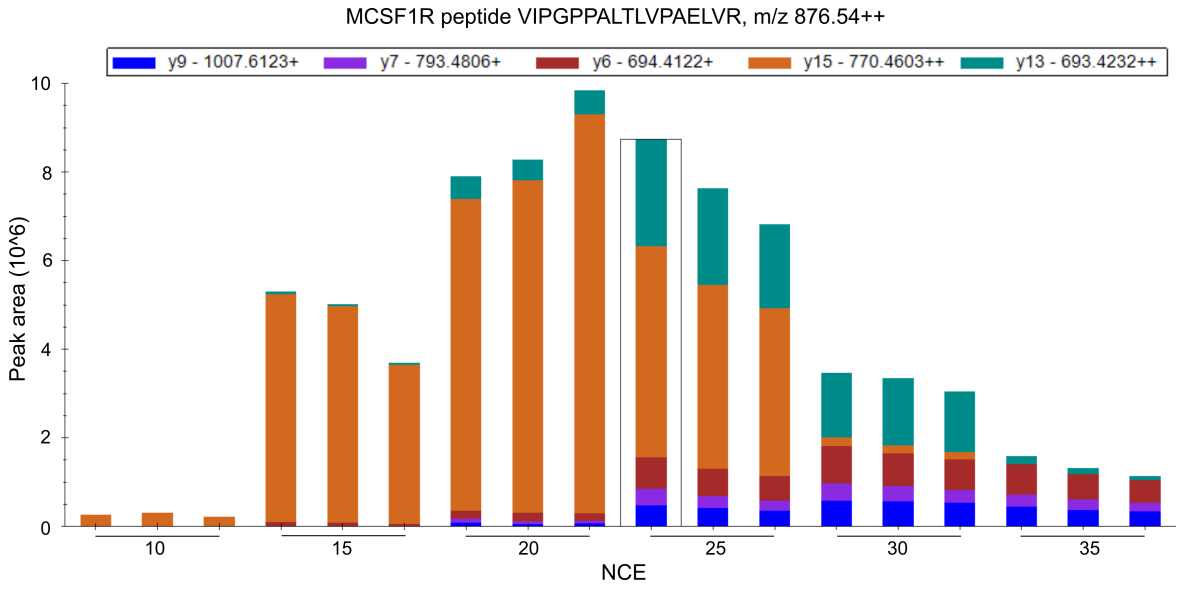

Figure 13: Impact of normalized collision energy (NCE) on peptide detection and quantification. Exemplary fragment pattern and peak intensities produced by MS/MS measurement of the human MCSF1R peptide using a NCE ranging from 10 to 35 (n = 3 for each NCE with 100 fmol peptide on column per run). Highest summed peak intensity: NCE of 20. Best peak pattern: NCE of 25 (framed).

Furthermore, double and triple charged precursor ions were tested and the precursor ions with highest resulting peak intensities were chosen (**Table 13**). The fragments (at least four) with highest peak intensity were listed as well and were chosen for peptide quantification to further increase the specificity of peptide quantification. Usually, peptides were isotopically labeled with C-terminal lysine or arginine due to the cleavage specificity of trypsin. However, no lysine or arginine could be chosen for isotope-labeling of the ccK18 peptide due to its characteristic C-terminal caspase-cleavage site (-DALD). Thus, leucine was chosen for labeling and isotope-labeled amino acids were chosen for both N-terminal leucines to increase peptide mass and the difference between labeled

and endogenous peptide. In this case, b-ions were chosen for peptide quantification due to the labeled N-terminus instead of labeled C-terminus.

Table 13: Precursor ions and fragments selected for peptide quantification. Isotope-labeled amino acids shown in **bold**

Protein	Peptide	Precursor (m/z) non-labeled	Precursor (m/z) labeled	NCE	Fragments for quantification
OPN	YPDAVATWLNPDPSQ**K**	901.44++	905.45++	25	y4+, y6+, y7+, y11+
	HSDAVATWLKPDPSQ**K**	593.97+++	596.64+++	25	y4+, y6+, y7+, y8+, y15++
HMGB1	GEHPGLSIGDVA**K**	640.34++	644.34++	25	y7+, y9+, y10+, y10++, y11++
	RPPSAFFLFCSEYRP**K**	668.01+++	670.68+++	25	y4+, y7+, y8+, y8++
GLDH	HGGTIPVVPTAEFQD**R**	869.45++	874.45++	25	y8+, y9+, y11+, y12+, y14+
	HGGTIPVVPTAEFQD**R**	593.97+++	596.64+++	20	y6+, y8+, y8++, y9++
ccK18	**LL**EDGEDFNLGDALD	818.37++	825.39++	10	b10+, b13+, b12++, b13++, b14++
	SSNSMQTIQ**K**	569.27++	574.27++	20	y5+, y6+, y7+, y8+, y8++
K18	AQIFANTVDNA**R**	660.34++	665.34++	20	y7+, y8+, y9+, y10+, y10++
	AQIFANSVDNA**R**	653.33++	658.34++	20	y7+, y8+, y9+, y10+, y10++
	LLEDGEDFNLGDALDSS-NSMQTIQK	914.09+++	916.76+++	20	y4+, y7+, y8+, y10+, y11+, y12+
MCSF1R	VIPGPPALTLVPAELV**R**	871.53++	876.54++	25	y6+, y7+, y9+, y13++, y15++
	ESTSTGIWL**K**	561.30++	565.30++	20	y5+, y6+, y7+, y8+
	ESTSIGI**R**	431.74++	436.74++	20	y3+ to y7+, y3++ to y7++
	AHNNVGNSSQFF**R**	739.35++	744.35++	25	y8+, y9+, y10+, y11+, y12++

4.1.2 K18 and ccK18 peptide stability and chromatographic performance

A set of calibration samples comprising a dilution curve of non-labeled synthetic peptide in constant stable isotope-labeled standard (SIS) peptide concentration was tested for quantification performance of the peptides. Calibrators were tested in serial 1:3 dilution starting from 1,000 fmol for ccK18. Major carryover was observed when measuring wash runs (0.1% FA, 1 µL on column) after calibrators for the ccK18 peptide with the C-terminus ending in -DALD (**Figure 14A, B**).

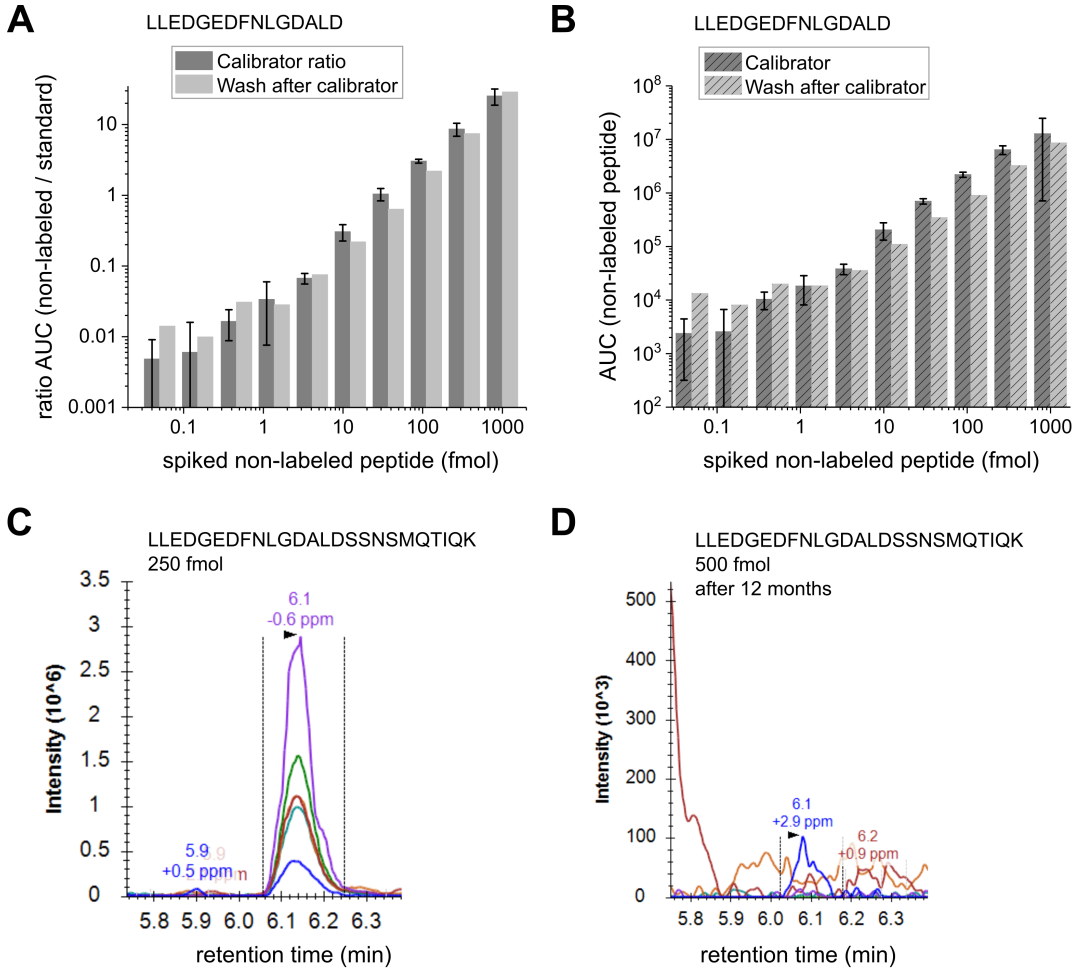

Figure 14: Carryover or intensity loss of ccK18 or K18 peptide. (A, B) Calibrators (0.05 fmol to 1,000 fmol non-labeled peptide in 35 fmol standard per IP well, n = 3) and wash runs (0.1%FA, n = 1) were measured for the ccK18 peptide. **(A)** Peptide ratios of calibrators and wash runs or **(B)** intensity of non-labeled peptide (5 µL calibrator eluate on column, 1 µL wash on column). **(C, D)** Calibrator for the K18 peptide with non-labeled peptide was measured within a time period of 12 months. Peptides were stored in stock solution (20% DMSO). Peaks of non-labeled peptide of **(C)** 250 fmol non-labeled peptide per IP well with 5 µL calibrator eluate on column and **(D)** 500 fmol non-labeled peptide per IP well with 5 µL calibrator eluate on column after 12 months storage of stock are shown.

This was observed either with AUC ratios (**Figure 14A**) or with plain intensity signals (**Figure 14B**). A complete loss of signal was observed after 12 months for the long K18 peptide comprising the non-cleaved caspase-cleavage site (**Figure 14C, D**). Moreover, precipitations were observed in the stock solution indicating aggregated peptide. This was observed for the available analog peptide from other species and also to a certain extent for the ccK18 peptide stock (peptide ending in -DALD). No reproducible results with regard to calibration curves could be generated for these peptides (data not shown).
Due to the observed carryover of the ccK18 peptide (-DALD) and the instability of the long K18 peptide, the peptides SSNSMQTIQK / SSNSMQTVQR (ccK18, human, rat) and AQIFANTVDNAR / AQIFANSVDNAR (K18, human, rat) were further investigated for the respective proteins (see **4.1.4** and **4.2**). ELISA kits were available for human specimen and quantification of K18 and ccK18 was continued with the ELISA approach for human samples involving investigation of matrix and sampling effects (see **4.3**).

4.1.3 Effect of antibody and spiked internal standard amount on peptide recovery

Two major parameters influencing peptide quantification are antibody (AB) and stable internal standard (SIS) amount per sample well during peptide enrichment. Endogenous HMGB1 peptide was initially hardly detectable in human plasma. First, this peptide was tested in 1 µL to 15 µL human plasma (n = 3 per volume) with varying AB and internal standard amount per IP well (**Figure 15**). Increasing AB amount improved recovery of endogenous HMGB1 leading to reproducible measurement using 5 µg AB even in 5 µL human plasma (**Figure 15C**). However, due to higher AB amount also the blank signal increased more than 2-fold in comparison to 1 µg AB. The blank sample comprised surrogate matrix with 15 µL of 60 mg/mL BSA in PBS to mimic the protein content of 15 µL plasma sample. Second, SIS amounts of 2 fmol and 10 fmol per well resulted in improved AUC ratios using the lower amount of standard (**Figure 15E**). Surprisingly, also the blank signal (BSA control) increased using 2 fmol internal standard (**Figure 15E**) compared to 5 fmol internal standard (**Figure 15D**). Two different AB purification Lots were used for optimizing AB (**Figure 15A-C**) and SIS amounts (**Figure 15D,E**), hence, the ratios and background of (**Figure 15C**) and (**Figure 15D**) cannot be compared directly. A combination fo 5 µg AB and 5 fmol SIS per IP was selected for further HMGB1 measurement, because a stable signal of endogenous HMGB1 could be measured even in 1 µL plasma (**Figure 15D**). Furthermore, a fold change of 6 was observed when using 5 fmol SIS between endogenous HMGB1 signal in 15 µL plasma compared to the BSA control, which shows higher sensitivity than using 2 fmol SIS with a fold change of 4.8 for the same signal-to-noise comparison.

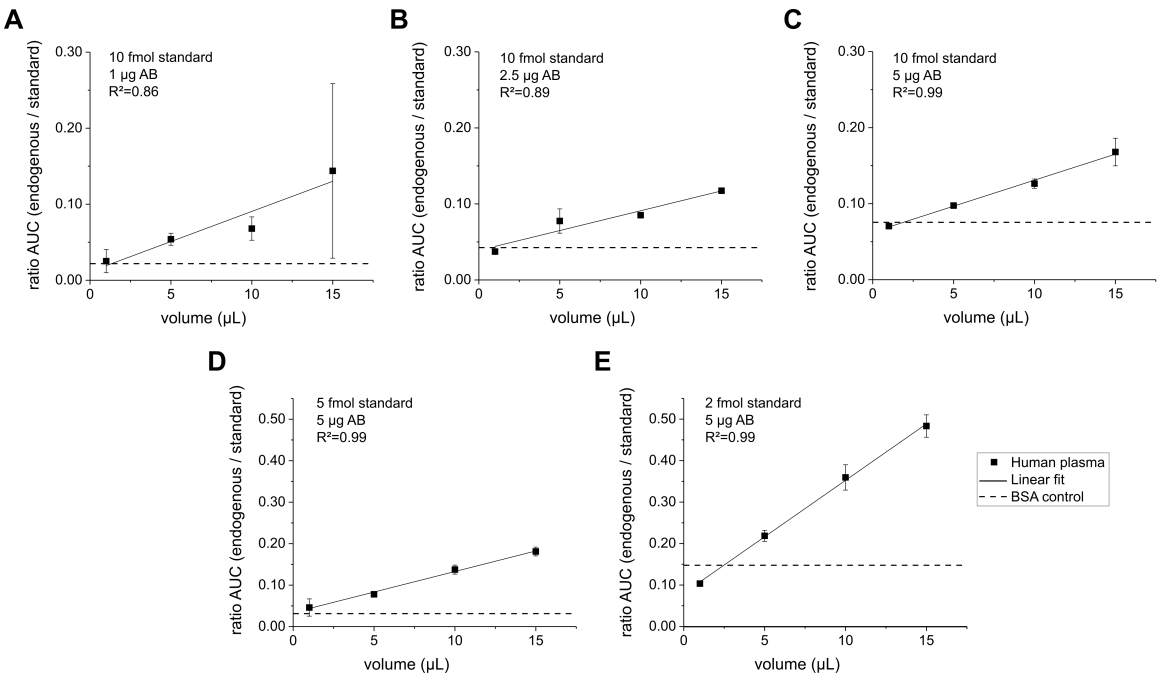

Figure 15: Impact of antibody (AB) and internal standard amount on HMGB1 peptide quantification in human plasma. The HMGB1 peptide GEHPGLSIGDVAK was measured in 1 µL to 15 µL human plasma (n = 3 per volume) with increasing AB amount from 1 µg to 5 µg **(A-C)** and decreasing internal standard amount **(D, E)**. Endogenous peptide signals improve with increasing AB or decreasing SIS amount. BSA control = blank with 15 µL surrogate matrix comprising 60 mg/mL BSA in PBS.

To determine the optimal sample volume, different volumes of plasma from a healthy volunteer were analyzed (**Figure 16A-D**). In total, 15 µL plasma was digested in a final digestion volume of 150 µL and the equivalent volumes compared to 1 µL, 5 µL, 10 µL, and 15 µL, were used for the peptide enrichments, e.g., 100 µL digestion product was used for IP to enrich peptide from 10 µL plasma sample. Peptide enrichment was multiplexed for the shown peptides by adding all antibodies in one IP well. Regression analysis showed good regression coefficients ($R^2 = 0.99$) for all investigated analytes indicating well performing peptide enrichment throughout 1 µL to 15 µL plasma. A sample volume of 15 µL was used for all further experiments to provide maximum sensitivity in case unknown samples have less endogenous peptide than the plasma sample used here.

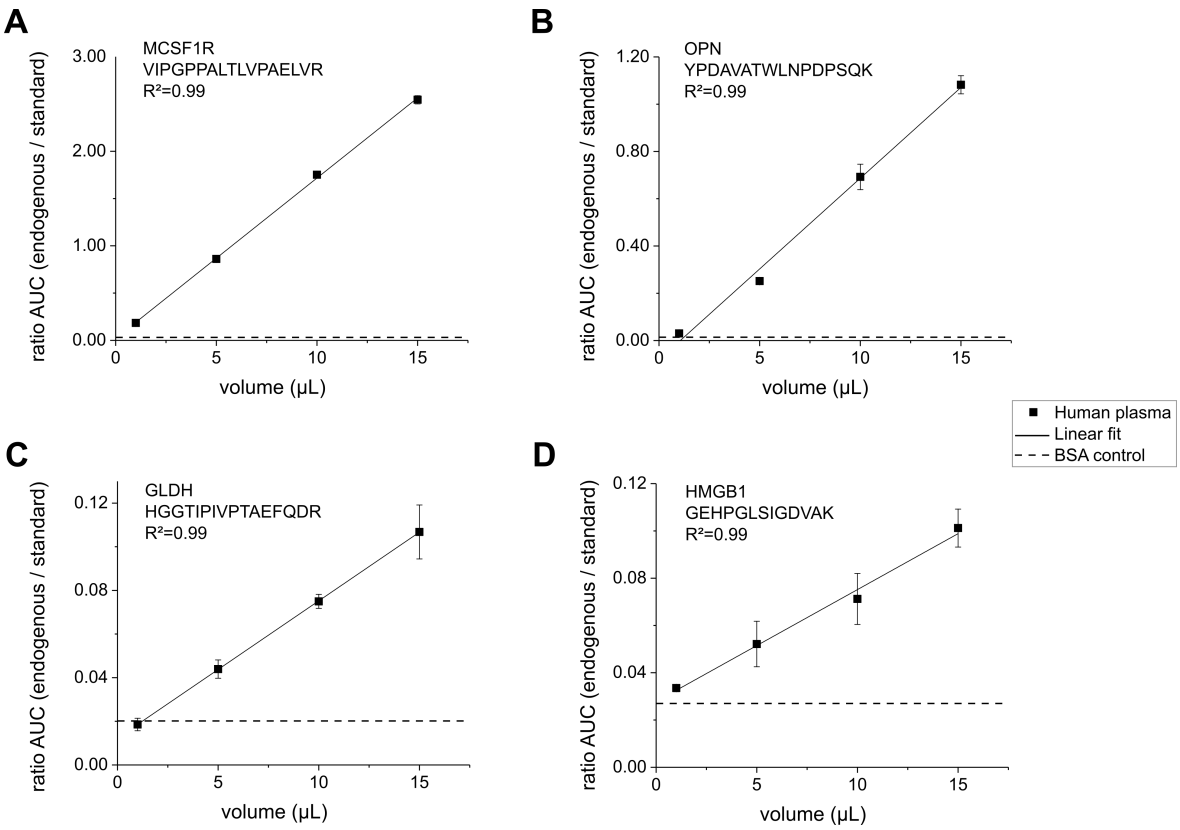

Figure 16: Endogenous DILI-related proteins measured by IA-LC-MS/MS in human plasma. **(A)** MCSF1R (2.5 µL AB, 25 fmol SIS), **(B)** OPN (2.5 µL AB, 25 fmol SIS), **(C)** GLDH (2.5 µL AB, 10 fmol SIS), and **(D)** HMGB1 (5 µL AB, 5 fmol SIS) could be measured in at least 5 µL to 15 µL human plasma (n = 3 per volume). Only MCSF1R could be measured in 1 µL plasma, whereas OPN, GLDH, and HMGB1 peptide signals were close to or the same as the ratio in the BSA control (surrogate matrix).

4.1.4 Impact of trypsin on peptide release and recovery

K18 and ccK18 were hardly detectable in plasma presumably due to its high dynamic range in protein concentration caused by high content of serum albumin or IgG and low concentration in relevant DILI analytes. Liver cell line lysate (HepG2) was expected to have high concentrations in K18 since this protein is part of the intermediate filament in one-layered epithelial cells of inner organs such as the liver. To determine whether K18 quantification was affected by plasma protein content, 20 µg HepG2 lysate was measured in the presence and absence of 15 µL plasma (**Figure 17**). The AUC ratio of the K18 peptide AQIFANTVDNAR was about 70-fold less in plasma-spiked lysate than in non-spiked HepG2 lysate. Non-spiked plasma showed an AUC ratio similar to the blank AUC ratio (BSA control). This was investigated further by measuring

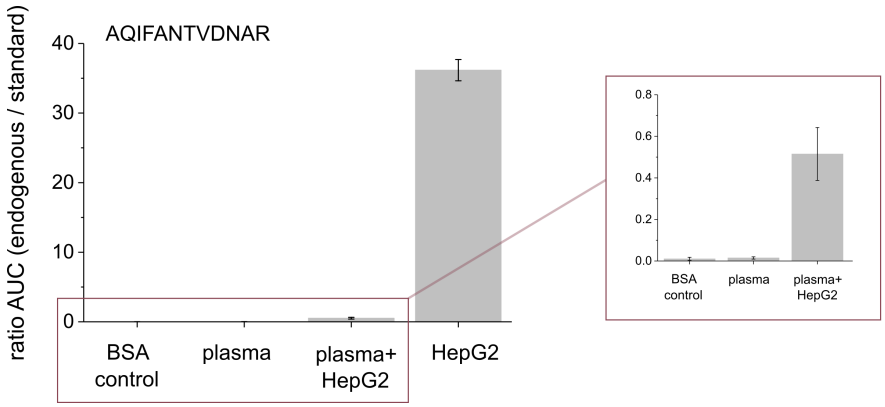

Figure 17: Loss of endogenous K18 peptide in plasma. K18 peptide AQIFANTVDNAR recovery was compared in non-spiked HepG2 cell lysate (20 µg) and spiked into plasma (20 µg lysate in 15 µL plasma) measured with 10 fmol SIS and 5 µg AB (n = 3 per sample). A 70-fold decrease was observed in the spiked plasma sample. K18 recovery in non-spiked plasma was comparable to the observed AUC ratio of the BSA control.

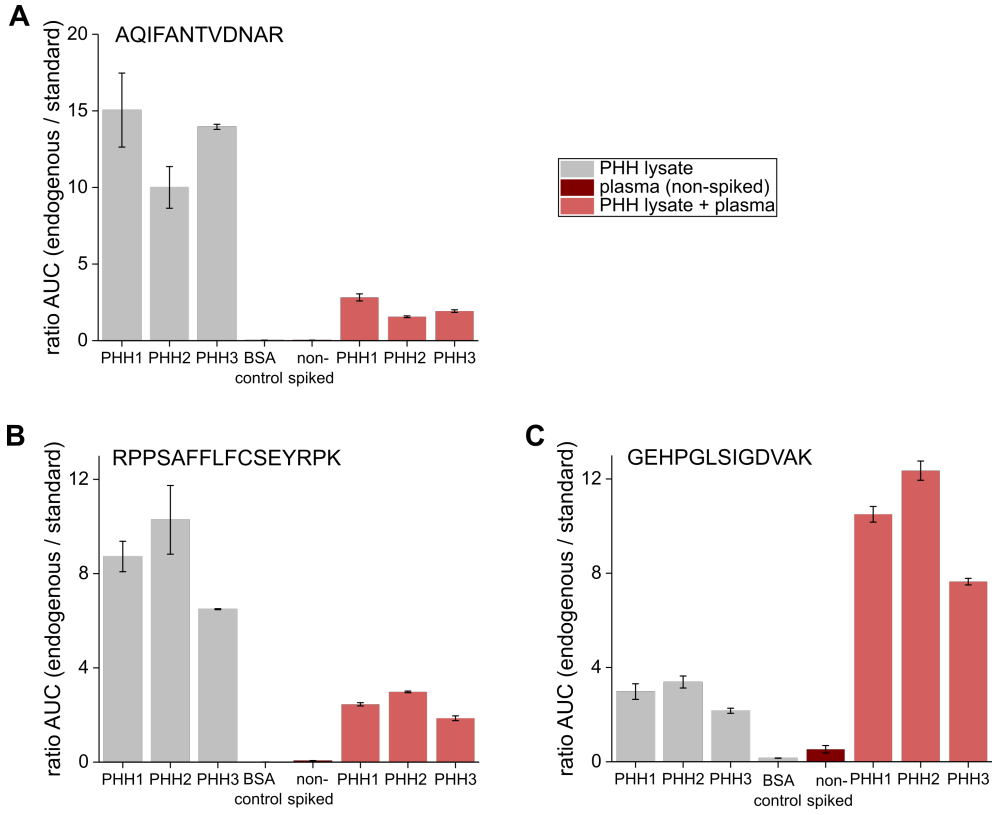

Figure 18: Impact of sample matrix on K18 and HMGB1 peptide recovery. Loss of peptide was confirmed for **(A)** the K18 peptide (5 fmol SIS, 5 µg AB) and **(B)** the HMGB1 peptide RPPSAFFLFCSEYRPK (4 fmol SIS, 5 µg AB) by measurement of 10 µg primary human hepatocytes (PHH, n = 3) without plasma or spiked in 15 µL plasma. **(C)** Recovery of the HMGB1 peptide GEHPGLSIGDVAK was improved by spiking lysate in plasma (4 fmol SIS, 5 µg AB).

primary human hepatocytes (PHH) of three donors spiked in plasma and non-spiked (**Figure 18A**). PHH were selected for investigation to resemble liver cells better than HepG2 cells. The loss in K18 signal in plasma was observed for all three PHH samples but with a fold change of about 6 instead of 70, which might be caused by the change in type of lysate. The internal standard amount of the K18 peptide was decreased from 10 fmol to 5 fmol to increase sensitivity. Nevertheless, the AUC ratios in BSA control and plasma without lysate was still similar. In addition to the K18 peptide, both HMGB1 peptides were investigated in the experimental set-up with PHH cells in the course of investigating HMGB1 recovery during method development (**Figure 18B, C**). Similar to the K18 results, peptide loss was observed for the HMGB1 peptide RPPSAFFLFCSEYRPK in samples with plasma (**Figure 18B**). In contrast to this, recovery of the HMGB1 peptide GEHPGLSIGDVAK was even increased when PHH was measured spiked in human plasma (**Figure 18C**).
The major difference in digestion procedure between plasma-spiked and non-spiked PHH lysate was the increased trypsin amount per IP well to proteolyze the plasma-spiked samples with a trypsin to protein ratio of 1:20 (45 µg trypsin versus about 900 µg plasma protein plus 20 µg PHH lysate compared to 0.5 µg trypsin versus 10 µg PHH lysate).
Therefore, the effect of different trypsin to protein ratios (1:20 and 1:100) was investigated by digesting PHH lysate accordingly (**Figure 19**). The investigated K18 peptide and the HMGB1 peptide RPPSAFFLFCSEYRPK showed again a similar response to decreasing the trypsin amount compared to total protein amount for each of the three PHH lysates (**Figure 19A, B**). In contrast to the K18 peptide and the HMGB1 peptide ending in -YRPK, less endogenous HMGB1 peptide GEHPGLSIGDVAK was observed with less trypsin in relation to total protein amount (**Figure 19C**).
Due to the contrary effect of trypsin amount on the recovery of both HMGB1 peptides, digestion kinetics were investigated by digesting HepG2 lysate for K18 (**Figure 20A**) or 200 fmol recombinant HMGB1 protein (**Figure 20B, C**), both spiked in plasma and processed in triplicates. Recombinant protein was used for HMGB1 since the experiments were performed at a later time point and HepG2 lysate was used due to sample availability. Peptide loss over 16 h proteolysis time was observed for the K18 peptide and the HMGB1 peptide RPPSAFFLFCSEYRPK, whereas the highest concentration of the HMGB1 peptide GEHPGLSIGDVAK was observed after 16 h proteolysis. The samples for a proteolysis time of zero hours were prepared by adding 10 mM PMSF directly before trypsin addition. Peptide ratios above an AUC ratio of 4 were measured in samples with zero proteolysis time for the K18 peptide and the HMGB1 peptide RPPSAFFLFCSEYRPK (**Figure 20A, B**). However, almost no peptide from recombinant protein was observed for the HMGB1 peptide GEHPGLSIGDVAK in the corresponding sample.

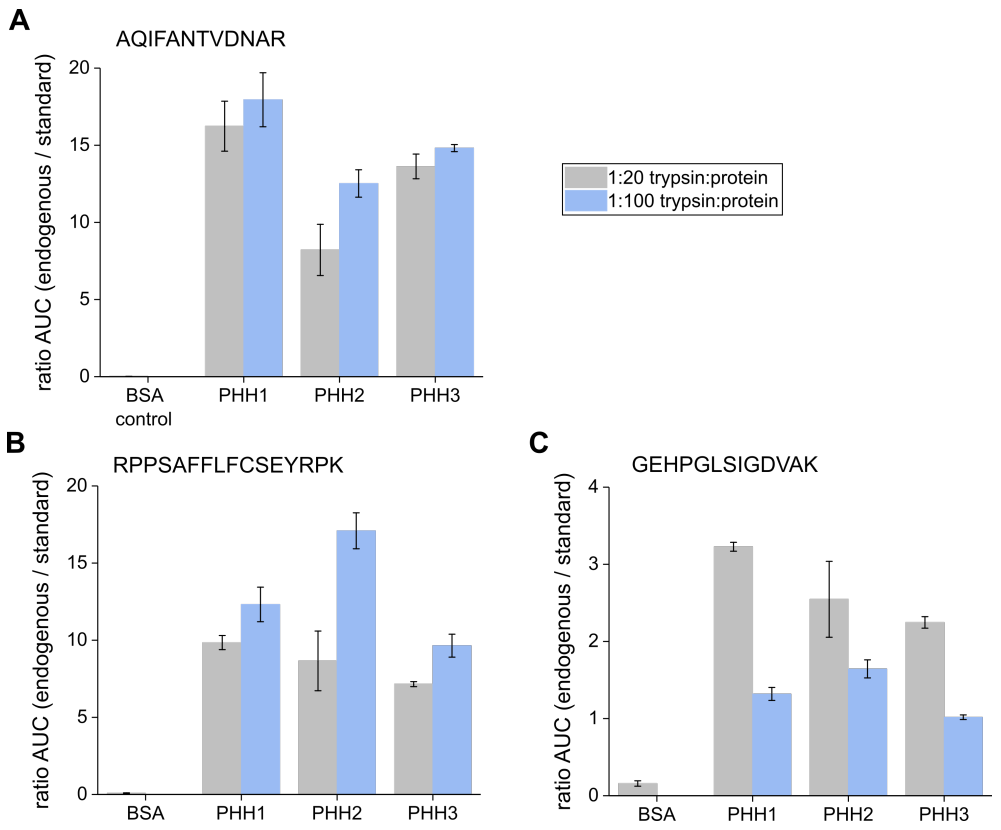

Figure 19: Different effect of trypsin to protein ratio on K18 and HMGB1 recovery. Primary human hepatocytes (PHH, 10 µg per sample, n = 3) were proteolyzed with trypsin to protein ratios of 1:20 and 1:100. Using less trypsin resulted in improved recovery of **(A)** the K18 peptide AQIFANTVDNAR and **(B)** the HMGB1 peptide RPPSAFFLFCSEYRPK. **(C)** Less trypsin during proteolysis resulted in less endogenous HMGB1 peptide GEHPGLSIGDVAK.

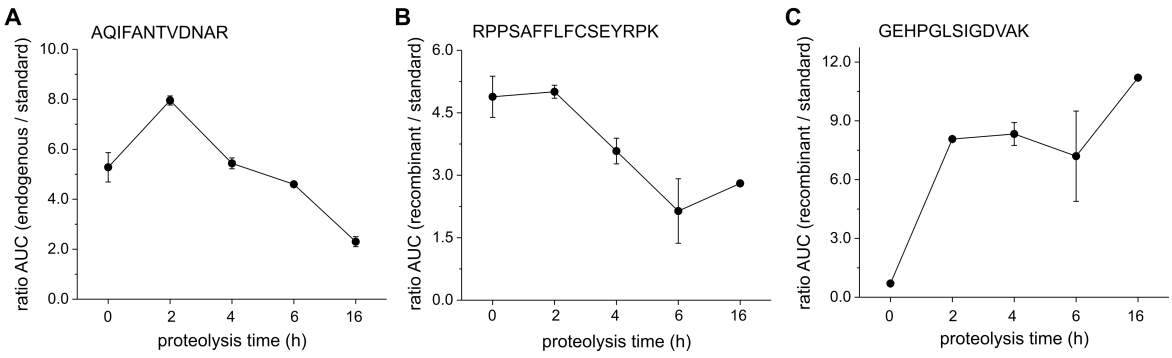

Figure 20: Digest kinetics for the K18 and HMGB1 peptides. HepG2 lysate (10 µg) spiked in 15 µL plasma was used for K18 assessment and recombinant protein (200 fmol) spiked in 15 µL plasma was used for HMGB1 assessment (5 fmol SIS for K18, 4 fmol SIS for HMGB1. 5 µg AB for all peptides). Peptide loss between 0 h and 16 h (n = 3 per time point) was observed for **(A)** the K18 peptide AQIFANTVDNAR and **(B)** the HMGB1 peptide RPPSAFFLFCSEYRPK, whereas the highest recovery for the HMGB1 peptide GEHPGLSIGDVAK was observed after 16 h **(C)**.

Since both trypsin-to-protein ratio and proteolysis time affected the peptide recovery of K18 and HMGB1, contamination of chymotrypsin or tryptic side reactivity was assumed as a possible reason for peptide loss. Hence, all three peptides were investigated *in silico* for chymotryptic cleavage sites by the online tool PeptideCutter[139] (**Figure 21A-C**). Furthermore, the corresponding synthetic isotope-labeled HMGB1 and K18 peptides were treated with trypsin and the theoretically possible chymotryptic fragments and the full length peptides were then targeted as precursor ions by MS (**Figure 21D-F**). Digestion solution without peptide and trypsin and samples without trypsin treatment (only peptide) or without added peptide (only trypsin) served as controls. Loss of full-length peptide was observed for the K18 peptide and the HMGB1 peptide RPPSAFFLFCSEYRPK (**Figure 21D, E**). The recovery of full length HMGB1 peptide GEHPGLSIGDVAK after trypsin treatment was not clear due to the high standard deviation (**Figure 21F**). The measured three replicates provided an AUC range between $1x10^6$ and $1x10^7$ possibly caused by instable MS measurement since this analysis was based on raw signals without normalization. However, AUC measurement without ratios is required in this case since internal standards were not available for the precursors with chymotryptic cleavage sites. Peptide fragments matching to the chymotryptic cleavage sites were detected in the trypsin treated sample for the HMGB1 peptide RPPSAFFLFCSEYRPK (**Figure 21E**). Especially the fragments RPPSAFFLF and RPPSAFFLFCSEY were represented.

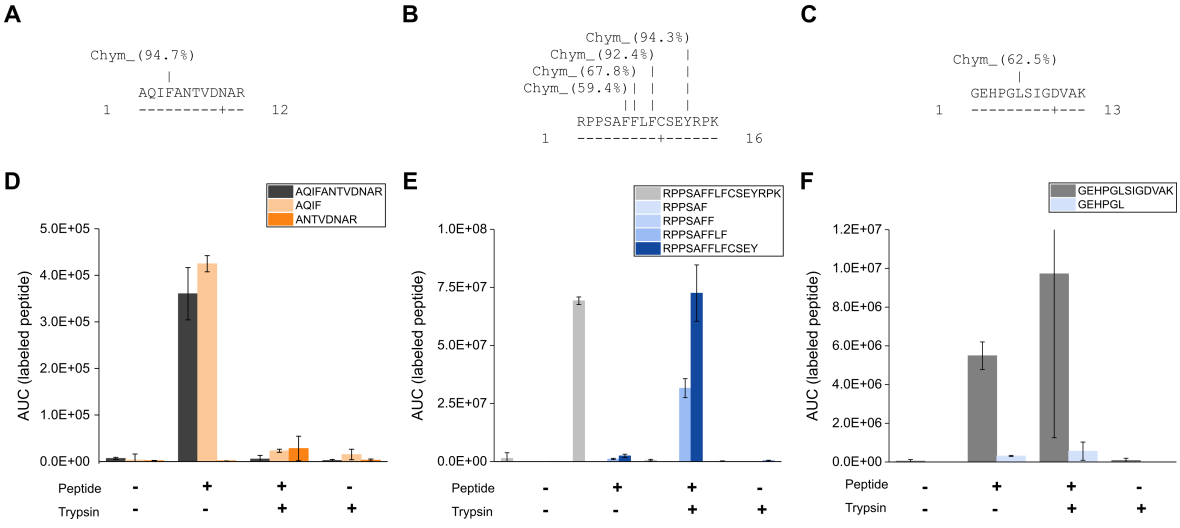

Figure 21: Full-length and chymotryptic fragments of the K18 and HMGB1 peptides on MS/MS level. (A - C) Chymotryptic fragments of the K18 and HMGB1 peptides were investigated *in silico* using the PeptideCutter environment[139]. **(D - F)** An amount of 100 fmol labeled peptide (trypsin treated or controls) was loaded on LC column and peptide fragments and the full length peptides were targeted by PRM. Peptide fragments were observed in presence of trypsin for the HMGB1 peptide RPPSAFFLFCSEYRPK **(E)**.

Fragments for the K18 peptide and the HMGB1 peptide GEHPGLSIGDVAK could not be confirmed in the samples comprising peptide and trypsin (**Figure 21F**). The fragment AQIF was observed in the K18 peptide sample (**Figure 21D**). However, the fragment ions b2 and b3 were measured for this peptide, which are too short for reliable confirmation of this fragment. Due to the chymotryptic N-terminal fragments observed for the HMGB1 peptide RPPSAFFLFCSEYRPK, the tryptic and chymotryptic activity of trypsin was then investigated (**Figure 22A, B**) and chymotrypsin was used as control (**Figure 22C, D**). This was performed using the method described by DelMar *et al.* in 1979. In case of an IA-LC-MS/MS approach, autolytic trypsin fragments are not impacting the MS analysis since they are removed during the immunoaffinity step. Hence, we are using a non-stabilized trypsin for digesting the high protein amounts in plasma (Worthington trypsin). We compared the chymotryptic activity of trypsin produced by Worthington with mass spectrometry-grade trypsin Gold from Promega, which is modified to increase resistance against autolytic digestion. Trypsin from both providers is treated with TPCK, a chymotrypsin-specific inhibitor[148]. The conversion of 100 nmol trypsin substrate (Nα-Benzoyl-L-arginine-4-nitroanilide hydrochloride) or chymotrypsin-specific substrate (N-Succinyl-Ala-Ala-Pro-Phe-p-nitroanilide) was monitored for 20 h. Various inhibitors including the general serine protease inhibitor PMSF, TPCK, and the trypsin-specific inhibitor TLCK[148] were tested for their impact on substrate conversion by trypsin or chymotrypsin. Blanks without substrate or without enzyme and substrate were carried as negative controls.
Less trypsin substrate was converted by Worthington trypsin than Promega Gold trypsin in presence of TLCK (**Figure 22A**). Other inhibitors did not affect the conversion of trypsin substrate. Chymotrypsin substrate was also converted but at a smaller conversion rate, which is why the inhibitors were added 180 min after start instead of 20 min after start as for the trypsin substrate. Promega Gold trypsin indicated a higher chymotryptic activity in general than Worthington trypsin (**Figure 22B**). Interestingly, chymotryptic activity was affected the most by the trypsin-specific inhibitor TLCK, followed by the serin protease inhibitor PMSF. TPCK did not affect the conversion of chymotrypsin substrate by both types of trypsin. PMSF and TLCK had an inhibitory impact on the conversion of chymotrypsin substrate by Worthington trypsin comparable to the effects observed for Promega Gold trypsin.
Chymotrypsin was used to study substrate and inhibitor specificity as a control. The inhibibtors PMSF, TPCK, and TLCK were added directly before substrate addition for maximum effect. The results showed that the trypsin substrate is indeed trypsin-specific since no substrate could be converted by chymotrypsin (**Figure 22C**). Almost the complete added chymotrypsin substrate was converted by chymotrypsin, even in presence of PMSF, TPCK, or TLCK. The inhibitors did not affect chymotrypsin substrate conversion by chymotrypsin (**Figure 22D**). The corresponding activity tests in presence of 15 µL plasma showed a slower conversion of tryptic substrate by trypsin and no signs of chymotryptic activity by trypsin (appendix **Figure 49**).

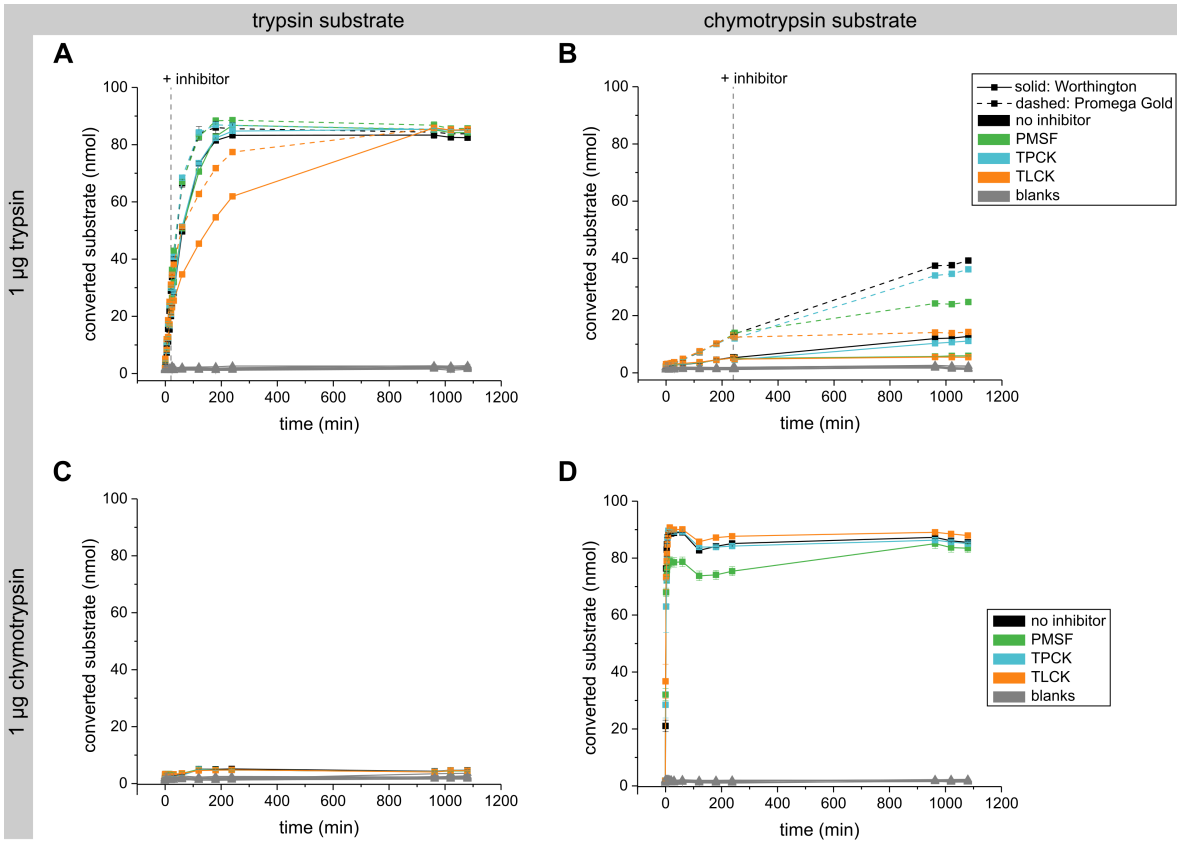

Figure 22: Conversion of trypsin and chymotrypsin substrate and its inhibition. **(A)** Trypsin substrate and **(B)** chymotrypsin substrate was converted in the presence of 1 µg trypsin (provided by Worthington or Promega Gold, n = 3 per condition, 100 nmol substrate per well). The following inhibitors were added to trypsin substrate or chymotrypsin substrate wells 20 min or 180 min after start, respectively: 1 mM PMSF, 100 µM TPCK, 100 µM TLCK. TLCK inhibited the conversion of chymotrypsin stubstrate the most. **(C)** Trypsin substrate was not converted in the presence of 1 µg chymotrypsin. **(D)** The conversion of chymotrypsin substrate in the presence of 1 µg chymotrypsin was not affected by inhibitors (added before start, n = 3 per condition). Blanks included samples without substrate and samples without enzyme and substrate.

Blank samples containing plasma but no trypsin or inhibitor showed neither tryptic nor chymotryptic activity (appendix **Figure 49**). In order to investigate the observed inhibitory effects on potential chymotryptic activity of trypsin, the impact of PMSF addition was tested on the recovery of the K18 peptide AQIFANTVDNAR and both HMGB1 peptides (**Figure 23**). PMSF was used since this reagent is easier accessible than TLCK. Concentrations of 1 mM to 10 mM PMSF were added directly before trypsin addition to plasma samples spiked with 200 fmol recombinant protein (n = 3 per PMSF level). BSA and addition of EtOH without PMSF to plasma served as controls.

Increasing the PMSF concentration before proteolysis resulted in improving recovery of the K18 peptide and the HMGB1 peptide RPPSAFFLFCSEYRPK (**Figure 23A, B**). However, PMSF addition resulted also in considerable loss of the HMGB1 peptide GEHPGLSIGDVAK with increasing PMSF concentration (**Figure 23C**). The observed rescue of the K18 and HMGB1 peptides AQIFANTVDNAR and RPPSAFFLFCSEYRPK was further investigated in rat plasma and liver samples of preclinical studies provided by Sanofi. Due to a change in one amino acid within the K18 peptide sequence between the protein sequences of human and rat, the peptide AQIFANSVDNAR was used for quantification in rat samples. The HMGB1 sequence is highly conserved, thus, the same peptide was used in rat samples.

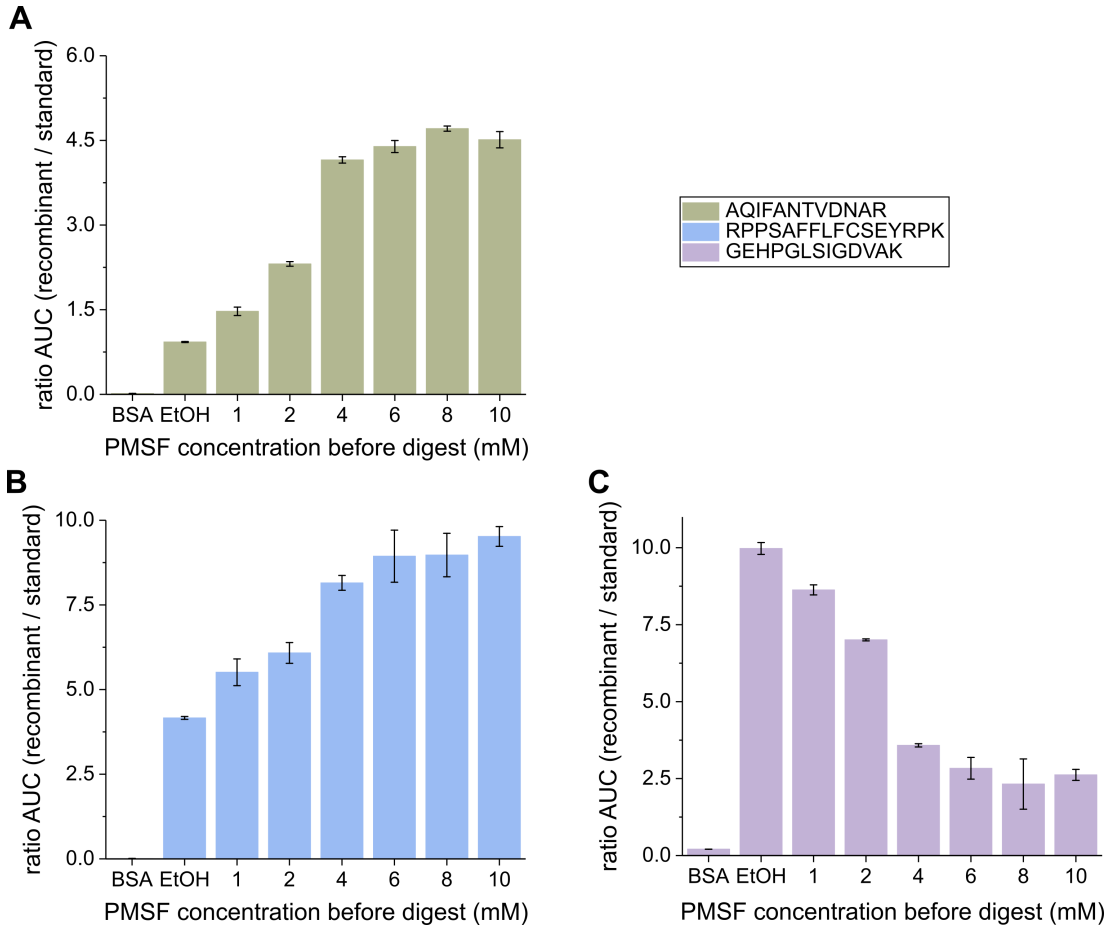

Figure 23: Effect of PMSF addition before proteolysis on K18 and HMGB1 peptide recovery. Recovery of 200 fmol recombinant protein in 15 µL plasma was tested (K18: 5 fmol SIS, HMGB1: 4 fmol SIS, K18 & HMGB1: 5 µg AB, n = 3 per condition). Peptide rescue was confirmed for **(A)** the K18 peptide AQIFANTVDNAR and **(B)** the HMGB1 peptide RPPSAFFLFCSEYRPK by PMSF addition before proteolysis. **(C)** Addition of PMSF before proteolysis resulted in loss of the HMGB1 peptide GEHPGLSIGDVAK.

Plasma samples of the study groups control and DAPM treated (250 mg/kg, sampling 24 h after treatment) were measured for K18 supplemented with and without 4 mM PMSF before proteolysis (**Figure 24A, B**). A peptide recovery plateau was reached with this PMSF concentration, therefore, further peptide rescue experiments were performed with this concentration. All control sample results remained below the BSA control blank even with PMSF addition (**Figure 24A**). Peptide rescue with PMSF was shown for 6 / 6 plasma samples of the treated rat group since higher AUC ratios than the blank ratio were observed compared to only 2 / 6 plasma samples above blank without PMSF (**Figure 24B**).

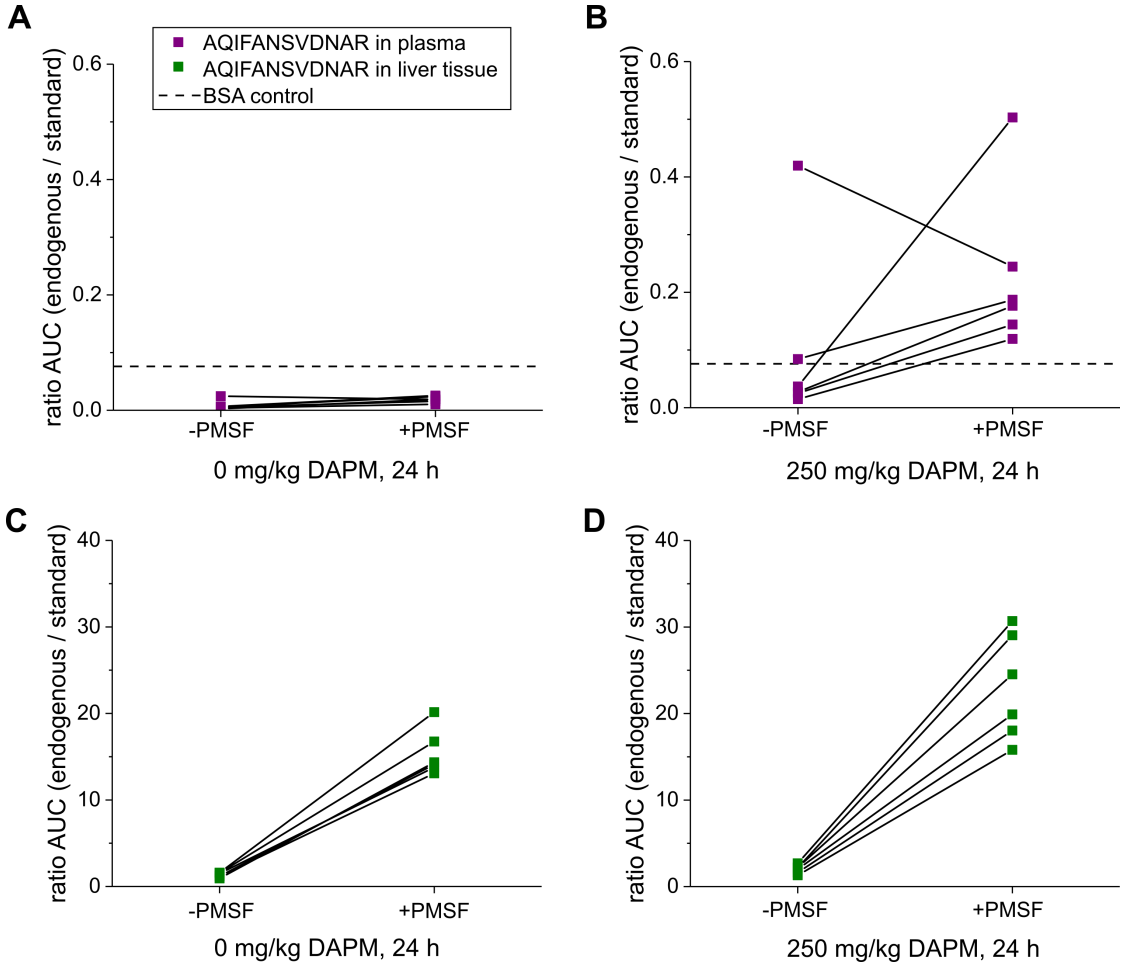

Figure 24: K18 peptide rescue in rat plasma and rat liver tissue. (A, B) Rat plasma (15 µL) and **(C, D)** rat liver samples (8 µg tissue lysate in 15 µL surrogate matrix) of control and DAPM treated rats (24 h after treatment) were measured without and with addition of 4 mM PMSF before proteolysis (5 fmol SIS, 5 µg AB, n = 2 replicates per sample, 6 samples per group). The K18 peptide could be rescued in the plasma samples of treated animals since all signals are above the blank signal when digested with PMSF **(B)**.

One sample showed less K18 peptide ratios in the sample with PMSF compared to the same sample without PMSF. K18 could be monitored in all liver rat samples compared to the BSA control independent of PMSF addition. Nevertheless, K18 peptide recovery was greatly increased by PMSF addition with a fold change of 11.8 ±2.1 or 11.5 ±1.1 (mean ±SD) for control or treated group, respectively (**Figure 24C, D**).
Similar results were observed for the HMGB1 peptide RPPSAFFLFCSEYRPK in rat plasma and rat liver from control and treated rats (**Figure 25**). HMGB1 was measurable in all samples and the peptide recovery was improved by PMSF with a fold change of 3.3 ±0.3 or 3.6 ±0.7 (mean ±SD) for plasma samples of the control or treated group, respectively (**Figure 25A, B**). The recovery was increased in liver samples by 2.6 ±0.5-fold or 2.8 ±0.3-fold for control or treated group (**Figure 25C, D**).

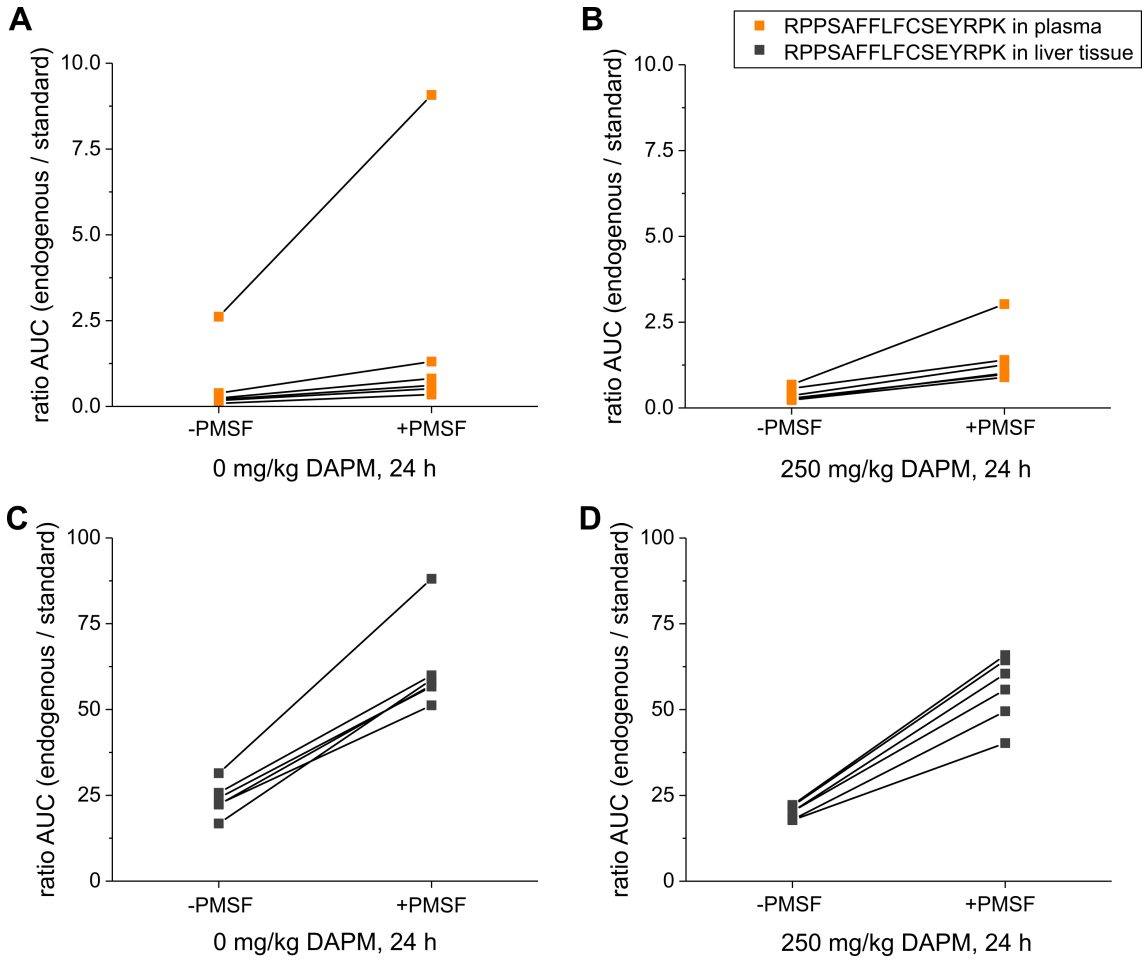

Figure 25: Improvement of HMGB1 peptide measurement in rat plasma and rat liver tissue. (A, B) Rat plasma (15 µL) and **(C, D)** rat liver samples (8 µg tissue lysate in 15 µL surrogate matrix) of control and DAPM treated rats (24 h after treatment) were measured without and with addition of 4 mM PMSF before proteolysis (4 fmol SIS, 5 µg AB, n = 2 replicates per sample, 6 samples per group). Recovery of the HMGB1 peptide was improved in both samples types.

Due the different proteolysis strategy, K18 could not be added to the multiplex for DILI analyte measurent in rat samples. Therefore, validation of the multiplexed method for DILI biomarker quantification in rat specimen was focused on the HMGB1 peptide GEHPGLSIGDVAK together with the other DILI-related proteins MCSF1R, OPN, GLDH, and ccK18 (see **4.2**).

4.1.5 New insights into the rat MCSF1R protein sequence

Due to different peptide sequences between different species within the corresponding protein regions of MSCF1R, two peptides were used for quantification in human, mouse, and rat plasma (**Figure 26**). Endogenous MCS1F1R could be measured readily in human plasma with the peptide VIPGPPALTLVPAELVR (**Figure 26A**). The analog peptide sequence in rats and mice is theoretically truncated to VHPEPPQIK, LEPSK, and LVR by tryptic cleavage sites (Uniprot ID Q00495 for rat and P09581 for mouse). Therefore, the peptide ESTSTGIWLK was initially targeted in rat and mouse specimen using IA-LC-MS/MS. The corresponding antibody was specificly produced against the entire peptide sequence for highest possible specificity. Endogenous MCSF1R could be measured in 1 µL to 15 µL mouse plasma with this AB-peptide combination, even with 50 fmol internal standard (**Figure 26B**). Endogenous rat MCSF1R could not be detected even with the minimum amount of 1 fmol internal standard per IP well (**Figure 26C**). Tests with altered IP conditions such as longer peptide enrichment time from 1 h to 3 h or even overnight could not recover the peptide in rat plasma (data not shown), which was easily detectable in mouse plasma.

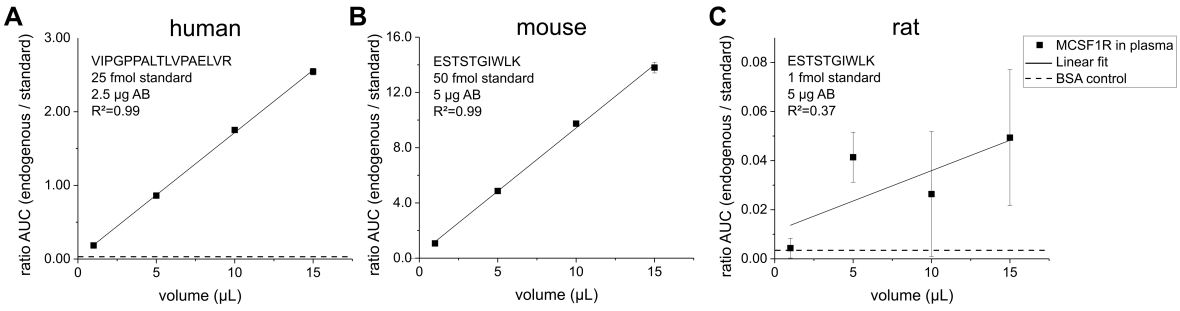

Figure 26: MCSF1R analyses in human, mouse, and rat plasma. MCSF1R could be quantified in 1 µL to 15 µL **(A)** human plasma and **(B)** mouse plasma. Another peptide was targeted in mouse plasma than in human plasma because the corresponding mouse / rat MCSF1R sequence comprises two tryptic cleavage sites compared to the human MCSF1R sequence. Due to sequence identity, the same peptides were targeted to measure MCSF1R in mouse and rat plasma, but MCSF1R could not be measured in rat plasma **(C)**.

Therefore, a proposed isoform of rat MCSF1R with the Uniprot ID D4ACA7 with unreviewed status was investigated. Database search on the online platform PeptideAtlas[149] revealed the experimentally identified peptides for both MCSF1R rat sequences with Uniprot IDs Q00495 and D4ACA7 (**Figure 27**). The underlying experimental evidence is a comprehensive in-depth analysis of rat liver tissue by proteomics using various proteolytic enzymes presented by Low *et al.* in 2013[150]. The sequence coverage of MCSF1R rat with Uniprot ID Q00495 was shown about 4%, whereas one fourth of the complete MCSF1R rat protein sequence with Uniprot ID D4ACA7 was identified.

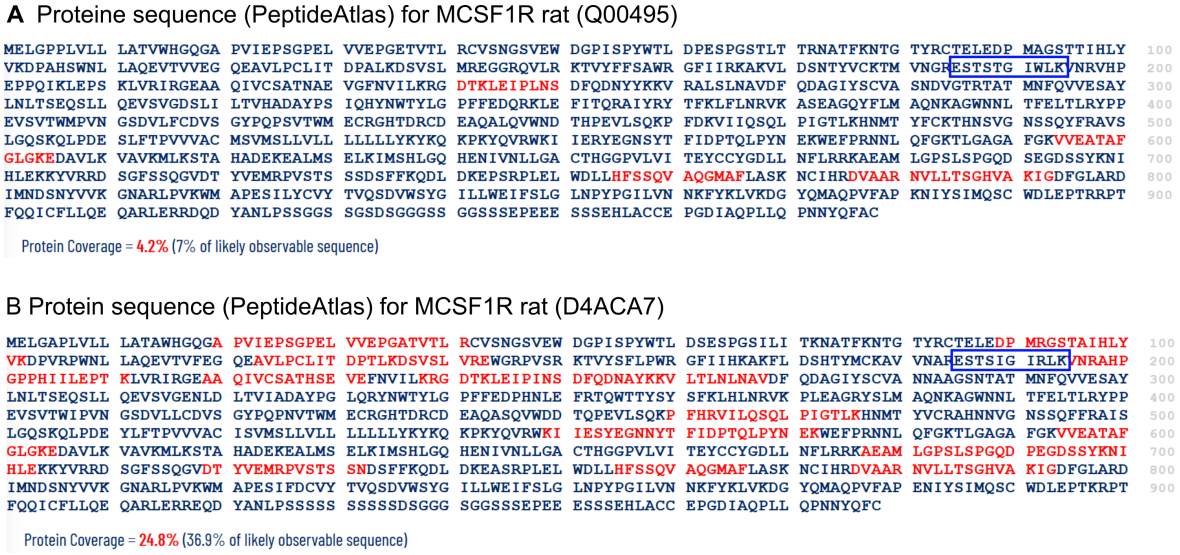

Figure 27: MCSF1R rat sequence comparison. Sequence comparison between **(A)** reviewed (Uniprot ID Q00495) and **(B)** unreviewed (Uniprot ID D4ACA7) protein sequence was performed via PeptideAtlas[149]. Experimentally identified peptides are displayed in red. The initially investigated peptide in the reviewed protein sequence (Uniprot ID Q00495) and its analog peptide within the unreviewed protein sequence (Uniprot ID D4ACA7) are framed in blue **(A, B)**.

The analog peptide of MCSF1R with Uniprot ID D4ACA7 (ESTSIGIR) shows a C-terminus truncated by two amino acids compared to MCSF1R with Uniprot ID Q00495 (ESTSTGIWLK). Trypsin cleaves this corresponding peptide two amino acids upstream due to the exchanged tryptophane with arginine. Furthermore, one threonine is part of the sequence instead of isoleucine compared to the MCSF1R sequence with Uniprot ID Q00495.

In order to test endogenous MCSF1R in rat plasma, several peptides were selected as candidates for quantification of MCSF1R with the Uniprot ID D4ACA7. Peptide selection was approached by digesting and measuring commercially available recombinant MCSF1R via full-scan MS mode. Recombinant MCSF1R protein (2 µg) was digested in solution with a 1:20 trypsin to protein ratio (Worthington trypsin), acidified with 100% FA after digestion and 130 ng digested product was loaded on column for MS

read-out. Full-scan mode provided several precursor peaks covering the MCSF1R protein sequence with Uniprot ID D4ACA7 (**Figure 28A**). The peptide ESTSIGIR and two other peptides were confirmed via PRM measurement with well observed fragment-patterns (**Figure 28A**). These peptides were selected for PRM measurement based on in-house available antibodies with at least two matching amino acids to enable peptide enrichment from plasma. The annotated MS/MS spectrum of the peptide AHNNVGNSSQFFR shows a good coverage with most of the y- and b-ions of this peptide confirmed (**Figure 28B**).

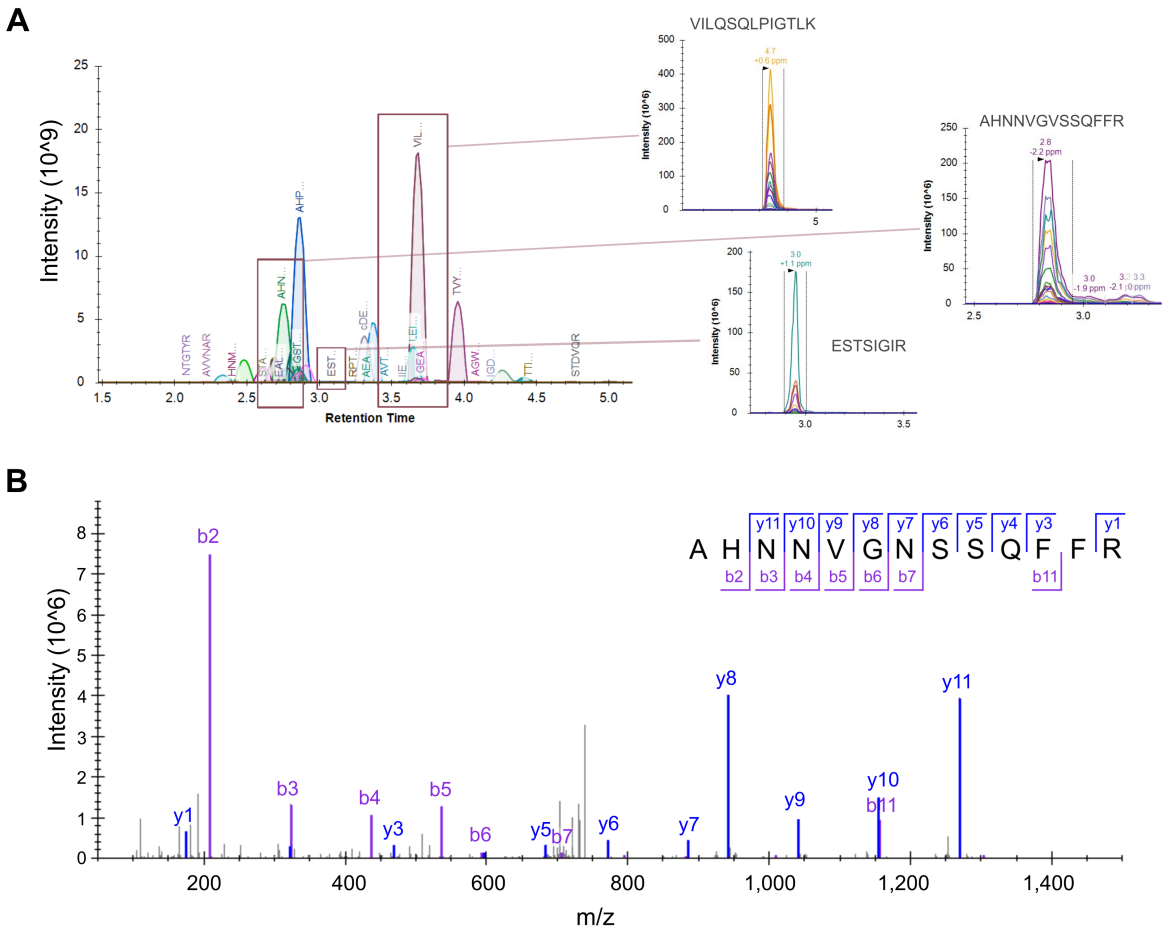

Figure 28: MS and MS/MS measurement of recombinant MCSF1R rat with the protein sequence according to Uniprot ID D4ACA7. (A) The peptide pattern of digested recombinant MCSF1R rat protein (130 ng on column) was well observed using full-scan LC-MS (left) and three peptides were picked for measurement by PRM (right). **(B)** Almost all peptide fragments (y-, b-ions) were observed on the MS/MS level of the peptide AHNNVGNSSQFFR (this spectrum was obtained during full-scan LC-MS).

Peptide enrichment was tested by spiking 50 fmol or 1,000 fmol recombinant MCSF1R into rat plasma and measuring with the IA-LC-MS/MS method (**Figure 29**). Surrogate matrix and non-spiked plasma served as controls. Two generated polyclonal antibodies were available for enrichment of each of the peptides VILQSQLPIGTLK, AHNNVGNSSQFFR, and ESTSIGIR. There was no antibody available with an epitope matching 100% to the targeted peptides, but enrichment is known to be possible even with less then four matching amino acids[151]. Furthermore, the same antibody that was used to capture endogenous ESTSTGIWLK in mouse plasma, was tested here for capturing ESTSIGIR and ESTSTGIWLK from digested recombinant MCSF1R. Internal standards were not available for spiking, thus, peak intensity of the non-labeled peak was investigated. High background signals were observed for VILQSQLPIGTLK (**Figure 29**, blue). The peptide ESTSTGIWLK was not enriched from the digested recombinant MCSF1R with a sequence according to Uniprot ID D4ACA7 (**Figure 29**, orange). To confirm this antibody's enrichment ability, isotope-labeled peptide ESTSTGIWLK was spiked (5 fmol) and captured (see AUC signal, dashed line). The peptide ESTSIGIR could not be enriched from digested recombinant protein using the antibody with the epitope ESTSTGIWLK (**Figure 29**, dark blue). Notable peak intensity was observed for the peptide AHNNVGNSSQFFR in the samples with spiked recombinant protein (**Figure 29**, purple). A fold change of 17 between the signals from 1,000 fmol versus 50 fmol spiked sample was found, which was roughly expected.

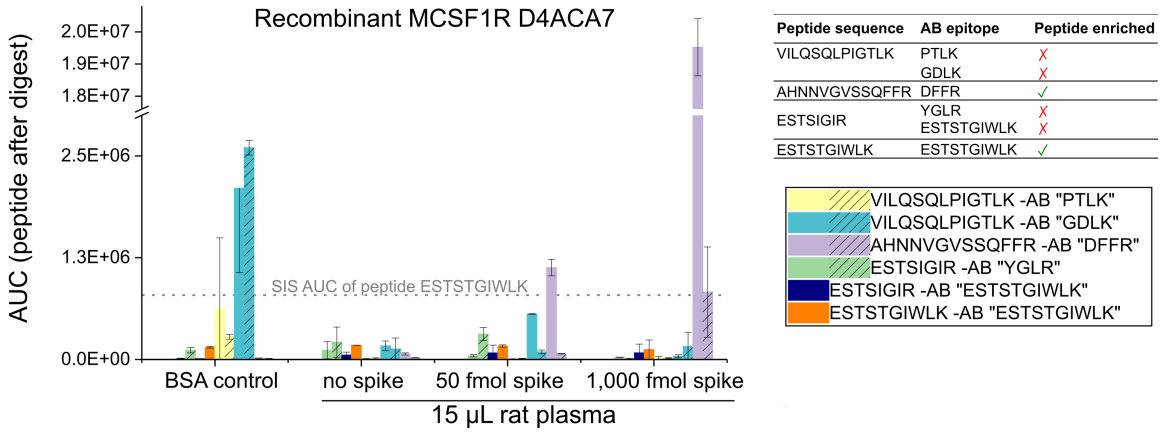

Figure 29: Immunoaffinity enrichment of peptides from recombinant MCSF1R rat (Uniprot ID D4ACA7). Several peptides were targeted with polyclonal antibodies for peptide enrichment from 15 µL plasma spiked or non-spiked with recombinant MCSF1R protein (50 fmol and 1,000 fmol spiked MCSF1R, 5 µg AB per IP well, n = 2 per test condition). Furthermore, 5 fmol SIS peptide ESTSTGIWLK was spiked in 15 µL plasma and enrichment was performed with the AB with the epitope "ESTSTGIWLK". The peptide AHNNVGNSSQFFR from digested recombinant MCFS1R (purple) and the SIS peptide ESTSTGIWLK were enriched (dashed line). Two polyclonal ABs generated against the same epitope were tested (plain and shaded colors).

Especially one of the two available ABs with the epitope "DFFR" was thereby able to enrich this peptide from plasma (**Figure 29**, purple, plain). On the basis of these findings, the peptide AHNNVGNSSQFFR was used to validate the method for MCSF1R quantification (see **4.2**) and was used for measurement of rat specimen from preclinical DILI studies (see **4.4**).

4.1.6 DILI biomarker quantification in human and rat specimen

At a more advanced development stage, IA-LC-MS/MS assays required calibration curves for precise and accurate calculation of the peptide concentration in unknown samples. The calibration samples consisted of digested surrogate matrix spiked with a constant isotope-labeled peptide concentration and varying concentration levels of non-labeled synthetic peptides. The curve was generally prepared with non-labeled synthetic peptides serially diluted 1:3. Due to the enrichment step with antibodies, such calibration curves could have a logistic or a more linear character, exemplary shown for the GLDH and MCSF1R rat peptides in **Figure 30**. With calibration curve obtained from the measured calibrator AUC ratios, calibrator levels could be back-calculated using logistic fit models for both types of curves (**Figure 30A, B**). The back-calculated curves showed acceptable results for 8 / 8 GLDH calibrators and 6 / 8 MCSF1R calibrators marking the lower and upper limit of quantification (LLOQ, ULOQ), respectively (**Figure 30A, B**, see acceptance criteria in **3.2.13**). The lowest MCSF1R calibrator could not be back-calculated with the curve fit, thus, missing in the plot (**Figure 30B**). Using the logistic fit models, quality control (QC) samples with plasma and lysate or recombinant protein along with unknown samples could be accurately back-calculated within the calibration range between LLOQ and ULOQ ($R^2 = 0.99$). Multiplexed assays for analyte quantification in human or rat samples were developed and the specifications were summarized in the following overview (**Table 14**). DILI analytes in human samples were measured with the assay termed MPh-dev and matrix and sampling effects were investigated with this assay (see below **4.3**). Assay performance was monitored and qualified across experiments using calibration curves and QC samples. Synthetic peptides were available but not quantified by amino acid analysis (ASA) at that time. Apart from this qualification, no further validation experiments were performed for this assay at that time, hence, the assay extension "dev" for MPh-dev under development. Assay performance for the DILI-related peptides from rat was evaluated by method validation and this multiplexed assay was termed MPr (see **4.2**). The detergent CHAPS was used initially for MPh-dev to prevent remnants of beads in the sample plate, but was later not included in processing for MPr because the detergent NOG from digestion buffer seemed to sufficiently prevent bead remnants. Weighting for preparation of the calibration curve was refined during method validation for MPr compared to MPh-dev (**Table 14**).

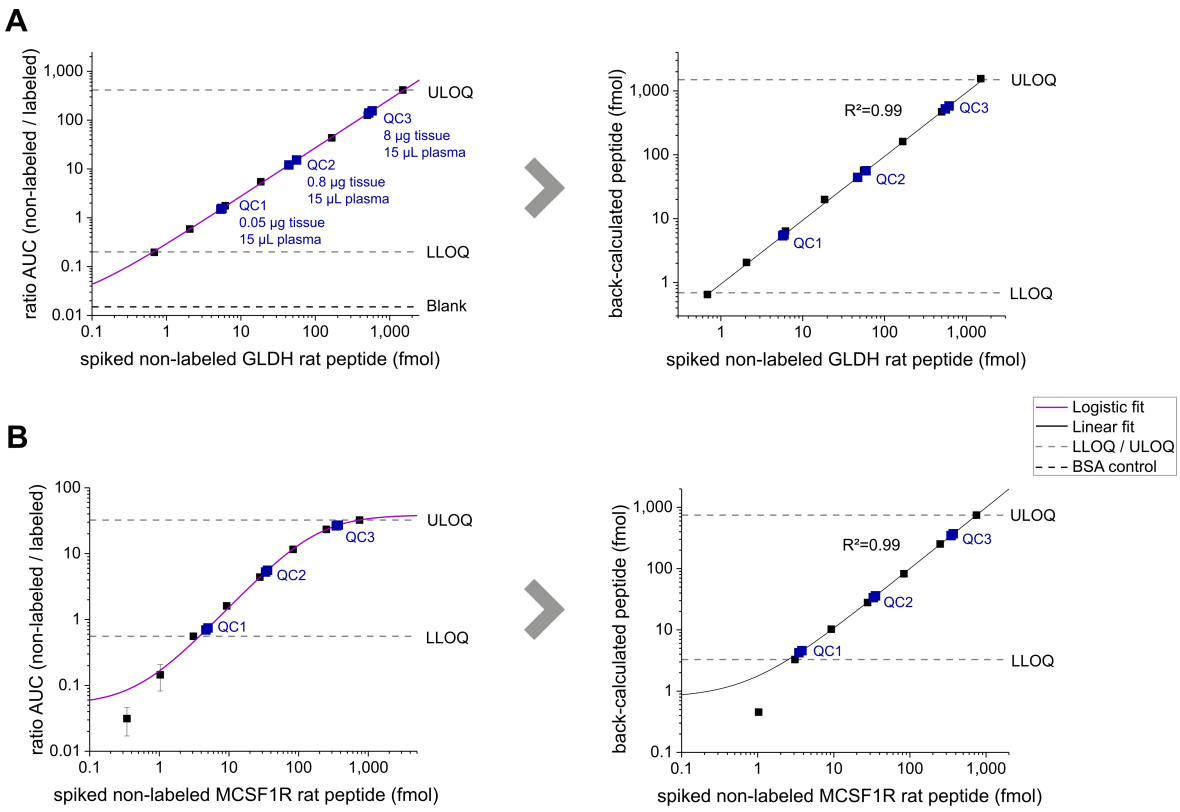

Figure 30: Exemplary calibration curves and QC samples with raw data and back-calculated values for the GLDH and MCSF1R rat peptides. Synthetic non-labeled peptide was diluted in a peptide solution with constant isotope-labeled standard peptide concentration to prepare calibration curves for **(A)** the GLDH rat and **(B)** the MCSF1R rat peptides. The AUC ratios were plotted exemplary for both peptides and ratios measured from contrived QC samples are displayed in the calibration ranges. Logistic fits were used to back-calculate calibrators and QC samples. See run 1 under 4.2 for the corresponding curve data.

Table 14: Assay-related specifications for IA-LC-MS/MS assays and protein measurements. MPh-dev = multiplex human, MPr = multiplex rat, EN = synthetic non-labeled peptide, S1 = highest calibrator

Assay, species	Protein	Peptide sequence	SIS amount / well (fmol)	EN amount (S1) / well (fmol)	AB amount / well (µg)	Bead suspension / well (µL)	CHAPS (%)	Fit model	Weighting
MPh-dev, human	MCSF1R	VIPGPPALTLVPAELVR	25	1,500	2.5	25	0.03	logistic	instrumental
	OPN	YPDAVATWLNPDPSQK	25	1,500	2.5				instrumental
	HMGB1	GEHPGLSIGDVAK	4	250	5.0				instrumental
	GLDH	HGGTIPIVPTAEFQDR	5	1,500	2.5				instrumental
MPr, rat	MCSF1R	AHNNVGNSSQFFR	5	750	5.0	45	0.00	logistic	no weights
	OPN	HSDAVATWLKPDPSQK	25	1,500	2.5				1/y
	HMGB1	GEHPGLSIGDVAK	4	250	5.0				1/y
	GLDH	HGGTIPVVPTAEFQDR	5	1,500	2.5				$1/y^2$
	ccK18	SSNSMQTIQK	50	1,500	5.0				1/y

4.2 Method validation of IA-LC-MS/MS assay for protein quantification in rat specimen

In order to accurately quantify DILI-relevant analytes in rat speciment, several aspects of method validation were performed on the basis of FDA recommendations[126] resulting in partial validation of the IA-LC-MS/MS assay MPr proposed in **Table 14** (see above **4.1.6**). This partial validation included evaluation of accuracy and precision of calibrator and QC sample values for inter assay variation, accuracy and precision of QC sample values for intra assay variation, parallelism of endogenous sample diluted in surrogate matrix, and reproducibility of sample measurement. Preclinical rat samples were under investigation here instead of clinical samples, hence, three independent accuracy and precision runs were performed instead of the proposed six runs, thus, being a partial validation. Contrived QC samples with rat plasma, liver tissue lysate, and recombinant protein were used to assess accuracy and precision. The respective QC and calibrator sample preparation was described in **Table 9** (see **3.2.2**). An assay run always comprised a calibration curve in duplicates (from digest to MS read-out), three QC levels each processed in duplicates and samples to be investigated (e.g., from parallelism, reproducibility, or unknown samples). Limits of quantification were determined on the basis of accuracy and precision experiments with calibration samples and QC samples measured in three independent runs. Acceptance criteria for limits of quantification, parallelism, and reproducibility were defined in section **3.2.13**. Nominal values for QC samples were determined with three independent QC sample sets (data not shown). A preliminary experiment with 0.5 µg to 5 µg cell lysate from taxol treated HepG2 cells showed enrichment of endogenous human ccK18 peptide SSNSMQTIQK spiked in 20 µg BSA or in human EDTA plasma (appendix **Figure 50**). Hence, the peptide SSNSMQTVQR was included in the MPr assay to target ccK18 in rat samples.

4.2.1 Accuracy & precision

Calibrators S1 to S8 with synthetic non-labeled and labeled peptide spiked in digested surrogate matrix were measured in three independent runs in duplicates per run. Blank samples comprised only the labeled standard peptide. Calibrator AUC ratios are shown here exemplary for GLDH and MCSF1R (**Table 15, 16**). Further peak area data for OPN, HMGB1, and ccK18 are listed in the appendix (**Table 26** to **Table 28**). The measured ratio at S8 for GLDH was still above the blank signal plus six times the blank standard deviation, which means even at low concentration level, measured signal could be distinguished from the blank signal. The ratios at their respective LLOQs were also for the other analytes above the blank signal plus six times the blank standard deviation (**Table 26** to **Table 28**). From each independent run, a calibration curve was established and the respective calibrators were back-calculated in fmol peptide using the curve. Protein concentrations were calculated by converting

the measured absolute peptide amount (fmol) per IP well into protein concentrations (ng/mL) considering the molecular weight of the corresponding protein and the 15 µL sample volume. Back-calculated calibrator results were summarized for GLDH and MCSF1R in **Table 17** and **Table 18**. Results for OPN, HMGB1 and ccK18 were listed in the appendix (**Table 29** to **Table 31**). The assay range met the acceptance criteria when comprising calibration samples S1-S8 in case of GLDH, S1-S7 for OPN, and S1-S6 for MCSF1R, HMGB1, and ccK18. The lower and upper calibrators marking the calibration range with accurate quantification are termed lower and upper limit of quantification (LLOQ, ULOQ; marked in **bold** in each data table). Calibrators in the lower calibration ranges of MCSF1R, OPN, HMGB1, and ccK18 exceeded the accuracy and precision criteria, thus, these calibrators were not included in the curve fits.

Table 15: Peak area ratio data of calibrators and blank for GLDH (MPr), ratio = area under the curve (AUC) of non-labeled peptide peak over isotope-labeled peptide peak. LLOQ/ULOQ ratios labeled in **bold**

Run	Unit	B	S8	S7	S6	S5	S4	S3	S2	S1
1	ratio	0.01	0.20	0.58	1.74	5.27	15.7	44.8	126	430
1	ratio	0.03	0.20	0.60	1.80	5.66	15.3	42.2	126	397
2	ratio	0.00	0.14	0.45	1.45	4.22	13.3	36.2	123	368
2	ratio	0.02	0.13	0.46	1.44	4.36	12.8	34.4	113	305
3	ratio	0.00	0.19	0.56	1.66	5.81	16.1	49.3	127	356
3	ratio	0.01	0.18	0.55	1.70	5.70	15.0	43.6	130	441
Mean value, n=6	ratio	0.01	**0.17**	0.53	1.63	5.17	14.7	41.7	124	**383**
SD	ratio	0.01	0.03	0.06	0.15	0.71	1.32	5.58	5.63	50.6
blank + 6x SD	ratio	0.07	-	-	-	-	-	-	-	-

Table 16: Peak area ratio data of calibrators and blank for MCSF1R (MPr), ratio = area under the curve (AUC) of non-labeled peptide peak over isotope-labeled peptide peak. LLOQ/ULOQ ratio labeled in **bold**

Run	Unit	B	S8	S7	S6	S5	S4	S3	S2	S1
1	ratio	0.00	0.02	0.10	0.54	1.61	4.44	12.3	23.4	32.4
1	ratio	0.00	0.04	0.19	0.57	1.61	4.35	11.0	23.3	32.3
2	ratio	0.00	0.01	0.10	0.45	1.64	4.53	13.7	24.6	29.9
2	ratio	0.00	0.01	0.15	0.49	1.61	4.88	12.8	24.1	29.9
3	ratio	0.00	0.01	0.09	0.50	1.77	5.73	12.6	25.7	32.8
3	ratio	0.00	0.00	0.10	0.45	1.93	5.52	12.2	26.5	34.2
Mean value, n=6	ratio	0.00	0.02	0.12	**0.50**	1.70	4.91	12.4	24.6	**31.9**
SD	ratio	0.00	0.01	0.04	0.05	0.13	0.59	0.90	1.28	1.70
blank + 6x SD	ratio	0.00	-	-	-	-	-	-	-	-

Table 17: Calibrator validation results for GLDH (MPr). TE = total error. LLOQ/ULOQ labeled in **bold**

Run	Unit	S8	S7	S6	S5	S4	S3	S2	S1
1	ng/mL	2.65	8.26	25.6	78.5	236	678	1,928	6,606
1	ng/mL	2.66	8.63	26.5	84.5	230	639	1,923	6,103
2	ng/mL	2.63	8.70	27.6	78.1	239	635	2,153	6,840
2	ng/mL	2.46	8.97	27.5	80.7	231	604	1,979	5,559
3	ng/mL	2.84	8.24	24.5	85.7	237	726	1,890	5,580
3	ng/mL	2.69	8.18	25.2	84.1	221	642	1,934	7,048
Mean value, n=6	ng/mL	2.66	8.50	26.2	81.9	232	654	1,968	6,289
SD	ng/mL	0.12	0.32	1.24	3.25	6.50	42.5	95.1	640
CV	%	5	4	5	4	3	7	5	10
Nominal value	ng/mL	**2.81**	8.42	25.3	76	227	682	2,046	**6,138**
Accuracy	%	-5	1	4	8	2	-4	-4	2
TE	%	10	5	8	12	5	11	9	13

Table 18: Calibrator validation results for MCSF1R (MPr). TE = total error. LLOQ/ULOQ labeled in **bold**

Run	Unit	S8	S7	S6	S5	S4	S3	S2	S1
1	ng/mL	#	#	12.7	41.3	114	355	1,023	3,020
1	ng/mL	#	1.83	13.7	41.3	111	308	1,009	2,988
2	ng/mL	#	#	11.4	47.0	108	347	1,059	2,934
2	ng/mL	#	#	13.0	43.0	116	316	993	2,969
3	ng/mL	#	#	10.4	41.8	131	313	1,034	2,510
3	ng/mL	#	#	8.93	45.4	126	300	1,114	3,363
Mean value, n=6	ng/mL	-	-	11.7	42.7	118	323	1,039	2,964
SD	ng/mL	-	-	1.79	1.63	8.97	22.4	43.3	272
CV	%	-	-	15	4	8	7	4	9
Nominal value	ng/mL	1.38	4.14	**12.4**	37.3	112	336	1,007	**3,021**
Accuracy	%	-	-	-6	15	5	-4	3	-2
TE	%	-	-	21	18	1	3 11	7	11

#Calibrators could not be back-calculated with curve fit

Accuracy and precision results for QC samples are shown here for GLDH and MCSF1R in **Tables 19** and **20** and listed in the appendix for OPN, HMGB1, and ccK18 (**Table 32** to **Table 35**). Intra and inter assay accuracy and precision within the acceptance criteria was given for all analytes at each QC level except for HMGB1. The first QC1 replicate for HMGB1 inter assay accuracy and precision (**Table 32**) was below LLOQ (out of calibration range for this batch). Since the assay showed

robust performance in this range for intra assay QC1 sample accuracy and precision (**Table 34**) as well as for calibrator accuracy and precision (**Table 30**), the results for HMGB1 were considered as acceptable.

Table 19: QC inter assay validation results for GLDH and MCSF1R (MPr)

		GLDH			MCSF1R		
Run	**Unit**	**QC1**	**QC2**	**QC3**	**QC1**	**QC2**	**QC3**
1	ng/mL	22.0	181	2,138	18.4	145	1,489
1	ng/mL	22.9	230	2,373	17.0	135	1,393
2	ng/mL	26.8	260	2,196	16.5	133	1,541
2	ng/mL	26.7	255	2,113	18.1	128	1,637
3	ng/mL	22.5	248	2,140	15.6	114	1,319
3	ng/mL	20.3	238	1,857	16.1	169	1,733
Mean value, n=6	ng/mL	23.5	235	2,136	17.0	137	1,519
SD	ng/mL	2.64	28.6	166	1.10	18.6	153
CV	%	11	12	8	7	14	10
Nominal value	ng/mL	23.2	241	2,110	17.4	127	1,308
Accuracy	%	1	-2	1	-3	8	16
TE	%	13	15	9	9	22	26

Table 20: QC intra assay validation results for GLDH and MCSF1R (MPr)

		GLDH			MCSF1R		
Run	**Unit**	**QC1**	**QC2**	**QC3**	**QC1**	**QC2**	**QC3**
Measurement 1	ng/mL	20.6	192	2,172	17.3	126	1,233
Measurement 2	ng/mL	23.2	219	2,110	18.1	129	1,361
Measurement 3	ng/mL	19.6	235	2,105	18.2	135	1,194
Measurement 4	ng/mL	19.7	215	2,548	18.8	123	1,461
Measurement 5	ng/mL	19.9	209	2,316	16.7	124	1,234
Measurement 6	ng/mL	21.9	214	2,096	19.0	126	1,250
Mean value, n=6	ng/mL	20.8	214	2,225	18.0	127	1,289
SD	ng/mL	1.45	13.9	178.6	0.87	4.28	101
CV	%	7	7	8	5	3	8
Nominal value	ng/mL	23.2	241	2,110	17.4	127	1,308
Accuracy	%	-10	-11	5	3	1	-1
TE	%	17	18	13	8	4	9

4.2.2 Parallelism of endogenous analyte diluted in surrogate matrix

Parallelism was addressed by the analysis of plasma or liver samples diluted in surrogate matrix to determine whether plasma or liver can be diluted in case the results of undiluted samples exceed the determined calibration range, thereby exceeding the ULOQ. Parallelism was assessed using six plasma samples with high endogenous DILI biomarker levels (15 µL plasma per sample) and six liver tissue samples (8 µg lysate in 15 µL surrogate matrix per sample) three times diluted 1:2 in surrogate matrix (P1-6_dil1-4, PT1-6_dil1-4). A minimum of two serial dilutions within the assay range was needed to evaluate parallelism of endogenous analyte in a given sample. Parallelism is given if the obtained calculated protein concentration meets the general acceptance criteria for at least two dilutions within the assay range for 80% of a minimum of six samples. The measured protein concentration of the diluted samples should be multiplied with the corresponding dilution factor and should be within an accuracy of ±20% of the reference value (the corresponding undiluted sample). Plasma samples and liver tissue samples were evaluated separately. Parallelism of plasma samples diluted in surrogate matrix could be confirmed for GLDH, OPN, and HMGB1 within the acceptance criteria until a dilution of 1:8 (**Table 21** and appendix **Tables 36, 37**).

Table 21: Parallelism of endogenous GLDH in plasma samples diluted in surrogate matrix (MPr)

Parallelism samples P1-P6 (plasma) diluted in surrogate matrix					
Dilution factor (DF)	**Unit**	**1 (undiluted)**	**2**	**4**	**8**
P1 measured value	ng/mL	298	149	81.4	42.4
P1 x DF	ng/mL	298	298	326	339
Accuracy	%	0	0	9	14
P2 measured value	ng/mL	1,396	713	335	173
P2 x DF	ng/mL	1,396	1,426	1,341	1,382
Accuracy	%	0	2	-4	-1
P3 measured value	ng/mL	1,361	670	361	177
P3 x DF	ng/mL	1,361	1,340	1,445	1,415
Accuracy	%	0	-2	6	4
P4 measured value	ng/mL	250	110	61.5	29.1
P4 x DF	ng/mL	250	220	246	233
Accuracy	%	0	-12	-2	-7
P5 measured value	ng/mL	433	217	113	60.5
P5 x DF	ng/mL	433	435	453	484
Accuracy	%	0	0	5	12
P6 measured value	ng/mL	444	222	113	53.7
P6 x DF	ng/mL	444	443	452	430
Accuracy	%	0	0	2	-3

Parallelism of MCSF1R and ccK18 in plasma samples could not be assessed since endogenous samples were not available with high analyte concentration (for dilution up to at least 1:4). Parallelism of liver tissue samples diluted in surrogate matrix was well observed for GLDH until a dilution of 1:8, whereas not one dilution step was possible for HMGB1 (appendix **Tables 38, 39**). Therefore, always the same liver protein amount must be processed for HMGB1 within one study to ensure correct sample comparison within a study.

4.2.3 Reproducibility of quantification of endogenous analyte

At least six plasma and liver tissue samples from individual animals were tested undiluted in two independent runs to evaluate the reproducibility of sample measurement. The percentage difference of the results between the first and the second analysis was determined as described above (see 3.2.13). The acceptance criteria were fulfilled when results from two independent runs were below CV≤30% in 80% of the samples.
Well performing assay reproducibility was confirmed in plasma for GLDH, OPN, and HMGB1 (**Table 22**, appendix **Tables 40, 41**). Reproducibility for ccK18 and MCSF1R in plasma could not be assessed since the measured sample levels were below the lower limit of quantification (data not shown). Assay reproducibility for GLDH and HMGB1 was also well observed in liver tissue (appendix **Tables 42, 43**). OPN, MCSF1R, and ccK18 showed signals below lower limit of quantification in liver tissue (data not shown).
All validation results were summarized in **Table 23** and the MPr assay was used for measurement of preclinical study samples of rats (plasma and liver) treated with several drugs and compounds (see **4.4**).

Table 22: Reproducibility of endogenous GLDH levels in rat plasma (MPr)

		Reproducibility samples of animals 1 to 8							
Run	**Unit**	**1**	**2**	**3**	**4**	**5**	**6**	**7**	**8**
Run 1	ng/mL	13.7	14.0	10.6	9.32	13.4	11.6	11.0	3.48
Run 2	ng/ml	17.3	16.9	12.4	11.7	16.5	14.1	14.5	5.02
Difference %		23	19	16	22	21	20	27	**36**

Table 23: Validation results for the assay MPr. Run number for accuracy and precision (% CV): n = 3. TE = total error. n/a = not applicable due to missing endogenous signals

Protein	LLOQ (ng/mL)	ULOQ (ng/mL)	Inter assay calibrators (% accuracy, % CV, % TE)	Inter assay QC (% accuracy, % CV, % TE)	Intra assay QC (% accuracy, % CV, % TE)	Reproducibility (% difference)	Parallelism: dilution in surrogate matrix
GLDH	2.81	6,138	-5 to 8 3 to 10 5 to 13	-2 to 1 8 to 12 9 to 15	-11 to 5 7 to 8 13 to 18	<30% for 7/8	until 1:8
MCSF1R	12.4	3,021	-6 to 15 4 to 15 7 to 21	-3 to 16 7 to 14 9 to 26	-1 to 3 3 to 8 4 to 9	n/a	n/a
OPN	4.86	3,540	-2 to 7 4 to 13 4 to 20	3 to 6 5 to 9 11 to 15	7 to 11 4 to 6 8 to 14	<30% for 8/8	until 1:8
HMGB1	1.70	412	-2 to 6 2 to 11 3 to 16	1 to 5 5 to 16 8 to 17	5 to 12 3 to 9 8 to 21	<30% for 7/8	until 1:8
ccK18	1.53	373	-8 to 5 3 to 12 3 to 20	2 to 11 8 to 10 12 to 19	8 to 14 5 to 9 13 to 22	n/a	n/a

4.3 Matrix and sampling effects on quantification of potential human protein biomarkers of DILI

This chapter was adapted from **Anselm, V.**, Sommersdorf, C., Carrasco-Triguero, M., Katavolos, P., Planatscher, H., Steinhilber, A., Joos, T., Poetz, O., Matrix and Sampling Effects on Quantification of Protein Biomarkers of Drug-Induced Liver Injury. *Journal of Proteome Research.* 20(11):4985-4994. doi:10.1021/acs.jproteome.1c00478 (Nov 2021).

Serum and plasma specimen are both clinically relevant types of matrices commonly collected when biomarkers are investigated in blood of patients. Independent of the analyses method, the type of sample matrix or preanalytical factors such as stability during serum and plasma preparation could impact analyte concentration in specimen. Thus, comparability of analyte quantification in serum and plasma and benchtop stability between sample collection and centrifugation were investigated in the following. Matched samples including EDTA plasma, serum, and serum gel (serum collection tubes with gel) samples from 10 healthy volunteers (donor 1 to donor 10) were used for matrix comparison regarding DILI biomarker concentration. Furthermore, each sample type was collected three times per subject and the incubation times of 15 min, 30 min, or 60 min at room temperature between sample collection and centrifugation were investigated.
K18 and ccK18 were measured by immunoassays and MCSF1R, OPN, HMGB1, and GLDH levels were measured by IA-LC-MS/MS using the assay MPh-dev. Samples were measured in duplicates with the IA-LC-MS/MS assay and in singlicates with ELISAs due to limited sample volume. An IA-LC-MS/MS assay was not available for K18 or ccK18 due to the presented peptide instability and chromatographic performance (see **4.1.2**). The impact of trypsin (see **4.1.4**) was not recognized at the time of measurement of this study, hence, ELISAs were used for K18 and ccK18 quantification.

4.3.1 Effects of sample matrix on DILI biomarkers

All samples showed detectable levels of the analytes except for K18 where all the samples comprised undetectable levels (**Figure 31**). Detailed median sample results and results from the corresponding calibration curves and QC samples are listed in the appendix (**Tables 44** to **48**). Only analyte results which were measured within the corresponding calibration ranges were displayed. Differences between matrices were investigated by paired t-test with significance level $p < 0.05$. For better overview, statistical and mean differences were listed in **Tables 24** and **25**. The carried calibration curves and QC samples showed good accuracy (within ±20% accuracy of the nominal values) and precision ($CV < 20\%$) across the measured sample plates (appendix **Tables 45** to **48**). Donor 2 showed outliers in ccK18 levels consistently throughout

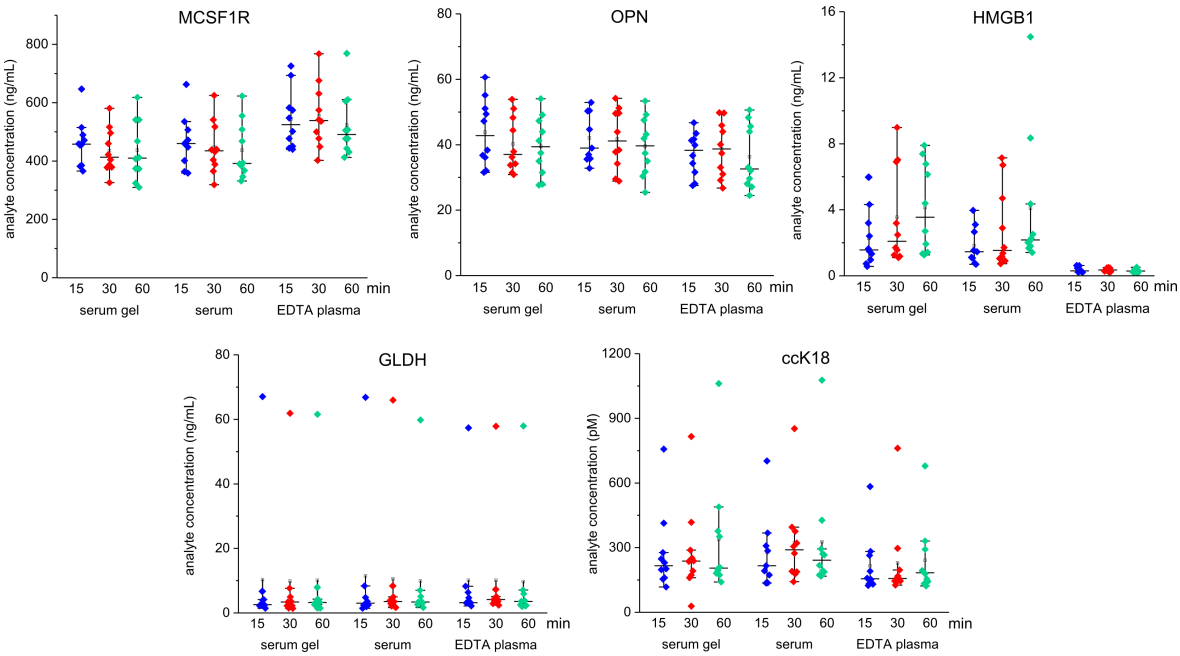

Figure 31: DILI biomarker in serum gel, serum, and EDTA plasma. Matched samples from 10 healthy volunteers were investigated. Sample tubes were incubated between 15 min and 60 min at RT between sample collection and centrifugation. The multiplexed assay MPh-dev was used to measure MCSF1R, OPN, HMGB1, and GLDH by IA-LC-MS/MS. K18 and ccK18 were measured by immunoassays, but K18 was undetectable in all donors.

Table 24: Statistical comparison between DILI biomarker concentration in matched serum gel, serum, and EDTA plasma samples (paired t-test, significance level $p < 0.5$ shown in **bold**). Time = benchtop time

Matrix	**Time (min)**	**p-value**				
		MCSF1R	**OPN**	**HMGB1**	**GLDH**	**ccK18**
Serum gel	15	6.55E-01	9.08E-01	9.39E-01	1.92E-01	5.87E-01
vs	30	2.46E-01	3.08E-01	2.87E-01	1.66E-01	2.99E-01
Serum	60	9.74E-01	1.00E+00	9.79E-01	4.05E-01	5.26E-01
Serum gel	15	**1.59E-03**	**2.87E-03**	**2.94E-02**	8.99E-01	**4.51E-02**
vs	30	**3.09E-05**	1.64E-01	**8.94E-03**	6.77E-01	8.93E-02
EDTA plasma	60	**7.40E-05**	**4.07E-02**	**1.48E-03**	4.46E-01	6.46E-02
Serum	15	**3.35E-05**	**2.20E-04**	**2.12E-02**	7.77E-01	8.05E-02
vs	30	**2.65E-07**	**2.22E-02**	**1.27E-02**	6.56E-01	**1.02E-03**
EDTA plasma	60	**6.12E-05**	**4.05E-02**	**1.83E-02**	5.37E-01	6.29E-02

Table 25: Mean difference between DILI biomarker concentration in matched serum gel, serum, and EDTA plasma samples measured by IA-LC-MS/MS. Time = benchtop time

Matrix	Time (min)	Mean difference (ng/mL)				(pM)
		MCSF1R	OPN	HMGB1	GLDH	ccK18
Serum gel	15	-4.14	-0.08	0.03	-0.37	9
vs	30	-12.2	-1.54	0.70	-0.72	-42
Serum	60	0.21	0.00	0.03	0.22	10
Serum gel	15	-81.4	6.72	1.75	0.18	60
vs	30	-121	1.51	3.44	-0.25	51
EDTA plasma	60	-86.7	3.22	3.82	0.40	96
Serum	15	-86.7	5.63	1.37	0.45	55
vs	30	-109	3.05	2.68	0.47	92
EDTA plasma	60	-86.9	3.22	3.79	0.19	86

all matrices and donor 3 showed consistent outlier results for GLDH in all matrices (**Figure 31**). GLDH levels were below the lowest calibration standard (2.56 ng/mL) in all samples of donor 7 (data not shown). In total, 11 samples were below the lowest calibration standard for HMGB1 (0.19 ng/mL). A sample of donor 4 with 15 min benchtop time was not available. Only duplicate samples with a precision below 30% CV were further analyzed.

Significant differences between matrices were especially observed for MCSF1R, HMGB1, and OPN (**Table 24**). MCSF1R revealed higher concentration in EDTA plasma compared to serum or serum gel for all investigated benchtop times (mean difference 81.35 - 120.70 ng/mL **Table 25**, p = 1.59E-3 to p = 2.65E-7). In contrast to this, HMGB1 showed significantly lower concentrations in EDTA plasma compared to serum or serum gel for all benchtop times with a mean difference of 1.37 - 3.82 ng/mL (p = 2.94E-2 to p = 1.48E-3). This represents a 4- to 12-fold mean difference compared to the median HMGB1 concentration in EDTA plasma (0.29-0.35 ng/mL).

OPN levels were significantly decreased in plasma compared to serum or serum gel (p = 4.07E-2 to p = 2.20E-4) but this only accounted about 10% compared to the measured values (about 3 - 4 ng/mL mean difference compared to about 30 - 40 ng/mL OPN levels (**Table 25**, appendix **Table 44**). GLDH levels were comparable in all investigated matrices. Significantly elevated ccK18 concentration was indicated only for two benchtop time comparisons, in serum gel compared to EDTA plasma (15 min benchtop time, p = 4.51E-02) and serum compared to EDTA plasma (30 min benchtop time, p = 1.03E-03).

Individual matching of results across the different matrices was investigated by correlating analyte concentrations from matching samples. Two donors showed 4- and 20-fold increase in ccK18 or GLDH concentration compared to the other donors. Thus, these

results were confirmed as outliers based on Tukey's method[152] for all matrices and the donors were excluded from correlation to avoid bias in the analyses (donor 2 for ccK18 and donor 3 for GLDH).
Comparing all DILI biomarkers in matched samples revealed a generally positive correlation across all matrices except for HMGB1 and ccK18 (**Figure 32**). MCSF1R and OPN provided the best correlation ($R^2 = 0.78$ to 0.92) when comparing all results from the three matrices. However, concentration of the analytes differed if results for the matrices were compared. In the case of MCSF1R, the data obtained from plasma and serum from the same assay shows an off-set of about 90 ng/mL (about 20% difference) between the two matrices, while OPN concentrations show a moderate matrix-dependent differences of about 3 ng/mL (about 10% difference) (appendix **Table 44**). GLDH concentrations correlated moderately between EDTA plasma and serum gel or serum samples ($R^2 = 0.47$), whereas a high positive correlation was observed between serum and serum gel results ($R^2 = 0.89$). HMGB1 levels between EDTA plasma and serum gel or serum samples did not correlate (R^2 = -0.02 or -0.01). Furthermore, HMGB1 levels between serum gel and serum showed a low positive correlation ($R^2 = 0.37$) and a negligible to low positive correlation was seen for ccK18 across all matrices ($R^2 = 0.25$ to 0.33).
DILI biomarkers measured with the MPh-dev assay were also investigated by immunoassays (MCSF1R, OPN, HMGB1) and enzymatic activity (GLDH) for comparison between IA-LC-MS/MS and standard methods (see below, detailed method comparison **4.3.3**). According to the vendor's instruction manual of the enzymatic activity kit, GLDH was measured only in serum and serum gel samples. Correlation of biomarker concentration between matched samples was comparable to the IA-LC-MS/MS results for MCSF1R, HMGB1, and GLDH (**Figure 33**). OPN concentration did not match between EDTA plasma and serum or serum gel using the immunoassay read-out (R^2 = -0.04 to 0.11). However, OPN results between serum and serum gel seem to match better ($R^2 = 0.64$). Correlation between the IA-LC-MS/MS and immunoassay methods is presented below (see **4.3.3**).

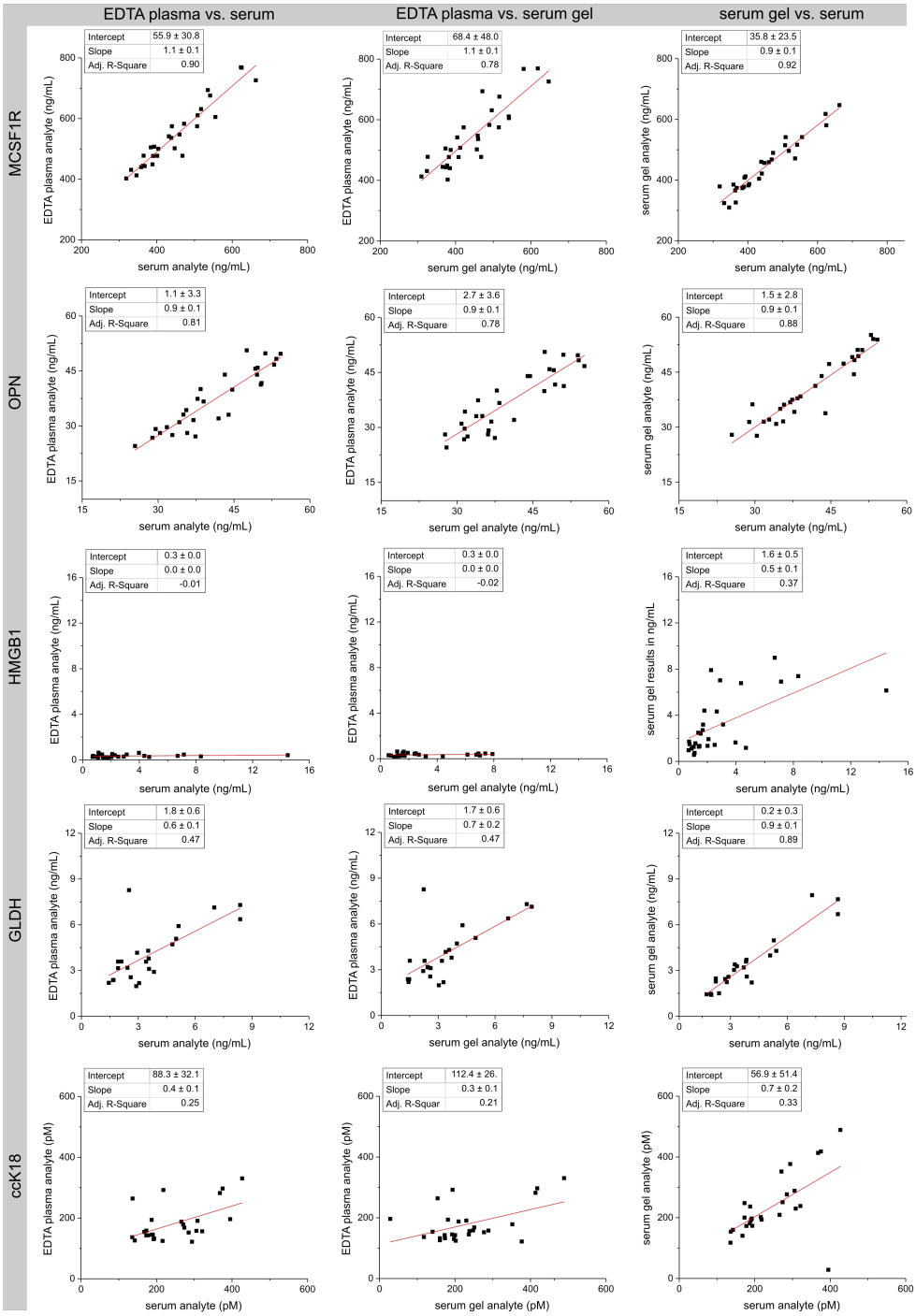

Figure 32: Correlation of DILI biomarker concentrations in serum gel, serum, and EDTA plasma of matched samples by IA-LC-MS/MS (MPh-dev) and ELISA (ccK18). Analyte levels in EDTA plasma samples were compared to results from serum (column 1) and serum gel (column 2). Furthermore, serum with and without gel in the collection tubes was compared (column 3). Donor 3 and donor 2 were excluded from correlation to avoid a bias towards these samples with high analyte levels for GLDH or ccK18, respectively.

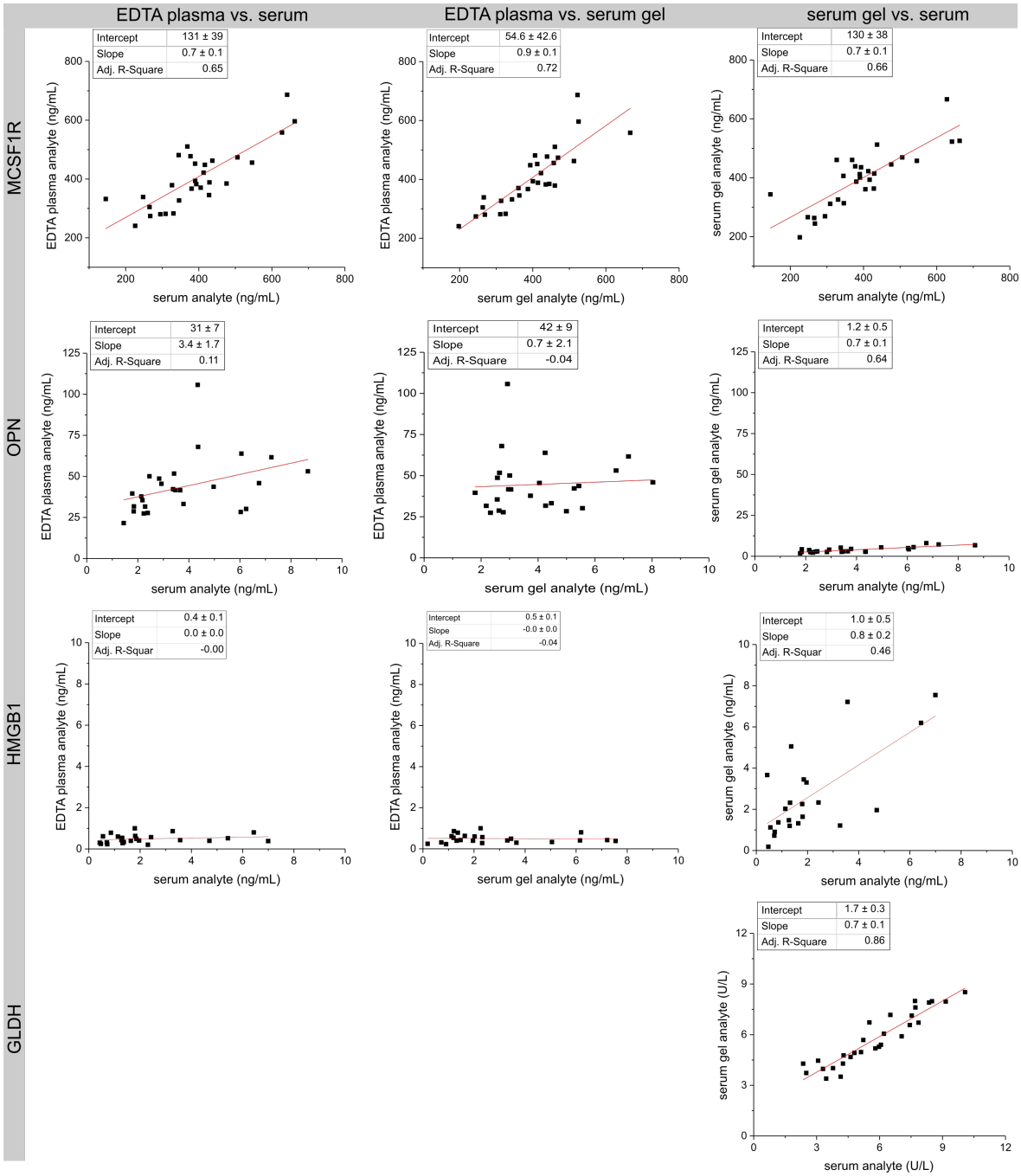

Figure 33: Correlation of DILI biomarker concentrations in matched serum gel, serum, and EDTA plasma samples measured by immunoassays and enzyme activity. MCSF1R, OPN, and HMGB1 levels were assessed with sandwich immunoassays. GLDH activity was measured only in serum and serum gel samples according to the vendor's instruction manual of the enzymatic activity assay kit.

4.3.2 Effects of sample benchtop time on DILI biomarkers

Benchtop time between sample collection and centrifugation was investigated with one-way repeated measures ANOVA with Bonferroni correction to reveal potential sampling time-dependent changes in DILI biomarker concentrations (significance level: $p < 0.05$). Analyte concentrations, which were measured with 15 min benchtop time, were considered as the reference time point and set as 100%. The difference in analyte concentrations between 15 min to 30 min, 15 min to 60 min, and between 30 min to 60 min was calculated in percent. The mean differences in analyte concentration across the tested samples from 10 healthy volunteers (HVs) are displayed in percent for the investigated time intervals (**Figure 34**). Each DILI biomarker (rows) was investigated in serum gel (column 1), serum (column 2), and EDTA plasma (column 3). Positive mean differences show an increase in analyte level over time and negative mean differences show decreased analyte levels. Depending on the analyte, changes in DILI biomarker concentrations over time were observed.
Especially HMGB1 levels changed over time in serum gel and serum samples (see wider mean difference scale and the observed wide mean difference bars). A significant increase in HMGB1 concentration was observed between serum gel samples with 15 min and 60 min benchtop time ($p = 7.83E\text{-}03$). HMGB1 levels increased over this time period of 45 min by 112% ±126% (mean ±SD) in serum gel and remained comparably steady in EDTA plasma with a mean decrease of -8% ±36% (mean ±SD).
The mean differences in OPN, MCSF1R, and GLDH concentrations remained within ±25% across all time intervalls and matrices. Nonetheless, significantly less OPN concentration was observed in serum gel samples with 60 min benchtop time compared to samples with 15 min benchtop time ($p = 3.52E\text{-}02$).
The protein levels of ccK18 showed a higher variation over time based on the higher mean difference (wider bars) in serum gel or serum compared to plasma. However, the mean % differences across benchtop time points were not statistically significant.

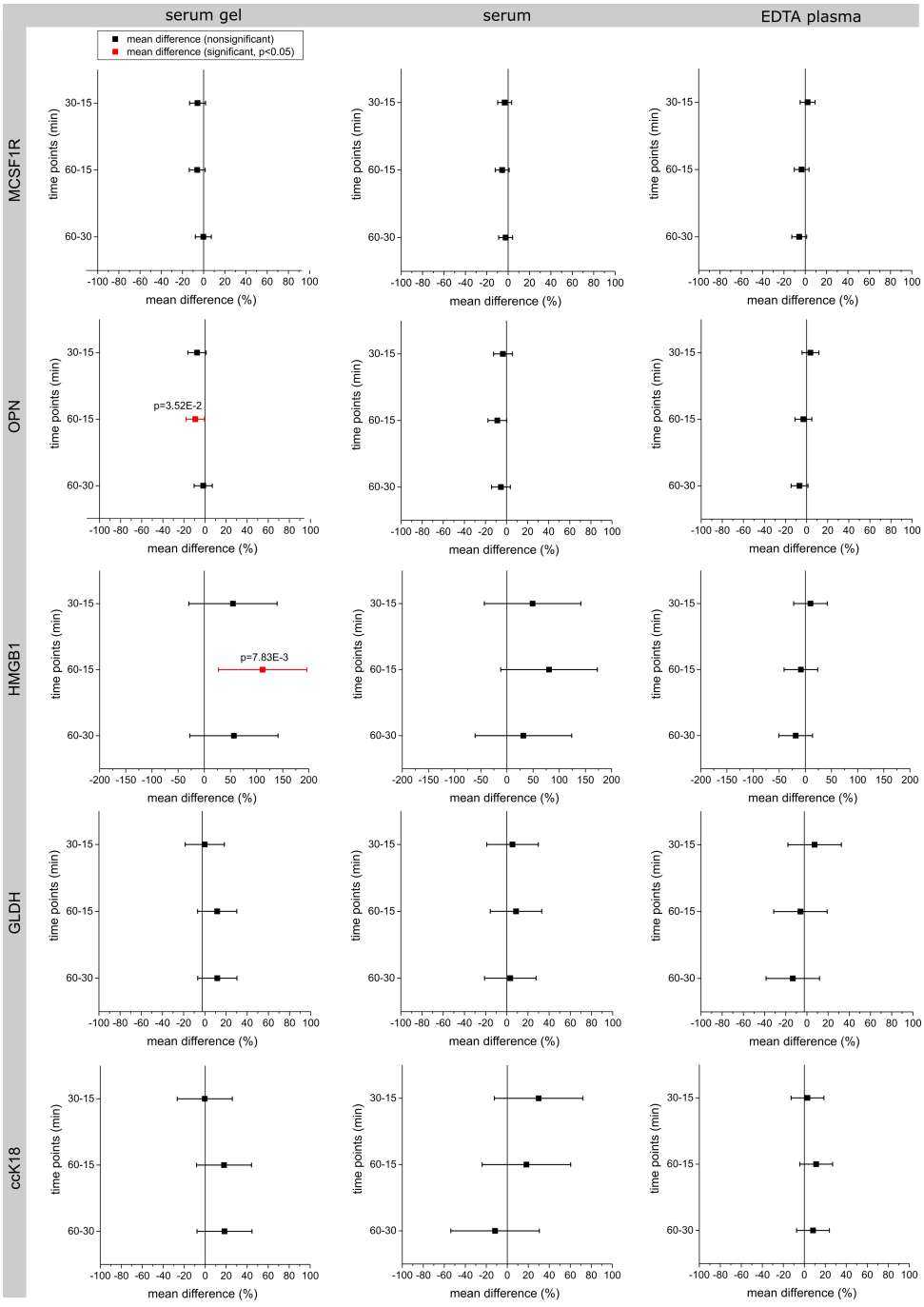

Figure 34: Change in analyte concentrations during benchtop stability between 15 min and 60 min benchtop time. One-way repeated measures ANOVA testing with Bonferroni correction ($p < 0.05$) was used to test significant changes in DILI analyte concentrations over time in all sample types. Incubation time intervals (15 - 30 min, 15 - 60 min, 30 - 60 min) between sample collection and centrifugation were investigated for the samples obtained from 10 HVs. Positive mean difference reveals an increase in analyte level over time and negative mean differences show decreased analyte levels over time. Measurement results of IA-LC-MS/MS (MPh-dev) and ELISA (ccK18). Note: HMGB1 data are shown with a larger difference range in the diagram due to stronger observed changes.

4.3.3 Correlation between standard methods and IA-LC-MS/MS

DILI-related biomarkers were measured in serum gel, serum, and EDTA plasma samples from 10 donors using the MPh-dev assay for OPN, MCSF1R, HMGB1, and GLDH with quantification based on the IA-LC-MS/MS method and the ELISA kits for quantification of ccK18 and K18. The same samples were measured using single-analyte immunoassays (Luminex: OPN and MCSF1R; ELISA: HMGB1) and an enzymatic activity assay (GLDH) as available standard methods to assess the impact of the quantification approach on biomarker concentration. The extent of correlation between protein quantification with IA-LC-MS/MS compared to immunoassay or enzymatic assay was investigated for all samples. Results of serum gel, serum, and EDTA plasma measurements collected for all benchtop incubation times were included in this comparison (**Figure 35**). The measured MCSF1R results showed a moderate positive correlation ($R^2 = 0.64$) between results from the IA-LC-MS/MS method and the immunoassay method. Very high correlation was observed for HMGB1 assessed via IA-LC-MS/MS and ELISA (**Figure 35**, $R^2 = 0.91$).

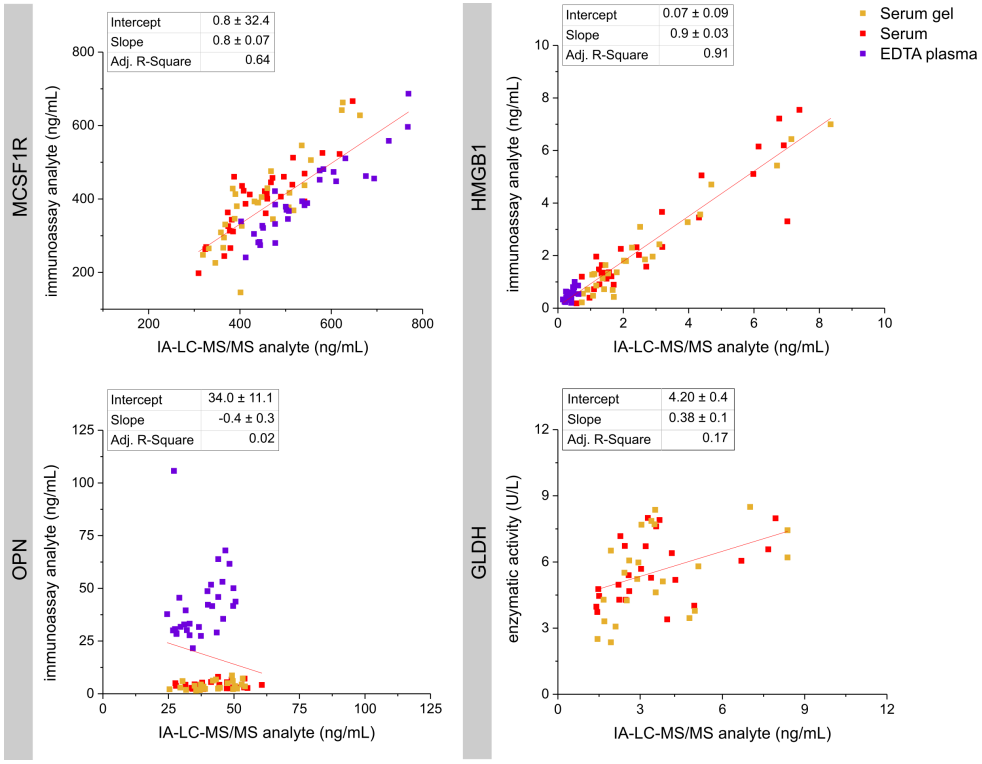

Figure 35: IA-LC-MS/MS and immunoassay or enzyme assay method comparison. DILI biomarker results of samples across all matrices measured with different methods were compared (MCSF1R: immunoassay vs IA-LC-MS/MS, n = 89; HMGB1: ELISA vs IA-LC-MS/MS, n = 78; OPN: immunoassay vs IA-LC-MS/MS, n = 82; GLDH: enzyme activity vs IA-LC-MS/MS, n = 47). No IA-LC-MS/MS assay was available for K18 and ccK18. Donor 3 was excluded from GLDH result correlation to avoid a bias towards samples with high GLDH levels.

HMGB1 levels in EDTA plasma appear in the lower ng/mL concentration range measured with both methods. Consistenly lower OPN concentrations were measured in serum gel and serum samples by quantification via the immunoassay compared to quantification via IA-LC-MS/MS. Thus, no correlation was observed between results of both methods ($R^2 = 0.02$). Furthermore, only a low positive correlation was observed when comparing only EDTA plasma samples between both methods ($R^2 = 0.37$, plot not shown here, excluded donor 10 (60 min), $n = 29$). Donor 3 (60 min) with 106 ng/mL OPN concentration was excluded for this correlation analysis to avoid bias towards higher OPN concentration. The measured GLDH activity did not correlate with GLDH protein concentration across serum gel and serum samples ($R^2 = 0.17$). Results of donor 3 were excluded for GLDH method correlation analysis to avoid bias towards higher GLDH concentration.

4.4 Translational protein biomarkers for DILI investigation in preclinical studies with APAP, DAPM, thioacetamide, bromobenzene, and CCl_4

This chapter was adapted from the manuscript **Anselm, V.**, Meisinger, T., Laurent, S., Sautier, L., Poetz, O., Elevated GLDH and OPN levels in plasma of rats treated with APAP or DAPM. (in preparation)

The impact of drugs or compounds known to induce liver injury was investigated in animals including APAP, DAPM thioacetamide, bromobenzene, and CCl_4. Rats were treated with single drugs or compounds according to the summary given in **3.2.4**. EDTA plasma samples were kindly provided by Sanofi and MSD. Furthermore, rat liver specimen for the APAP and DAPM studies were provided by Sanofi. Studies with APAP, thioacetamide, and bromobenzene included dose-ascending or escalation, whereas the effects of DAPM and CCl_4 were investigated over time. Each collaboration partner provided samples from APAP studies, Sanofi with 1,500 mg/kg APAP dosage and MSD with 1,000 mg/kg APAP dosage. CCl_4 was dosed daily. Control animals received the corresponding vehicle solutions without drug or compound at the same time as the treated animals. Enzyme activity of ALT was measured in serum samples at the corresponding collection site, the data was kindly provided by the collaborators and then analyzed by me. All samples were analyzed using the developed multiplex IA-LC-MS/MS assay MPr including measurement of OPN, GLDH, HMGB1, MCSFR, and ccK18. Due to limited sample volume, K18 could not be analyzed. EDTA plasma (2 x 15 µL per sample) and liver tissue samples (2 x 8 µg per sample in 15 µL surrogate matrix) were processed and measured in duplicates with the respective calibration curves and QC samples. Only results with CV below 30% were taken into account.

Results below LLOQ were generally not back-calculated in fmol or ng/mL but reported as AUC ratios. Data points for the potential DILI biomarkers OPN, GLDH, HMGB1, and MCSF1R measured in rat EDTA plasma were displayed color-coded according to the respective ALT activity result (**Figures 37, 39, 42,** and **44**). A common reference range for ALT values in rats could not be used since reference ranges in literature vary between 10 - 40 U/L and 52 - 224 U/L[153,154]. Hence, the lowest ALT activity range used for color-coding was calculated based on the range in ALT activity measured in all samples of control animals of the here presented studies (6 - 91 U/L).

4.4.1 ALT

Significantly higher enzymatic ALT activity was observed in serum of rats treated with all tested drugs (**Figure 36**, Mann-Whitney test). ALT activity is significantly elevated in serum of rats treated either with 1,000 mg/kg or 1,500 mg/kg APAP (**Figure 36A, B**). Thereby, a median ALT activity of 87 U/L and 169 U/L was observed compared to the control groups with 34 U/L or 27 U/L, respectively ($n = 5$ - 6 per group). Furthermore, a dose-dependent increase in ALT activity was monitored for thioacetamide (**Figure 36C**). Significant increase was observed between the control group and the 50 or 100 mg/kg treated group ($p < 0.05$). Dosage with 300 mg/kg bromobenzene resulted in exceedingly high ALT activity (median 2,412 U/L) and an ALT activity of 610 U/L (median) was observed with a higher dose of bromobenzene (750 mg/kg) (**Figure 36D**). ALT activity was still about 27-fold higher with high-dose bromobenzene treatment compared to the control group (23 U/L ALT activity). A single dose with 250 mg/kg DAPM resulted in significantly increased ALT activity (300 U/L) in rats after 24 h compared to the control group with 53 U/L ALT activity (**Figure 36E**, $p < 0.01$). A significantly increased ALT activity of 134 U/L was also observed 96 h after DAPM treatment compared to the control group. Furthermore, a significantly increased ALT activity was observed when comparing samples of rats 3 h after treatment with 24 h or 96 h after treatement ($p < 0.01$). The control group seems to have slightly higher ALT activity 24 h after dosage with vehicle solution compared to the 96 h control group.
Daily dosing with CCl_4 resulted in time-correlated elevations of ALT activity when comparing control samples with samples of treated animals (8 day treatment, 15 day treatment). Furthermore, an increased activity was observed when comparing animals treated for 15 days with animals treated for 4 days or 8 days (**Figure 36F**). Moreover, a small significant change in ALT activity was observed between the control animals treated for 8 days and 15 days with vehicle solution. Samples of study day 3 were not analyzed for ALT activity.

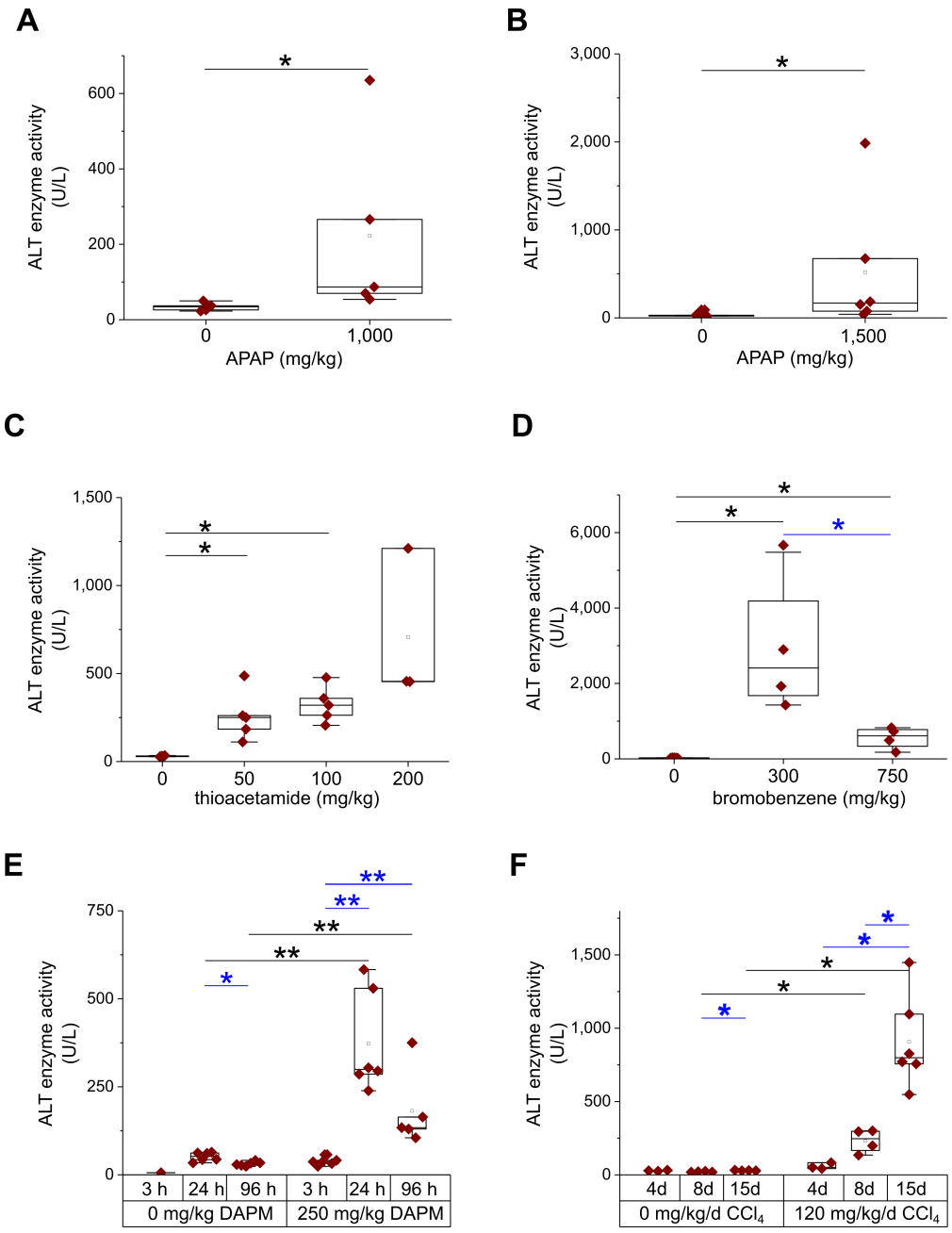

Figure 36: Enzymatic ALT activity in serum of preclinical DILI studies with rats. Serum samples were analyzed for ALT activity in U/L at Sanofi and MSD (n = 3 to 6 animals per group). Data for analysis was kindly provided by Sanofi **(B, E)** and MSD **(A, C, D, F)**. CCl_4 was dosed daily. Each data point represents a sample from an individual animal, time-course experiments were also performed with individual animals per monitored time interval, thus, results are not paired. Mann-Whitney significance test (*$p < 0.05$, **$p < 0.01$) with comparison between control and treated (black) or within the respective groups (blue). Day of treatment: study day 1. Day of sampling: DAPM & CCl_4: as shown; APAP: study day 2; thioacetamide: study day 2; bromobenzene: study day: 3.

4.4.2 OPN

OPN protein concentration was measured in EDTA plasma and liver samples of the preclinical studies using the MPr assay. Treatment with APAP (1,500 mg/kg), thioacetamide, DAPM, and CCl_4 led to elevated OPN levels in rat plasma (**Figure 37**). One sample of the bromobenzene study (300 mg/mL bromobenzene) and three samples of the thioacetamide study (100 and 200 mg/kg thioacetmide) were measured above ULOQ (3,540 ng/mL), thus, these samples were diluted 1:8 in surrogate matrix and reprocessed. OPN was significantly increased in samples of rats treated with 1,500 mg/kg APAP (Mann-Whitney test, $p < 0.05$, **Figure 37B**), but was not significantly increased in samples of rats treated with 1,000 mg/kg APAP (**Figure 37A**).
A dose-dependent significant increase in OPN plasma concentration between thioacetamide treated rats (50 and 100 mg/kg) and control rats was observed ($p < 0.05$) (**Figure 37C**). Furthermore, elevated OPN levels were observed in the groups treated with 100 mg/kg or 200 mg/kg thioacetamide compared to the animal group treated with 50 mg/kg thioacetamide. Treatment with thioacetamide caused generally high elevations of OPN plasma concentration (up to 7,300 ng/mL).
No significant increase was observed in animals treated with bromobenzene (**Figure 37D**). However, the OPN increase in samples collected of bromobenzene treated animals was almost up to 20-fold, 4,000 ng/mL OPN in treated samples compared to 200 - 300 ng/mL control samples. The outlier results for the bromobenzene control group with high OPN plasma value was confirmed by reprocessing (OPN concentration in run1: 2,479 ng/mL; in run2: 2,358 ng/mL, -5% difference).
Treating rats with a single dose of DAPM resulted in a significant increase from 192 ng/mL (median) OPN concentration in EDTA plasma of control animals to a meadian of 475 ng/mL OPN concentration in EDTA plasma of treated animal within 24 h ($p < 0.01$, **Figure 37E**). Shortly after treatment (3 h), OPN levels were still within the normal range. OPN levels were 96 h after treatement at a median level of 297 ng/mL, which is less then the measured OPN levels in samples of the 24 h after treatment group. Daily administration of 120 mg/kg CCl_4 resulted in significant increases of OPN concentration 8 days and 15 days after treatment compared to control ($p < 0.05$) (**Figure 37F**). Furthermore, 15 days of CCl_4 treatment led to elevated OPN levels when compared to 3 days or 4 days of treatment.
OPN concentration was increased along with higher ALT activity especially for thioacetamide, bromobenzene, DAPM, and CCl_4 treatment. The observed outlier of the bromobenzene control group observed for OPN did not correlate with high ALT activity. No significant difference was detected in OPN concentration between the results of CCl_4 study day 8 and 15, whereas higher ALT activity was measured in the 15 day treatment group compared to 8 days of daily dosing.

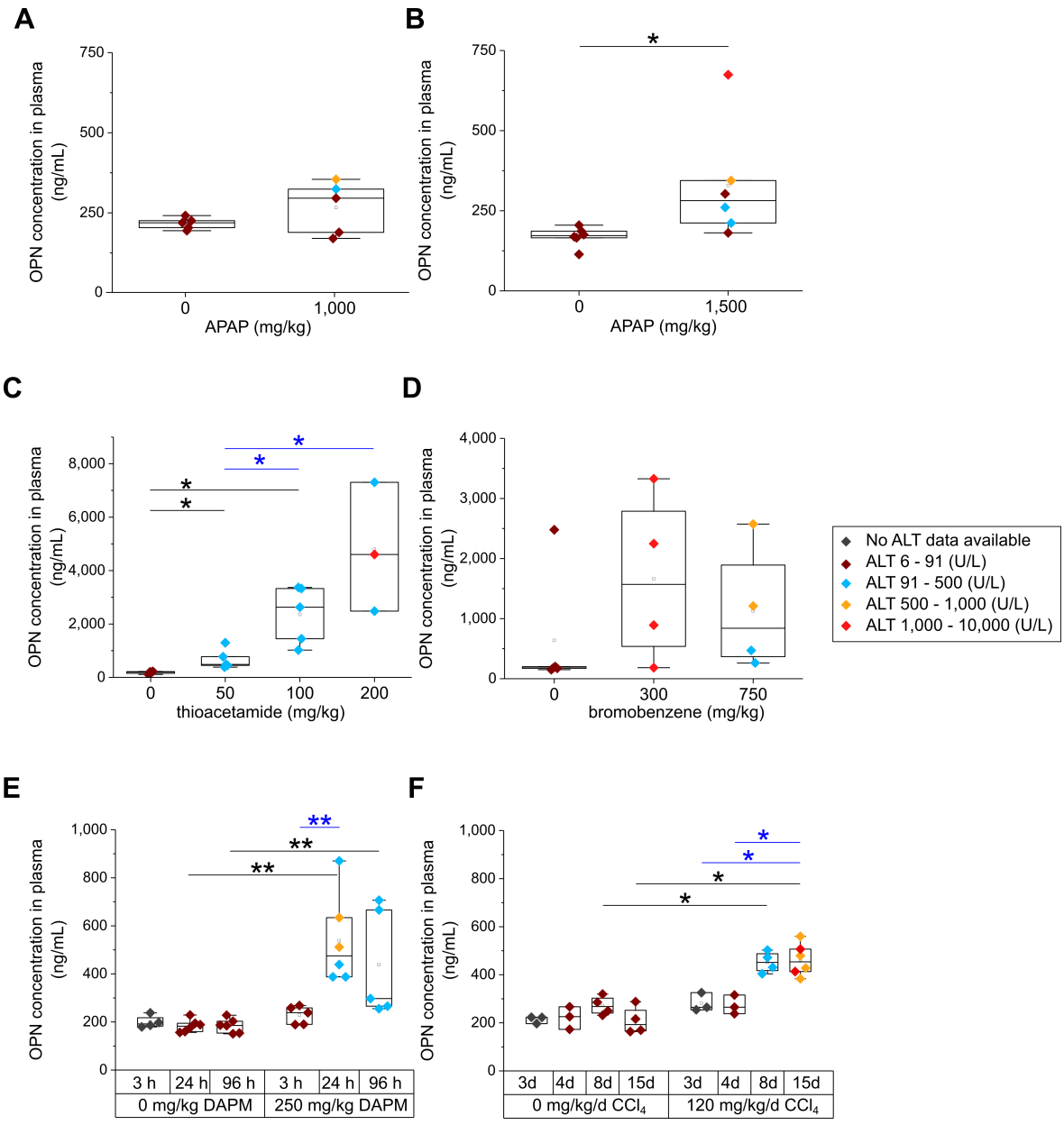

Figure 37: OPN concentration in EDTA plasma of preclinical DILI studies with rats. OPN concentration was analyzed in rat plasma samples using the IA-LC-MS/MS assay MPr (n = 3 to 6 animals per group). **(A - F)** Data points are colored by their corresponding sample result for ALT activity. CCl_4 was dosed daily. Each data point represents a sample from an individual animal, time-course experiments were also performed with individual animals per monitored time interval, thus, results are not paired. Mann-Whitney significance test (*$p < 0.05$, **$p < 0.01$) with comparison between control and treated (black) or within the respective groups (blue). Day of treatment: study day 1. Day of sampling: DAPM & CCl_4: as shown; APAP: study day 2; thioacetamide: study day 2; bromobenzene: study day: 3.

OPN measurement was performed on liver tissue samples which were obtained from the studies including APAP (1,500 mg/kg) and DAPM (24 h after treatement) (**Figure 38**). The measured OPN peptide ratio was below the LLOQ ratio for all samples. The shown LLOQ ratio was determined during validation of the MPr assay across three independent runs with two calibration curves per run (**Table 26**). Thus, OPN was not measureable in liver tissue samples in quantifyable amounts.

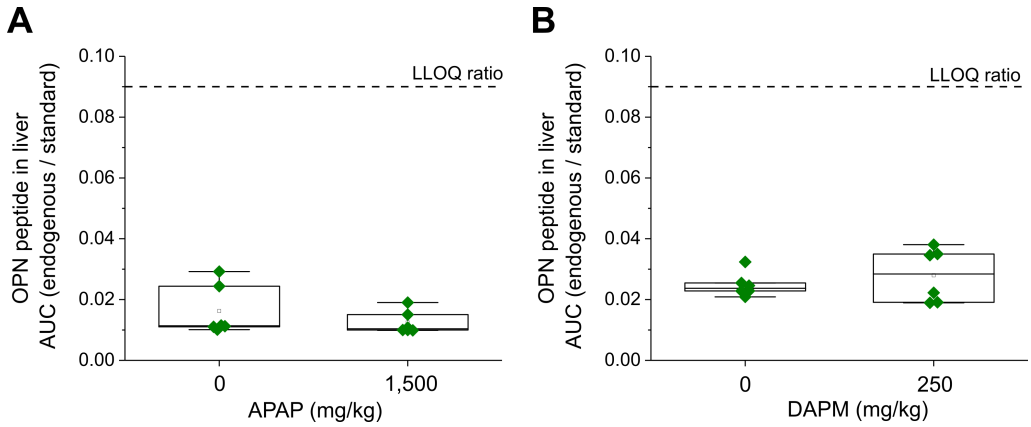

Figure 38: OPN concentration in liver tissue of preclinical DILI studies with rats.
(A, B) OPN concentration was analyzed in 8 µg rat liver tissue samples using the IA-LC-MS/MS assay MPr for the available studies with APAP and DAPM (n = 6 animals per group). AUC ratios of the measured OPN peptide and the corresponding LLOQ ratio from MPr validation are shown. Day of treatment: study day 1. Day of sampling: APAP: study day 2; DAPM: 24 h.

4.4.3 GLDH

Along with the IA-LC-MS/MS assay MPr, GLDH protein concentration was measured in rat EDTA plasma samples of the preclinical DILI studies under investigation. Changes in GLDH concentration were observed for all studies except with bromobenzene (**Figure 39**). One sample of the thioacetamide study and three samples of the bromobenzene study exceeded the ULOQ for GLDH (6,138 ng/mL). Hence, these samples were diluted 1:8 in surrogate matrix and reprocessed. GLDH protein concentration increased by 19-fold when treated with 1,000 mg/kg APAP (**Figure 39A**) or by about 4-fold for the higher APAP dosage of 1,500 mg/kg (**Figure 39B**) with generally higher GLDH concentration when treated with the higher APAP dosage. However, the median of GLDH concentration in control EDTA plasma samples differed between the study from MSD (median 13.9 ng/mL GLDH) and the study from Sanofi (median 199 ng/mL GLDH) by a fold change of 14.
A significant increase in GLDH levels was indicated after thioacetamide treatment in a dose-dependent manner ($p < 0.05$, **Figure 39C**). The increase was observed between control group and 50 mg/kg (91-fold change) or 100 mg/kg (356-fold change) thioacetamide treated group. Furthermore, a significant increase was indicated between sam-

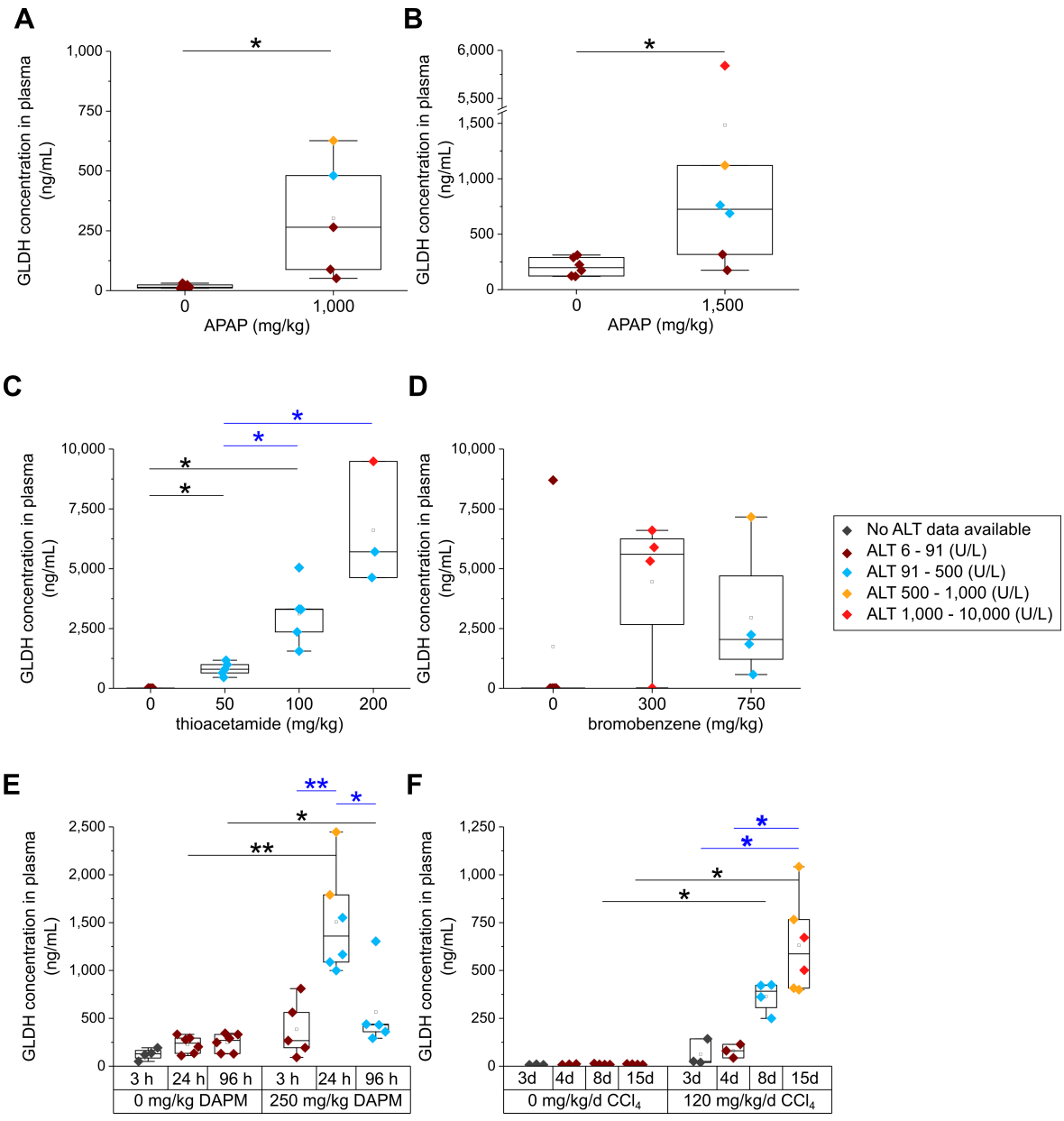

Figure 39: GLDH concentration in EDTA plasma of preclinical DILI studies with rats. GLDH concentration was analyzed in rat plasma samples using the IA-LC-MS/MS assay MPr (n = 3 to 6 animals per group). **(A - F)** Data points are colored by their corresponding sample result for ALT activity. CCl_4 was dosed daily. Each data point represents a sample from an individual animal, time-course experiments were also performed with individual animals per monitored time interval, thus, results are not paired. Mann-Whitney significance test (*$p < 0.05$, **$p < 0.01$) with comparison between control and treated (black) or within the respective groups (blue). Day of treatment: study day 1. Day of sampling: DAPM & CCl_4: as shown; APAP: study day 2; thioacetamide: study day 2; bromobenzene: study day: 3.

ples of low-dose (50 mg/kg) and higher-dose (100 mg/kg and 200 mg/kg) treated rats with fold changes of 4 and 2, respectively. The GLDH protein concentration in rat plasma was highly affected by administration of thioacetamide or bromobenzene since the levels increased up to about 9,000 ng/mL GLDH (**Figure 39C, D**). However, one sample in the control group of the bromobenzene study resulted in similarly high GLDH concentration. Reprocessing of this sample confirmed the obtained high GLDH level (run1: > ULOQ, run2 (diluted and back-calculated with dilution factor): 8,697 ng/mL). No significant differences were observed throughout the bromobenzene study for GLDH. It is not clear whether samples were mixed up during shipment for this study, thus, no further statistical testing without outliers were performed for this compound.
A single-dose treatment with 250 mg/kg DAPM resulted in elevated levels of GLDH 24 h after treatment compared to control ($p < 0.01$, **Figure 39E**). Elevated levels were still observable 96 h after DAPM treatment ($p < 0.05$). Within the treated groups, a fast increase could be observed between 3 h and 24 h after treatment ($p < 0.01$), which resulted then in significant recovery of GLDH levels 96 h compared to 24 h after treatment($p < 0.05$).
After 8 days and 15 days of CCl_4 treatment, GLDH levels rise significantly compared to samples of non-treated animals ($p < 0.05$, **Figure 39F**), which was also the case when comparing samples of rats treated for 15 days with treatment for 3 days or 4 days.
Comparable to higher ALT activity, higher GLDH protein levels were observed in the CCl_4, thioacetamide, DAPM, and bromobenzene studies. The outlier in GLDH concentration observed in the bromobenzene control group was not confirmed with high ALT activity.
GLDH activity was measured in rat serum for the animal studies with DAPM and APAP (1,500 mg/kg) at Sanofi (**Figure 40**). GLDH activity was significantly elevated in serum of APAP-treated as well as of DAPM-treated animals when compared to their respective control group (**Figure 40A, B**). GLDH activity and GLDH protein concentration of the corresponding samples was compared by linear regression using results of the treated animal groups (above LLOQ of 5 U/L). Results of control groups were excluded since most of the results were below LLOQ and outliers of the treated groups were excluded according to Tukey's method[152]. A moderate correlation was observed between the GLDH activity and GLDH protein concentration of the corresponding samples (**Figure 40C**).
Rat liver tissue samples of the studies including APAP (1,500 mg/kg) and DAPM (24 h after treatement) dosage were examined by digesting 8 µg tissue material in surrogate matrix and measurement with the MPr assay. GLDH was well observed in rat liver tissue with between 2 to about 9 ng GLDH per total protein amount (**Figure 41**). However, no significant differences were observed in any of the here investigated studies (Mann-Whitney significance test).

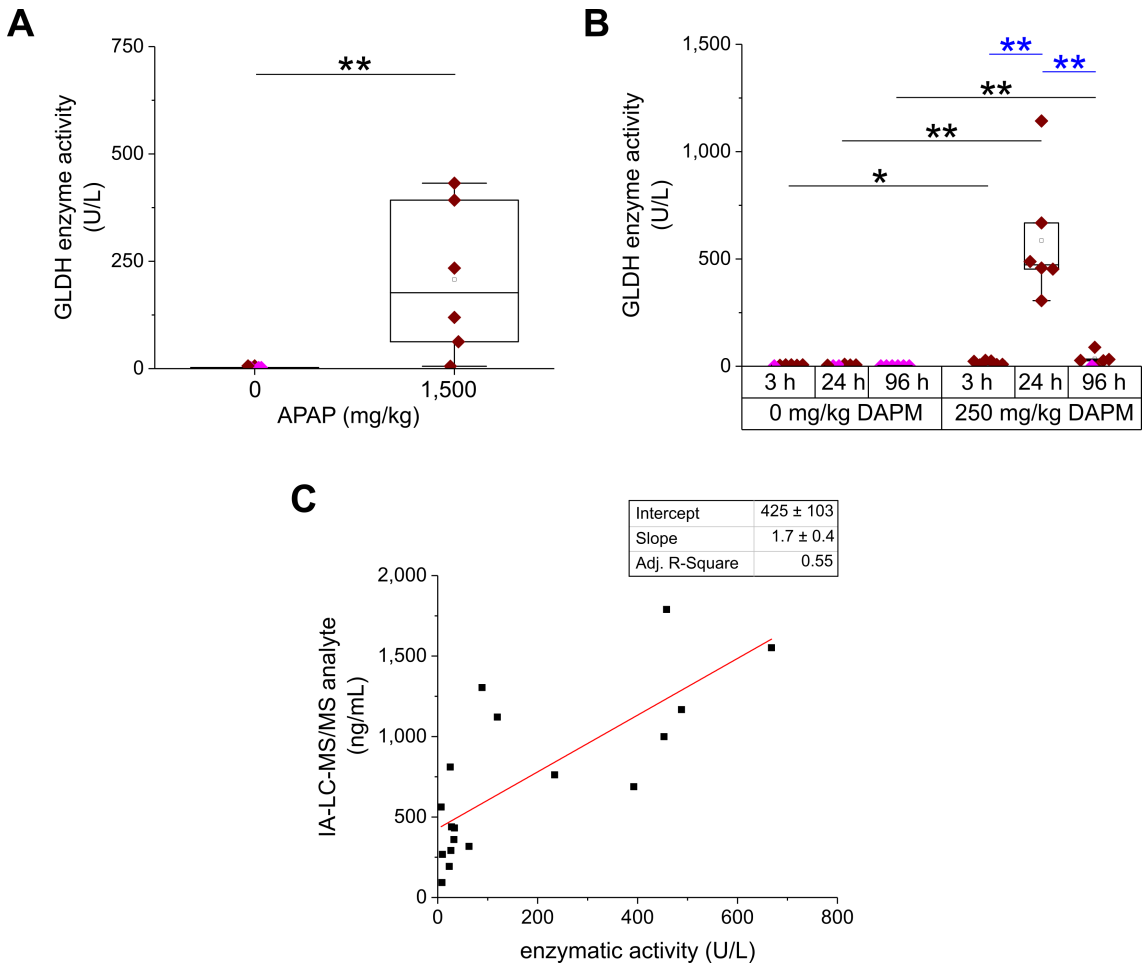

Figure 40: GLDH activity results in studies with APAP (1,500 mg/kg) and DAPM and correlation with protein concentration data. (A, B) GLDH activity in rat serum was measured at Sanofi (n = 6 animals per group). Results below LLOQ were represented in pink as LLOQ/2 according to Wakefield's method[140]. Each data point represents a sample from an individual animal, time-course experiments were also performed with individual animals per monitored time interval, thus, results are not paired. Mann-Whitney significance test (*$p < 0.05$, **$p < 0.01$) with comparison between control and treated (black) or within the respective groups (blue). Day of treatment: study day 1. Day of sampling: APAP: study day 2; DAPM: as shown. **(C)** GLDH activity and protein concentration was compared with all results of the treated animal groups excluding outliers according to Tukey's method[152] (n = 18).

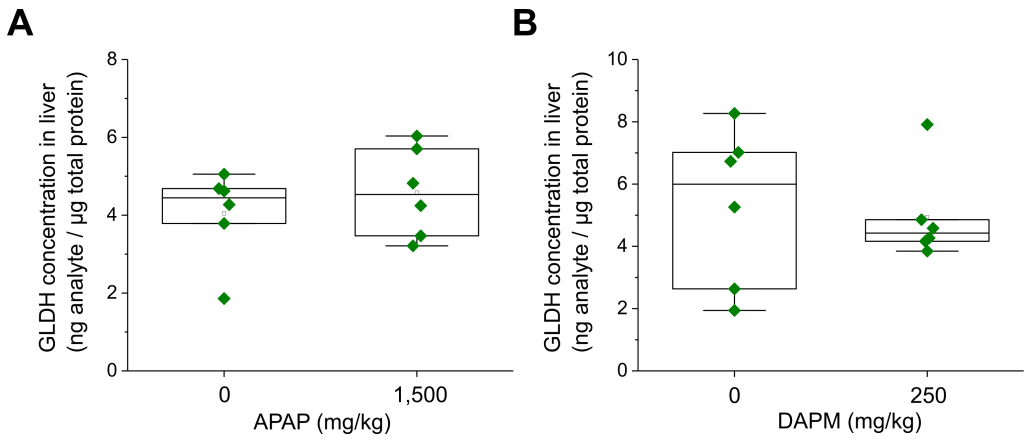

Figure 41: GLDH concentration in liver tissue of preclinical DILI studies with rats. **(A, B)** GLDH concentration was analyzed in 8 µg rat liver tissue samples using the IA-LC-MS/MS assay MPr for the available studies with APAP and DAPM (n = 6 animals per group). GLDH could be quantified in all liver tissue samples in ng GLDH per µg total protein. Day of treatment: study day 1. Day of sampling: APAP: study day 2; DAPM: 24 h.

4.4.4 HMGB1

HMGB1 protein concentration was measured in EDTA plasma samples of rats treated with drugs and compounds including APAP, thioacetamide, bromobenzene, DAPM, and CCl_4. Several samples showed HMGB1 protein concentrations below the LLOQ (1.70 ng/mL). Hence, half of the LLOQ value was used for plotting and statistical analysis of results for HMGB1 plasma levels below LLOQ. Significant increases in HMGB1 levels were observed for thioacetamide, bromobenzene, DAPM, and CCl_4 treatment according to the Mann-Whitney significance test (**Figure 42**). APAP treatment did not result in significant changes of HMGB1 levels between control and treated groups (**Figure 42A, B**).

HMGB1 protein concentration was highly affected in the thioacetamide treated groups compared to the respective control group ($p < 0.05$, **Figure 42C**). All treated groups showed elevated HMGB1 levels compared to control and the median increased up to 35-fold between the non-treated group (0.85 ng/mL) and the high-dose treated group (200 mg/kg thioacetamide, 29.5 ng/mL HMGB1). Furthermore, a dose-dependent increase in HMGB1 plasma concentration was observed between samples of rats treated with 50 mg/kg and 100 mg/kg or 200 mg/kg thioacetamide and between samples of rats treated with 100 mg/kg and 200 mg/kg thioacetamide. Bromobenzene resulted in elevated HMGB1 levels betwen high-dose samples (750 mg/kg bromobenzene) and control samples (**Figure 42D**). In case of DAPM, the only significant elevation of HMGB1 concentration was observed 3 h after dosing with DAPM compared to the corresponding control group (**Figure 42E**).

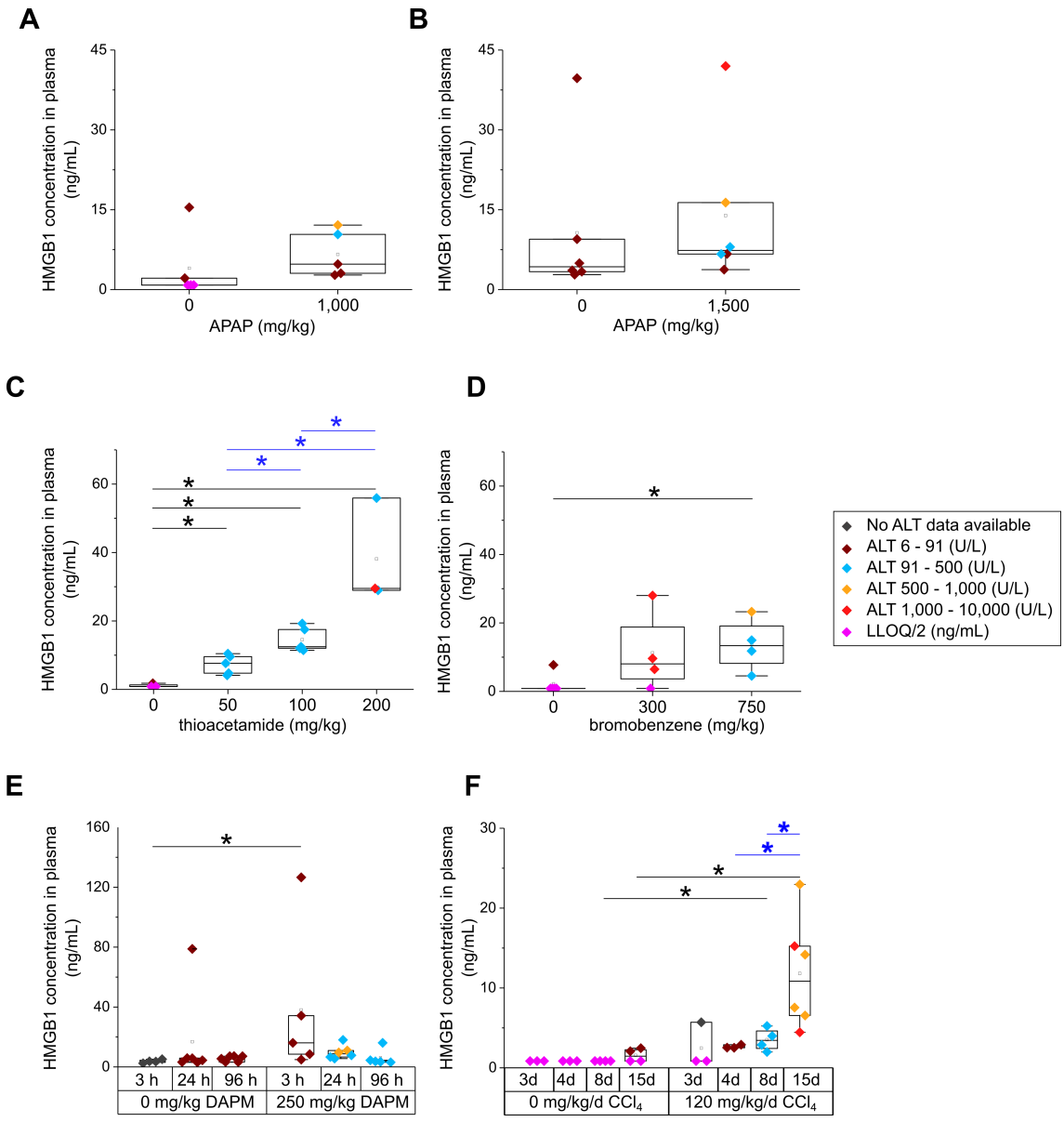

Figure 42: HMGB1 concentration in EDTA plasma of preclinical DILI studies with rats. HMGB1 concentration was analyzed in rat plasma samples using the IA-LC-MS/MS assay MPr ($n = 3$ to 6 animals per group). **(A - F)** Data points are colored by their corresponding sample result for ALT activity. CCl_4 was dosed daily. Each data point represents a sample from an individual animal, time-course experiments were also performed with individual animals per monitored time interval, thus, results are not paired. Mann-Whitney significance test (*$p < 0.05$) with comparison between control and treated (black) or within the respective groups (blue). Day of treatment: study day 1. Day of sampling: DAPM & CCl_4: as shown; APAP: study day 2; thioacetamide: study day 2; bromobenzene: study day: 3.

Treatment with 120 mg/kg CCl_4 per day resulted in significant elevations of HMGB1 protein concentration 8 days and 15 days after treatment compared to control ($p < 0.05$) (**Figure 42F**). Moreover, HMGB1 levels were significantly elevated 15 days after daily CCl_4 treatment in comparison to HMGB1 levels in the samples of animals with 4 days or 8 days of daily CCl_4 administration. Elevated levels in HMGB1 concentration along with increased ALT activity were measured in the study samples with thioacetamide, bromobenzene, and CCl_4. Likewise, an increase in HMGB1 concentration could be monitored between 8 day and 15 day CCl_4 treatment. Results of both biomarkers are especially not comparable within the DAPM study, since HMGB1 protein concentration did not increase over time, whereas higher ALT activity was monitored over time after DAPM dosing.
Rat liver tissue samples were available of the studies with APAP (1,500 mg/kg) and DAPM (24 h after treatement). According to the MPr assay workflow, 8 µg tissue material was digested in surrogate matrix and HMGB1 levels were quantified. HMGB1 could be measured in all available rat liver tissue samples (**Figure 43**). Consistent protein amounts between 0.2 and 0.8 ng HMGB1 per total protein amount were demonstrated but significant differences between samples of control and treated animals could not be confirmed according to the Mann-Whitney significance test.

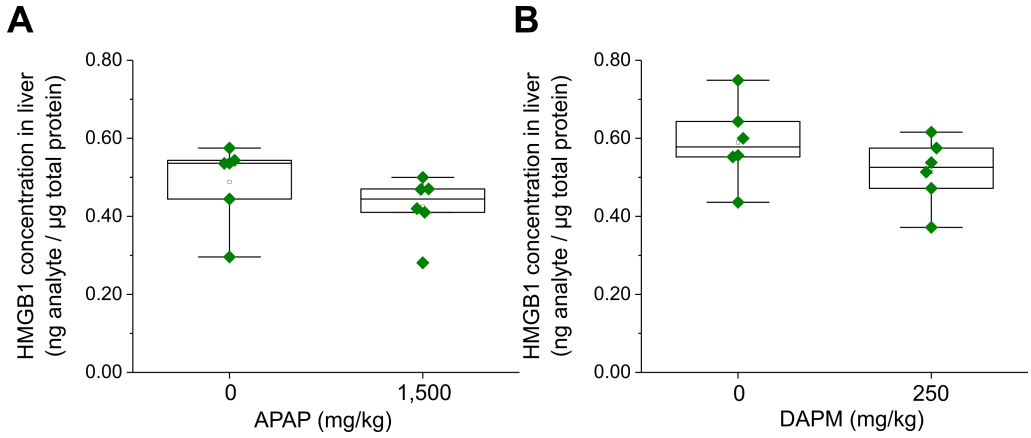

Figure 43: HMGB1 concentration in liver tissue of preclinical DILI studies with rats. (A, B) HMGB1 concentration was analyzed in 8 µg rat liver tissue samples using the IA-LC-MS/MS assay MPr for the available studies with APAP and DAPM (n = 6 animals per group). HMGB1 was quantified in all liver tissue samples in ng HMGB1 protein per µg total protein amount. Day of treatment: study day 1. Day of sampling: APAP: study day 2; DAPM: 24 h.

4.4.5 MCSF1R

MCSF1R protein was quantified in preclinical DILI samples using the multiplexed IA-LC-MS/MS assay MPr. In total, five samples showed MCSF1R levels above the LLOQ (12.4 ng/mL). Thus, AUC ratios of the MCSF1R peptide measured with CV < 30% in duplicate samples and the corresponding LLOQ ratio from MPr validation were

presented (**Figure 44**, LLOQ ratio: **Table 16**). MCSF1R results of the studies with APAP (1,000 mg/kg), thioacetamide, and bromobenzene are not shown because the corresponding QC sample results for MCSF1R were not within ±30% of the nominal QC values (failed QC accuracy for the measured batch). These samples could not be reprocessed due to limited sample volume. The measured MCSF1R peptide signals did not reveal changes in peptide ratios after APAP (1,500 mg/kg) treatment (**Figure 44A**). Significantly elevated MCSF1R peptide ratios were observed when comparing ratios between control and DAPM treated animal samples (96 h) or between 24 h and 96 h after DAPM treatment (Mann-Whitney test, $p < 0.05$, **Figure 44B**). One of the samples with 96 h after DAPM treatment reached a MCSF1R peptide ratio above the LLOQ

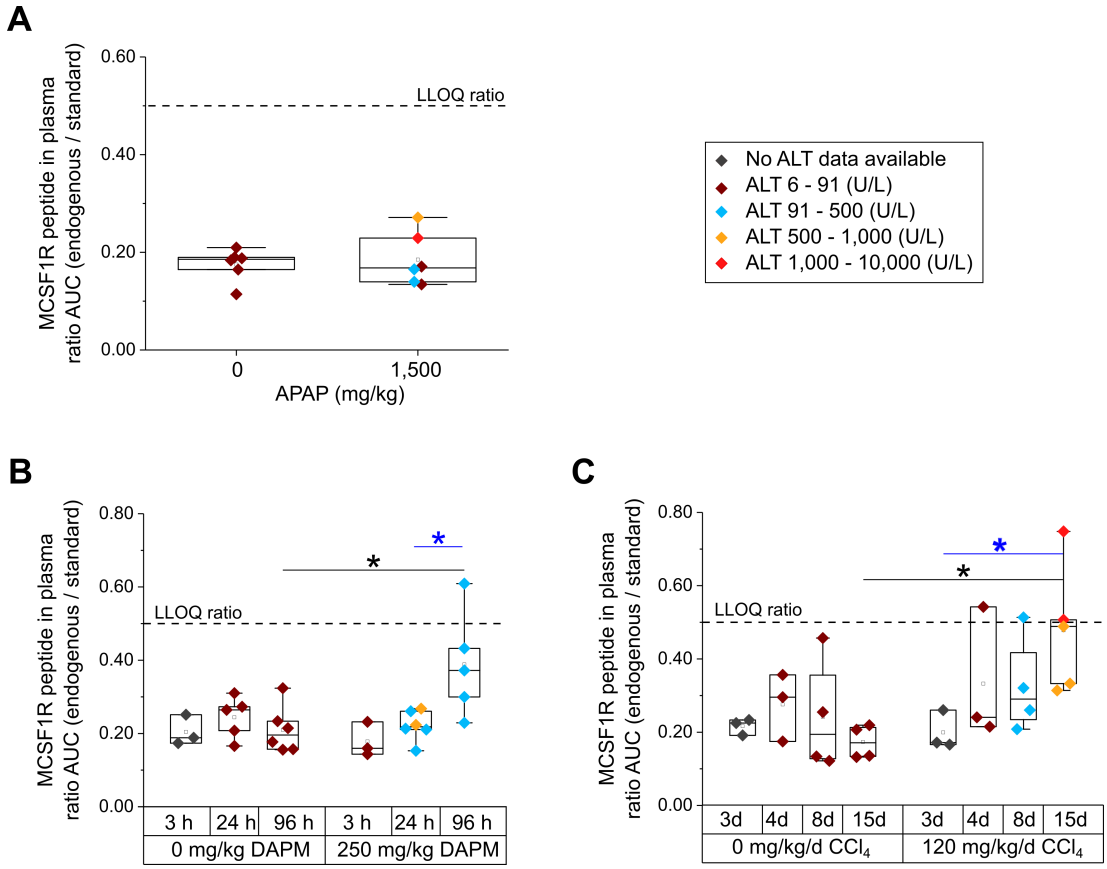

Figure 44: MCSF1R peptide ratio in EDTA plasma of preclinical DILI studies with rats. MCSF1R content was analyzed in rat plasma samples using the IA-LC-MS/MS assay MPr ($n = 3$ to 6 animals per group). **(A - C)** AUC ratios of the MCSF1R peptide measured with $CV < 30\%$ in duplicate samples and the corresponding LLOQ ratio from MPr validation are presented. Data points are colored by their corresponding sample result for ALT activity. CCl_4 was dosed daily. Each data point represents a sample from an individual animal, time-course experiments were also performed with individual animals per monitored time interval, thus, results are not paired. Mann-Whitney significance test ($^*p < 0.05$) with comparison between control and treated (black) or within the respective groups (blue). Day of treatment: study day 1. Day of sampling: DAPM & CCl_4: as shown; APAP: study day 2.

ratio. Daily treatment with CCl_4 resulted also in increased MCSF1R peptide ratios compared to the control group (**Figure 44C**). The first of four samples above the LLOQ ratio within this study was observed on the fourth study day. Significant increase in ratios was seen for MCSF1R on the 15th study day after daily treatment compared to the corresponding control group ($p < 0.05$). In addition, MCSF1R results were elevated within the treated animal group between 3 days and 15 days after daily treatment ($p < 0.05$). Along with elevated ALT activity in specimen of animals treated with DAPM or CCl_4, MCSF1R concentration was increased in EDTA plasma. This effect was observed especially 96 h after DAPM administration or after 15 days of daily CCl_4 dosing. The corresponding liver tissue samples of the APAP (1,500 mg/kg) and DAPM studies did not indicate any MCSF1R peptide ratios close to the LLOQ ratio (**Figure 45**). All ratios were close to zero, hence, no MCSF1R could be measured in liver tissue samples with this assay.

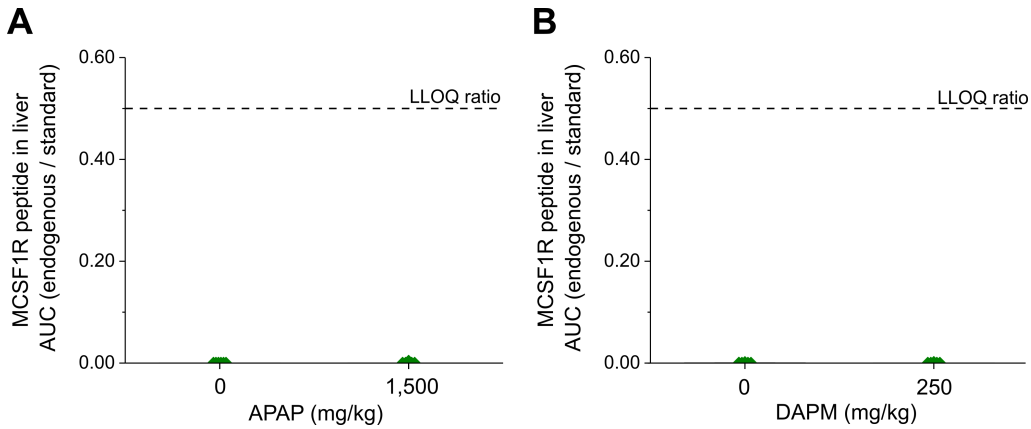

Figure 45: MCSF1R peptide ratio in liver tissue of preclinical DILI studies with rats. **(A, B)** MCSF1R concentration was analyzed in 8 µg rat liver tissue using the IA-LC-MS/MS assay MPr for the studies including APAP and DAPM (n = 6 animals per group). All measured MCSF1R peptide ratios were below the LLOQ ratio which was determined during method validation. Day of treatment: study day 1. Day of sampling: APAP: study day 2, DAPM: 24 h.

4.4.6 ccK18

Analysis of EDTA plasma samples and the corresponding liver tissue samples of the preclinical DILI studies with the assay MPr included also read-out of ccK18 levels. Endogenous ccK18 could not be measured in any of the EDTA plasma or liver tissue samples (**Figures 46A - C** and **47A, B**). Only AUC ratios were shown when duplicate measurements could be measured with a precision below 30% CV. Since this requirement failed for more than 80% of the ccK18 results of the APAP (1,000 mg/kg), thioacetamide, and bromobenzene studies, the according data was not shown. The respective ALT activity color-coding was not applied for ccK18 results since all AUC ratios were close to zero.

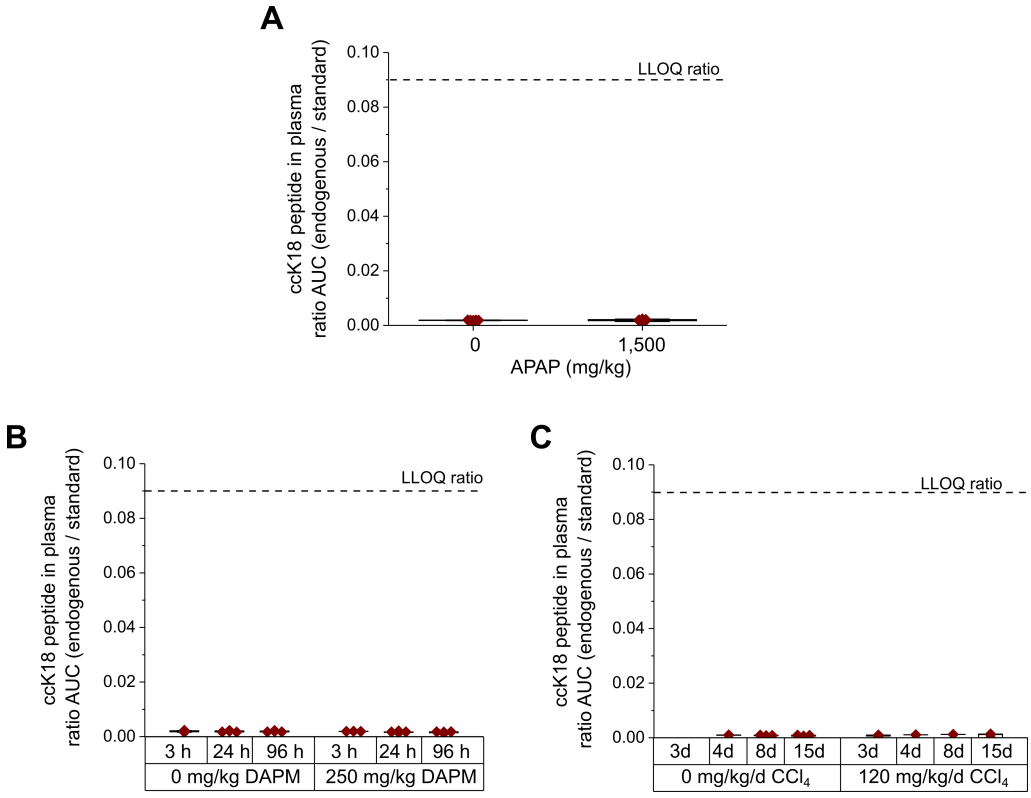

Figure 46: ccK18 peptide ratio in EDTA plasma of preclinical DILI studies with rats. ccK18 content was analyzed in rat plasma samples using the IA-LC-MS/MS assay MPr (n = 3 to 6 animals per group). **(A - C)** AUC ratios of the ccK18 peptide measured with CV < 30% in duplicate samples and the corresponding LLOQ ratio from MPr validation are presented. CCl_4 was dosed daily. Day of treatment: study day 1. Day of sampling: DAPM & CCl_4: as shown; APAP: study day 2.

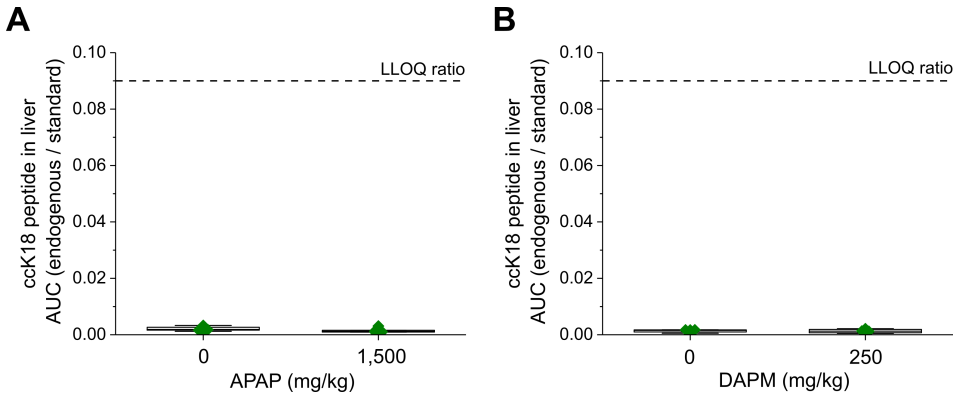

Figure 47: ccK18 peptide ratio in liver tissue of preclinical DILI studies with rats. **(A, B)** ccK18 content was analyzed in 8 µg rat liver tissue using the IA-LC-MS/MS assay MPr for the studies including APAP and DAPM (n = 6 animals per group). Results of the measured ccK18 peptide ratios were below the LLOQ ratio. Day of treatment: study day 1. Day of sampling: APAP: study day 2, DAPM: 24 h.

4.5 Specificity of DILI protein biomarkers in rat tissue

The investigated potential DILI biomarkers are proposed to come from underlying mechanisms such as hepatocellular apoptosis, necrosis, and inflammation[155]. To investigate tissue specificity of the potential DILI biomarkers, various types of rat tissue were investigated for DILI biomarker content. Types of tissue ranging from brain, lung, kidney to ovaries were lyzed according to the procedure described for liver tissue lysis, total protein content was determined and 8 µg tissue was proteolyzed in 15 µL surrogate matrix according to the liver tissue proteolysis. Pancreas samples from three animals were available. GLDH and HMGB1 could be measured in all investigated types of tissue (**Figure 48A, B**), whereas OPN, MCSF1R, and ccK18 were not measurable. Only AUC values measured for OPN below LLOQ were shown since more than 80% of the samples measured in duplicates resulted in measurement with CV below 30% (**Figure 48C**), which was not the case for MCSF1R or ccK18 measurements. GLDH was highly abundant in liver, followed by kidney, pancreas and brain. HMGB1 showed concentration values above the ULOQ for ovaries and lung tissue. Tissue was not diluted for these samples since parallelism of liver tissue samples diluted in surrogate matrix failed.

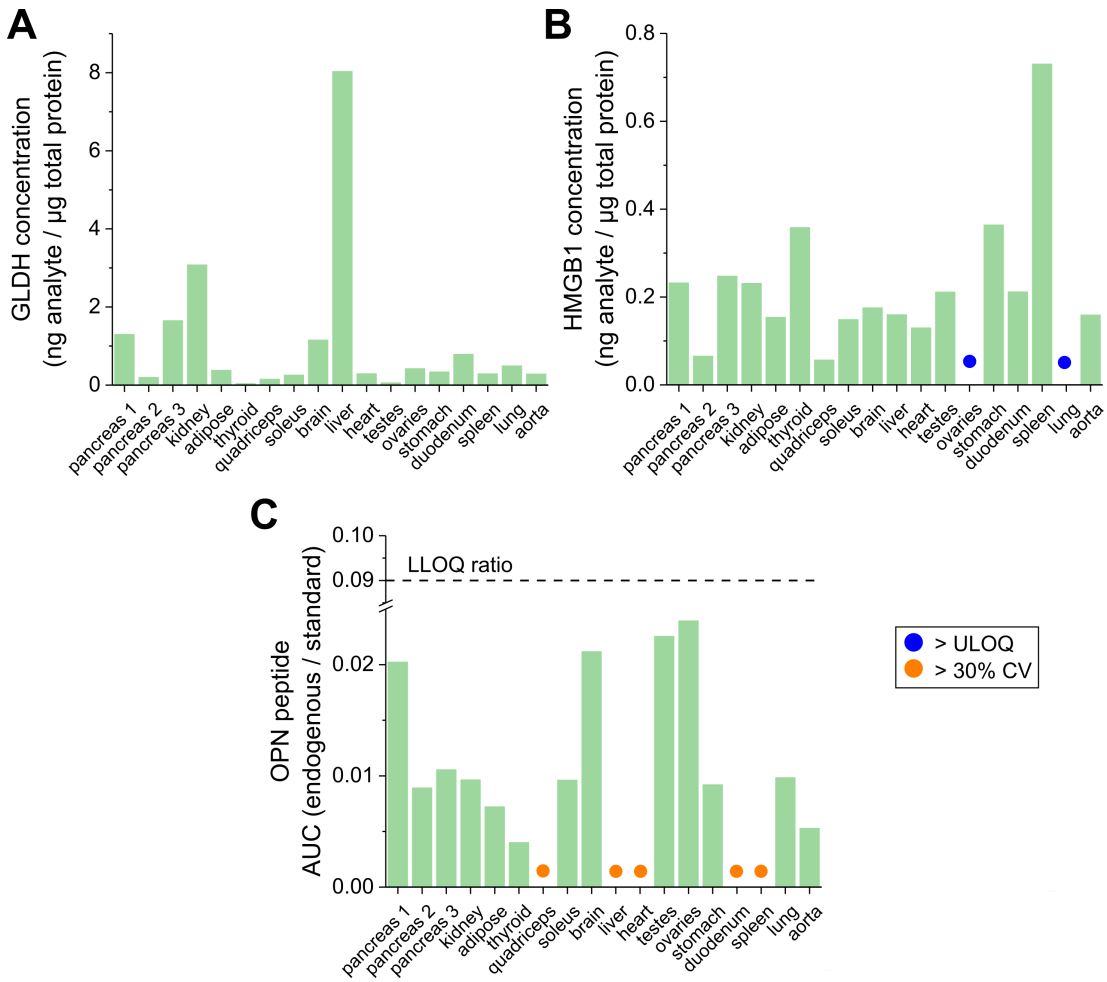

Figure 48: Specificity of DILI biomarkers in rat tissue. **(A)** GLDH and **(B)** HMGB1 concentration could be measured in various rat tissue samples (n=3 for pancreas, n=1 for other tissue, duplicate measurement for each tissue sample). HMGB1 concentration in ovaries and lung tissue was measured above ULOQ. **(C)** OPN was measured consistently below LLOQ in all tissue samples. Duplicate measurements for quadriceps, liver, heart, duodenum, and spleen tissue showed more than 30% CV. MCSF1R and ccK18 results are not shown because more than 80% of the sample replicates were measured below LLOQ and with a CV above 30%.

5 Discussion

5.1 IA-LC-MS/MS assays applied to analyses in plasma

5.1.1 Combining sensitivity and selectivity in IA-LC-MS/MS assays

Plasma remains a challenging type of specimen for protein analysis, yet this type of body fluid is readly accessible and often sampled for diverse analyses regarding patient health and disease[156]. Common analysis approaches include measurement of enzyme activity and assessment of protein concentration using immunoassays, e.g., sandwich immunoassays. This type of immunoassay struggles with lack of concordance across different platforms, presence of autoantibodies, saturation of reagent antibodies, protein denaturation, protein degradation, and cross-reactivity all possibly leading to falsified analyte quantification[106]. An emerging approach for protein quantification is provided by immunoaffinity-mass spectrometry (IA-MS)[109] termed IA-LC-MS/MS when coupled to liquid chromatography and read-out based on MS^2 fragments. Using this approach only one antibody is required to enrich and quantify proteins on the peptide-level in plasma as opposed to two required antibodies for sandwich immunoassays (e.g., ELISA[103,157] or Luminex technology[158]). Furthermore, autoantibodies may mask biomarker quantification on protein level making it impossible to quantify, for example, HMGB1 or thyroglobulin with a sandwich immunoassay in plasma[110,159]. This shows the need for alternative approaches such as peptide-based approaches that do not require enrichment via the protein's structure, e.g., the IA-LC-MS/MS method. This method is sensitive enough to measure MCSF1R, HMGB1, OPN, and GLDH in at least 5 µL human plasma (**Figure 16**) in 96-well format with a total plate processing time of 23 h and 12 min measurement time per sample (**Figure 12**). This results in less than one hour processing and measurement time per sample when considering 36 samples being processed in duplicates along with calibration curve and QC samples. Plasma proteome profiling by Geyer *et al.* showed in 2016 about 300 reproducibly measurable plasma proteins without use of antibodies. Among these proteins, only MCSF1R could be quantified in 9 of 15 runs by label-free quantification (LFQ). Peptide pre-fractionation increased the number of identified proteins to more than 1,000. This deep plasma proteome profiling enabled LFQ-based quantification of OPN and HMGB1. Furthermore, GLDH peptides were identified in plasma using this approach but could not be quantified. In comparison, MCSF1R and OPN could be quantified with internal peptide standards in all 89 human plasma and serum samples, which were investigated for matrix and sampling comparison (section **4.3**). HMGB1 and GLDH

were quantified in at least 80% of these measured samples, thereby showing the depth of sensitivity introduced by IA-LC-MS/MS compared to standard plasma proteome profiling[102,160]. Especially increasing the antibody amount and decreasing the internal standard peptide amount seem beneficial for better assay sensitivity (**Figure 15**). Both approaches for increasing sensitivity hold the concept of increasing the number of antibody binding sites for endogenous peptides from the protein of interest. On the one hand, more antibodies can simply bind more peptides, on the other hand, less internal standard peptides result in more free binding sites for endogenous peptides during competition for antibody binding sites. However, the antibody amount can only be increased in reasonable extent due to limited antibody availability and due to limited transfer capacity of the semi-automated procedure used here for peptide enrichment since a maximum amount of 25 µg antibody can be transferred using 50 µL of bead suspension (data not shown here). Alternatively, an immunoprecipitation approach using antibodies coupled to columns can be employed for affinity enrichment. Coupling can involve binding of the Fc region of the antibody by protein G or by strepatavidin capturing of biotinylated antibody. Depending on the size of the column, the binding capacity can be increased and online peptide enrichment can be performed before MS read-out. However, high background signals due to the high binding capacity also incorporating unspecific binding or carryover are common issues when using columns for peptide enrichment[109]. The internal standard peptide amount can only be decreased to improve the signal-to-noise ratio as long as the peak intensity is still sufficient to be read-out with MS. The peak intensity depends on the ionization efficiency of the peptide, which is in turn determined by its amino acid composition with basic amino acids having higher ionization efficiency[161].
However, focusing on peptides also has certain pitfalls which have to be considered for using the IA-LC-MS/MS technique. Peptide properties such as hydrophobicity influence the performance in chromatography as shown for the ccK18 peptide (**Figure 14**). Due to carryover and peptide aggregation, quantification of ccK18 and K18 was not possible using IA-LC-MS/MS, which is why ELISA kits were required to quantify these proteins for matrix and sampling comparison (section **4.3**). The elution time of both investigated peptides were both after minute six of the gradient (K18: elution time at 6.1 min **Figure 14**; ccK18: elution time at 6.8 min, peak not shown), which is technically already within the wash phase of the gradient with 99% of eluent B (LC elution solvent). The later the elution time compared to the gradient, the more hydrophobic is the structure eluted from the chromatographic column[162]. Furthermore, both peptides comprise many leucines, which is a very hydrophobic amino acid. However, according to Kyte and Doolittle[163], the investigated peptides show a hydrophobicity score of -0.4 and -0.7. It was expected, that such late eluting peptides would have a higher hydrophobicity score. Since especially the ccK18 peptide LLEDGEDFNLGDALD comprises 40% of hydrophobic amino acids, the high percentage of hydrophobic amino acids compared to the total length of the peptide might cause the long retention time on the

column with C18-material.
Additionally to physical or chemical peptide properties, selecting the right peptide for protein quantification is highly important also in biological context. Protein sequence parts need to be targeted that are available in the investigated context, such as for MCSF1R it was highly important to target a peptide which is theoretically part of the external receptor area and might be shedded during activation of the receptor[74]. In case of OPN, a truncated protein variant produced by activated thrombin had to be taken into account which is elaborated below in section **5.2**. Post-translational modifications (PTMs) and single nucleotide polymorphisms (SNPs) also alter the mass-to-charge ratio of endogenous peptide, thereby altering the enrichment efficiency[164] and required mass-to-charge ratio to be targeted for MS read-out. Since this quantification approach depends on internal standard peptides as reference peptides, any change of the endogenous peptide properties would exclude them from quantification.
Considering selectivity, the IA-LC-MS/MS approach has the advantage that potential cross-reactivity between antibodies and similar proteins can be completely neglected. For instance, HMGB1 and HMGB2 are highly similar, forcing high caution when selecting the right antibodies for HMGB1 or HMGB2 identification and quantification[165]. Using MS as read-out, the antibody for enrichment would be irrelevant, when either HMGB1- or HMGB2-specific peptides are chosen for quantification. Both peptides selected for HMGB1 in this work are specific for this protein (**Table 12**). Moreover, the ability of mass spectrometers to measure their target in the low ppm area has the advantage to confirm endogenous proteins highly selective based on their amino acid sequence. With this MS feature, isoforms of the MCSF1R rat sequences with Uniprot ID Q00495 and D4ACA7 were investigated since endogenous MCSF1R was easily accessible in mouse plasma, but not in rat plasma (**Figure 26**). The experimental evidence for the unreviewed MCSF1R rat sequence with Uniprot ID D4ACA7[150] seemed more reliable due to a higher coverage of experimentally identified peptides compared to the reviewed sequence with Uniprot ID Q00495 (**Figure 27**). Hence, this protein was followed up to be enriched on the peptide level by in-house available antibodies (**Figures 28** and **29**). A different antibody than initially planned was used targeting the peptide sequence AHNNVGNSSQFFR (Uniprot ID D4ACA7) instead of ESTSTGIWLK (Uniprot ID Q00495). This was done because the corresponding sequence ESTSIGIR could not be enriched with the available antibody immunized against the sequence ESTSTGIWLK (**Figure 29**) presumably due to the shorter C-terminus. Especially the two C-terminal amino acids of a peptide sequence are crucial for peptide antibody binding, since the immunogens used for AB production were conjugated via the N-terminus to the carrier protein, thus, not being accessible for binding[151]. Hence, antibodies in animals are produced rather against the C-terminal peptide site than the N-terminal site. Targeting the peptide AHNNVGNSSQFFR (Uniprot ID D4ACA7) enabled quantification of endogenous MCSF1R in plasma of rats treated with drugs or compounds, which is further discussed below in section **5.3.5**.

A partial method validation of this multiplexed IA-LC-MS/MS measurement approach showed that synthetic peptides and contrived QC samples could be measured with acceptable accuracy and precision across three independent runs for MCSF1R, GLDH, OPN, HMGB1, and ccK18 (**Table 23**). Endogenous GLDH, OPN, and HMGB1 could be reproducibly measured in plasma samples of control animals (**Tables 22**, **40**, **41**), whereas MCSF1R was only observed in plasma of drug- or compound-treated animals and ccK18 could not be measured endogenously at all (sections **4.4.5** and **4.4.6**, respectively). The peptide SSNSMQTVQR was selected to quantify rat ccK18 since preliminary experiments with taxol-treated HepG2 cell lysate showed increased concentration of human ccK18 peptide SSNSMQTIQK whether lysate was spiked in plasma or in 20 µg BSA (appendix **Figure 50**). Taxol-treated HepG2 cells were used because taxol is known to induce apoptosis, in turn leading to caspase-3-mediated cleavage of keratin 18 in these treated cells[166,167]. Since the endogenous human ccK18 peptide could be quantified although several serine phosphorylation sites are known for this peptide[168], and the N-terminal site of the caspase-cleavage site of K18 seem to be hydrophobic for measurement via LC-MS (**Figure 14**), the C-terminal site was considered as the next option to target caspase-cleaved K18. However, phosphorylation occupancy of peptides may differ depending on the biological condition[169]. Therefore, the antibody, which was immunized against the sequence SSNSMQTIQK, may not able to enrich the phosphorylated rat-specific peptide. This peptide could possibly be phosphorylated to a larger extent in rats than in human samples measured here (appendix **Figure 50**), hence, decreasing the enrichment efficiency of endogenous rat peptide. Alternatively, the rat-specific peptide sequence may have a different amino acid composition as reported or comprises amino acid positions with potentially not known SNP, both leading to failing read-out of endogenous rat ccK18. Furthermore, this peptide-antibody combination might not provide a sufficient sensitivity to quantify endogenous ccK18 in rat samples.

Testing parallelism by diluting plasma or liver tissue samples in surrogate matrix showed that the same liver tissue amount should be used in case of HMGB1 quantification (**Table 39**), whereas plasma could be diluted 1:8 if required (**Table 37**). Parallelism of GLDH and OPN in plasma was demonstrated and samples comprising high GLDH and OPN concentration could be diluted in surrogate matrix to be quantified within the calibration range (see sections **4.4.2** and **4.4.3**). Taken together, this partial validation demonstrated that the analytes OPN, HMGB1, GLDH, and MCSF1R under investigation in DILI-related rat samples can be quantified confidently in a multiplexed fashion with only 30 µL sample volume (15 µL per replicate). In case of ccK18, endogenous available peptide could not be confirmed with this assay (see **4.4.6**).

5.1.2 Peptide rescue by inhibition of trypsin side reactivity

The peptide initially investigated for the analysis of K18 (LLEDGEDFNLGDALDSSNSMQTIQK) was not suitable for measurement since the stock solution of the standard peptide was not stable under the storage conditions (**Figure 14**). The other peptide investigated for the analysis of K18 (AQIFANTVDNAR) showed a particularly weaker recovery in plasma compared to the recovery in cell lysate (**Figure 17**). The type of matrix was seen to influence the performance in recovery not only for this K18 peptide but also for two HMGB1 peptides under investigation (**Figure 18**). In case of the K18 peptide and one of the HMGB1 peptides (RPPSAFFLFCSEYRPK), spiking in plasma reduced their recovery by at least 4-fold compared to spiking in cell lysate. Quantification of the other HMGB1 peptide (GEHPGLSIGDVAK) performed better in plasma than in cell lysate. The ratio between trypsin and protein content was found to drive the observed peptide recovery (**Figure 19**). Interestingly, the longer the digestion procedure was, the less K18 peptide or HMGB1 peptide RPPSAFFLFCSEYRPK was observed by 2- to 3- fold (**Figure 20**). In contrast, peptide release was improved with longer proteolysis time for the HMGB1 peptide GEHPGLSIGDVAK. Adding 10 mM PMSF seemed to be insufficient to rapidly inactivate the release of the K18 peptide and the HMGB1 RPPSAFFLFCSEYRPK since considerable peptide signal was observed at a proteolysis time of zero hours. There is a time frame of about 5 min between subsequent PMSF and trypsin addition until the 5 min heating step at 99 °C, which might be suffient for release of the observed peptides by the high trypsin amount in this test set-up. Moreover, incomplete trypsin inhibition or denaturation would also lead to an extended incubation of 2 h instead of 5 min during the immunoprecipitation. Further investigations revealed that addition of trypsin to synthetic peptides resulted in a decrease of the full length K18 peptide signal and the HMGB1 peptide signal for RPPSAFFLFCSEYRPK (**Figure 21**). Additionally, N-terminal fragments were monitored for the peptide RPPSAFFLFCSEYRPK cleaved after phenylalanines possibly indicating break-down products suggesting chymotryptic cleavage activity. Tryptic cleavage after lysine and arginine was considered almost 100% specific as shown by Olsen *et al.*[84] in 2004. However, tryptic side-reactivity, autolytic trypsin reactivity, and contamination of trypsin with chymotrypsin are discussed in literature to cause peptide cleavage driven other than specificly after lysine or arginine[170–172]. Picotti *et al.*[170] characterized a tryptic digest of five bovine standard proteins in depth and revealed numerous peptide by-products. Perutka & Šebela[171] analyzed three forms of trypsin (α-, β-, ψ- trypsin) including pseudotrypsin (ψ- trypsin), which was first described by Keil-Dlouhá *et al.* in 1971[173]. This described form of trypsin is produced by tryptic autolysis and shows chymotrypsin-like activity including cleavage after Phe and Tyr additionally to the common tryptic cleavage specificity after Arg and Lys[174]. However, pseudotrypsin is not sensitive to tosyl phenylalanyl chloromethyl ketone (TPCK), a chymotrypsin-specific inhibitor[148]. Burkhart *et al.*[172] compared trypsin of different

providers coming to the conclusion that different levels of contamination with chymotrypsin may influence the degree of non-specific cleavage. Moreover, Fang *et al.*[175] suggested chymotryptic activity in plain human serum possibly by freely circulating proteases.
The here observed release of K18 and HMGB1 peptides led to the question what is indeed causing peptide recovery in opposing directions even when released from the same protein as in the case of HMGB1. It was not clear if the plasma matrix itself, contamination with chymotrypsin or tryptic side-reactivity, e.g., in form of pseudotrypsin, influenced the peptide recovery. Therefore, chymotryptic and tryptic activity was closely investigated with the conversion of trypsin[176]- or chymotrypsin[145,177]-specific substrates and the effect of various enzyme-specific inhibitors here on (**Figure 22**). Worthington trypsin and mass spectrometry-grade Promega Gold trypsin were compared. Trypsin from both providers are chromatographically purified and treated with TPCK. The Promega trypsin is additionally modified by reductive methylation to improve autolytic resistance[178]. Substrate conversion and the influence of inhibitors was also investigated for chymotrypsin since this enzyme is considered as contaminant of trypsin from natural sources. Several conclusions were drawn from the activity test results presented in **Figure 22** and appendix **Figure 49**: (i) Trypsin showed chymotryptic activity, higher for Promega trypsin than for Worthington trypsin. (ii) Conversion of trypsin and chymotrypsin substrate could be inhibited by the trypsin-specific inhibitor TLCK (iii) PMSF was also able to inhibit conversion of chymotrypsin substrate but in lesser extent than TLCK. (iv) Tryptic activity in plasma was quenched presumably due to the high amount of protein (about 900 µg in 15 µL plasma and 1 µg trypsin). (v) Chymotryptic activity in plasma itself was not observed as opposed to the suggested chymotryptic activity in serum[175]. (vi) Neither trypsin nor chymotrypsin were inhibited by TPCK. It was surprising that chymotrypsin could not be inhibited by TPCK at the conditions investigated with 1 µg enyzme amount per well, buffer pH at 8.0, and at an inhibitor concentration of 100 µM TPCK, which is within the common working concentration of this inhibitor. The pH should have been possibly adjusted to 7.0 because the rate of inhibition was seen to be majorly influenced by the pH with a decrease of the inactivation rate by TPCK of about 50% when adjusting pH conditions by 0.5 up or down[179]. Approximately 0.04 nmol chymotrypsin was treated with 10 nmol TPCK per well, which is enough inhibitor per enzyme ratio but chymotrypsin seemed to convert substrate faster than being inhibited by TPCK at pH 7.8. The steep curves observed for substrate conversion by chymotrypsin may indicate that the reaction between chymotrypsin and substrate might be too fast for inhibition of chymotrypsin by PMSF or TPCK. Preincubation of chymotrypsin with these irreversible inhibitors could result in more successful inhibition of chymotrypsin substrate conversion.
The most striking results on two different platforms were first, the observed chymotryptic fragments on MS level (**Figure 21**) and second, the inhibition of trypsin to convert chymotrypsin substrate by the inhibitor TLCK (**Figure 22**). Since the here observed

chymotrypsin-like activity was inhibited with the trypsin-specific inhibitor TLCK, pseudotrypsin might be the most-likely reason for cleavage of the K18 peptide and the HMGB1 peptide RPPSAFFLFCSEYRPK. To finally rule out chymotrypsin contamination as reason for chymotryptic activity, recombinant trypsin should be tested for chymotryptic activity.
The effect of PMSF was exploited to rescue the K18 peptide in plasma samples of DAPM-treated rats (**Figures 24**). The recovery of K18 in liver tissue could be improved by about 12-fold by this approach. Furthermore, the rescuing effect by PMSF was confirmed in plasma and liver tissue samples as well for the HMGB1 peptide RPPSAFFLFCSEYRPK but only with a fold change increase between 2- and 4- fold (**25**). This HMGB1 peptide is possibly more prone to pseudotryptic activity and could be more susceptible to remaining active pseudotrypsin. PMSF was used instead of TLCK since TLCK is highly instable in solution, thus, handling with PMSF was considered more practical. Addition of lower trypsin amounts added at several time points may also recover the K18 peptide sufficiently but the resulting fold change should be compared with the PMSF approach. Further assay validation of this adjusted IA-LC-MS/MS workflow could provide an reliable assay to quantify K18 in rat plasma, which would answer the current demand for a K18 assay to be used for rat specimen[180].

5.2 Matrix, sampling, and methodological effects on quantification of human protein biomarkers of DILI

This chapter was adapted from **Anselm, V.**, Sommersdorf, C., Carrasco-Triguero, M., Katavolos, P., Planatscher, H., Steinhilber, A., Joos, T., Poetz, O., Matrix and Sampling Effects on Quantification of Protein Biomarkers of Drug-Induced Liver Injury. *Journal of Proteome Research.* 20(11):4985-4994. doi:10.1021/acs.jproteome.1c00478 (Nov 2021).

Diverse DILI studies involve analysis of different sample types such as plasma or serum[60,181,182]. Plasma comprises anticoagulants to prevent blood clotting, whereas serum includes this process step in its preparation workflow[183,184]. Plasma has been evaluated for quality marker panels showing that published biomarkers might be rather artefacts caused by sample handling or processing[160]. A major variable during plasma or serum preparation across several collection sites is the benchtop time between sample collection and centrifugation of sample collection tubes. It can range from direct centrifugation after sample collection (in case of plasma) up to a whole day benchtop time prior to centrifugation depending on the specimen handling by the medical staff[185,186]. The time frame between 15 min and 60 min between sample collection and centrifugation was chosen to investigate potential immediate effects within the first hour of sampling, which is expected to cover the complete clotting time in serum[185]. It is understood that 15 min incubation deviates from the recommended clotting time

of at least 30 min for serum but this short time was selected based on the investigation of plasma and serum in combination to cover recommended prompt centrifugation in case of plasma and clotting time of up to 60 min for serum. HMGB1 and OPN were investigated previously for matrix and sampling dependent differences[129–131,187]. However, it was not clear if MCSF1R, GLDH, K18, and ccK18 protein concentration might be influenced by matrix or sampling effects. Therefore, potential changes in protein concentration caused by these effects were investigated here additionally for these biomarkers.

Weng *et al.*[129] reported in 2018 higher HMGB1 concentrations in serum compared to plasma within their study and summarized this as well from literature. Ottestad *et al.*[187] found in 2020 that HMGB1 levels in plasma increased exponentially over time when incubated for more than 6 h at room temperature prior to centrifugation. In another study by Lehner *et al.*[188] in 2012, HMGB1 levels were shown to increase in serum after 6 h incubation at room temperature prior to centrifugation. Taken together, it remained unclear if the differences occur in serum with or without gel as well and if HMGB1 was released over benchtop time especially within the time frame of less than 6 h incubation before centrifugation of serum. With this work, higher median levels in HMGB1 concentration were observed in serum samples compared to plasma across all tested benchtop times (**Figure 31**, **Table 25**) confirming the reported higher HMGB1 concentrations in serum compared to plasma[129]. Furthermore, it was shown that already within a time frame of 45 min, significant elevation of HMGB1 concentration occurs in serum (**Figure 34**). Overall, the mean differences are consiberably high for HMGB1 concentration in serum going up over time to more than 200% increase in HMGB1 concentration. Most important, this increase in HMGB1 concentration was observed in both types of serum tubes, with gel and without gel. However, only a low positive correlation of HMGB1 concentration with $R^2 = 0.37$ was seen between these matched serum samples (**Figure 32**) although no general significant differences were observed between these serum types by proteome profiling performed by Geyer *et al.*[160]. A rather random release of HMGB1 in serum samples might occur during platelet aggregation as HMGB1 was demonstrated to promote this step[189] causing elevated HMGB1 levels in serum over time. Since no signifcant changes were observed for plasma within 60 min of sampling time prior to centrifugation, the use of plasma is recommended for HMGB1 quantification. However, sampling should not take more than 6 h according to the elevated plasma HMGB1 concentration observed after this sampling time by Ottestad *et al.*[187]. Both investigated quantification methods, IA-LC-MS/MS and the ELISA kit, can be used to determine HMGB1 levels due to the observed high correlation of HMGB1 concentration results (**Figure 35**).

MCSF1R shows reproducibly higher levels of about 90 ng/mL in plasma compared to serum (**Figure 31**, **Table 25**) without any change in MCSF1R levels during a sampling time of up to 60 min (**Figure 34**). Despite of this difference of about 20% compared to total MCSF1R concentration, the MCSF1R results correlated highly between EDTA

plasma and serum regardless if gel was included in serum or not (**Figure 32**). Based on this finding, it is recommended to only compare studies for MCSF1R that include the same sample matrix. Results from serum and plasma samples should not be evaluated in comparison. These results extend the knowledge on MCSF1R as candidate DILI biomarker since the impact of matrix and sampling effects on MCSF1R were not investigated prior to this work. MCSF1R results from IA-LC-MS/MS and sandwich immunoassay measurement correlated only moderately which might be caused by the used internal standard without prior amino acid quantification (**Figure 35**).
OPN measurement is highly comparable in serum and plasma using the IA-LC-MS/MS method (**Figure 31**, **Figure 32**) with a small decrease in serum gel OPN concentration between 15 min and 60 min benchtop incubation time (**Figure 34**). The decrease was significant but rather small (maximum 10%) compared to the median OPN concentration in healthy volunteer plasma or serum (**Table 44**). Due to the observed low percent difference throughout all matrices, the matrix and sampling impact on OPN concentration in clinical sample testing is expected to be low for measurements with the IA-LC-MS/MS assay. Interestingly, the well observed correlation between plasma and serum OPN results is not reflected in OPN quantification using the sandwich immunoassay method (**Figure 33**). Plasma and serum OPN concentration does not correlate in matched samples, whereas serum and serum gel shows a moderate positive correlation. Furthermore, method comparison showed that OPN quantification results were not comparable between the investigated methods (**Figure 35**). Serum results were consistently lower by 5- to 25-fold compared to plasma OPN levels confirming previously reported higher OPN concentration in plasma than in serum[130,131]. Since even OPN plasma results do not match between the two quantification methods (**Figure 35**) and different types of plasma or ELISA kits were seen to influence the OPN concentration[190], OPN quantification may has to be considered cautiously when using sandwich immunoassays. The concept of protein-targeted quantification to enrich OPN using antibodies against the protein as opposed to the peptide-targeted quantification with IA-LC-MS/MS assay might be a reason for the observed differences between the methods under investigation. The protein's structure and its prevalence in endogenous conditions might influence the enrichment efficiency during the capture and detection step of the sandwich immunoassay method. Numerous phosphorylation sites of OPN and their interaction with calcium determine the protein structure of OPN, thus, making its structure sensitive to the present calcium concentration[191]. The calcium concentration in the sample is determined by the presence of anticoagulants such as EDTA, which decrease the present calcium concentration by forming chelate complexes with calcium[192]. Changes in the calcium concentration would result in conformational changes in the structure of OPN, making it either more or less accessible for the antibodies in use for protein enrichment. Since the OPN concentration in plasma is higher than in serum when measured in protein-targeted mode, it might be that OPN is more accessible with less prevalent calicum ions as it is the case in EDTA plasma.

The differences in various types of plasma could also be explained by this hypothesis because the final calcium concentration in plasma depends on the type of anticoagulant such as EDTA, citrate, or heparin[193]. Moreover, different ELISA kits usually include antibodies from different providers, thus, the antibodies might differ in their affinity and specificity to capture OPN across ELISA kits.
Apart from the calcium-sensitive protein structure, thrombin-activated cleavage of OPN is likely to alter the accessibility of OPN between serum or plasma when measured in protein-targeted approach with antibody enrichment. OPN comprises a thrombin cleavage site within the SVVYGLR motif resulting in a neoepitope at R168 after cleavage, which is then converted from R168 to L168 by thrombin-activated carboxypeptidase B[194]. This truncated form has been discussed in view of liver fibrosis showing that cleaved OPN promotes activation of hepatic stellate cells[195]. Since thrombin is a key player during the clotting process, it is likely that higher thrombin activity results in higher concentration of truncated OPN which might be less recognized by antibodies used in ELISA kits or sandwich immunoassays, in turn, resulting in less serum OPN than in plasma. Both hypotheses might apply depending on the specificity of the corresponding antibody used for protein enrichment. An advantage of the IA-LC-MS/MS method used in this work is the peptide-targeted approach of enrichment regardless of the corresponding protein structure. If the appropriate peptide is selected for enrichment, this approach might be less prone to matrix-induced changes in the protein conformation as pointed out here with the well observed correlation between serum and plasma results for OPN (**Figure 32**).
GLDH protein concentration or GLDH activity was not affected whether gel was present in serum tubes or not and matched samples correlated well by their GLDH concentration or activity independent of the measurement approach (**Figures 32** and **Figure 33**). Although there was no significant difference between plasma and serum GLDH concentration using the IA-LC-MS/MS approach (**Table 24**), only a low positive correlation was shown between matched EDTA plasma and both types of serum samples (**Figure 32**). GLDH protein concentration did not change within a benchtop time of 60 min (**Figure 34**), thus, sampling could be excluded as source for the difference in GLDH concentration between matched plasma and serum samples. Based on the observed matrix differences, studies with GLDH protein measurement only should be compared when the underlying sample type is the same and the same sample type should be used within one study. There are several studies investigating GLDH activity in plasma[196] and serum[64,197], although the benchmark assay manufactured by Randox Labs Ltd (Roche) and other commercial activity kits such as the one used here (SigmaAldrich, Cat# MAK099) recommend using serum. GLDH activity results from plasma should be considered carefully and no comparison across studies is recommended until comparability of GLDH activity in serum and plasma is evaluated in the future.
When comparing protein and activity data for GLDH measured in human serum and

plasma, no correlation was observed (**Figure 35**). Furthermore, donor 3 showed about 20-fold higher GLDH protein concentration across all serum and plasma samples independent of the benchtop time (**Figure 31**). Enzyme activity results were all within the assay range of 2 and 10 U/L for all donors without any outlier, which is consistent with previously measured GLDH activity in normal healthy volunteer serum[60,63]. Substrate concentration and reaction rate are known to be in non-linear regression context to each other[198]. It might be that the fold change in the reference range of GLDH protein concentration is wider (e.g. between 2 and 100 ng/mL) compared to the GLDH activity reference range of 1 to 10 U/L[63], which might be reflected in this non-linear regression model. Much higher elevated GLDH levels would then be required to be measurable with higher GLDH activity. To confirm this hypothesis, comparison of GLDH concentration and activity results with more subjects are required in the future. Measurement of GLDH protein concentration could be beneficial to evaluate DILI events in the future possibly by earlier onset of elevated GLDH levels after drug-treatment compared to GLDH activity. Additionally, long-term stability of GLDH on the peptide level might exceed reproducible measurement of GLDH activity in serum samples, which is currently accepted for storage at 4 °C for 14 days or storage at -80 °C for 36 months[76].
K18 and ccK18 could not be measured with the IA-LC-MS/MS approach due to the peptide features presented in section **4.1.2**. Therefore, the impact of matrix and sampling on K18 and ccK18 was assessed by ELISA measurement. Unexpectedly, there was no correlation observed between ccK18 activity when comparing serum samples with or without gel as well as when comparing EDTA plasma with both types of serum (**Figures 32**). Furthermore, relatively wide mean differences of up to 80% were especially observed in serum during benchtop time investigation (**Figure 34**). This shows a tendency towards increasing ccK18 activity with longer incubation time between sample collection and centrifugation, although statistically not significant. Especially due to the lack in correlation between serum gel and serum samples, the question arises if ccK18 can be measured reliably in serum without this potential matrix artefact. Since the ccK18 activity remains more stable in plasma than in serum (**Figure 34**), plasma is recommended as matrix of choice for studies involving ccK18. In contrast to ccK18, the ELISA's sensitivity was not sufficient to measure K18 in plasma or serum of healthy volunteers. Therefore, matrix and sampling effects could not be evaluated for this biomarker.
Taken together, the usage of plasma is recommended for investigation of these potential DILI biomarkers mainly based on the low to non-existent correlation between serum HMGB1 and ccK18 in tubes with and without gel. Furthermore, plasma is more reliable compared to the observed statistically significant increase in HMGB1 concentration in serum samples by up to 200% when incubated for as short as 60 min before centrifugation.

5.3 Translational protein biomarkers as potential DILI markers in preclinical studies

This chapter was adapted from the manuscript **Anselm, V.**, Meisinger, T., Laurent, S., Sautier, L., Poetz, O., Elevated GLDH and OPN levels in plasma of rats treated with APAP or DAPM. (in preparation)

The effect of known DILI-inducing drugs and agents on the clinical DILI marker ALT and on emerging protein biomarkers in rat plasma was investigated by measurement of ALT activity and protein concentration determination using the multiplexed IA-LC-MS/MS assay MPr for OPN, GLDH, HMGB1, MCSF1R, and ccK18 quantification. Results for K18 measurement revealed that the proteolysis conditions used for the MPr assay could not be applied to quantify K18 (see sections **4.1.4** and **5.1.2**), thus, extending the MPr multiplex by K18 was not possible. Due to limited sample availability, DILI-related samples were measured only by the MPr assay and ALT activity measurement was conducted. Each potential translational DILI biomarker is discussed in relation to ALT in the following sections **5.3.1** to **5.3.6**. The panel of potential biomarkers and their preclinical value is discussed in section **5.3.7**.

5.3.1 ALT

Alanine aminotransferase (ALT) activity was significantly elevated in serum of rats treated with APAP. The median ALT activity doubled from 87 U/L with 1,000 mg/kg APAP treatment to 169 U/L with 1,500 mg/kg APAP treatment in independent studies (**Figure 36**). Concordingly to the study presented by McGill *et al.*[199], Sprague-Dawley rats were administered with APAP and sampling was performed 24 h after treatment for this work. However, McGill *et al.* observed no significant difference between treated and control even with APAP treatments up to 2,000 mg/kg (n = 3 - 4 per group). Furthermore, histological investigation of the corresponding rat livers did show only little to no injury. Mice were treated in the same experimental set-up by McGill *et al.* with 300 mg/kg APAP resulting in considerable increase in ALT activity and large areas of liver necrosis in histological examination. The results obtained from the mice specimen in this study coincide with a previous study showing that APAP treatment induces hepatocellular injury in form of necrosis rather than apoptosis[33]. Based on the result of McGill *et al.,* it was postulated that mitochondrial damage and oxidative stress was greatly observed in mice but not in rats[27,200]. It was concluded that rats are highly resistant to APAP-induced liver injury compared to mice. However, other studies showed increasing ALT activity already within 3 h after administration of 300 mg/kg APAP to rats[201], significantly elevated ALT levels 24 h after treatment with 500 mg/kg APAP[202], and elevated ALT activity in specimen of rats treated with 1,000 or 1,500 mg/kg APAP

24 h after administration[203]. Interestingly, our two studies with different APAP concentration were performed at two different collaboration sites (Sanofi and MSD) and both study results showed significant differences in ALT activity between control and treated groups (Mann-Whitney test, $p < 0.05$) as opposed to the study by McGill *et al.*[199]. Within our studies, ALT serum activity spread over the range between 41 and up to 1,985 U/L for the treated animals. Thus, future studies investigating hepatocellular damage by APAP measuring ALT activity could include more animals to account for such a wide-spread ALT activity upon treatment which might be a reason why McGill *et al.* did not observe liver injury effects in rats induced by APAP.
Reactive conversion products of thioacetamide converted by cytochrome P450 enzymes can drive hepatoxicity[204,205]. Elevated ALT activity could already be observed in this study in serum of animals treated with 50 mg/kg thioacetamide (**Figure 36**). The widespread results for ALT activity and the low number of animals treated with 200 mg/kg thioacetamide might be the reason why no significant difference was observed here between serum of control and high-dose thioacetamide treated animals. Thioacetamide was also previously seen to induce increased ALT activity in Wistar or Sprague-Dawley rats dosed with 300 mg/kg[206,207]. Liver damage induced by thioacetamide might be mediated by TNF-α as key player resulting in hepatocellular necrosis according to Lin *et al.*[207].
Tremendous ALT activity was shown in samples of rats treated with the mid-dose of bromobenzene (300 mg/kg) but significantly less ALT activity was observed for higher dose of bromobenzene (750 mg/kg, **Figure 36**). Tanaka *et al.*[208] demonstrated with ALT activity measurements that rats acquired resistance after repeated bromobenzene treatment. Tanaka *et al.*[209] showed later that this repeated treatment with bromobenzene also caused increased expression levels of the gene abcc3 (multidrug resistance protein; MRP3), which may contribute to bromobenzene resistance by facilitated drug elimination in the liver within the phase III reaction[210]. Multidrug resistance proteins (MRP) are known as subfamily of ATP binding cassette transporters being part of the phase III reaction during xenobiotic metabolism[13]. The high dosage with bromobenzene might be sufficient to induce a similar effect of resistance, which would explain the recovery in ALT levels between high-dose and mid-dose levels of bromobenzene. Coinciding with the results presented here, a toxicology report[46] provided by the U.S. Environmental Protection Agency (EPA) showed high ALT values in serum of rats treated with 400 mg/kg bromobenzene, whereas considerably lower ALT activity was observed when treated with 600 mg/kg. Interestingly, the reported mean ALT activity was about 900 U/L, which is considerably lower than the here observed median of 2,412 U/L. There is possibly already bromobenzene resistance observable with 400 mg/kg compared to the dosage used here with 300 mg/kg bromobenzene.
Dosage with DAPM resulted in a significant increase in ALT activity when comparing control and treated groups 24 h and 96 h after DAPM administration as well when comparing these samples from treated group to the serum samples drawn 3 h after DAPM

treatment (**Figure 36**). Furthermore, a tendency of ALT recovery can be seen after 96 h compared to the 24 h group. These results could reflect the initial impairment of biliary epithelial cells resulting in impaired bile duct flow, in turn leading to cholestasis and hepatocellular necrosis[41,211]. The bile duct then recovers by transdifferentiation of hepatocytes to biliary epithelial cells[42], which could possibly be reflected by the lower ALT activity measured 96 h after DAPM treatment.
CCl_4 induces mitochondrial damage and oxidative stress resulting in hepatocellular necrosis mediated by its reactive metabolite produced during biotransformation[35]. This compound can be used to model chronic liver injury in animal studies[212,213]. Daily dosage CCl_4 resulted in a stepwise increase of serum ALT activity of treated animals (**Figure 36**). Significantly higher ALT activity was observed in test groups starting from 8 days treatment with CCl_4 compared to the control group. Furthermore, ALT activity was even significantly increased between 8 and 15 days of CCl_4 treatment.

5.3.2 OPN

Among its various functions, OPN is actively involved in inflammatory processes such as chemotaxis and cell activation since it is released as cytokine by macrophages, dendrites, or other immune cells[214]. Elevated OPN concentrations were observed in rat plasma for all drugs and compounds (**Figure 37**). Hepatocellular damage as well as biliary injury seem to induce increased OPN concentration in rat plasma of treated animals. This was previously confirmed for patients with acute liver failure induced by hepatocyte necrosis[181]. A tendency of increasing OPN concentration could be seen with 1,000 mg/kg APAP dosage compared to the control group, but a significant increase was first observed with 1,500 mg/kg APAP (**Figure 37A, B**). Higher APAP concentrations seem to be required to induce significant OPN response compared to the already observable significant ALT response on 1,000 mg/kg APAP (**Figure 36**). The highest measured OPN value within the APAP studies was also measured in the sample with highest ALT activity in serum of APAP treated animals, which presumably reflects higher immune response caused by more necrotic liver cells. He *et al.*[215] presented a dual role of OPN being both protective and harmful during APAP toxicity. Hepatic OPN exhibits its protective role by inhibiting APAP metabolism via preventing an increased expression of cytochrome P450 enzymes that are involved in APAP turn over, thus, decreasing the rate of reactive metabolite NAPQI. According to He *et al.,* OPN shows its harming role by later promoting toxicity during inflammatory stage by proinflammatory cytokine expression and enhancing inflammatory infiltration, ultimately leading to cell death of stressed hepatocytes. Hepatic OPN could not be observed in liver tissue of rats treated with APAP and DAPM (**Figure 38**). The MPr assay seems not sensitive enough to quantify OPN in 8 µg liver tissue protein. OPN was previously measured between 2-8 pg analyte per gramm tissue using an ELISA kit[216]. PTMs are not reported for the peptide used for OPN quantification (**Table 12**), hence,

tissue specific changes in the PTM-state of the peptide are not likely to cause this lack in measurable OPN peptide in liver tissue.
Interestingly, the OPN concentration in rats treated with thioacetamide increased with higher fold change compared to the controls (more than 10-fold with 100 mg/kg thioacetamide) than the observed changes in ALT activity with almost all treated samples remaining below 500 U/L ALT activity (**Figure 37C**). OPN was indeed to be up-regulated during thioacetamide-induced liver fibrosis in rats[216,217] confirming the here observed OPN response to thioacetamide treatment of rats (**Figure 37C**). The inflammatory reaction might be induced more by thioacetamide than by APAP since exceedingly high OPN concentration was measured compared to the APAP-induced in OPN concentration.
Similar to the OPN results from thioacetamide treatment, bromobenzene treatment resulted in exceedingly high OPN levels, especially within the animal group dosed with 300 mg/kg bromobenzene (**Figure 37D**). However, no significant difference was observed presumably due to outlier in the control group with about 2,500 ng/mL OPN compared to the usual 200 ng/mL OPN in healthy animal plasma. Since this sample was measured twice, a sample mix up at our site is not likely. Similar to ALT, a decrease in OPN concentration could be observed for the high-dose treated group but not as clear as for the ALT results. The resistance mechanism induced by bromobenzene treatment might be indicated also by OPN, but not as strongly as by ALT activity. The two samples with the highest ALT activity within the high-dose animal group displayed also the highest OPN concentration. However, these results have to be considered carefully since significant differences in OPN concentration were not observed within this study.
A single dose of DAPM showed elevated OPN concentration 24 h after dosing which then recovery for three of five animals after 96 h (**Figure 37E**). Such a variability in concentration of more than 3-fold within one group was not seen for ALT activity in the 96 h-animal group (**Figure 36E**). A longer monitoring would have been interesting for the animals with higher OPN concentration to see if there is an adverse outcome potentially predicted by these prolonged elevated OPN levels. OPN was previously associated as potential predictor of liver failure in clinical studies[60,182].
Treatment with CCl_4 resulted in higher OPN plasma concentration of rats which were treated for 8 days and 15 days (**Figure 37F**). Interestingly, the increase between day 8 and day 15 regarding ALT activity was not pointed out by OPN concentration since the OPN levels were comparable between both groups. OPN was also previously linked to liver fibrosis in mice by OPN-mediated activation of hepatic stellate cells during CCl_4 treatment[218].

5.3.3 GLDH

GLDH can be found in high amounts in liver tissue (**Figure 48**) since this protein is a mitochondrial protein involved in the urea cycle[61]. A similar GLDH concentration was measured in all liver tissue samples of control and treated animals of the APAP (1,500 mg/kg) and DAPM studies. Since GLDH protein is suggested to be released by necrotic hepatocytes into the blood stream[155], there would be a decrease in necrotic areas of the liver tissue. However, the same amount of liver protein is used for proteloysis irrelevant of the area of necrosis, therefore, a change in GLDH concentration is rather expected in plasma (**Figure 39**) than in liver lysate (**Figure 41**).
Consistent with the ALT activity results of the APAP studies presented in this work (**Figure 36A, B**), the GLDH concentration increased significantly in plasma of rats treated either with 1,000 mg/kg or with 1,500 mg/kg APAP (**Figure 39A, B**). The observed GLDH concentration pattern in the high-dose treated group was comparable with the ALT activity in the same samples (**Figure 39B**). The fold change in GLDH protein concentration between treated and control within the 1,000 mg/kg APAP study was about 19-fold, which is considerably higher and by two days earlier than the GLDH activity with fold change of maximum 10 with 1,000 mg/kg APAP observed by Thulin *et al.*[203]. Furthermore, GLDH activity peaked in plasma of humans three days after hospitalization and abnormal liver function tests[197]. However, the control sample baseline in the study with 1,500 mg/kg APAP was about 10-fold higher than the baseline of the 1,000 mg/kg APAP study, which in turn, resulted in a smaller fold change of 4-fold for the 1,500 mg/kg APAP treated animals compared to the control animals. This might have been a result of different diet or vehicle administration between the two APAP studies from Sanofi and MSD. Further investigation of GLDH baseline across different collection sites should be investigated for clarification. Studying GLDH activity in serum revealed an even higher significant difference in GLDH activity (**Figure 40**) than GLDH protein concentration (**Figure 39**) with both measured in samples collected 24 h after treatment with 1,000 mg/kg APAP. Similarly, a stronger significance was observed for changes in GLDH activity after DAPM treatement compared to the measured GLDH concentration. The concordance of GLDH activity and protein concentration should be investigate further to shed more light on the here moderately observed correlation with higher sample numbers than $n = 18$ (**Figure 40C**).
Thioacetamide showed great impact on the GLDH concentration in plasma starting already with administration of 50 mg/kg thioacetamide (**Figure 39C**). Similar to OPN, the fold change in GLDH concentration between control (median 30 ng/mL GLDH) and treated groups, e.g., 3,298 ng/mL GLDH with 100 mg/kg thioacetamide, was by one magnitude higher than observed for the ALT activity results (100-fold for GLDH compared to 10-fold for ALT). Giffen *et al.*[219] demonstrated an increase in GLDH activity of more than 60-fold in plasma of rats 30 h after treatment with 150 mg/kg thioacetamide showing less fold change with higher drug dosing.

The corresponding sample showed an exceedingly high GLDH concentration in the control group of the bromobenzene study as observed with OPN results (**Figures 39D** and **37D**). Three of four samples showed a GLDH concentration above 5,000 ng/mL in the animal group treated with 300 mg/kg bromobenzene and three of four samples showed the tendency to recover with regard to GLDH concentration with high-dose bromobenzene. Every test group in this study comprises outliers according to Tukey's method[152], which is why conclusions on GLDH concentration upon bromobenzene treatment are limited. In a study with rats treated with 1,500 mg/kg bromobenzene, GLDH activity increased from a fold change of 50 to more than 300 between treated and non-treated rat plasma samples within 31 h and 54 h after treatment[219]. Such a high dose would have been expected to result in a bromobenzene resistance as it was seen for ALT[208,209] and corresponding to the here observed tendency towards recovery for OPN and GLDH levels (**Figures 39D** and **37D**).
GLDH concentration increased significantly 24 h after DAPM treatment and recovered again after 96 h (**Figures 39E**). Such a significance in recovery was not observed for ALT activity or OPN concentration, but was better observed with GLDH activity (**Figure 40**). An increase of GLDH concentration was observed starting from day 8 in the CCl_4 study comparable to the OPN and ALT results (**Figure 39F**). Coinciding with the ALT activity results, the GLDH concentration in rat plasma significantly increased between day 8 and day 15 of the study. Overall, GLDH reflected the ranking in ALT activity values very well in most cases when comparing results from the same samples, e.g., the highest ALT activity was almost always observed in samples with the highest GLDH concentration (except for two samples of the CCl_4 study and the bromobenzene study). This supports the opinion that GLDH and ALT are at least well comparable as biomarkers for DILI studies in rats[220].

5.3.4 HMGB1

HMGB1 is considered to be released during hepatocellular necrosis and may act as damage-associated molecular pattern to promote further cell death[155]. However in the studies investigated here, HMGB1 plasma levels in rats treated with APAP were not consistently different from their respective control groups (**Figure 42A, B**). Former studies reported HMGB1 involvement in clinical APAP hepatotoxicity and in preclinical studies with mice[221,222]. Acetylated HMGB1 as well as total HMGB1 concentration were shown significantly increased in APAP overdose patients and loss of oxidized HMGB1 was believed to show the involvement of HMGB1 in induction of inflammation during APAP toxicity but both studies were retracted due to scientific misconduct[223,224]. Despite that active HMGB1 secretion was shown *in vitro* in studies involving APAP[225,226], it remains questionable if this marker can be used *in vivo* for acute liver injury studies. In our studies involving acute liver toxicity via APAP or DAPM treatment, HMGB1 levels were not increased compared to their corresponding

control groups (**Figure 42A, B, E**). High HMGB1 concentration did not always match with high ALT activity (**Figure 42A, B, E**). Additionally, HMGB1 concentration was seen to be highly influenced by the matrix and the sampling procedure (section **4.3**) which supports the doubt that HMGB1 can serve as reliable biomarker for acute liver injury.
HMGB1 results from the bromobenzene study showed similar response in both bromobenzene dosing groups (**Figure 42D**), which does not fit to bromobenzene resistance reported in literature and reflected here by significant changes in ALT[208,209]. Interestingly, HMGB1 shows its most significant response in studies with the compounds thioacetamide and CCl_4, which are used to model liver fibrosis in animal studies[227] (**Figure 42C, F**). This observation supports a study by Arriazu *et al.*[218] who showed that HMGB1 mediates liver fibrosis together with OPN, which acts upstream of HMGB1. Mice were treated with CCl_4 to induce liver fibrosis in this study. Furthermore, HMGB1 was observed elevated in plasma of thioacetamide treated rats[207] with both studies supporting the involvement of HMGB1 in fibrosis.
Similar to GLDH in liver tissue, HMGB1 concentration was not significantly different in liver specimen of the studies with DAPM, or with 1,500 mg/kg APAP, presumably since always the same liver amount was processed and by necrosis depleted HMGB1 from liver tissue would not be measurable (**Figure 43**). Investigation of acetylated HMGB1 in hepatocytocellular macrophages, thereby acting as cytokine[66], would have been interesting but early experiments in this direction with acetylated HMGB1 showed only a small protein and peptide enrichment efficiency (data not shown), hence, this was not followed up.

5.3.5 MCSF1R

The soluble receptor part of MCSF1R could be detected endogenously in samples of treated animals within the DAPM and CCl_4 studies (**Figure 44B, C**). The peptide sequence targeted with this IA-LC-MS/MS assay is part of the unreviewed MCSF1R rat sequence with the Uniprot ID D4ACA7 and our findings support previously identified MCSF1R in rat specimen by mass spectrometry[150] (see above **5.1.1**).
Notably, two samples showed a MCSF1R concentration above the LLOQ in the animal group treated for 15 days with CCl_4. Furthermore, the median ratio AUC is highest in this group which might indicate prolonged activation of macrophages, thus, resulting in increased plasma MCSF1R levels by shedding the extracellular receptor part[74,228]. Moreover, the animal group with the longest recovery time after single-dosing with DAPM showed a significantly increased median MCSF1R ratio AUC compared to the control group or the group with sampling 24 h after DAPM treatment possibly also showing prolonged activated macrophage response.
Treatment with APAP seemed not to trigger elevated MCSF1R plasma concentration in treated animals (**Figure 44A**). This might aggree with the demonstrated elevated

MCSF1R levels in human plasma of patients treated with flupirtine, a drug known for idiosyncratic DILI, as opposed to the MCSF1R results of APAP-related clinical samples within the same DILI study[60]. However, it is also possible that this assay is not sensitive enough to quantify significant changes within the APAP study. Compared to the base level of MCSF1R concentration in human plasma or serum specimen (**Figure 31**), it was already surprising to find very low concentration of MCSF1R in rat plasma. This might be caused by a potential glycosylation site within the peptide AHNNVGNSSQFFR (Uniprot ID D4ACA7). The corresponding sequence in the reviewed sequence THNSVGNSSQYFR with Uniprot ID Q00495 shows a N-linked glycosylation site (position 491) found by sequence analysis due to the consensus sequence for N-linked glycosulation in this area[229] (Asn-Xaa-Ser/Thr). Since this consensus sequence is also present in the peptide AHNNVGNSSQFFR, it might be that endogenous MSCF1R is glycosylated within this part, however, the N-glycosylation site occupancy is not known. In this case, the assay results could be influenced. Either the enrichment efficiency between glycosylated peptide and antibody is impaired or the mass-to-charge ratio is altered by the glycosylation site resulting in a different peptide mass compared to the internal standard, thus not being measureable with this particulary assay setup. The concentration of hepatic macrophages was appearently not high enough to allow measurement of endogenous MCSF1R in liver tissue lysate (**Figure 45**). Since MCSF1R is mainly expressed by macrophages, it is not surprising that samples containing primarily hepatocytes from rat liver tissue do not comprise sufficient amounts of MCSF1R peptide for measurement.

5.3.6 ccK18

Caspase-cleaved keratin 18 (ccK18) is a known marker for apoptosis and leaks into circulation during this process[147]. As part of the apoptotic index, quantification of ccK18 might shed light on the prognosis of drug-induced liver injury[155]. Measurement of rat liver tissue as well as rat plasma measurement of the investigated studies did not reveal any ccK18 signals above the LLOQ (**Figures 46** and **47**). The analog human peptide could be measured in cell lysate of taxol-treated HepG2 cells, therefore, lacking ccK18 signal was not expected, neither in liver tissue nor in plasma of treated animals. Further assay implications were discussed above in section **5.1.1**.

5.3.7 Relationship between potential biomarkers and their preclinical value for DILI

DILI is well investigated as seen from the many studies involving the investigated proteins measured with different approaches in form of protein concentration or activity (see sections **5.3.1** to **5.3.6**). The most effects across the investigated potential biomarkers were observed for ALT, OPN, GLDH, HMGB1, and MCSF1R in the CCl_4

study, where all potential biomarkers were observed significantly elevated in plasma samples of treated animals compared to controls. The reactive metabolites produced during biotransformation of CCl_4 seem to influence these biomarkers possibly caused by a combination of induced liver fibrosis and hepatocellular injury[35,218,227]. MCSF1R was shown to increase specificity to predict severe DILI or even serve as marker for idiosyncratic DILI[60]. However, this should be carefully considered for rats since DAPM and CCl_4 both resulted in significantly increased signals for MCSF1R in plasma samples of treated animals. GLDH was most specificly observed in liver tissue (**Figure 48**), which underlines the function of GLDH as mitochondrial matrix protein involved in the urea cycle. However, GLDH was also quantified in kidney but about 3-fold less than in liver tissue. This was also observed with RNA expression patterns presented in the Human Proteome Atlas[230]. Thioacetamide and bromobenzene were both observed to induce kidney injury[231,232], which might explain the high fold change in increased GLDH concentration upon treatment with these compounds. Further studies with kidney injury-inducing drugs such as cisplatin[233] could reveal if GLDH indeed may serve as liver-specific biomarker. Alternatively, GLDH could indicate a combinatory damage of liver and kidney depending on the GLDH levels to be measured. Results from this work support the response of GLDH on the hepatotoxicity-inducing drug APAP in humans[63,64], mice[196], and rats[203] but contradict a study[199] where mitochondrial toxicity induced by APAP was not observed for rats. Whether GLDH can be used as marker for mitotoxicity, is not clear yet, since release of GLDH protein into circulation may occur by any type of drug-induced necrosis or apoptosis. GLDH shows greater potential to show acute liver injury in a time-resolved manner since significant recovery was observed for GLDH (**Figure 39**) as opposed to ALT activity and OPN protein concentration (**Figures 36** and **37**). Interestingly, OPN concentration was not elevated when comparing CCl_4 study days 8 and 15 (**Figure 37**), but the GLDH concentration was elevated with longer daily CCl_4 treatment (**Figure 39**). This may suggest that immune response is not triggered more intensively between these study days, but hepatic necrosis may continue within this time frame resulting in more and more increasing GLDH protein in circulation. A combinatory assessment of these potential biomarkers could reflect drug-induced apoptosis and necrosis by GLDH additionally with inflammatory response by OPN assessment. Since OPN displays major issues when quantifying different sample matrices with ELISA kits (see section **5.2**), it could be of advantage to measure both analytes with the presented IA-LC-MS/MS technique in multiplexed manner on the peptide level. Following to this work, animal studies including drugs with known idiosyncratic DILI outcome such as flupirtine[60] will be interesting to shed light on the influence of these drugs on the investigated biomarkers in preclinical studies.

6 Conclusions

Candidate biomarkers for evaluation of DILI in human- and rat- derived body fluid or liver tissue samples were investigated in terms of quantification method, matrix and sampling effects, and change in biomarker concentration upon drug or compound treatment of rats as animal models. These candidate biomarkers included the proteins MCSF1R, OPN, GLDH, HMGB1, K18, and ccK18. The following conclusions were drawn based on the results presented in this work:

1. Method development for DILI-related protein quantification using IA-LC-MS/MS
   - 1.1. IA-LC-MS/MS assays can be improved in their sensitivity by increasing the antibody amount or decreasing the internal standard peptide amount for enrichment. A multiplexed IA-LC-MS/MS assay MPh-dev could be developed to quantify MCSF1R, OPN, HMGB1, and GLDH in human serum or plasma.
   - 1.2. Pseudotrypsin (ψ-trypsin) produced by autolysis and its chymotrypsin-like activity should be taken into account when investigating proteins on their peptide level. Peptides susceptible to this activity could be rescued by PMSF addition before start of proteolysis. Endogenous K18 could be observed by this approach in plasma of DAPM-treated rats.
   - 1.3. The unreviewed MCSF1R rat protein sequence with Uniprot ID D4ACA7 represents more likely the endogenously prevalent protein sequence instead the MCSF1R sequence with Uniprot ID Q00495 due to more experimental evidence in this work and in literature.
   - 1.4. Partial method validation of DILI-related protein quantification with the multiplexed assay MPr demonstrated reproducible measurement of OPN, HMGB1, GLDH in rat plasma and GLDH and HMGB1 in rat liver tissue. Detectable levels of MCSF1R were observed later in plasma samples of animals treated with DILI-related drugs or compounds. Endogenous ccK18 was only detected in cell lysate of taxol-treated human HepG2 cells and could not be quantified in rat-related samples.

2. Study of preanalytical matrix and sampling effects in human serum and plasma specimen regarding DILI biomarker quantification
   - 2.1. Matched samples did not correlate in HMGB1 and ccK18 concentration between EDTA plasma or serum. Comparability was also not given for serum collected with tubes with gel or without gel, which calls into question the results of previous HMGB1 and ccK18 studies based on serum, since the concentration of these analytes in this matrix seems rather random. Correlation was given for MCSF1R and OPN in all matrices but MCSF1R shows

consistently about 20% higher concentration in EDTA plasma compared to serum. GLDH protein concentration is most comparable in serum with and without gel. Taken together, studies investigating these proteins should be compared only when the same underlying sample type was used.

2.2. In general, plasma showed more stable protein biomarker levels within the first hour of benchtop time prior to sample centrifugation for HMGB1 and ccK18. Especially HMGB1 concentrations in serum increased up to 200% within this time frame. No impact of sampling time was observed for GLDH, MCSF1R, or OPN. In summary, plasma is recommended as matrix of choice to study the investigated proteins.

2.3. The IA-LC-MS/MS method and sandwich immunoassays are comparable for HMGB1 and MCSF1R. OPN protein concentration is highly influenced by the matrix in use when quantified on the protein level with sandwich immunoassays. GLDH activity and protein concentration did not correlate. Potential earlier onset of GLDH protein concentration compared to GLDH activity in plasma samples of DILI-related patients or animals might be investigated in future studies.

3. Study of translational protein biomarkers for DILI investigation in preclinical studies including rat animal models

3.1. The developed IA-LC-MS/MS assay could be used to quantify OPN, GLDH, and HMGB1 plasma samples of the investigated studies. Endogenous MCSF-1R was confirmed in plasma samples of rats treated with DAPM or CCL_4, whereas no endogenous ccK18 peptide could be measured. GLDH reflected the response in ALT activity as gold standard for drug treatment best. Additionally to GLDH as marker for hepatic cell death, OPN may complement DILI research as biomarker for liver failure in rat animal studies because a response of GLDH and OPN concentration was observed on drug treatment for almost all of the investigated studies. These potential biomarkers are worth to be explored in preclinical studies involving drugs known to cause idiosyncratic DILI and they are worth to be tested as panel for prediction of liver failure in animal models. HMGB1 seems rather a biomarker for liver fibrosis than hepatocellular or biliary injury in the investigated animal studies.

3.2. GLDH and HMGB1 were confirmed in rat liver tissue, but endogenous OPN, MCSF1R, and ccK18 could not be measured. Either lacking assay sensitivity or the absence of endougenous peptide may caused this. No significant differences were observed for GLDH and HMGB1 content between specimen of control and treated animal groups.

3.3. HMGB1 can be measured endogenously across all investigated tissue samples, thus, HMGB1 measurement would not be specific for liver injury. GLDH pro-

tein content showed a similar pattern in distribution across the investigated tissue types as observed with RNA expression. Liver tissue beares the most GLDH content, followed by kidney and brain tissue. Drugs known to cause specificly kidney or brain injury can be used to test further specificity of GLDH as liver injury marker when using plasma specimen.

References

1. Trefts, E., Gannon, M. & Wasserman, D. H. The liver. eng. *Current biology: CB* **27,** R1147–R1151. doi:10.1016/j.cub.2017.09.019 (Nov. 2017).
2. Cunningham, R. P. & Porat-Shliom, N. Liver Zonation - Revisiting Old Questions With New Technologies. *Frontiers in Physiology* **12,** 1433. doi:10.3389/fphys.2021.732929 (2021).
3. Kling, S. *et al.* Characterization of hepatic zonation in mice by mass-spectrometric and antibody-based proteomics approaches. *Biological Chemistry.* doi:10.1515/hsz-2021-0314 (2021).
4. Dixon, L. J., Barnes, M., Tang, H., Pritchard, M. T. & Nagy, L. E. Kupffer cells in the liver. eng. *Comprehensive Physiology* **3,** 785–797. doi:10.1002/cphy.c120026 (Apr. 2013).
5. Tsuchida, T. & Friedman, S. L. Mechanisms of hepatic stellate cell activation. *Nature Reviews Gastroenterology and Hepatology* **14,** 397–411. doi:10.1038/nrgastro.2017.38 (2017).
6. Tabibian, J. H., Masyuk, A. I., Masyuk, T. V., O'Hara, S. P. & LaRusso, N. F. Physiology of cholangiocytes. eng. *Comprehensive Physiology* **3,** 541–565. doi:10.1002/cphy.c120019 (Jan. 2013).
7. Fujiwara, R. *et al.* Systemic regulation of bilirubin homeostasis: Potential benefits of hyperbilirubinemia. *Hepatology* **67,** 1609–1619. doi:10.1002/hep.29599 (Apr. 2018).
8. Li, T. & Chiang, J. Y. L. Bile acid signaling in metabolic disease and drug therapy. eng. *Pharmacological reviews* **66,** 948–983. doi:10.1124/pr.113.008201 (Oct. 2014).
9. Li, T. & Chiang, J. (eds Arias, I. *et al.*) chap. Bile Acid Metabolism in Health and Disease (John Wiley and Sons Ltd, 2020). doi:10.1002/9781119436812.ch23.
10. Guerra Ruiz, A. R. *et al.* Measurement and clinical usefulness of bilirubin in liver disease. *Advances in Laboratory Medicine / Avances en Medicina de Laboratorio* **2,** 352–361. doi:10.1515/almed-2021-0047 (2021).
11. Esteves, F., Rueff, J. & Kranendonk, M. The Central Role of Cytochrome P450 in Xenobiotic Metabolism - A Brief Review on a Fascinating Enzyme Family. *Journal of Xenobiotics* **11.** doi:10.3390/jox11030007 (2021).
12. Grillo, M. P. *Bioactivation by Phase-II-Enzyme-Catalyzed Conjugation of Xenobiotics* doi:10.1002/9780470921920.edm074 (2012).
13. Xu, C., Li, C. Y.-T. & Kong, A.-N. T. Induction of phase I, II and III drug metabolism/transport by xenobiotics. *Archives of Pharmacal Research* **28,** 249. doi:10.1007/BF02977789 (2005).
14. Hailfinger, S., Jaworski, M., Braeuning, A., Buchmann, A. & Schwarz, M. Zonal gene expression in murine liver: Lessons from tumors. *Hepatology* **43,** 407–414. doi:10.1002/hep.21082 (Mar. 2006).

15. Kullak-Ublick, G. A. *et al.* Drug-induced liver injury: recent advances in diagnosis and risk assessment. *Gut* **66,** 1154–1164. doi:10.1136/gutjnl-2016-313369 (6 June 2017). ppublish.

16. Hoofnagle, J. H. & Björnsson, E. S. Drug-Induced Liver Injury - Types and Phenotypes. *The New England Journal of Medicine* **381,** 264–273. doi:10.1056/NEJMra1816149 (July 2019).

17. Russmann, S., Kullak-Ublick, G. A. & Grattagliano, I. Current concepts of mechanisms in drug-induced hepatotoxicity. eng. *Current medicinal chemistry* **16,** 3041–3053. doi:10.2174/092986709788803097 (2009).

18. Robin, M.-A., Roy, M. L., Descatoire, V. & Pessayre, D. Plasma membrane cytochromes P450 as neoantigens and autoimmune targets in drug-induced hepatitis. *Journal of Hepatology* **26,** 23–30. doi:10.1016/S0168-8278(97)82329-X (Jan. 1997).

19. Cory, S. & Adams, J. M. The Bcl2 family: regulators of the cellular life-or-death switch. *Nature Reviews Cancer* **2,** 647–656. doi:10.1038/nrc883 (2002).

20. Malhi, H. & Gores, G. J. Cellular and molecular mechanisms of liver injury. eng. *Gastroenterology* **134,** 1641–1654. doi:10.1053/j.gastro.2008.03.002 (May 2008).

21. Andrade, R. J. *et al.* Drug-induced liver injury. *Nature reviews. Disease primers* **5,** 58. doi:10.1038/s41572-019-0105-0 (1 Aug. 2019). epublish.

22. Nicoletti, P. *et al.* Association of liver injury from specific drugs, or groups of drugs, and other genes in a genome-wide association study. *Gastroenterology* **152,** 1078–1089. doi:10.1053/j.gastro.2016.12.016 (Apr. 2017).

23. Urban, T. J. *et al.* Minocycline hepatotoxicity: Clinical characterization and identification of HLA-B-35:02 as a risk factor. *Journal of Hepatology* **67,** 137–144. doi:10.1016/j.jhep.2017.03.010 (July 2017).

24. Reuben, A. *et al.* Outcomes in Adults With Acute Liver Failure Between 1998 and 2013. *Annals of Internal Medicine* **164,** 724–732. doi:10.7326/M15-2211 (Apr. 2016).

25. Donnelly, M. C. *et al.* Acute liver failure in Scotland: changes in aetiology and outcomes over time (the Scottish Look-Back Study). *Alimentary Pharmacology and Therapeutics* **45,** 833–843. doi:10.1111/apt.13943 (Mar. 2017).

26. Stevens, J. L. & Baker, T. K. The future of drug safety testing: expanding the view and narrowing the focus. *Drug Discovery Today* **14,** 162–167. doi:10.1016/j.drudis.2008.11.009 (2009).

27. McGill, M. R. & Jaeschke, H. Animal models of drug-induced liver injury. eng. *Biochimica et biophysica acta. Molecular basis of disease* **1865,** 1031–1039. doi:10.1016/j.bbadis.2018.08.037 (May 2019).

28. Hecker, N., Sharma, V. & Hiller, M. Convergent gene losses illuminate metabolic and physiological changes in herbivores and carnivores. *Proc Natl Acad Sci USA* **116,** 3036. doi:10.1073/pnas.1818504116 (Feb. 2019).

29. Sharma, C. V. & Mehta, V. Paracetamol: mechanisms and updates. *Continuing Education in Anaesthesia Critical Care and Pain* **14,** 153–158. doi:10.1093/bjaceaccp/mkt049 (Aug. 2014).

30. Yan, M., Huo, Y., Yin, S. & Hu, H. Mechanisms of acetaminophen-induced liver injury and its implications for therapeutic interventions. *Redox Biology* **17,** 274–283. doi:10.1016/j.redox.2018.04.019 (2018).

31. Qiu, Y., Benet, L. Z. & Burlingame, A. L. Identification of the Hepatic Protein Targets of Reactive Metabolites of Acetaminophen in Vivoin Mice Using Two-dimensional Gel Electrophoresis and Mass Spectrometry. *Journal of Biological Chemistry* **273,** 17940–17953. doi:10.1074/jbc.273.28.17940 (1998).

32. Du, K. *et al.* Editor's Highlight: Metformin Protects Against Acetaminophen Hepatotoxicity by Attenuation of Mitochondrial Oxidant Stress and Dysfunction. *Toxicological Sciences* **154,** 214–226. doi:10.1093/toxsci/kfw158 (Dec. 2016).

33. Gujral, J. S., Knight, T. R., Farhood, A., Bajt, M. L. & Jaeschke, H. Mode of Cell Death after Acetaminophen Overdose in Mice: Apoptosis or Oncotic Necrosis? *Toxicol Sci* **67,** 322–328. doi:10.1093/toxsci/67.2.322 (June 2002).

34. Scholten, D., Trebicka, J., Liedtke, C. & Weiskirchen, R. The carbon tetrachloride model in mice. *Laboratory Animals* **49,** 4–11. doi:10.1177/0023677215571192 (Apr. 2015).

35. Weber, L. W. D., Boll, M. & Stampfl, A. Hepatotoxicity and Mechanism of Action of Haloalkanes: Carbon Tetrachloride as a Toxicological Model. *Critical reviews in toxicol* **33,** 105–136. doi:10.1080/713611034 (Jan. 2003).

36. Tan, Z. *et al.* IL-17A Plays a Critical Role in the Pathogenesis of Liver Fibrosis through Hepatic Stellate Cell Activation. *The Journal of Immunology* **191,** 1835. doi:10.4049/jimmunol.1203013 (Aug. 2013).

37. Marcher, A.-B. *et al.* Transcriptional regulation of Hepatic Stellate Cell activation in NASH. *Scientific Reports* **9,** 2324. doi:10.1038/s41598-019-39112-6 (2019).

38. Xu, R., Zhang, Z. & Wang, F.-S. Liver fibrosis: mechanisms of immune-mediated liver injury. *Cellular and Molecular Immunology* **9,** 296–301. doi:10.1038/cmi.2011.53 (2012).

39. CDC-ATSDR (Agency for Toxic Substances and Disease Registry) Toxic Substances Portal. *Carbon Tetrachloride* https://wwwn.cdc.gov/TSP/substances/ToxSubstance.aspx?toxid=35.

40. European Union. *Risk Assessment Report* tech. rep. (Institute for Health and Consumer Protection, 2001). https://echa.europa.eu/documents/10162/ba567fa3-282c-4b37-bcba-f82fd9ae52bc.

41. Kanz, M. F., Kaphalia, L., Kaphalia, B. S., Romagnoli, E. & Ansari, G. A. S. Methylene dianiline: Acute toxicity and effects on biliary function. *Toxicology and Applied Pharmacology* **117,** 88–97. doi:10.1016/0041-008X(92)90221-D (1992).

42. Limaye, P. B., Bowen, W. C., Orr, A., Apte, U. M. & Michalopoulos, G. K. Expression of hepatocytic- and biliary-specific transcription factors in regenerating bile ducts during hepatocyte-to-biliary epithelial cell transdifferentiation. eng. *Comparative hepatology* **9,** 9–9. doi:10.1186/1476-5926-9-9 (Dec. 2010).

43. Mehendale, H. M., Chilakapati, J. & McQueen, C. A. *Comprehensive Toxicology (Second Edition)* 627–638 (Elsevier, Oxford, 2010). doi:10.1016/B978-0-08-046884-6.01029-0.

44. Ledda-Columbano, G. M. *et al.* Induction of two different modes of cell death, apoptosis and necrosis, in rat liver after a single dose of thioacetamide. eng. *The American journal of pathology* **139,** 1099–1109. https://www.ncbi.nlm.nih.gov/pmc/articles/PMC1886348/ (Nov. 1991).

45. Matsuo, M. *et al.* Novel liver fibrosis model in Macaca fascicularis induced by thioacetamide. *Scientific Reports* **10,** 2450. doi:10.1038/s41598-020-58739-4 (2020).

46. Smallwood, C. & Lamber, J. *Toxicological review of bromobenzene* tech. rep. (U.S. Environmental Protection Agency (EPA), Sept. 2009). doi:https://iris.epa.gov/static/pdfs/1020tr.pdf.

47. Manautou, J. E., Campion, S. N., Aleksunes, L. M. & McQueen, C. A. *Comprehensive Toxicology (Second Edition)* 175–220 (Elsevier, Oxford, 2010). doi:10.1016/B978-0-08-046884-6.01008-3.

48. Lau, S. S. & Monks, T. J. The contribution of bromobenzene to our current understanding of chemically-induced toxicities. *Life Sciences* **42,** 1259–1269. doi:10.1016/0024-3205(88)90219-6 (1988).

49. Park, J. H. *et al.* Prevalence and clinical characteristics of antibiotics associated drug induced liver injury. eng. *Annals of translational medicine* **9,** 642–642. doi:10.21037/atm-20-5144 (Apr. 2021).

50. Kleiner, D. E. Drug-induced Liver Injury: The Hepatic Pathologist's Approach. eng. *Gastroenterology clinics of North America* **46,** 273–296. doi:10.1016/j.gtc.2017.01.004 (June 2017).

51. Kobayashi, A., Suzuki, Y. & Sugai, S. Specificity of transaminase activities in the prediction of drug-induced hepatotoxicity: *The Journal of Toxicological Sciences* **45,** 515–537. doi:10.2131/jts.45.515 (2020).

52. Wulkan, R. W. & Leijnse, B. Alkaline Phosphatase and Cholestasis. *Annals of Clinical Biochemistry* **23,** 405–412. doi:10.1177/000456328602300405 (July 1986).

53. Sharma, U., Pal, D. & Prasad, R. Alkaline phosphatase: an overview. eng. *Indian journal of clinical biochemistry* **29,** 269–278. doi:10.1007/s12291-013-0408-y (July 2014).

54. Turan, S. *et al.* Serum alkaline phosphatase levels in healthy children and evaluation of alkaline phosphatase z-scores in different types of rickets. eng. *Journal of clinical research in pediatric endocrinology* **3,** 7–11. doi:10.4274/jcrpe.v3i1.02 (2011).

55. Pravastatin Multicenter Study Group II. Comparative Efficacy and Safety of Pravastatin and Cholestyramine Alone and Combined in Patients With Hypercholesterolemia. *Archives of Internal Medicine* **153,** 1321–1329. doi:10.1001/archinte.1993.0041011-0029006 (June 1993).

56. Dukes, G. *et al.* Transaminase Elevations in Patients Receiving Bovine or Porcine Heparin. *Annals of Internal Medicine* **100,** 646–650. doi:10.7326/0003-4819-100-5-646 (May 1984).

57. Temple, R. Hy's law: predicting serious hepatotoxicity. *Pharmacoepidem. Drug Safe.* **15,** 241–243. doi:10.1002/pds.1211 (Apr. 2006).

58. Aithal, G. P. *et al.* Case Definition and Phenotype Standardization in Drug-Induced Liver Injury. *Clinical Pharmacology and Therapeutics* **89,** 806–815. doi:10.1038/clpt.2011.58 (June 2011).

59. Pacifico, L. *et al.* Upper limit of normal for alanine aminotransferase: Quo vadis? *Clinica Chimica Acta* **422,** 29–39. doi:10.1016/j.cca.2013.03.030 (2013).

60. Church, R. J. *et al.* Candidate biomarkers for the diagnosis and prognosis of drug-induced liver injury: An international collaborative effort. *Hepatology* **69,** 760–773. doi:10.1002/hep.29802 (2 Feb. 2019).

61. Schmidt, E. S. & Schmidt, F. W. Glutamate dehydrogenase: biochemical and clinical aspects of an interesting enzyme. *Clinica Chimica Acta* **173,** 43–55. doi:10.1016/0009-8981(88)90356-7 (1988).

62. Lindena, J., Sommerfeld, U., Höpfel, C. & Trautschold, I. Catalytic Enzyme Activity Concentration in Tissues of Man, Dog, Rabbit, Guinea Pig, Rat and Mouse. Approach to a Quantitative Diagnostic Enzymology, III. Communication. *Journal of clinical chemistry and clinical biochemistry* **24,** 35–48. doi:10.1515/cclm.1986.24.1.35 (1986).

63. Schomaker, S. *et al.* Assessment of Emerging Biomarkers of Liver Injury in Human Subjects. *Toxicological Sciences* **132,** 276–283. doi:10.1093/toxsci/kft009 (Apr. 2013).

64. Schomaker, S. *et al.* Serum glutamate dehydrogenase activity enables early detection of liver injury in subjects with underlying muscle impairments. *PLOS ONE* **15,** e0229753. doi:10.1371/journal.pone.0229753 (May 2020).

65. Scaffidi, P., Misteli, T. & Bianchi, M. E. Release of chromatin protein HMGB1 by necrotic cells triggers inflammation. *Nature* **418,** 191–195. doi:10.1038/nature00858 (2002).

66. Bonaldi, T. *et al.* Monocytic cells hyperacetylate chromatin protein HMGB1 to redirect it towards secretion. eng. *The EMBO journal* **22,** 5551–5560. doi:10.1093/emboj/cdg516 (Oct. 2003).

67. Gaskell, H., Ge, X. & Nieto, N. High-Mobility Group Box-1 and Liver Disease. eng. *Hepatology communications* **2,** 1005–1020. doi:10.1002/hep4.1223 (Sept. 2018).

68. Moll, R., Divo, M. & Langbein, L. The human keratins: biology and pathology. eng. *Histochemistry and cell biology* **129,** 705–733. doi:10.1007/s00418-008-0435-6 (June 2008).

69. Thulin, P. *et al.* Keratin-18 and microRNA-122 complement alanine aminotransferase as novel safety biomarkers for drug-induced liver injury in two human cohorts. *Liver International* **34,** 367–378. doi:10.1111/liv.12322 (Mar. 2014).

70. Rutherford, A. *et al.* Development of an accurate index for predicting outcomes of patients with acute liver failure. eng. *Gastroenterology* **143,** 1237–1243. doi:10.1053/j.gastro.2012.07.113 (Nov. 2012).

71. Singh, A., Gill, G., Kaur, H., Amhmed, M. & Jakhu, H. Role of osteopontin in bone remodeling and orthodontic tooth movement: a review. *Progress in Orthodontics* **19,** 18. doi:10.1186/s40510-018-0216-2 (2018).

72. Kawashima, R. *et al.* Expression of Osteopontin in Kupffer Cells and Hepatic Macrophages and Stellate Cells in Rat Liver after Carbon Tetrachloride Intoxication: A Possible Factor for Macrophage Migration into Hepatic Necrotic Areas. *Biochemical and Biophysical Research Communications* **256,** 527–531. doi:10.1006/bbrc.1999.0372 (1999).

73. Kahles, F., Findeisen, H. M. & Bruemmer, D. Osteopontin: A novel regulator at the cross roads of inflammation, obesity and diabetes. *Molecular Metabolism* **3,** 384–393. doi:10.1016/j.molmet.2014.03.004 (2014).

74. Andersson, U. *et al.* A systems biology approach to understanding elevated serum alanine transaminase levels in a clinical trial with ximelagatran. *Biomarkers : biochemical indicators of exposure, response, and susceptibility to chemicals* **14,** 572–586. doi:10.3109/13547500903261354 (8 Dec. 2009). ppublish.

75. United States Department of Health and Human Services. *Food and Drug Administration Letter of Support for Drug-Induced Liver Injury (DILI) Biomarker(s)* 2016. https://www.fda.gov/media/99532/%20download.

76. Sauer, J. M. & King, N. *Qualification Plan for Glutamate Dehydrogenase as a Biomarker of Drug Induced Liver Injury in Individuals with Skeletal Muscle Degeneration* tech. rep. (Critical Path Institute (PSTC), 2018). doi:https://www.fda.gov/media/138319/download.

77. Aebersold, R. & Mann, M. Mass-spectrometric exploration of proteome structure and function. *Nature* **537,** 347–355. doi:10.1038/nature19949 (2016).

78. Bian, Y. *et al.* Robust, reproducible and quantitative analysis of thousands of proteomes by micro-flow LC-MS/MS. *Nature Communications* **11,** 157. doi:10.1038/s41467-019-13973-x (2020).

79. Doll, S. & Burlingame, A. L. Mass Spectrometry-Based Detection and Assignment of Protein Posttranslational Modifications. *ACS Chem. Biol.* **10,** 63–71. doi:10.1021/cb500904b (Jan. 2015).

80. Huttlin, E. L. *et al.* Architecture of the human interactome defines protein communities and disease networks. *Nature* **545,** 505–509. doi:10.1038/nature22366 (2017).

81. Richards, A. L., Eckhardt, M. & Krogan, N. J. Mass spectrometry-based protein-protein interaction networks for the study of human diseases. *Molecular Systems Biology* **17,** e8792. doi:10.15252/msb.20188792 (Jan. 2021).

82. Catherman, A. D., Skinner, O. S. & Kelleher, N. L. Top Down proteomics: facts and perspectives. eng. *Biochemical and biophysical research communications* **445,** 683–693. doi:10.1016/j.bbrc.2014.02.041 (Mar. 2014).

83. Zhang, Y., Fonslow, B. R., Shan, B., Baek, M.-C. & Yates John R, 3. Protein analysis by shotgun/bottom-up proteomics. eng. *Chemical reviews* **113,** 2343–2394. doi:10.1021/cr3003533 (Apr. 2013).

84. Olsen, J. V., Ong, S.-E. & Mann, M. Trypsin Cleaves Exclusively C-terminal to Arginine and Lysine Residues. *Molecular and Cellular Proteomics* **3,** 608–614. doi:10.1074/mcp.T400003-MCP200 (June 2004).

85. Craig, R., Cortens, J. P. & Beavis, R. C. The use of proteotypic peptide libraries for protein identification. *Rapid Communications in Mass Spectrometry* **19,** 1844–1850. doi:10.1002/rcm.1992 (July 2005).

86. Stewart, E. *et al.* Identification of Therapeutic Targets in Rhabdomyosarcoma through Integrated Genomic, Epigenomic, and Proteomic Analyses. *Cancer Cell* **34,** 411–426.e19. doi:10.1016/j.ccell.2018.07.012 (2018).

87. Hu, A., Noble, W. S. & Wolf-Yadlin, A. Technical advances in proteomics: new developments in data-independent acquisition. eng. *F1000Research* **5,** F1000 Faculty Rev–419. doi:10.12688/f1000research.7042.1 (Mar. 2016).

88. Gillet, L. C. *et al.* Targeted data extraction of the MS/MS spectra generated by data-independent acquisition: a new concept for consistent and accurate proteome analysis. eng. *Molecular and cellular proteomics : MCP* **11,** O111.016717–O111.016717. doi:10.1074/mcp.O111.016717 (June 2012).

89. Shi, T. *et al.* Advances in targeted proteomics and applications to biomedical research. eng. *Proteomics* **16,** 2160–2182. doi:10.1002/pmic.201500449 (Aug. 2016).

90. Gallien, S. *et al.* Targeted proteomic quantification on quadrupole-orbitrap mass spectrometer. eng. *Molecular and cellular proteomics : MCP* **11,** 1709–1723. doi:10.1074/mcp.O112.019802 (Dec. 2012).

91. Ronsein, G. E. *et al.* Parallel reaction monitoring (PRM) and selected reaction monitoring (SRM) exhibit comparable linearity, dynamic range and precision for targeted quantitative HDL proteomics. eng. *Journal of proteomics* **113,** 388–399. doi:10.1016/j.jprot.2014.10.017 (Jan. 2015).

92. Neue, U. *et al.* Ultra-Performance Liquid Chromatography Technology and Applications. *Advances in chromatography* **48,** 99–143. doi:10.1201/9781420084542-c3 (Jan. 2010).

93. Yates, J. R., Ruse, C. I. & Nakorchevsky, A. Proteomics by Mass Spectrometry: Approaches, Advances, and Applications. *Annu. Rev. Biomed. Eng.* **11,** 49–79. doi:10.1146/annurev-bioeng-061008-124934 (July 2009).

94. Banerjee, S. & Mazumdar, S. Electrospray ionization mass spectrometry: a technique to access the information beyond the molecular weight of the analyte. eng. *International journal of analytical chemistry* **2012,** 282574–282574. doi:10.1155/2012/282574 (2012).

95. Scheltema, R. A. *et al.* The Q Exactive HF, a Benchtop Mass Spectrometer with a Pre-filter, High-performance Quadrupole and an Ultra-high-field Orbitrap Analyzer. *Molecular and Cellular Proteomics* **13,** 3698–3708. doi:10.1074/mcp.M114.043489 (2014).

96. Schuhmann, K. *et al.* Bottom-Up Shotgun Lipidomics by Higher Energy Collisional Dissociation on LTQ Orbitrap Mass Spectrometers. *Analytical Chemistry* **83,** 5480–5487. doi:10.1021/ac102505f (July 2011).

97. Steen, H. & Mann, M. The abc's (and xyz's) of peptide sequencing. *Nature Reviews Molecular Cell Biology* **5,** 699–711. doi:10.1038/nrm1468 (2004).

98. Geyer, P. E., Holdt, L. M., Teupser, D. & Mann, M. Revisiting biomarker discovery by plasma proteomics. *Mol Syst Biol* **13,** 942. doi:10.15252/msb.20156297 (Sept. 2017).

99. Makarov, A., Denisov, E., Lange, O. & Horning, S. Dynamic range of mass accuracy in LTQ orbitrap hybrid mass spectrometer. *Journal of the American Society for Mass Spectrometry* **17,** 977–982. doi:10.1016/j.jasms.2006.03.006 (July 2006).

100. Qian, W.-J. *et al.* Enhanced Detection of Low Abundance Human Plasma Proteins Using a Tandem IgY12-SuperMix Immunoaffinity Separation Strategy. *Molecular and Cellular Proteomics* **7,** 1963–1973. doi:10.1074/mcp.M800008-MCP200 (Oct. 2008).

101. Tu, C. *et al.* Depletion of abundant plasma proteins and limitations of plasma proteomics. eng. *Journal of proteome research* **9,** 4982–4991. doi:10.1021/pr100646w (Oct. 2010).

102. Geyer, P. E. *et al.* Plasma Proteome Profiling to Assess Human Health and Disease. *Cell systems* **2,** 185–195. doi:10.1016/j.cels.2016.02.015 (3 Mar. 2016). ppublish.

103. Engvall, E. The ELISA, Enzyme-Linked Immunosorbent Assay. *Clin Chem* **56,** 319–320. doi:10.1373/clinchem.2009.127803 (Feb. 2010).

104. Engvall, E., Jonsson, K. & Perlmann, P. Enzyme-linked immunosorbent assay. II. Quantitative assay of protein antigen, immunoglobulin g, by means of enzyme-labelled antigen and antibody-coated tubes. *Biochimica et Biophysica Acta (BBA) - Protein Structure* **251,** 427–434. doi:10.1016/0005-2795(71)90132-2 (1971).

105. Schmidt, S. D., Mazzella, M. J., Nixon, R. A. & Mathews, P. M. *Amyloid Proteins: Methods and Protocols* (eds Sigurdsson, E. M., Calero, M. & Gasset, M.) 507–527 (Humana Press, Totowa, NJ, 2012). doi:10.1007/978-1-61779-551-0_34.

106. Hoofnagle, A. N. & Wener, M. H. The fundamental flaws of immunoassays and potential solutions using tandem mass spectrometry. eng. *Journal of immunological methods* **347,** 3–11. doi:10.1016/j.jim.2009.06.003 (Aug. 2009).

107. Sotnikov, D. V., Zherdev, A. V., Zvereva, E. A., Eremin, S. A. & Dzantiev, B. B. *Changing Cross-Reactivity for Different Immunoassays Using the Same Antibodies: Theoretical Description and Experimental Confirmation* 2021. doi:10.3390/app11146581.

108. Anderson, N. L. *et al.* Mass Spectrometric Quantitation of Peptides and Proteins Using Stable Isotope Standards and Capture by Anti-Peptide Antibodies (SISCAPA). *Journal of proteome research* **3,** 235–244. doi:10.1021/pr034086h (Apr. 2004).

109. Neubert, H. *et al.* Protein Biomarker Quantification by Immunoaffinity Liquid Chromatography–Tandem Mass Spectrometry: Current State and Future Vision. *Clinical Chemistry* **66,** 282–301. doi:10.1093/clinchem/hvz022 (Jan. 2020).

110. Hoofnagle, A. N., Becker, J. O., Wener, M. H. & Heinecke, J. W. Quantification of thyroglobulin, a low-abundance serum protein, by immunoaffinity peptide enrichment and tandem mass spectrometry. eng. *Clinical chemistry* **54,** 1796–1804. doi:10.1373/clinchem.2008.109652 (Nov. 2008).

111. Hoeppe, S. *et al.* Targeting peptide termini, a novel immunoaffinity approach to reduce complexity in mass spectrometric protein identification. *Molecular and cellular proteomics: MCP* **10,** M110.002857. doi:10.1074/mcp.M110.002857 (2 Feb. 2011). ppublish.

112. Weiss, F. *et al.* Catch and measure-mass spectrometry-based immunoassays in biomarker research. *Biochimica et Biophysica Acta (BBA) - Proteins and Proteomics* **1844,** 927–932. doi:10.1016/j.bbapap.2013.09.010 (2014).

113. Poetz, O., Hoeppe, S., Templin, M. F., Stoll, D. & Joos, T. O. Proteome wide screening using peptide affinity capture. *Proteomics* **9,** 1518–1523. doi:10.1002/pmic.200800842 (Mar. 2009).

114. Cox, J. *et al.* Accurate proteome-wide label-free quantification by delayed normalization and maximal peptide ratio extraction, termed MaxLFQ. eng. *Molecular and cellular proteomics : MCP* **13,** 2513–2526. doi:10.1074/mcp.M113.031591 (Sept. 2014).

115. Lundgren, D. H., Hwang, S.-I., Wu, L. & Han, D. K. Role of spectral counting in quantitative proteomics. *Expert Review of Proteomics* **7,** 39–53. doi:10.1586/epr.09.69 (Feb. 2010).

116. Al Shweiki, M. H. D. R. *et al.* Assessment of Label-Free Quantification in Discovery Proteomics and Impact of Technological Factors and Natural Variability of Protein Abundance. *Journal of proteome research* **16,** 1410–1424. doi:10.1021/acs.jproteome.6b00645 (Apr. 2017).

117. Ong, S.-E. *et al.* Stable Isotope Labeling by Amino Acids in Cell Culture, SILAC, as a Simple and Accurate Approach to Expression Proteomics. *Molecular and Cellular Proteomics* **1,** 376–386. doi:10.1074/mcp.M200025-MCP200 (May 2002).

118. Soufi, B. *et al.* Stable Isotope Labeling by Amino Acids in Cell Culture (SILAC) Applied to Quantitative Proteomics of Bacillus subtilis. *Journal of Proteome Research* **9,** 3638–3646. doi:10.1021/pr100150w (July 2010).

119. Deng, J., Erdjument-Bromage, H. & Neubert, T. A. Quantitative Comparison of Proteomes Using SILAC. eng. *Current protocols in protein science* **95,** e74–e74. doi:10.1002/cpps.74 (Feb. 2019).

120. Boersema, P. J., Raijmakers, R., Lemeer, S., Mohammed, S. & Heck, A. J. R. Multiplex peptide stable isotope dimethyl labeling for quantitative proteomics. *Nature Protocols* **4,** 484–494. doi:10.1038/nprot.2009.21 (2009).

121. Ross, P. L. *et al.* Multiplexed Protein Quantitation in Saccharomyces cerevisiae Using Amine-reactive Isobaric Tagging Reagents. *Molecular and Cellular Proteomics* **3,** 1154–1169. doi:10.1074/mcp.M400129-MCP200 (Dec. 2004).

122. Thompson, A. *et al.* Tandem Mass Tags: A Novel Quantification Strategy for comparative analysis of complex protein mixtures. *Analytical Chemistry* **75,** 1895–1904. doi:10.1021/ac0262560 (Mar. 2003).

123. Macklin, A., Khan, S. & Kislinger, T. Recent advances in mass spectrometry based clinical proteomics: applications to cancer research. *Clinical Proteomics* **17,** 17. doi:10.1186/s12014-020-09283-w (2020).

124. Gerber, S. A., Rush, J., Stemman, O., Kirschner, M. W. & Gygi, S. P. Absolute quantification of proteins and phosphoproteins from cell lysates by tandem MS. *Proc Natl Acad Sci USA* **100,** 6940. doi:10.1073/pnas.0832254100 (June 2003).

125. Frantzi, M., Latosinska, A., Kontostathi, G. & Mischak, H. Clinical Proteomics: Closing the Gap from Discovery to Implementation. *Proteomics* **18,** 1700463. doi:10.1002/pmic.201700463 (July 2018).

126. United States Department of Health and Human Services. *Bioanalytical method validation* tech. rep. (United States Food and Drug Administration (FDA), 2018). http://resource.nlm.nih.gov/101734209.

127. Committee for Medicinal Products for Human Use (CHMP). *Guideline on bioanalytical method validation* tech. rep. (European Medicines Agency, 2012). https://www.ema.europa.eu/en/documents/scientific-guideline/guideline-bioanalytical-method-validation_en.pdf.

128. Andreasson, U. *et al.* A Practical Guide to Immunoassay Method Validation. eng. *Frontiers in neurology* **6,** 179–179. doi:10.3389/fneur.2015.00179 (Aug. 2015).

129. Weng, L., Guo, L., Vachani, A., Mesaros, C. & Blair, I. A. Quantification of Serum High Mobility Group Box 1 by Liquid Chromatography/High-Resolution Mass Spectrometry: Implications for Its Role in Immunity, Inflammation, and Cancer. *Analytical chemistry* **90,** 7552–7560. doi:10.1021/acs.analchem.8b01175 (12 June 2018). ppublish.

130. Lanteri, P., Lombardi, G., Colombini, A., Grasso, D. & Banfi, G. Stability of osteopontin in plasma and serum. *Clinical chemistry and laboratory medicine* **50,** 1979–1984. doi:10.1515/cclm-2012-0177 (11 Nov. 2012). ppublish.

131. Cristaudo, A. *et al.* Comparison between Plasma and Serum Osteopontin Levels: Usefulness in Diagnosis of Epithelial Malignant Pleural Mesothelioma. *International Journal of Biological Markers* **25,** 164–170. doi:10.1177/172460081002500307 (2010).

132. Anselm, V., Steinhilber, A., Sommersdorf, C. & Poetz, O. Immunoaffinity-Based Liquid Chromatography Mass Spectrometric Assay to Accurately Quantify the Protein Concentration of HMGB1 in EDTA Plasma. *Methods in molecular biology (Clifton, N.J.)* **2261,** 277–289. doi:10.1007/978-1-0716-1186-9_17 (2021). ppublish.

133. *Ganong's review of medical physiology* 24. ed. (eds Barrett, K. E. & Ganong, W. F.) Literaturangaben. IX, 752 (McGraw-Hill Med., New York [u.a.], 2012).

134. Anselm, V. *et al.* Matrix and Sampling Effects on Quantification of Protein Biomarkers of Drug-Induced Liver Injury. *Journal of proteome research.* doi:10.1021/acs.jproteome.1c00478 (Sept. 2021). aheadofprint.

135. Smith, P. K. *et al.* Measurement of protein using bicinchoninic acid. *Analytical biochemistry* **150,** 76–85. doi:10.1016/0003-2697(85)90442-7 (1 Oct. 1985). ppublish.

136. Perez-Riverol, Y. *et al.* The PRIDE database and related tools and resources in 2019: improving support for quantification data. *Nucleic Acids Research* **47,** D442–D450. doi:10.1093/nar/gky1106 (Jan. 2019).

137. Pino, L. K. *et al.* The Skyline ecosystem: Informatics for quantitative mass spectrometry proteomics. *Mass Spectrometry Reviews* **39,** 229–244. doi:10.1002/mas.21540 (May 2020).

138. Bateman, A. *et al.* UniProt: the universal protein knowledgebase in 2021. *Nucleic Acids Research* **49,** D480–D489. doi:10.1093/nar/gkaa1100 (2021).

139. Gasteiger, E. *et al.* (ed J.M., W.) 571–607 (Humana Press, 2005). doi:10.1385/1-59259-890-0:571.

140. Wakefield, J. & Racine-Poon, A. An Application of Bayesian Population Pharmacokinetic/Pharmacodynamic Models to Dose Recommendation. *Statistics in Medicine* **14,** 971–986. doi:10.1002/sim.4780140917 (May 1995).

141. Mukaka, M. M. Statistics corner: A guide to appropriate use of correlation coefficient in medical research. eng. *Malawi medical journal: the journal of Medical Association of Malawi* **24,** 69–71. https://www.ncbi.nlm.nih.gov/pmc/articles/PMC3576830/ (Sept. 2012).

142. Poetz, O. *et al.* Peptide-Based Sandwich Immunoassay for the Quantification of the Membrane Transporter Multidrug Resistance Protein 1. *Analytical Chemistry* **90,** 5788–5794. doi:10.1021/acs.analchem.8b00152 (May 2018).

143. Wroblewski, F. & Ladue, J. S. Serum glutamic pyruvic transaminase in cardiac with hepatic disease. *Proceedings of the Society for Experimental Biology and Medicine. Society for Experimental Biology and Medicine (New York, N.Y.)* **91,** 569–571. doi:10.3181/00379727-91-22330 (4 Apr. 1956). ppublish.

144. Bergmeyer, H. U. & Horder, M. International federation of clinical chemistry. Scientific committee. Expert panel on enzymes. IFCC document stage 2, draft 1; 1979-11-19 with a view to an IFCC recommendation. IFCC methods for the measurement of catalytic concentration of enzymes. Part 3. IFCC method for alanine aminotransferase. *Journal of clinical chemistry and clinical biochemistry.* **8,** 521–524 (Aug. 1980).

145. DelMar, E. G., Largman, C., Brodrick, J. W. & Geokas, M. C. A sensitive new substrate for chymotrypsin. *Analytical biochemistry* **99,** 316–320. doi:10.1016/s0003-2697(79)80013-5 (2 Nov. 1979). ppublish.

146. Swinehart, D. F. The Beer-Lambert Law. *Journal of Chemical Education* **39,** 333–335. doi:10.1021/ed039p333 (July 1962).

147. Caulín, C., Salvesen, G. S. & Oshima, R. G. Caspase cleavage of keratin 18 and reorganization of intermediate filaments during epithelial cell apoptosis. *The Journal of cell biology* **138,** 1379–1394. doi:10.1083/jcb.138.6.1379 (6 Sept. 1997). ppublish.

148. Shaw, E. Site-specific reagents for chymotrypsin, trypsin, and other serine proteases. *Methods in enzymology* **25,** 655–660. doi:10.1016/S0076-6879(72)25062-5 (1972). ppublish.

149. Schwenk, J. M. *et al.* The Human Plasma Proteome Draft of 2017: Building on the Human Plasma PeptideAtlas from Mass Spectrometry and Complementary Assays. *Journal of proteome research* **16,** 4299–4310. doi:10.1021/acs.jproteome.7b00467 (Dec. 2017).

150. Low, T. Y. *et al.* Quantitative and qualitative proteome characteristics extracted from in-depth integrated genomics and proteomics analysis. *Cell reports* **5,** 1469–1478. doi:10.1016/j.celrep.2013.10.041 (5 Dec. 2013). ppublish.

151. Weiss, F. *et al.* Indirect protein quantification of drug-transforming enzymes using peptide group-specific immunoaffinity enrichment and mass spectrometry. *Scientific reports* **5,** 8759. doi:10.1038/srep08759 (Mar. 2015).

152. Tukey, J. W. *Exploratory data analysis* https://www.worldcat.org/oclc/03058187 (Addison-Wesley, 1977).

153. Hasan, K. M. M., Tamanna, N. & Haque, M. A. Biochemical and histopathological profiling of Wistar rat treated with Brassica napus as a supplementary feed. *Food Science and Human Wellness* **7,** 77–82. doi:10.1016/j.fshw.2017.12.002 (Mar. 2018).

154. *The Laboratory Rat* 2nd (eds Suckow, M., Weisbroth, S. & Franklin, C.) (2005).

155. Church, R. J. & Watkins, P. B. The transformation in biomarker detection and management of drug-induced liver injury. *Liver international : official journal of the International Association for the Study of the Liver* **37,** 1582–1590. doi:10.1111/liv.13441 (11 Nov. 2017).

156. Végvári, Á., Welinder, C., Lindberg, H., Fehniger, T. E. & Marko-Varga, G. Biobank resources for future patient care: developments, principles and concepts. *Journal of Clinical Bioinformatics* **1,** 24. doi:10.1186/2043-9113-1-24 (2011).

157. Uotila, M., Ruoslahti, E. & Engvall, E. Two-site sandwich enzyme immunoassay with monoclonal antibodies to human alpha-fetoprotein. *Journal of Immunological Methods* **42,** 11–15. doi:10.1016/0022-1759(81)90219-2 (1981).

158. Stoecker, W. & Schlumberger, W. *Lexikon der Medizinischen Laboratoriumsdiagnostik* (eds Gressner, A. M. & Arndt, T.) 1–2 (Springer Berlin Heidelberg, Berlin, Heidelberg, 2018). doi:10.1007/978-3-662-49054-9_1980-1.

159. Abdulahad, D. A. *et al.* High mobility group box 1 (HMGB1) and anti-HMGB1 antibodies and their relation to disease characteristics in systemic lupus erythematosus. *Arthritis Research and Therapy* **13.** doi:10.1186/ar3332 (2011).

160. Geyer, P. E. *et al.* Plasma Proteome Profiling to detect and avoid sample-related biases in biomarker studies. *EMBO Mol Med* **11,** e10427. doi:10.15252/emmm.201910427 (Nov. 2019).

161. Liigand, P., Kaupmees, K. & Kruve, A. Influence of the amino acid composition on the ionization efficiencies of small peptides. *Journal of Mass Spectrometry* **54,** 481–487. doi:10.1002/jms.4348 (June 2019).

162. Xindu, G. & Regnier, F. E. Retention model for proteins in reversed-phase liquid chromatography. *Journal of Chromatography A* **296,** 15–30. doi:10.1016/S0021-9673(01)96399-X (1984).

163. Kyte, J. & Doolittle, R. F. A simple method for displaying the hydropathic character of a protein. *Journal of molecular biology* **157,** 105–132. doi:10.1016/0022-2836(82)90515-0 (1 May 1982).

164. Fuchs, S. M. & Strahl, B. D. Antibody recognition of histone post-translational modifications: emerging issues and future prospects. *Epigenomics* **3,** 247–249. doi:10.2217/epi.11.23 (June 2011).

165. Davies, J. E., Apta, B. H. R. & Harper, M. T. Cross-reactivity of anti-HMGB1 antibodies for HMGB2. eng. *Journal of immunological methods* **456,** 72–76. doi:10.1016/j.jim.2018.02.006 (May 2018).

166. Wang, T.-H., Wang, H.-S. & Soong, Y.-K. Paclitaxel-induced cell death. *Cancer* **88,** 2619–2628 (June 2000).

167. Impens, F. *et al.* Mechanistic insight into taxol-induced cell death. *Oncogene* **27,** 4580–4591. doi:10.1038/onc.2008.96 (2008).

168. Bian, Y. *et al.* An enzyme assisted RP-RPLC approach for in-depth analysis of human liver phosphoproteome. *Journal of Proteomics* **96,** 253–262. doi:10.1016/j.jprot.2013.11.014 (2014).

169. Von Stechow, L., Francavilla, C. & Olsen, J. V. Recent findings and technological advances in phosphoproteomics for cells and tissues. eng. *Expert review of proteomics* **12,** 469–487. doi:10.1586/14789450.2015.1078730 (2015).

170. Picotti, P., Aebersold, R. & Domon, B. The Implications of Proteolytic Background for Shotgun Proteomics. *Molecular and Cellular Proteomics* **6,** 1589–1598. doi:10.1074/mcp.M700029-MCP200 (Sept. 2007).

171. Perutka, Z. & Šebela, M. Pseudotrypsin: A Little-Known Trypsin Proteoform. eng. *Molecules* **23,** 2637. doi:10.3390/molecules23102637 (Oct. 2018).

172. Burkhart, J. M., Schumbrutzki, C., Wortelkamp, S., Sickmann, A. & Zahedi, R. P. Systematic and quantitative comparison of digest efficiency and specificity reveals the impact of trypsin quality on MS-based proteomics. *Journal of Proteomics* **75,** 1454–1462. doi:10.1016/j.jprot.2011.11.016 (2012).

173. Keil-Dlouhá, V., Zylber, N., Imhoff, J.-M., Tong, N.-T. & Keil, B. Proteolytic activity of pseudotrypsin. *FEBS Letters* **16,** 291–295. doi:10.1016/0014-5793(71)80373-3 (1971).

174. Dycka, F. *et al.* Evaluation of Pseudotrypsin Cleavage Specificity Towards Proteins by MALDI-TOF Mass Spectrometry. *Protein and Peptide Letters* **22,** 1123–1132. doi:10.2174/0929866522666151008151617 (2015).

175. Fang, P. *et al.* Controlling nonspecific trypsin cleavages in LC-MS/MS-based shotgun proteomics using optimized experimental conditions. *Analyst* **140,** 7613–7621. doi:10.1039/C5AN01505G (2015).

176. Erlanger, B. F., Kokowsky, N. & Cohen, W. The preparation and properties of two new chromogenic substrates of trypsin. *Archives of Biochemistry and Biophysics* **95,** 271–278. doi:10.1016/0003-9861(61)90145-X (1961).

177. Erlanger, B. F., Edel, F. & Cooper, A. G. The action of chymotrypsin on two new chromogenic substrates. *Archives of Biochemistry and Biophysics* **115,** 206–210. doi:10.1016/S0003-9861(66)81058-5 (1966).

178. Rice, R. H., Means, G. E. & Brown, W. D. Stabilization of bovine trypsin by reductive methylation. *Biochimica et Biophysica Acta (BBA) - Protein Structure* **492,** 316–321. doi:10.1016/0005-2795(77)90082-4. https://www.sciencedirect.com/science/article/pii/0005279577900824 (1977).

179. Schoellmann, G. & Shaw, E. Direct Evidence for the Presence of Histidine in the Active Center of Chymotrypsin. *Biochemistry* **2,** 252–255. doi:10.1021/bi00902a008 (Mar. 1963).

180. Korver, S. *et al.* The application of cytokeratin-18 as a biomarker for drug-induced liver injury. *Archives of Toxicology* **95,** 3435–3448. doi:10.1007/s00204-021-03121-0 (2021).

181. Srungaram, P. *et al.* Plasma osteopontin in acute liver failure. *Cytokine* **73,** 270–276. doi:10.1016/j.cyto.2015.02.021 (2015).

182. Liu, L. *et al.* Serum osteopontin is a predictor of prognosis for HBV-associated acute-on-chronic liver failure. *Biomedical Reports* **8,** 166–171. doi:10.3892/br.2017.1027 (2018).

183. Yu, Z. *et al.* Differences between human plasma and serum metabolite profiles. eng. *PloS one* **6,** e21230–e21230. doi:10.1371/journal.pone.0021230 (2011).

184. Barelli, S., Crettaz, D., Thadikkaran, L., Rubin, O. & Tissot, J.-D. Plasma/serum proteomics: pre-analytical issues. *Expert Reviews of Proteomics* **4,** 363–370. doi:10.1586/14789450.4.3.363 (June 2007).

185. Tuck, M. K. *et al.* Standard operating procedures for serum and plasma collection: early detection research network consensus statement standard operating procedure integration working group. *Journal of proteome research* **8,** 113–117. doi:10.1021/pr800545q (1 Jan. 2009). ppublish.

186. Hsieh, S.-Y., Chen, R.-K., Pan, Y.-H. & Lee, H.-L. Systematical evaluation of the effects of sample collection procedures on low-molecular-weight serum/plasma proteome profiling. *Proteomics* **6,** 3189–3198. doi:10.1002/pmic.200500535 (May 2006).

187. Ottestad, W. *et al.* HMGB1 concentration measurements in trauma patients: assessment of pre-analytical conditions and sample material. *Molecular Medicine.* doi:10.1186/s10020-019-0131-0 (2020).

188. Lehner, J. *et al.* Methodological and preanalytical evaluation of an HMGB1 immunoassay. *Anticancer Research* **32,** 2059–62 (May 2012).

189. Yang, X. *et al.* HMGB1: a novel protein that induced platelets active and aggregation via Toll-like receptor-4, NF-κB and cGMP dependent mechanisms. eng. *Diagnostic pathology* **10,** 134–134. doi:10.1186/s13000-015-0348-3 (Aug. 2015).

190. Vordermark, D. *et al.* Plasma osteopontin levels in patients with head and neck cancer and cervix cancer are critically dependent on the choice of ELISA system. *BMC Cancer* **6,** 207. doi:10.1186/1471-2407-6-207 (2006).

191. Denhardt, D. T. & Guo, X. Osteopontin: a protein with diverse functions. *The FASEB Journal* **7,** 1475–1482. doi:10.1096/fasebj.7.15.8262332 (Dec. 1993).

192. Banfi, G., Salvagno, G. L. & Lippi, G. The role of ethylenediamine tetraacetic acid (EDTA) as in vitro anticoagulant for diagnostic purposes. *Clinical chemistry and laboratory medicine* **45,** 565–576. doi:10.1515/CCLM.2007.110 (2007).

193. Mohri, M. & Rezapoor, H. Effects of heparin, citrate, and EDTA on plasma biochemistry of sheep: Comparison with serum. *Research in Veterinary Science* **86,** 111–114. doi:10.1016/j.rvsc.2008.05.010 (2009).

194. Sharif, S. A. *et al.* Thrombin-activatable carboxypeptidase B cleavage of osteopontin regulates neutrophil survival and synoviocyte binding in rheumatoid arthritis. *Arthritis and Rheumatism* **60,** 2902–2912. doi:10.1002/art.24814 (Oct. 2009).

195. Cui, G. *et al.* Thrombin cleavage of osteopontin controls activation of hepatic stellate cells and is essential for liver fibrogenesis. *Journal of Cellular Physiology* **234,** 8988–8997. doi:10.1002/jcp.27571 (June 2019).

196. Church, R. J. *et al.* Glutamate dehydrogenase as a biomarker for mitotoxicity; insights from furosemide hepatotoxicity in the mouse. eng. *PloS one* **15,** e0240562–e0240562. doi:10.1371/journal.pone.0240562 (Oct. 2020).

197. McGill, M. R. *et al.* The mechanism underlying acetaminophen-induced hepatotoxicity in humans and mice involves mitochondrial damage and nuclear DNA fragmentation. *Journal of Clinical Investigation* **122,** 1574–1583. doi:10.1172/JCI59755 (Apr. 2012).

198. Johnson, K. A. & Goody, R. S. The Original Michaelis Constant: Translation of the 1913 Michaelis-Menten Paper. *Biochemistry* **50,** 8264–8269. doi:10.1021/bi201284u (Oct. 2011).

199. McGill, M. R., Williams, C. D., Xie, Y., Ramachandran, A. & Jaeschke, H. Acetaminophen-induced liver injury in rats and mice: comparison of protein adducts, mitochondrial dysfunction, and oxidative stress in the mechanism of toxicity. eng. *Toxicology and applied pharmacology* **264,** 387–394. doi:10.1016/j.taap.2012.08.015 (Nov. 2012).

200. Jaeschke, H., Xie, Y. & McGill, M. R. Acetaminophen-induced Liver Injury: from Animal Models to Humans. eng. *Journal of clinical and translational hepatology* **2,** 153–161. doi:10.14218/JCTH.2014.00014 (Sept. 2014).

201. Jarsiah, P., Nosrati, A., Alizadeh, A. & Hashemi-Soteh, S. M. B. Hepatotoxicity and ALT/AST Enzymes Activities Change in Therapeutic and Toxic Doses Consumption of Acetaminophen in Rats. *International Biological and Biomedical Journal* **3,** 119–124. http://ibbj.org/article-1-129-en.html (June 2017).

202. Aycan, İ. Ö. *et al.* Thymoquinone treatment against acetaminophen-induced hepatotoxicity in rats. *International Journal of Surgery* **12,** 213–218. doi:10.1016/j.ijsu.2013.12.013 (2014).

203. Thulin, P. *et al.* A longitudinal assessment of miR-122 and GLDH as biomarkers of drug-induced liver injury in the rat. *Biomarkers* **22,** 461–469. doi:10.1080/1354750X.2016.1269131 (July 2017).

204. Kang, J. S. *et al.* Role of CYP2E1 in thioacetamide-induced mouse hepatotoxicity. *Toxicology and Applied Pharmacology* **228,** 295–300. doi:10.1016/j.taap.2007.11.010 (2008).

205. Hajovsky, H. *et al.* Metabolism and Toxicity of Thioacetamide and Thioacetamide S-Oxide in Rat Hepatocytes. *Chem. Res. Toxicol.* **25,** 1955–1963. doi:10.1021/tx3002719 (Sept. 2012).

206. Zargar, S., Wani, T. A., Alamro, A. A. & Ganaie, M. A. Amelioration of thioacetamide-induced liver toxicity in Wistar rats by rutin. *International Journal of Immunopathology and Pharmacology* **30,** 207–214. doi:10.1177/0394632017714175 (June 2017).

207. Lin, Y.-Y., Hu, C.-T., Sun, D.-S., Lien, T.-S. & Chang, H.-H. Thioacetamide-induced liver damage and thrombocytopenia is associated with induction of antiplatelet autoantibody in mice. *Scientific Reports* **9,** 17497. doi:10.1038/s41598-019-53977-7 (2019).

208. Tanaka, K. *et al.* Acquired Resistance to Bromobenzene Hepatotoxicity by Repeated Treatment of Rats with Bromobenzene. *Journal of Toxicologic Pathology* **18,** 189–198. doi:10.1293/tox.18.189 (Jan. 2005).

209. Tanaka, K., Kiyosawa, N., Watanbe, K. & Manabe, S. Characterization of Resistance to Bromobenzene-induced Hepatoxicity by Microarray. *The Journal of Toxicological Sciences* **32,** 129–134. doi:10.2131/jts.32.129 (2007).

210. Wagner, M. *et al.* CAR and PXR agonists stimulate hepatic bile acid and bilirubin detoxification and elimination pathways in mice. *Hepatology* **42,** 420–430. doi:10.1002/hep.20784 (Aug. 2005).

211. Kanz, M. F., Wang, A. & Campbell, G. A. Infusion of bile from methylene dianiline-treated rats into the common bile duct injures biliary epithelial cells of recipient rats. *Toxicology Letters* **78,** 165–171. doi:10.1016/0378-4274(95)03251-F (1995).

212. Fortea, J. I. *et al.* Comparison of Two Protocols of Carbon Tetrachloride-Induced Cirrhosis in Rats - Improving Yield and Reproducibility. *Scientific Reports* **8,** 9163. doi:10.1038/s41598-018-27427-9 (2018).

213. De la M. Hall, P., Plummer, J. L., Ilsley, A. H. & Cousins, M. J. Hepatic fibrosis and cirrhosis after chronic administration of alcohol and "low-dose" carbon tetrachloride vapor in the rat. *Hepatology* **13,** 815–819. doi:10.1002/hep.1840130502 (May 1991).

214. Wang, K. X. & Denhardt, D. T. Osteopontin: Role in immune regulation and stress responses. *Cytokine and Growth Factor Reviews* **19,** 333–345. doi:10.1016/j.cytogfr.2008.08.001 (2008).

215. He, C.-y. *et al.* The dual role of osteopontin in acetaminophen hepatotoxicity. *Acta pharmacologica Sinica* **33,** 1004–1012. doi:10.1038/aps.2012.47 (Aug. 2012).

216. Ramadan, A. *et al.* Potential Therapeutic Role of Osteopontin Inhibition in Liver Fibrosis -Induced by Thioacetamide in Rats. en. *Journal of Applied Veterinary Sciences* **2,** 1–8. doi:10.21608/javs.2017.62129 (2017).

217. Arffa, M. L. *et al.* Epigallocatechin-3-Gallate Upregulates miR-221 to Inhibit Osteopontin-Dependent Hepatic Fibrosis. eng. *PloS one* **11,** e0167435–e0167435. doi:10.1371/journal.pone.0167435 (Dec. 2016).

218. Arriazu, E. *et al.* Signalling via the osteopontin and high mobility group box-1 axis drives the fibrogenic response to liver injury. *Gut* **66,** 1123. doi:10.1136/gutjnl-2015-310752 (June 2017).

219. Giffen, P. S., Pick, C. R., Price, M. A., Williams, A. & York, M. J. Alpha-Glutathione S-Transferase in the Assessment of Hepatotoxicity–Its Diagnostic Utility in Comparison with Other Recognized Markers in the Wistar Han Rat. *Toxicol Pathol* **30,** 365–372. doi:10.1080/01926230252929945 (Apr. 2002).

220. Sharapova, T. *et al.* Evaluation of miR-122 as a Serum Biomarker for Hepatotoxicity in Investigative Rat Toxicology Studies. *Vet Pathol* **53,** 211–221. doi:10.1177/0300985815591076 (June 2015).

221. Antoine, D. J. *et al.* RETRACTED: Molecular forms of HMGB1 and keratin-18 as mechanistic biomarkers for mode of cell death and prognosis during clinical acetaminophen hepatotoxicity. eng. *Journal of hepatology* **56,** 1070–1079. doi:10.1016/j.jhep.2011.12.019 (May 2012).

222. Antoine, D. J., Williams, D. P., Kipar, A., Laverty, H. & Park, B. K. Retracted: Diet restriction inhibits apoptosis and HMGB1 oxidation and promotes inflammatory cell recruitment during acetaminophen hepatotoxicity. eng. *Molecular medicine (Cambridge, Mass.)* **16,** 479–490. doi:10.2119/molmed.2010.00126. https://www.ncbi.nlm.nih.gov/pmc/articles/PMC2972397 (2010).

223. Antoine, D. J. *et al.* Retraction notice to "Molecular forms of HMGB1 and keratin-18 as mechanistic biomarkers for mode of cell death and prognosis during clinical acetaminophen hepatotoxicity": J Hepatol 56(2012)1070-1079. eng. *Journal of hepatology* **73,** 1297–1297. doi:10.1016/j.jhep.2020.08.022 (Nov. 2020).

224. Antoine, D. J., Williams, D. P., Kipar, A., Laverty, H. & Park, B. K. Retraction Note: Diet restriction inhibits apoptosis and HMGB1 oxidation and promotes inflammatory cell recruitment during acetaminophen hepatotoxicity. eng. *Molecular medicine (Cambridge, Mass.)* **26,** 130–130. doi:10.1186/s10020-020-00262-3 (Dec. 2020).

225. Liu, J. *et al.* Modulation of HMGB1 Release in APAP-Induced Liver Injury: A Possible Strategy of Chikusetsusaponin V Targeting NETs Formation. *Frontiers in Pharmacology* **12,** 1895. doi:10.3389/fphar.2021.723881 (2021).

226. Minsart, C. *et al.* New insights in acetaminophen toxicity: HMGB1 contributes by itself to amplify hepatocyte necrosis in vitro through the TLR4-TRIF-RIPK3 axis. *Scientific Reports* **10,** 5557. doi:10.1038/s41598-020-61270-1 (2020).

227. Wallace, M. C. *et al.* Standard Operating Procedures in Experimental Liver Research: Thioacetamide model in mice and rats. *Lab Animal* **49,** 21–29. doi:10.1177/002367721-5573040 (Apr. 2015).

228. Wei, Y. *et al.* Proteolytic Shedding of Human Colony-Stimulating Factor 1 Receptor and its implication. eng. *Journal of cellular and molecular medicine* **25,** 4516–4521. doi:10.1111/jcmm.16474 (May 2021).

229. Lowenthal, M. S., Davis, K. S., Formolo, T., Kilpatrick, L. E. & Phinney, K. W. Identification of Novel N-Glycosylation Sites at Noncanonical Protein Consensus Motifs. eng. *Journal of proteome research* **15,** 2087–2101. doi:10.1021/acs.jproteome.5b00733 (July 2016).

230. Mathias, U. *et al.* Tissue-based map of the human proteome. *Science* **347,** 1260419. doi:10.1126/science.1260419 (Jan. 2015).

231. Schyman, P. *et al.* Identification of the Toxicity Pathways Associated With Thioacetamide-Induced Injuries in Rat Liver and Kidney. eng. *Frontiers in pharmacology* **9,** 1272–1272. doi:10.3389/fphar.2018.01272 (Nov. 2018).

232. Vlasakova, K. *et al.* Evaluation of the Relative Performance of 12 Urinary Biomarkers for Renal Safety Across 22 Rat Sensitivity and Specificity Studies. *Toxicological Sciences* **138,** 3–20. doi:10.1093/toxsci/kft330 (Mar. 2014).

233. McSweeney, K. R. *et al.* Mechanisms of Cisplatin-Induced Acute Kidney Injury: Pathological Mechanisms, Pharmacological Interventions, and Genetic Mitigations. eng. *Cancers* **13,** 1572. doi:10.3390/cancers13071572 (Mar. 2021).

Appendices

A.A Tryptic and chymotryptic activity in plasma

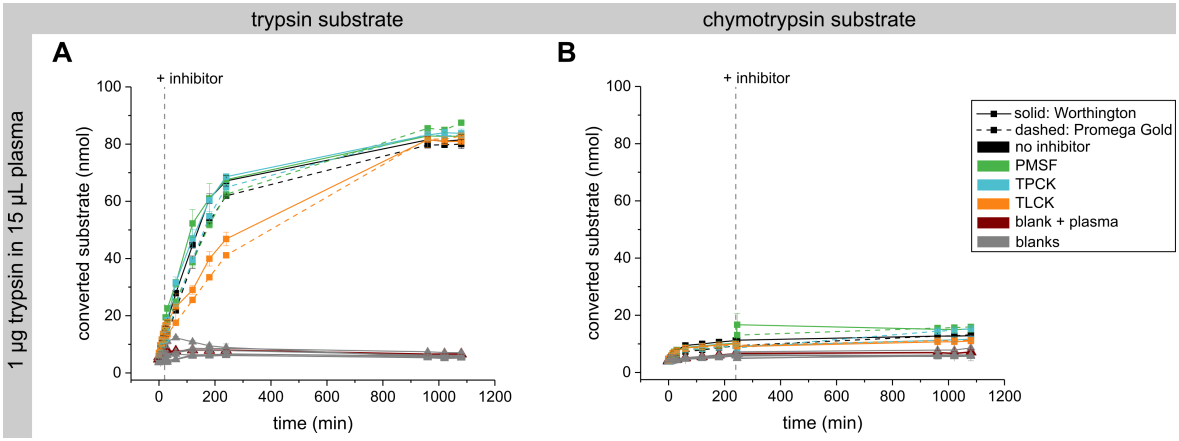

Figure 49: Tryptic and chymotryptic activity in plasma. (A) Trypsin substrate and **(B)** chymotrypsin substrate was converted in the presence of 15 µL human plasma and 1 µg trypsin (provided by Worthington or Promega Gold, n = 3 per condition, 100 nmol substrate per well). The following inhibitors were added to trypsin substrate or chymotrypsin substrate wells 20 min or 180 min after start, respectively: 1 mM PMSF, 100 µM TPCK, 100 µM TLCK. Blank + plasma sample included plasma and substrate but no trypsin or inhibitors. Further blanks without spiked plasma (grey) included samples without substrate and samples without trypsin and substrate.

A.B Endogenous human ccK18 peptide

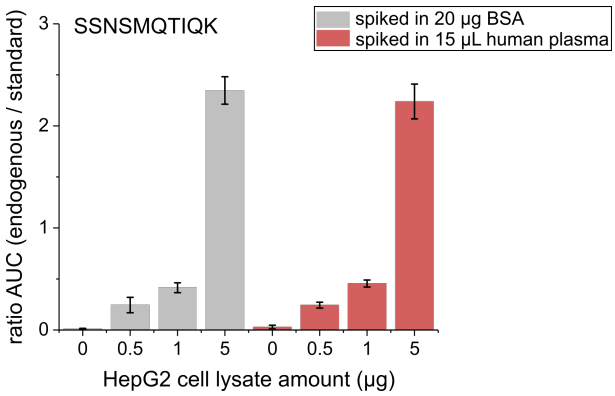

Figure 50: Enriched endogenous human ccK18 from cell lysate of taxol-treated HepG2 cells. Cell lysate from taxol-treated HepG2 cells was spiked either in 20 µg BSA or in 15 µL human plasma (n = 2; 0.5 µg to 5 µg total protein amount from lysate). The human ccK18 peptide SSNSMQTIQK was targeted for enrichment with 5 µg AB and 5 fmol spiked internal standard.

A.C Partial validation results for the IA-LC-MS/MS assay MPr

Table 26: Peak area ratio data of calibrators and blank for OPN (MPr), ratio = area under the curve (AUC) of non-labeled peptide peak over isotope-labeled peptide peak. LLOQ/ULOQ ratios labeled in **bold**

Run	Unit	B	S8	S7	S6	S5	S4	S3	S2	S1
1	ratio	0.01	0.03	0.08	0.22	0.73	2.05	5.53	16.8	54.8
1	ratio	0.01	0.04	0.09	0.25	0.69	2.09	6.03	18.6	60.9
2	ratio	0.01	0.03	0.09	0.27	0.76	2.29	6.94	19.9	59.5
2	ratio	0.01	0.04	0.09	0.26	0.77	2.39	6.55	20.0	62.6
3	ratio	0.01	0.04	0.09	0.26	0.82	2.24	6.97	20.3	58.0
3	ratio	0.01	0.03	0.09	0.27	0.75	2.28	6.70	21.2	66.4
Mean value, n=6	ratio	0.01	0.03	**0.09**	0.26	0.75	2.23	6.45	19.5	**60.4**
SD	ratio	0.00	0.01	0.01	0.02	0.04	0.13	0.57	1.55	3.97
blank + 6x SD	ratio	0.02	-	-	-	-	-	-	-	-

Table 27: Peak area ratio data of calibrators and blank for HMGB1 (MPr), ratio = area under the curve (AUC) of non-labeled peptide peak over isotope-labeled peptide peak. LLOQ/ULOQ ratios labeled in **bold**

Run	Unit	B	S8	S7	S6	S5	S4	S3	S2	S1
1	ratio	0.19	0.19	0.27	0.47	0.97	2.68	6.81	19.9	66.5
1	ratio	0.18	0.22	0.25	0.48	0.94	2.45	6.81	20.8	66.0
2	ratio	0.17	0.21	0.26	0.52	1.00	2.83	8.58	22.4	64.0
2	ratio	0.16	0.20	0.28	0.47	1.01	3.05	8.05	20.6	63.0
3	ratio	0.13	0.18	0.25	0.42	1.06	2.61	7.53	23.3	68.4
3	ratio	0.18	0.18	0.26	0.46	1.00	3.04	9.02	25.3	72.9
Mean value, n=6	ratio	0.17	0.20	0.26	**0.47**	1.00	2.78	7.80	22.1	**66.8**
SD	ratio	0.02	0.01	0.01	0.03	0.04	0.24	0.92	2.05	3.53
blank + 6x SD	ratio	0.30	-	-	-	-	-	-	-	-

Table 28: Peak area ratio data of calibrators and blank for ccK18 (MPr), ratio = area under the curve (AUC) of non-labeled peptide peak over isotope-labeled peptide peak. LLOQ/ULOQ ratios labeled in **bold**

Run	Unit	B	S8	S7	S6	S5	S4	S3	S2	S1
1	ratio	0.00	0.00	0.03	0.09	0.31	0.89	2.75	7.76	26.9
1	ratio	0.00	0.01	0.03	0.09	0.34	0.92	3.16	8.51	27.9
2	ratio	0.00	0.01	0.03	0.11	0.32	1.02	3.11	8.92	24.0
2	ratio	0.00	0.00	0.03	0.08	0.31	1.07	2.72	8.94	23.0
3	ratio	0.00	0.00	0.01	0.09	0.30	0.99	2.56	8.58	25.1
3	ratio	0.00	0.00	0.01	0.08	0.32	1.04	3.13	8.72	23.5
Mean value, n=6	ratio	0.00	0.00	0.02	**0.09**	0.32	0.99	2.91	8.57	**25.1**
SD	ratio	0.00	0.00	0.01	0.01	0.01	0.07	0.26	0.44	1.95
blank + 6x SD	ratio	0.01	-	-	-	-	-	-	-	-

Table 29: Calibrator validation results for OPN (MPr). LLOQ/ULOQ labeled in **bold**

Run	Unit	S8	S7	S6	S5	S4	S3	S2	S1
1	ng/mL	#	5.44	15.7	51.8	141	369	1,082	3,391
1	ng/mL	#	6.44	17.6	48.8	144	401	1,193	3,757
2	ng/mL	1.19	4.89	15.1	44.0	133	405	1,162	3,460
2	ng/mL	1.67	4.70	14.9	44.7	139	382	1,164	3,644
3	ng/mL	1.66	5.07	14.9	46.8	129	399	1,159	3,303
3	ng/mL	1.18	4.67	15.3	43.0	131	383	1,207	3,776
Mean value, n=6	ng/mL	1.42	5.20	15.6	46.5	136	390	1,161	3,555
SD	ng/mL	0.28	0.67	1.06	3.33	6.04	13.9	43.4	199
CV	%	19	13	7	7	4	4	4	6
Nominal value	ng/mL	1.62	**4.86**	14.6	43.7	131	393	1,180	**3,540**
Accuracy	%	-12	7	7	6	4	-1	-2	0
TE	%	31	20	14	14	8	4	5	6

#Calibrators excluded from curve fit due to non-acceptable CV of back-calculated S8 value in the corresponding batch

Table 30: Calibrator validation results for HMGB1 (MPr). LLOQ/ULOQ labeled in **bold**

Run	Unit	S8	S7	S6	S5	S4	S3	S2	S1
1	ng/mL	#	#	1.92	5.60	17.7	45.6	130	417
1	ng/mL	#	#	2.03	5.43	16.1	45.6	136	414
2	ng/mL	0.22	0.51	1.89	4.50	15.1	50.2	139	418
2	ng/mL	0.19	0.58	1.59	4.60	16.4	47.0	127	411
3	ng/mL	0.17	0.57	1.55	5.21	14.1	41.9	131	399
3	ng/mL	0.16	0.61	1.78	4.87	16.5	50.3	143	426
Mean value, n=6	ng/mL	0.19	0.57	1.79	5.04	16.0	46.8	134	414
SD	ng/mL	0.03	0.04	0.19	0.45	1.25	3.20	6.01	9.11
CV	%	15	8	11	9	8	7	4	2
Nominal value	ng/mL	0.19	0.57	**1.70**	5.09	15.3	45.8	138	**412**
Accuracy	%	-1	0	6	-1	5	2	-2	0
TE	%	16	8	16	10	12	9	7	3

#Calibrators excluded from curve fit due to non-acceptable accuracy values in the corresponding batch

Table 31: Calibrator validation results for ccK18 (MPr). LLOQ/ULOQ labeled in **bold**

Run	Unit	S8	S7	S6	S5	S4	S3	S2	S1
1	ng/mL	#	0.42	1.49	5.08	13.8	41.3	112	370
1	ng/mL	#	0.51	1.58	5.48	14.3	47.2	122	384
2	ng/mL	#	0.53	1.60	4.73	14.4	42.8	125	382
2	ng/mL	#	0.43	1.21	4.52	15.1	37.6	125	363
3	ng/mL	#	§	1.32	4.49	14.4	36.7	123	386
3	ng/mL	#	§	1.25	4.73	15.2	44.8	125	360
Mean value, n=6	ng/mL	-	0.47	1.41	4.84	14.5	41.7	122	374
SD	ng/mL	-	0.05	0.17	0.38	0.51	4.09	5.16	11.3
CV	%	-	12	12	8	4	10	4	3
Nominal value	ng/mL	0.17	0.51	**1.53**	4.60	13.8	41.4	124	**373**
Accuracy	%	-	-7	-8	5	5	1	-2	0
TE	%	-	19	20	13	9	10	6	3

#Calibrators excluded from curve fit due to non-acceptable CV of mean raw data in the corresponding batch
§ Calibrators excluded from curve fit due to non-acceptable accuracy in the corresponding batch

Table 32: QC inter assay validation results for OPN and HMGB1 (MPr)

		OPN			HMGB1		
Run	**Unit**	**QC1**	**QC2**	**QC3**	**QC1**	**QC2**	**QC3**
1	ng/mL	130	314	1,962	#	23.1	192
1	ng/mL	124	327	2,018	2.18	21.1	204
2	ng/mL	119	274	1,885	1.96	18.2	186
2	ng/mL	112	291	1,889	2.10	18.2	183
3	ng/mL	104	263	1,755	1.92	15.2	175
3	ng/mL	111	272	1,831	2.16	16.1	181
Mean value, n=6	ng/mL	117	290	1,890	2.06	18.7	187
SD	ng/mL	9.72	25.6	93.0	0.12	3.07	9.86
CV	%	8	9	5	6	16	5
Nominal value	ng/mL	113	275	1,832	1.96	18.5	182
Accuracy	%	3	6	3	5	1	3
TE	%	11	14	8	11	17	8

#First replicate of QC1 run 1 was out of batch calibration range

Table 33: QC inter assay validation results for ccK18 (MPr)

		ccK18		
Run	**Unit**	**QC1**	**QC2**	**QC3**
1	ng/mL	8.70	19.3	201
1	ng/mL	9.41	19.3	187
2	ng/mL	8.42	15.6	160
2	ng/mL	8.38	17.4	167
3	ng/mL	10.8	17.1	192
3	ng/mL	9.43	17.3	184
Mean value, n=6	ng/mL	9.19	17.7	182
SD	ng/mL	0.92	1.40	15.6
CV	%	10	8	9
Nominal value	ng/mL	8.99	15.9	175
Accuracy	%	2	11	4
TE	%	12	19	12

Table 34: QC intra assay validation results for OPN and HMGB1 (MPr)

		OPN			HMGB1		
Run	**Unit**	**QC1**	**QC2**	**QC3**	**QC1**	**QC2**	**QC3**
Measurement 1	ng/mL	133	261	1,873	2.35	19.7	187
Measurement 2	ng/mL	123	309	2,090	1.96	19.7	196
Measurement 3	ng/mL	124	293	1,956	1.96	21.3	195
Measurement 4	ng/mL	131	308	1,958	2.37	20.7	188
Measurement 5	ng/mL	121	298	1,894	2.19	21.7	182
Measurement 6	ng/mL	121	304	2,008	2.38	21.7	197
Mean value, n=6	ng/mL	125	295	1,963	2.20	20.8	191
SD	ng/mL	5.53	17.9	78.7	0.20	0.93	6.14
CV	%	4	6	4	9	4	3
Nominal value	ng/mL	113	275	1,832	1.96	18.4	182
Accuracy	%	11	7	7	12	12	5
TE	%	15	14	11	12	12	5

Table 35: QC intra assay validation results for ccK18 (MPr)

		ccK18		
Run	**Unit**	**QC1**	**QC2**	**QC3**
1	ng/mL	10.8	19.6	198
1	ng/mL	9.56	17.7	177
2	ng/mL	9.66	19.3	197
2	ng/mL	10.5	19.4	199
3	ng/mL	9.04	15.9	188
3	ng/mL	9.68	16.8	178
Mean value, n=6	ng/mL	9.86	18.1	190
SD	ng/mL	0.63	1.56	9.88
CV	%	6	9	5
Nominal value	ng/mL	8.99	15.9	175
Accuracy	%	10	14	8
TE	%	16	22	13

Table 36: Parallelism of endogenous OPN in plasma samples diluted in surrogate matrix (MPr)

Parallelism samples P1-P6 (plasma) diluted in surrogate matrix					
Dilution factor (DF)	**Unit**	**1 (undiluted)**	**2**	**4**	**8**
P1 measured value	ng/mL	246	127	68.5	34.0
P1 x DF	ng/mL	246	255	274	272
Accuracy	%	0	4	11	11
P2 measured value	ng/mL	344	162	85.0	40.4
P2 x DF	ng/mL	344	325	340	323
Accuracy	%	0	-6	-1	-6
P3 measured value	ng/mL	398	198	105	50.7
P3 x DF	ng/mL	398	396	420	406
Accuracy	%	0	0	6	2
P4 measured value	ng/mL	195	88.0	46.5	23.0
P4 x DF	ng/mL	195	176	186	184
Accuracy	%	0	-10	-5	-6
P5 measured value	ng/mL	209	104	54.4	27.1
P5 x DF	ng/mL	209	207	217	217
Accuracy	%	0	-1	4	4
P6 measured value	ng/mL	680	372	178	85.8
P6 x DF	ng/mL	680	743	711	687
Accuracy	%	0	9	5	1

Table 37: Parallelism of endogenous HMGB1 in plasma samples diluted in surrogate matrix (MPr)

Parallelism samples P1-P6 (plasma) diluted in surrogate matrix					
Dilution factor (DF)	**Unit**	**1 (undiluted)**	**2**	**4**	**8**
P1 measured value	ng/mL	39.1	20.1	10.3	5.43
P1 x DF	ng/mL	39.1	40.1	41.1	43.4
Accuracy	%	0	3	5	11
P2 measured value	ng/mL	19.3	9.81	5.25	2.65
P2 x DF	ng/mL	19.3	19.6	21.0	21.2
Accuracy	%	0	2	9	10
P3 measured value	ng/mL	17.8	8.40	4.60	2.30
P3 x DF	ng/mL	17.8	16.8	18.4	18.4
Accuracy	%	0	-6	3	3
P4 measured value	ng/mL	18.5	8.29	4.66	2.49
P4 x DF	ng/mL	18.5	16.6	18.7	19.9
Accuracy	%	0	-10	1	8
P5 measured value	ng/mL	81.3	39.9	21.3	11.4
P5 x DF	ng/mL	81.3	79.7	85.4	91.0
Accuracy	%	0	-2	5	12
P6 measured value	ng/mL	44.9	24.0	11.2	5.50
P6 x DF	ng/mL	44.9	47.9	44.6	44.0
Accuracy	%	0	7	-1	-2

Table 38: Parallelism of endogenous GLDH in liver tissue samples diluted in surrogate matrix (MPr)

Parallelism samples PT1-PT6 (liver tissue) diluted in surrogate matrix					
Dilution factor (DF)	**Unit**	**1 (undiluted)**	**2**	**4**	**8**
PT1 measured value	ng analyte / µg total protein	7.46	3.38	1.85	0.88
PT1 x DF	ng analyte / µg total protein	7.46	6.76	7.41	7.08
Accuracy	%	0	-9	-1	-5
PT2 measured value	ng analyte / µg total protein	8.35	4.36	2.08	0.97
PT2 x DF	ng analyte / µg total protein	8.35	8.73	8.33	7.72
Accuracy	%	0	4	0	-8
PT3 measured value	ng analyte / µg total protein	5.96	2.57	1.37	0.63
PT3 x DF	ng analyte / µg total protein	5.96	5.14	5.47	5.02
Accuracy	%	0	-14	-8	-16
PT4 measured value	ng analyte / µg total protein	5.89	2.85	1.34	0.64
PT4 x DF	ng analyte / µg total protein	5.89	5.70	5.36	5.09
Accuracy	%	0	-3	-9	-14
PT5 measured value	ng analyte / µg total protein	3.94	2.08	0.98	0.53
PT5 x DF	ng analyte / µg total protein	3.94	4.16	3.92	4.26
Accuracy	%	0	6	0	8
PT6 measured value	ng analyte / µg total protein	5.02	2.41	1.18	0.61
PT6 x DF	ng analyte / µg total protein	5.02	4.83	4.72	4.87
Accuracy	%	0	-4	-6	-3

Table 39: Parallelism of endogenous HMGB1 in liver tissue samples diluted in surrogate matrix (MPr). Accuracy exceeding the acceptance criteria (±20% accuracy compared to undiluted sample) are labeled in **bold**

Parallelism samples PT1-PT6 (liver tissue) diluted in surrogate matrix					
Dilution factor (DF)	**Unit**	**1 (undiluted)**	**2**	**4**	**8**
PT1 measured value	ng analyte / µg total protein	0.45	0.30	0.17	0.09
PT1 x DF	ng analyte / µg total protein	0.45	0.59	0.67	0.70
Accuracy	%	0	**31**	**47**	**55**
PT2 measured value	ng analyte / µg total protein	0.49	0.33	0.17	0.09
PT2 x DF	ng analyte / µg total protein	0.49	0.66	0.67	0.76
Accuracy	%	0	**36**	**38**	**56**
PT3 measured value	ng analyte / µg total protein	0.46	0.27	0.16	0.09
PT3 x DF	ng analyte / µg total protein	0.46	0.54	0.65	0.74
Accuracy	%	0	17	**40**	**59**
PT4 measured value	ng analyte / µg total protein	0.44	0.28	0.17	0.08
PT4 x DF	ng analyte / µg total protein	0.44	0.55	0.67	0.67
Accuracy	%	0	**25**	**52**	**52**
PT5 measured value	ng analyte / µg total protein	0.49	0.26	0.16	0.08
PT5 x DF	ng analyte / µg total protein	0.49	0.52	0.63	0.67
Accuracy	%	0	6	**28**	**37**
PT6 measured value	ng analyte / µg total protein	0.45	0.27	0.17	0.08
PT6 x DF	ng analyte / µg total protein	0.45	0.54	0.66	0.67
Accuracy	%	0	**21**	**47**	**49**

Table 40: Reproducibility of endogenous OPN levels in rat plasma (MPr)

		Reproducibility samples of animals 1 to 8							
Run	**Unit**	**1**	**2**	**3**	**4**	**5**	**6**	**7**	**8**
Run 1	ng/mL	141	166	179	130	174	177	275	125
Run 2	ng/ml	121	155	154	112	169	164	253	117
Difference	%	-15	-6	-15	-14	-3	-8	-8	-7

Table 41: Reproducibility of endogenous HMGB1 levels in rat plasma (MPr)

		Reproducibility samples of animals 1 to 8							
Run	**Unit**	**1**	**2**	**3**	**4**	**5**	**6**	**7**	**8**
Run 1	ng/mL	27.0	65.5	130	56.4	26.5	69.3	7.29	6.15
Run 2	ng/mL	29.4	30.5	134	64.5	31.9	74.1	8.44	6.27
Difference	%	9	**-73**	3	13	18	7	15	2

Table 42: Reproducibility of endogenous GLDH levels in liver tissue (MPr)

		Reproducibility samples of animals 1 to 6					
Run	**Unit**	**1**	**2**	**3**	**4**	**5**	**6**
Run 1	ng analyte / µg total protein	1.12	1.21	1.15	1.09	1.22	1.12
Run 2	ng analyte / µg total protein	1.37	1.60	1.43	1.33	1.33	1.35
Difference	%	20	28	21	19	9	19

Table 43: Reproducibility of endogenous HMGB1 levels in rat liver tissue (MPr)

		Reproducibility samples of animals 1 to 6					
Run	**Unit**	**1**	**2**	**3**	**4**	**5**	**6**
Run 1	ng analyte / µg total protein	7.46	8.35	5.96	5.89	3.94	5.02
Run 2	ng analyte / µg total protein	5.26	6.73	4.62	4.68	3.79	4.27
Difference	%	**-35**	-22	-25	-23	-4	-16

A.D Matrix and sampling comparison results for MPh-dev

Table 44: DILI biomarker concentration in matched serum gel, serum, and EDTA plasma samples. IA-LC-MS/MS assay MPh-dev and ELISA (ccK18). Time = benchtop time

Matrix	**Time (min)**	**median (ng/mL)**				**median (pM)**
		MCSF1R	**OPN**	**HMGB1**	**GLDH**	**ccK18**
Serum gel	15	458 ± 81.3	42.8 ± 10.2	1.56 ± 1.75	2.60 ± 21.3	216 ± 188
	30	413 ± 77.4	37.1 ± 8.50	2.09 ± 2.95	3.40 ± 19.6	237 ± 213
	60	410 ± 102	39.4 ± 9.14	3.55 ± 2.71	3.28 ± 19.4	205 ± 278
Serum	15	460 ± 94.8	39.0 ± 7.63	1.46 ± 1.15	3.04 ± 22.5	216 ± 177
	30	435 ± 90.9	41.2 ± 9.26	1.54 ± 2.46	3.52 ± 20.9	290 ± 206
	60	392 ± 97.6	39.7 ± 9.05	2.18 ± 4.20	3.41 ± 18.8	242 ± 275
EDTA plasma	15	525 ± 102	38.3 ± 6.59	0.30 ± 0.17	3.18 ± 17.8	155 ± 141
	30	539 ± 111	38.7 ± 8.51	0.35 ± 0.10	4.16 ± 18.0	157 ± 193
	60	491 ± 109	32.6 ± 9.77	0.29 ± 0.11	3.58 ± 18.2	183 ± 168

Table 45: Calibration curves for matrix and sampling comparison (MPh-dev assay, MCSF1R, OPN, HMGB1). Acc. = accuracy

Analyte	Theory spike-in		Measured analyte amount (fmol)						Mean	SD	CV	Acc.
			run 1		run 2		run 3					
	(fmol)	(ng/mL)	curve 1	curve 2	curve 1	curve 2	curve 1	curve 2	(fmol)	(fmol)	(%)	(%)
	0.69	2.61	0.63	0.84	0.31	1.88	0.00	0.99	0.77	0.6	84	13
	2.06	7.82	1.44	2.17	1.95	1.05	1.45	2.97	1.84	0.7	37	-11
MCSF1R	6.17	23.5	6.27	5.98	6.18	6.16	6.53	5.65	6.13	0.3	5	-1
	18.5	70.4	18.2	18.7	18.5	16.2	18.6	18.5	18.1	0.9	5	-2
	55.6	211	55.5	58.2	56.5	53.5	55.3	49.2	54.7	3.1	6	-2
	167	633	171	167	169	185	171	150	169	11.3	7	1
	500	1,899	499	487	473	510	508	576	509	35.9	7	2
	1,500	5,698	1,484	1,549	1,404	1,631	1,529	1,465	1,510	78.0	5	1
	0.69	1.62	0.73	0.66	0.73	0.65	0.71	0.80	0.71	0.1	8	4
	2.06	4.86	1.57	2.07	2.00	2.23	1.89	2.07	1.97	0.2	12	-4
OPN	6.17	14.6	6.07	6.28	6.06	6.21	6.32	6.54	6.25	0.2	3	1
	18.5	43.7	18.4	17.8	17.7	18.7	19.3	18.7	18.4	0.6	3	0
	55.6	131	57.1	56.0	55.6	57.6	55.2	57.2	56.5	1.0	2	2
	167	393	167	165	166	169	173	174	169	3.5	2	1
	500	1,180	491	501	497	486	489	510	496	8.9	2	-1
	1,500	3,540	1,566	1,484	1,490	1,523	1,597	1,633	1,549	60.2	4	3
	0.11	0.19	0.09	0.11	0.09	0.11	0.10	0.08	0.10	0.0	11	-15
	0.34	0.57	0.31	0.36	0.36	0.34	0.34	0.35	0.34	0.0	6	0
HMGB1	1.03	1.71	1.15	1.20	1.06	1.14	1.00	1.02	1.09	0.1	7	6
	3.09	5.12	3.13	3.33	2.82	3.32	3.50	3.26	3.23	0.2	7	5
	9.26	15.4	9.31	9.43	8.62	9.64	9.88	8.80	9.28	0.5	5	0
	27.8	46.1	28.3	28.8	25.5	26.5	27.7	27.1	27.3	1.2	4	-2
	83.3	138	77.9	86.3	82.4	84.1	83.6	85.9	83.4	3.1	4	0
	250	415	218	244	250	253	245	254	244	13.3	5	-2

Table 46: Calibration curves for matrix and sampling comparison (MPh-dev assay, GLDH). Acc. = accuracy

Analyte	Theory spike-in		Measured analyte amount (fmol)						Mean	SD	CV	Acc.
			run 1		run 2		run 3					
	(fmol)	(ng/mL)	curve 1	curve 2	curve 1	curve 2	curve 1	curve 2	(fmol)	(fmol)	(%)	(%)
	0.69	2.56	0.69	0.68	0.54	0.42	0.53	0.60	0.58	0.1	18	-16
	2.06	7.68	2.09	2.14	2.40	2.05	2.06	2.06	2.13	0.1	6	4
GLDH	6.17	23.0	6.09	6.26	7.03	6.71	6.11	6.71	6.48	0.4	6	5
	18.5	69.1	15.7	18.0	20.2	20.7	19.8	19.1	18.9	1.8	10	2
	55.6	207	50.1	47.5	53.0	60.0	52.9	46.8	51.7	4.8	9	-7
	167	622	181	151	181	157	149	153	162	15.1	9	-3
	500	1,866	508	487	499	498	467	491	492	13.8	3	-2
	1,500	5,597	1,671	1,589	1,534	1,544	1,568	1,538	1,574	51.7	3	5

Table 47: Quality control samples for matrix and sampling comparison (MPh-dev assay, GLDH). Rep = replicate. # Invalid result due to pipetting error

Analyte	Sample	Unit	Measured analyte amount (fmol)						Mean	SD	CV
			run 1		run 1		run 1		(fmol)	(fmol)	(%)
			rep 1	rep 2	rep 1	rep 2	rep 1	rep 2			
	endogenous QC1	fmol	1.71	1.57	2.05	1.51	1.51	1.59	1.66	0.20	12
	accuracy	%	3	-5	24	-9	-9	-4			
GLDH	spiked QC2	fmol	9.85	10.6	9.7	12.6	16.9	12.0	11.9	2.70	23
	accuracy	%	-17	-11	-19	5	42	1			
	spiked QC3	fmol	93.0	74.1	76.1	113	77.0	#	86.7	16.4	19
	accuracy	%	7	-15	-12	30	-11	-			

Table 48: Quality control samples for matrix and sampling comparison (MPh-dev assay, MCSF1R, OPN, HMGB1). Rep = replicate

Analyte	Sample	Unit	Measured analyte amount (fmol)						Mean (fmol)	SD (fmol)	CV (%)
			run 1		run 1		run 1				
			rep 1	rep 2	rep 1	rep 2	rep 1	rep 2			
	endogenous QC1	fmol	89.2	88.1	85.7	83.7	88.6	84.9	86.7	2.23	3
	accuracy	%	3	2	-1	-3	2	-2			
MCSF1R	spiked QC2	fmol	208	233	212	216	224	224	220	9.21	4
	accuracy	%	-5	6	-3	-2	2	2			
	spiked QC3	fmol	464	496	430	427	460	471	458	26.0	6
	accuracy	%	1	8	-6	-7	0	3			
	endogenous QC1	fmol	18.8	19.1	19.6	20.4	20.0	19.4	19.6	0.57	3
	accuracy	%	-4	-2	0	4	2	-1			
OPN	spiked QC2	fmol	157	163	167	168	168	165	165	4.44	3
	accuracy	%	-5	-1	2	2	2	0			
	spiked QC3	fmol	1,414	1,385	1,471	1,445	1,457	1,417	1,431	32.0	2
	accuracy	%	-1	-3	3	1	2	-1			
	endogenous QC1	fmol	1.00	1.23	1.03	1.02	1.13	1.08	1.08	0.09	8
	accuracy	%	-8	13	-5	-6	5	0			
HMGB1	spiked QC2	fmol	12.7	13.3	12.4	12.8	13.7	13.1	13.0	0.45	3
	accuracy	%	-2	2	-4	-2	5	1			
	spiked QC3	fmol	122	126	124	122	121	129	124	2.89	2
	accuracy	%	-1	1	0	-2	-3	4			